INL/EXT-19-53556

Light Water Reactor Sustainability Program

Risk-Informed Analysis for an Enhanced Resilient PWR with ATF, FLEX, and Passive Cooling

August 2019

U.S. Department of Energy

Office of Nuclear Energy

INL/EXT-19-53556

Risk-Informed Analysis for an Enhanced Resilient PWR with ATF, FLEX, and Passive Cooling

Zhegang Ma
Carlo Parisi
Cliff Davis
Jooyoung Park
Ronald Boring
Hongbin Zhang

August 2019

Prepared for the
U.S. Department of Energy
Office of Nuclear Energy

EXECUTIVE SUMMARY

This report documents the activities performed by Idaho National Laboratory (INL) during the fiscal year (FY) 2019 for the DOE Light Water Reactor Sustainability (LWRS) Program, Risk-Informed System Analysis (RISA) Pathway, Enhanced Resilient Plant (ERP) Systems research. The purpose of the RISA Pathway research and development is to support plant owner-operator decisions with the aim to improve the economics, reliability, and maintain the high levels of safety of current nuclear power plants over periods of extended plant operations. The concept of ERP refers to the combinations of Accident Tolerant Fuel (ATF), optimal use of Diverse and Flexible Coping Strategy (FLEX), enhancements to plant components and systems, and the incorporation of augmented or new passive cooling systems, as well as improved fuel cycle efficiency. The objective of the ERP research effort is to use the RISA methods and toolkit in industry applications, including methods development and early demonstration of technologies, in order to enhance existing reactors' safety features (both active and passive) and to substantially reduce operating costs through risk-informed approaches to plant design modifications to the plant and their characterization.

The FY 2019 efforts documented in this report are an extension of those conducted in FY 2018. The same analysis process, risk analysis approaches, and analysis tools as in FY 2018 are used for near-term ATF cladding (i.e., Iron-Chromium-Aluminum [FeCrAl] cladding and Chromium [Cr]-coated cladding) designs under the postulated loss of feedwater (LOFW) and steam generator tube rupture (SGTR) accident scenarios. In addition, FLEX analysis was presented for an overview of FLEX equipment and strategies implemented in the nuclear industry after the Fukushima accident. A FLEX model was developed and incorporated into the generic SAPHIRE model to assess the risk impact from FLEX. FLEX human reliability analysis (HRA) was performed, which suggested an approach to HRA with FLEX strategies. The passive cooling system analysis includes an overview of the dynamic natural convection (DNC) system, the RELAP5-3D simulations of the DNC system in selected station blackout (SBO) scenarios, and the evaluation of the DNC system risk impact using the generic probabilistic risk assessment (PRA) model.

In the ATF LOFW analysis, seven LOFW scenarios were developed and analyzed using RELAP5-3D for thermal hydraulic analysis with traditional fuel design and near-term ATF designs. The RELAP5-3D simulation results, as presented in Tables ES-1 and ES-2, show that the gain of coping time, or the delay of time to core damage due to the ATF designs, is less than 20 minutes for most LOFW scenarios. For FeCrAl, four of the seven analyzed LOFW scenarios have a gain of coping time from 6 to 14 minutes. The other three scenarios have a gain of coping time from 18 to 49 minutes, which is relatively small when comparing the time to core damage with Zircaloy in the associated scenarios (about 13 hours). For Chromite, four of the seven analyzed LOFW scenarios have a gain of coping time from 4 to 9 minutes, while the other three scenarios have a gain of coping time from 16 to 22 minutes. With these relatively small increases of the time to core damage, the risk benefit to the core damage frequency (CDF) brought by the ATF designs would be very small and was therefore not conducted in this analysis. However, the RELAP5-3D simulation results show the clear benefit in adopting ATFs with much less hydrogen produced at the time of core damage, which can be one or two orders of magnitude lower than the Zircaloy clad cases.

Table ES-1. Time to Core Damage Comparison for LOFW Scenarios with ATF Designs.

Scenario	Description	Time to Core Damage (hr:min)				
		Zircaloy	FeCrAl	Δt (FeCrAl)	Chromite	Δt (Chromite)
LOFW-1.0	Unmitigated Loss of All Feedwater	2:19	2:27	0:08	2:23	0:04
LOFW-2.0	Mitigated Loss of All Feedwater with FAB	13:21	14:10	0:49	13:42	0:21
LOFW-3.0	LOMFW with PORV LOCA	2:10	2:16	0:06	2:14	0:04
LOFW-4.0	LOMFW with LOSC-182	13:50	14:17	0:27	14:06	0:16
LOFW-4.1	LOMFW with LOSC-182 w/o Depressurization	8:23	8:34	0:11	8:29	0:06
LOFW-4.2	LOMFW with LOSC-76	13:11	13:29	0:18	13:20	0:09
LOFW-4.3	LOMFW with LOSC-480	6:05	6:19	0:14	6:27	0:22

Table ES-2. Comparing H_2 Productions for LOFW Scenarios with ATF Designs.

Scenario	Description	Total H_2 (kg)				
		Zircaloy	FeCrAl	H_2% (FeCrAl)	Chromite	H_2% (Chromite)
LOFW-1.0	Unmitigated Loss of All Feedwater	51.1	1.0	2.0%	5.5	10.8%
LOFW-2.0	Mitigated Loss of All Feedwater with FAB	88.0	2.3	2.6%	4.0	4.5%
LOFW-3.0	LOMFW with PORV LOCA	28.5	1.9	6.7%	7.3	25.6%
LOFW-4.0	LOMFW with LOSC-182	55.6	2.5	4.5%	15.6	28.1%
LOFW-4.1	LOMFW with LOSC-182 w/o Depressurization	37.0	2.1	5.7%	9.8	26.5%
LOFW-4.2	LOMFW with LOSC-76	79.6	2.0	2.5%	8.8	11.1%
LOFW-4.3	LOMFW with LOSC-480	15.2	0.8	5.3%	7.6	50.0%

In the ATF SGTR analysis, the SGTR accident sequences based on the PRA model do not reach core damage conditions within 48 hours. The reasons they were defined in the PRA model with the end state of core damage are probably from the conservative and qualitative assessment when developing the PRA model. With the slow progressing nature in an SGTR event, the time to core damage for most SGTR accident sequences could be much longer than the 24 hours one would see in other initiating events.

Additional SGTR accident scenarios were developed based on the U.S. Nuclear Regulatory Commission (NRC) State-of-the-Art Reactor Consequence Analyses (SOARCA) Report, NUREG/CR-7110, which assumes no operator actions for an extended time interval. The RELAP5-3D analysis results show similar ATF impacts as those in the LOFW analysis. Similarly, the risk impact on behalf of the CDF brought by the ATF designs is not conducted for SGTR. However, the benefit in much less hydrogen produced

at the time of core damage is obvious. The calculated amount of hydrogen produced during the transients for Zircaloy is 72.5 kg, but only 1.1 kg for FeCrAl (1.5% of the hydrogen production for Zircaloy), and 18.5 kg for Chromite (25% of the hydrogen production for Zircaloy).

The FLEX analysis presents an overview of FLEX, including FLEX characterizations and the crediting of FLEX in PRA, in an effort to develop and incorporate FLEX to the generic loss of offsite power (LOOP)/SBO SAPHIRE model. It also includes a case study of how to perform HRA for FLEX applications. Table ES-3 shows that the total LOOP CDF with FLEX from the generic model is 1.68E-6 per year, which is a 26% reduction when compared with the total LOOP CDF with no FLEX (2.28E-6 per year). These results represent the risk impact on a generic pressurized water reactor (PWR) plant. Plant-specific FLEX analyses should be conducted to evaluate specific risk impacts from the planned or implemented FLEX equipment and strategies. Every plant analysis might have different results presented here due to different structure, system, and component (SSC) configurations, different risk profiles, and different SSC risk contributions and significance.

Table ES-3. FLEX PRA Model Quantification Results.

LOOP ET	CDF No FLEX	CDF with FLEX	ΔCDF	ΔCDF%
LOOPGR	1.07E-06	8.12E-07	-2.55E-07	-23.9%
LOOPPC	6.21E-08	5.19E-08	-1.02E-08	-16.4%
LOOPSC	4.57E-07	3.58E-07	-9.85E-08	-21.6%
LOOPWR	6.89E-07	4.60E-07	-2.29E-07	-33.2%
LOOP Total	2.28E-06	1.68E-06	-5.93E-07	-26.1%

The FLEX HRA in this report provides a case study on how to perform HRA for FLEX applications. It utilizes South Korean operating experience and tries to use existing HRA methods for FLEX. The South Korean examples are particularly relevant to multi-unit sites but can be generalized to single-unit plants. The analyses characterize different types of accident scenarios that would require FLEX. To date, most U.S. PRAs have on FLEX has taken minimal HRA credit for FLEX deployment. The examples provided in this report demonstrate ways to account for FLEX and to use existing HRA methods without the need necessarily to adopt newer HRA techniques specifically to account for FLEX.

In the passive cooling system analysis, the DNC system designed by DYNAC Systems was reviewed and simulated with RELAP5-3D in selected SBO scenarios. The DNC system was modeled and incorporated into the generic PRA model by assuming that the DNC system is able to replace auxiliary feedwater (AFW) to provide secondary cooling after an initiating event (IE) has occurred. The quantification results show that the SBO CDF with DNC system is reduced from 2.28E-6 to 9.79E-7 per year, which represents a significant 57% reduction (Table ES-4). After applying the DNC system to other event trees, the plant total CDF is reduced from 3.17E-5 to 2.34E-5 per year, with about 25% reduction (Table ES-5). The smaller risk reduction on the total plant CDF is due to the DNC system, which may have no or little impact to initiators such as loss-of-coolant accidents (LOCAs), loss of component cooling water (LOCCW), and general transients.

Table ES-4. DNC Risk Impact on SBO CDF.

ET	CDF with AFW (/year)	CDF with DNC (/year)	ΔCDF (/year)	ΔCDF%
LOOPGR	1.07E-06	4.61E-07	-6.06E-07	-56.8%
LOOPPC	6.21E-08	2.20E-08	-4.01E-08	-64.6%
LOOPSC	4.57E-07	1.84E-07	-2.72E-07	-59.7%
LOOPWR	6.89E-07	3.11E-07	-3.78E-07	-54.8%
Total	2.28E-06	9.79E-07	-1.30E-06	-57.0%

Table ES-5. DNC Risk Impact on Plant Total CDF.

Event Tree	CDF with AFW (/year)	CDF with DNC (/year)	ΔCDF (/year)	ΔCDF%
ISL-HPI	3.85E-09	3.85E-09	0.00E+00	0.0%
ISL-LPI	3.84E-08	3.84E-08	0.00E+00	0.0%
ISL-RHR	6.65E-07	6.65E-07	0.00E+00	0.0%
LLOCA	2.01E-08	2.01E-08	0.00E+00	0.0%
LOACA	1.14E-05	4.60E-06	-6.81E-06	-59.7%
LOCCW	1.35E-09	1.33E-09	-1.30E-11	-1.0%
LOCHS	1.46E-07	1.35E-07	-1.13E-08	-7.8%
LODCA	3.71E-07	3.05E-07	-6.57E-08	-17.7%
LODCB	3.72E-07	3.05E-07	-6.71E-08	-18.0%
LOMFW	1.08E-07	9.98E-08	-8.29E-09	-7.7%
LONSW	1.43E-05	1.43E-05	0.00E+00	0.0%
LOOPGR	1.07E-06	4.61E-07	-6.06E-07	-56.8%
LOOPPC	6.21E-08	2.20E-08	-4.01E-08	-64.6%
LOOPSC	4.57E-07	1.84E-07	-2.72E-07	-59.7%
LOOPWR	6.89E-07	3.11E-07	-3.78E-07	-54.8%
MLOCA	6.28E-07	6.28E-07	0.00E+00	0.0%
SGTR	1.07E-07	1.12E-07	4.80E-09	4.5%
SLOCA	7.78E-08	7.78E-08	-5.00E-11	-0.1%
TRANS	1.07E-06	1.05E-06	-2.30E-08	-2.1%
XLOCA	1.00E-07	1.00E-07	0.00E+00	0.0%
Total	3.17E-05	2.34E-05	-8.28E-06	-26.1%

CONTENTS

FIGURES

TABLES

ACRONYMS

ACC	accumulator system
AFW	auxiliary feedwater
AOP	abnormal operating procedures
ASEP	accident sequence evaluation program
ATF	accident tolerant fuel
ATWS	anticipated transient without scram
BEPU	best estimate plus uncertainty
BWR	boiling water reactor
CBDT	cause-based decision tree
CCF	common cause failure
CD	complete dependence
CDF	core damage frequency
CS	containment spray
CSP	cognitive speaking process
CST	condensate storage tank
CEAM	CREAM-based communication error analysis method
CREAM	cognitive reliability and error analysis method
DEGB	double-ended guillotine break
DG	diesel generator
DNC	dynamic natural convection
DOE	Department of Energy
DPRA	dynamic probabilistic risk assessment
ECCS	emergency core cooling system
EDG	emergency diesel generator
ELAP	extended loss of AC power
EOP	emergency operating procedures
EPRI	Electric Power Research Institute
ERP	enhanced resilient plant
ERPS	enhanced resilient plant systems
EPS	emergency power system
FAB	feed and bleed

FLEX	diverse and flexible coping strategy
FSG	FLEX support guidelines
FY	fiscal year
HD	high dependence
HEP	human error probabilities
HFE	human failure event
HPI	high pressure injection
HPR	high pressure recirculation
HPIS	high pressure injection system
HPSI	high pressure safety injection
HRA	human reliability analysis
HX	heat exchanger
IGPWR	INL Generic PWR
IE	initiating event
INL	Idaho National Laboratory
LERF	large early release frequency
LBLOCA	large break loss of coolant accident
LD	low dependence
LOCA	loss of coolant accident
LOCCW	loss of component cooling water
LOFW	loss of feedwater
LOMFW	loss of main feedwater
LOOP	loss of offsite power
LOSC	loss of seal cooling
LPI	low pressure injection
LPR	low pressure recirculation
LS	limit surface
LWR	light water reactor
LWRS	light water reactor sustainability
MACST	multi-barrier accident coping strategy
MCP	main coolant pump
MCR	main control room
MD	moderate dependence
MDAFP	motor-driven auxiliary feedwater pump
MFW	main feedwater

MOP	MACST operating procedures
MSIV	main steam isolation valves
MSPI	mitigating systems performance index
NEI	Nuclear Energy Institute
NOED	notices of enforcement discretion
NPP	nuclear power plant
NRC	Nuclear Regulatory Commission
NUREG	nuclear regulatory report
OAT	one at a time
OPR	offsite power recovery
PCT	peak clad temperature
PORV	power-operated relief valve
PRA	probabilistic risk assessment
PRT	pressurizer relief tank
PRZ	pressurizer
PSF	performance-shaping factors
PWR	pressurized water reactor
R&D	research and development
RA	risk assessment
RAVEN	Risk Analysis and Virtual Control Environment
RCS	reactor cooling system
RCP	reactor coolant pump
RELAP5-3D	Reactor Excursion and Leak Analysis Program 5 – 3D
RHR	residual heat removal
RISA	risk-informed system analysis
RISMC	Risk Informed Safety Margin Characterization
ROM	reduced order model
RPS	reactor protection system
RPV	reactor pressure vessel
RWST	reactor water storage tank
SA	severe accident
SAMG	severe accident management guidelines
SBO	station blackout
SD	steam dump
SDP	significance determination process

SFW	start-up feedwater
SG	steam generator
SGTR	steam generator rupture
SI	safety injection
SIAS	safety injection actuation signal
SOARCA	state-of-the-art reactor consequence analyses
SPAR-H	standardized plant analysis risk – human reliability analysis
SSC	structure, system, and component
SRV	safety relief valve
TDAFP	turbine driven auxiliary feedwater pump
TDAFW	turbine driven auxiliary feedwater
TH	thermal-hydraulic
THERP	technique for human error rate prediction
TSC	technical support center
TSV	turbine stop valve
U.S.	United States
UTS	ultimate tensile strength
ZD	zero dependence

Risk-Informed Analysis for an Enhanced Resilient PWR with ATF, FLEX, and Passive Cooling

1. INTRODUCTION

This report documents the activities performed by Idaho National Laboratory (INL) during fiscal year (FY) 2019 for the U.S. Department of Energy (DOE) Light Water Reactor Sustainability (LWRS) Program, Risk-Informed Systems Analysis (RISA) Pathway, Enhanced Resilient Plant (ERP) Systems research (INL, 2018). The LWRS Program is a research and development (R&D) program that provides technical foundations for the continued operation of the nation's nuclear power plants, develops methods to support safe and economical long-term management and operation of existing nuclear power plants, and investigates new technologies to address enhanced nuclear power plant performance, economics, and safety. With the continuing economic challenges faced by nuclear power plants, the LWRS Program has redirected some of its R&D efforts to consider how to leverage the results from other ongoing R&D activities to improve the economic performance of LWRs in current and future energy markets. The RISA Pathway is one of the primary technical areas of R&D under the LWRS Program. This pathway supports decision-making related to economics, reliability, and safety by providing integrated plant system analysis and solutions through collaborative demonstrations to enhance economic competitiveness of operating nuclear power plants. The purpose of RISA Pathway R&D is to support plant owner-operator decisions to improve economics and reliability, and to maintain the high levels of safety of current nuclear power plants over periods of extended plant operations. The goals of the RISA Pathway are:

- To demonstrate risk-assessment methods coupled to safety margin quantification that can be used by decision-makers as a part of their margin recovery strategies
- To apply the "RISA toolkit" to enable more accurate representations of safety margins for the long-term benefit of nuclear assets.

One of the research efforts under the RISA Pathway is the ERP system analysis, which supports the DOE and industry initiatives including Accident Tolerant Fuel (ATF), Diverse and Flexible Coping Strategy (FLEX), and passive cooling system designs, in order to improve the safety and economic performance of the current fleet of nuclear power plants. The ATF, combined with the optimal use of FLEX, the enhancements to plant components and systems, the incorporation of augmented or new passive cooling systems, and the improved fuel cycle efficiency are called ERP Systems. The objective of the ERP research effort is to use the RISA methods and toolkit in industry applications, including methods development and early demonstration of technologies, in order to enhance existing reactors' safety features (both active and passive) and to substantially reduce operating costs through risk-informed approaches.

The purpose of the FY 2019 ERP R&D efforts is to demonstrate additional safety margins or risk benefits available to industry by integrating individual design and operational enhancements, such as near-term ATF concepts, FLEX equipment, and passive cooling systems through risk analysis for a more resilient plant. The FY 2019 efforts documented in this report are extensions of those conducted in FY 2018. There were two main focus areas in FY 2018 for the ERP R&D efforts. One was to evaluate the risk impact brought by ATF and FLEX in postulated selected accident scenarios including station blackout (SBO) and large break loss-of-coolant-accident (LBLOCA). The other was to investigate various approaches to accomplish the ERP research objective, i.e., use RISA methods and toolkit to enhance existing reactors safety features and reduce plant operating costs. The FY 2018 ERP report (Ma & al., 2018) also describes the ERP analysis process, ERP analysis tools, and various analysis approaches.

Probabilistic risk assessment (PRA) and multi-physics best estimate analyses were performed for risk impact introduced by near-term ATF cladding (i.e., Iron-Chromium-Aluminum [FeCrAl] cladding and Chromium [Cr] coated cladding) designs to a generic Westinghouse 3-loop pressurized water reactor (PWR) for postulated SBO and LBLOCA accident scenarios using SAPHIRE (Smith & Wood, 2011), RELAP5-3D (RELAP5-3D Code Development Team, 2018), and RAVEN (Alfonsi, et al., 2017) codes.

The same analysis process, risk analysis approaches, and analysis tools as in FY 2018 are used for FeCrAl and Cr-coated ATF designs under the postulated loss of feedwater (LOFW) and steam generator tube rupture (SGTR) accident scenarios. Additional analyses are performed for FLEX and passive cooling system analysis. It should be noted that part of FY 2019 ERP activities will be documented under an "add-on" project report. These activities include the ATF analysis for other accident scenarios such as anticipated transient without scram (ATWS) as well as general transients with turbine trip and PWR locked rotor. More in-depth risk analysis on FLEX and passive cooling system will also be documented in that report.

The remaining sections of the report are organized as below: Section 2 presents ATF risk analysis for LOFW and SGTR scenarios. Section 3 provides FLEX risk analysis including FLEX PRA modeling for risk impact analysis and FLEX human reliability analysis (HRA), Section 4 provides risk-informed analysis on a passive cooling systems, or the dynamic natural convection (DNC) system designed by DYNAC Systems. Section 5 provides a summary and the future work planning for ERP.

2. RISK-INFORMED ATF ANALYSIS

This section presents a risk-informed analysis on ATF with the same generic PWR plant SAPHIRE PRA model and the same INL Generic PWR (IGPWR) RELAP5-3D model used in FY 2018 activities (Ma & al., 2018). Loss of feedwater (LOFW) and SGTR accident scenarios are developed by reviewing the PRA model and then analyzed by RELAP5-3D code for near-term ATF designs, FeCrAl, and Cr-coated cladding.

2.1 LOFW SCENARIO ANALYSIS

2.1.1 LOFW PRA Model and Scenarios

The generic PRA model represents LOFW by the loss of main feedwater (LOMFW) event tree and a series of sub event trees that are transferred from the main event tree. Figure 2-1 shows the LOMFW event tree and Figure 2-2 shows the loss of seal cooling (LOSC) for reactor coolant pump (RCP) event tree that is transferred from LOFW Sequence 2.

The LOMFW event tree was quantified with SAPHIRE 8 using a truncation level of 1E-12. Table 2-1 presents the quantification results. The total LOMFW core damage frequency (CDF) is 1.24E-7/year. There are nine non-zero CDF sequences out of a total of 82 LOMFW accident sequences (i.e., the sequence end state is core damage). LOMFW Sequence 13-16 is the most risk-significant sequence with a CDF of 6.74E-8/year and contributes 54% of the total LOMFW CDF. In this sequence, the reactor protection system (RPS) fails to trip the reactor following the LOMFW initiating event (IE), the sequence transfers from the LOMFW Sequence 13 to the anticipated transient without scram (ATWS) event tree. In the ATWS event, if the reactor cooling system (RCS) pressure exceeds the design pressure of the reactor vessel (ATWS Sequence 16), core damage is assumed. LOMFW Sequence 12 is the second-most risk-significant sequence with a CDF of 4.25E-8/year, contributing 34% of the total LOMFW CDF. In this sequence, RPS trips the reactor successfully, but auxiliary feedwater (AFW) fails to supply sufficient cooling water to at least one steam generator. When feed-and-bleed cooling also fails to provide decay heat removal, core damage can't be prevented. Other significant LOMFW sequences include another ATWS sequence (LOMFW:13-14, contributing 7% of total LOMFW CDF) and a loss of RCP seal cooling sequence (LOMFW:02-02-09, contributing 3% of the total LOMFW CDF).

Table 2-1. Overview of LOFW Event Trees Quantification Results.

Sequence	CDF	Cut Set Count	% CDF
LOMFW Total	1.24E-07	1304	100.0%
LOMFW:02-02-09	3.89E-09	516	3.1%
LOMFW:02-02-10	1.80E-11	13	0.0%
LOMFW:02-03-09	9.78E-11	48	0.1%
LOMFW:02-04-10	2.62E-12	2	0.0%
LOMFW:11	1.13E-09	102	0.9%
LOMFW:12	4.25E-08	515	34.2%
LOMFW:13-14	9.05E-09	28	7.3%
LOMFW:13-15	6.91E-11	30	0.1%
LOMFW:13-16	6.74E-08	50	54.3%

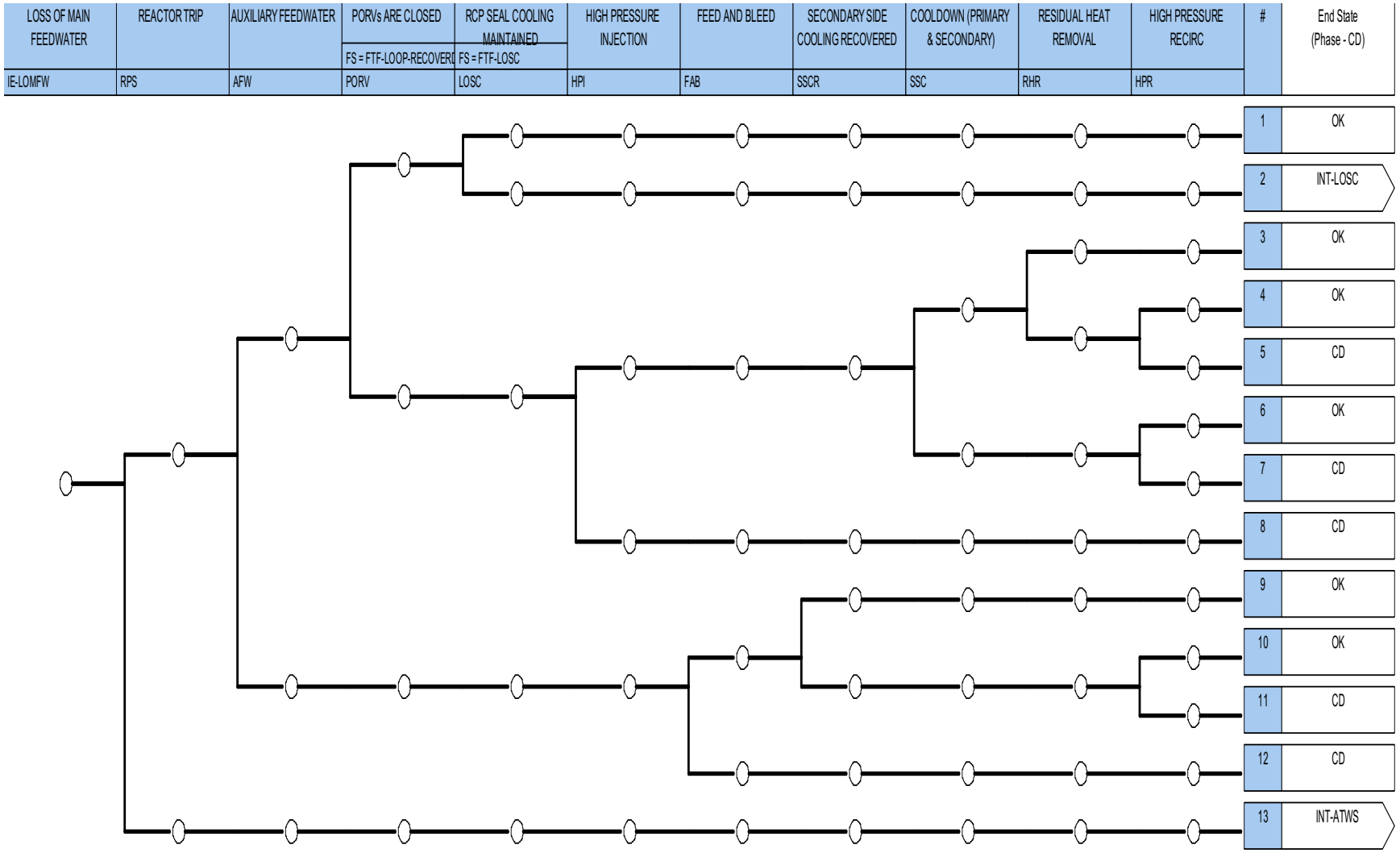

Figure 2-1. Generic PWR LOMFW Event Tree.

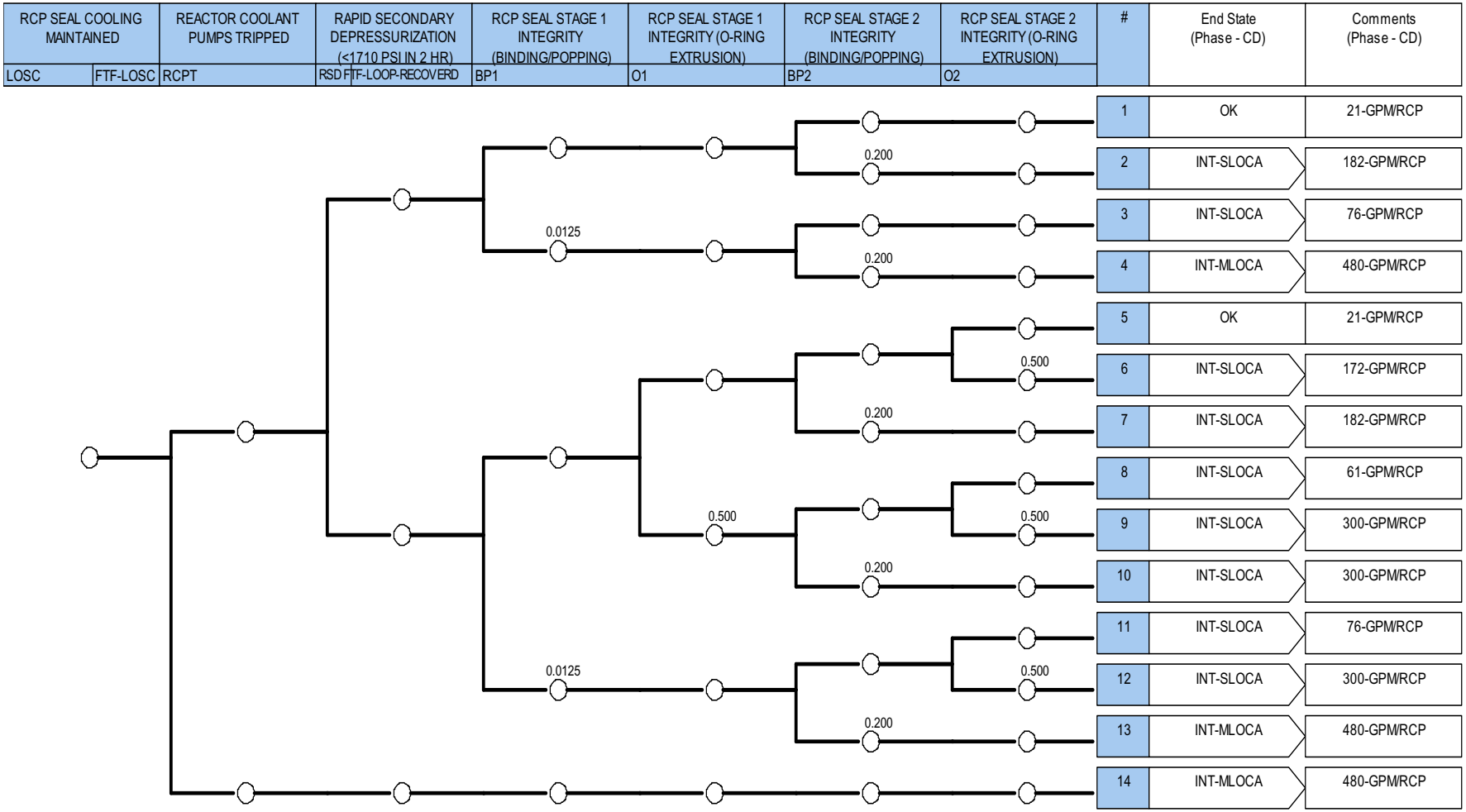

Figure 2-2. LOSC Event Tree – Transferred from LOMFW Sequence 2.

The following LOFW scenarios were developed as input for RELAP5-3D thermal hydraulic analysis with traditional fuel design and near-term ATF designs. The scenarios can be grouped into three categories: (1) loss of all feedwater scenarios (i.e., AFW is unavailable along with the LOMFW initiator); (2) loss of RCP seal cooling or power-operated relief valve (PORV) loss-of-coolant accident (LOCA) scenarios (also called RCP Seal LOCA), when a PORV opens and fails to reclose, leading to an LOCA; (3) ATWS scenarios.

Loss of All Feedwater Scenarios

LOFW-1.0: This is an unmitigated loss-of-all-feedwater scenario when an LOMFW initiating event occurs, RPS trips the reactor, but AFW is unavailable and feed-and-bleed (FAB) fails.

LOFW-2.0: This is a mitigated loss-of-all-feedwater with FAB scenario. An LOMFW initiating event occurs, RPS trips the reactor, AFW is unavailable, but FAB is successful with one PORV to open and remove decay heat, and high-pressure injection (HPI) provides early makeup water to RCS. However, when the reactor water storage tank (RWST) depletes, and high-pressure recirculation (HPR) fails to provide long-term cooling for the reactor, core damage occurs if there is no secondary side-cooling recovered.

RCP Seal LOCA/PORV LOCA Scenarios

LOFW-3.0 (PORV-1): This is a loss-of-main-feedwater with PORV LOCA scenario. An LOMFW initiating event occurs, RPS trips the reactor, one motor-driven auxiliary feedwater pump (MDAFP) starts and runs successfully, however, one PORV opens during the transient but cannot reclose. Primary injection is unavailable to provide makeup water to RCS and core damage occurs.

LOFW-4.0 (LOSC-182): This is a loss-of-main-feedwater with RCP Seal LOCA 182 gpm per RCP scenario. LOMFW initiating event occurs, RPS trips the reactor, one MDAFP starts and runs successfully, however, RCP seal LOCA occurs with a leakage rate of 182 gpm per pump. Although depressurization is successful, neither HPI nor low-pressure injection (LPI) is available to provide RCS makeup. Core damage occurs.

LOFW-4.1 (LOSC-182): This is a scenario similar to LOFW-4.0 other than that depressurization is not successful. HPI is not available while LPI is unable to operate due to high RCS pressure. Core damage will occur with no RCS water makeup.

LOFW-4.2 (LOSC-76): This is a scenario similar to LOFW-4.0 other than that RCP seal leakage rate is 76 instead of 182 gpm per pump.

LOFW-4.3 (LOSC-480): This is a scenario similar to LOFW-4.0 other than that RCP seal leakage rate is 480 instead of 182 gpm per pump.

ATWS Scenarios

LOFW-5.0 (ATWS-1): This is an ATWS-without-RCS pressure-relief scenario. An LOMFW initiating event occurs, RPS fails to trip the reactor, primary system PORVs and safety relief valves (SRVs) fail to control RCS pressure (RCS-P), which exceeds design pressure, and core damage is assumed.

LOFW-5.1 (ATWS-2): This is an ATWS-without-feedwater scenario. An LOMFW initiating event occurs, RPS fails to trip the reactor, RCS pressure does not increase beyond the design pressure of the reactor vessel, but MFW and AFW can't provide secondary cooling, and core damage occurs.

LOFW-5.2 (ATWS-3): This is an ATWS-without-boration scenario. An LOMFW initiating event occurs, RPS fails to trip the reactor, RCS pressure does not increase beyond the design pressure of the reactor vessel, the AFW system automatically starts and operates to provide sufficient cooling water to steam generators (SGs), however, boration fails to place the reactor in a subcritical state, and core damage finally occurs.

Table 2-2 presents an overview of the LOFW scenarios developed for RELAP5-3D analysis. After discussions with the RELAP5-3D analyst, the three LOFW ATWS scenarios (LOFW-5.0 to LOFW-5.2) would be similar with other transient ATWS scenarios, and thus won't analyzed in this section. All other scenarios would be run with RELAP5-3D, first with the current Zr-based fuel cladding design as the base case and then with the ATF design

(the FeCrAl design or the Cr-coated design). The times of peak cladding temperature (PCT) to reach melting point, the times to generate a half kilogram hydrogen, and the total amount of hydrogen generated when the run is terminated are compared between different cladding designs for each scenario. The estimated time differences for PCT to reach melting point from RELAP5-3D are then considered for PRA model changes to evaluate the risk impacts from the proposed ATF design.

Table 2-2. LOFW Scenarios for RELAP-5 3D Analysis.

RELAP-5 Scenario	Scenario Description	LOFW					PORV or RCP Seal LOCA							ATWS		
		RPS	AFW	FAB	SSCR	HPR	PORV	RCP Seal	HPI	ACC	AFW	SSC	LPI	RCS-P	AFW	Boration
LOFW-1.0	LOFW with No Mitigation	Trip	No AFW	No FAB												
LOFW-2.0	LOFW with F&B but No HPR	Trip	No AFW	FAB	No SSCR	No HPR										
LOFW-3.0 (PORV-1)	LOFW with PORV LOCA and No HPI	Trip	AFW				PORV LOCA		No HPI							
LOFW-4.0 (LOSC-182)	LOFW with RCP Seal LOCA (182 gpm) and No HPI/LPI	Trip	AFW				PORV OK	182 gpm	No HPI			SSC	No LPI			
LOFW-4.1 (LOSC-182)	LOFW with RCP Seal LOCA (182 gpm) and No HPI & No Depressurization	Trip	AFW				PORV OK	182 gpm	No HPI			No SSC				
LOFW-4.2 (LOSC-76)	LOFW with RCP Seal LOCA (76 gpm) and No HPI/LPI	Trip	AFW				PORV OK	76 gpm	No HPI			SSC	No LPI			
LOFW-4.3 (LOSC-480)	LOFW with RCP Seal LOCA (480 gpm) and No HPI/LPI	Trip	AFW				PORV OK	480 gpm	No HPI	ACC	AFW	SSC	No LPI			
LOFW-5.0 (ATWS-1)	LOFW with ATWS & Overpressure	No Trip												RCS-P Fail		
LOFW-5.1 (ATWS-2)	LOFW with ATWS & No AFW	No Trip												RCS-P Good	No AFW	
LOFW-5.2 (ATWS-3)	LOFW with ATWS & No Boration	No Trip												RCS-P Good	AFW	No Boration

2.1.2 LOFW RELAP5-3D Model

The same RELAP5-3D INL Generic PWR (IGPWR) model as in (Ma & al., 2018) was used in this analysis. The details of this are described in (Carlo Parisi, 2016). The model is based on a generic Westinghouse three-loop PWR. In order to simulate LOFW, several modifications to the base IGPWR input deck have been performed, as detailed below.

In order to properly calculate the LOFW transient, representation of the containment feedback had to be included in the simulation. Some PRA branches of the LOFW accident assume extended discharge of the primary coolant through the PRZ PORVs to the PRT, and from there to the containment. The successive actuation of the containment sprays significantly increases the rate of depletion of the RWST (the containment spray's mass flow rate is 445 lbm/second versus a total HPIS mass flow rate of about 63 lbm/second). Therefore, a simplified containment response model has been developed and added to the IGPWR model. The containment main parameters are reported in Table 2-3, based on Surry Power Station Final Safety Analysis Report (FSAR) (Dominion, 2007). The nodalization scheme is shown in Figure 2-3.

The containment model was developed using the RELAP5-3D pressurizer "prizer" component because such component has the following capabilities:

- Models a stack of hydraulic volumes with two-phase fluid and incondensable gases. This is the same capability of the "pipe" component
- Models the spray-induced condensation, using a dedicated junction and can let the user to specify the water droplet diameter in the annular/mist flow regime and the interfacial heat transfer coefficients between water and vapor
- Dedicated heat structures were connected to the hydraulic model of the containment in order to simulate the thermal inertia; the main structures considered are reported in Table 2-4.

A fan cooler system was also added in order to simulate the combined effect of spray and atmosphere mixing and cooling. The fan cooler and the containment spray characteristics are reported in Table 2-5 and Table 2-6. The logic of the fan coolers actuation was not available, therefore fan coolers were actuated with the same logic as the containment sprays (Table 2-6).

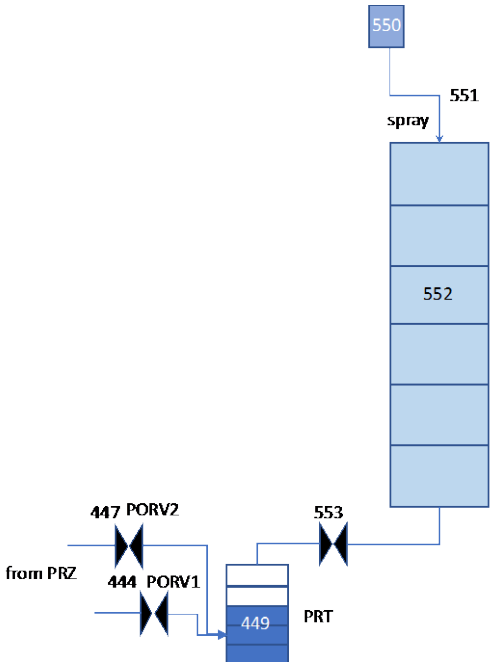

Figure 2-3. Containment and PRT Nodalization.

Table 2-3. Containment Parameters.

Parameters	Values
Max Free Volume (m^3)	49,000
Inside Diameter (m)	38.4
Interior Vertical height (m)	56.4
Steel Liner thickness (cm)	0.9525
Dome Spring Line above top of foundation mat (m)	37.2
Base of Foundation mats below finished ground grade (m)	20.1
Base Mat thickness (m)	3.05
Temperature Range (°C)	23.6 – 51.9
Air Partial Pressure Range (Pa)	62,100 – 71,000

Table 2-4. Containment Structures Parameters.

Parameters	Area (ft^2)	Thickness (inch)
Interior Concrete Wall 1	7740	6
Interior Concrete Wall 2	57435	12
Interior Concrete Wall 3	51,064	18
Interior Concrete Wall 4	10,691	24
Interior Concrete Wall 5	8,673	27
Interior Concrete Wall 6	3,353	36
Containment Wall Below Grade	20,108	54.375
Containment Wall Above Grade	24,576	54.375
Containment Dome	24,656	30.5
Containment Floor	11,757	146.65
Carbon Steel G2	66,345	0.439
Carbon Steel G5	7,000	2.9

Table 2-5. Fan Cooler Characteristics.

Parameters	Value
Number of Fan system	3
Total Volumetric Flow (cfm)	3 x 75,000

Table 2-6. Containment Spray Characteristics.

Parameters	Value
Number of Pumps	2
Rated mass flow at the spray nozzles at -4.0 psid (lbm/s)	376.6
Rated mass flow at the spray nozzles at 26.9 psid (lbm/s)	278.9
Spray Signal ON for pressure containment (psia)	>25
Spray Signal OFF for pressure containment (psia)	<12

Last, a Pressurizer Relief Tank (PRT) was added to the model and connected with the pressurizer PORV and SRV and with the containment. A trip valve simulates the PRT disk, which opens and discharges the primary coolant into the containment when the PRT pressure is greater than 100 psig. The main characteristics of the PRT are reported in Table 2-7.

Table 2-7. PRT Characteristics.

Parameters	Value
Total Volume (ft^3)	1,300
Water Volume (ft^3)	900
Disk failure pressure (psig)	100
Disk capacity (lbm/hour)	900,000

It should be remarked that the “prizer” component has not been validated for low pressure/containment conditions. Systematic validation at low pressure conditions, like the ones occurring in the IGPWR sub-atmospheric containment, has not been carried out since they are not within the scope of this project. However, the obtained results for a reference transient have been compared with the MELCOR analysis results in NUREG-1953 (NRC, 2010). Figure 2-4 shows an acceptable qualitative agreement between the two codes.

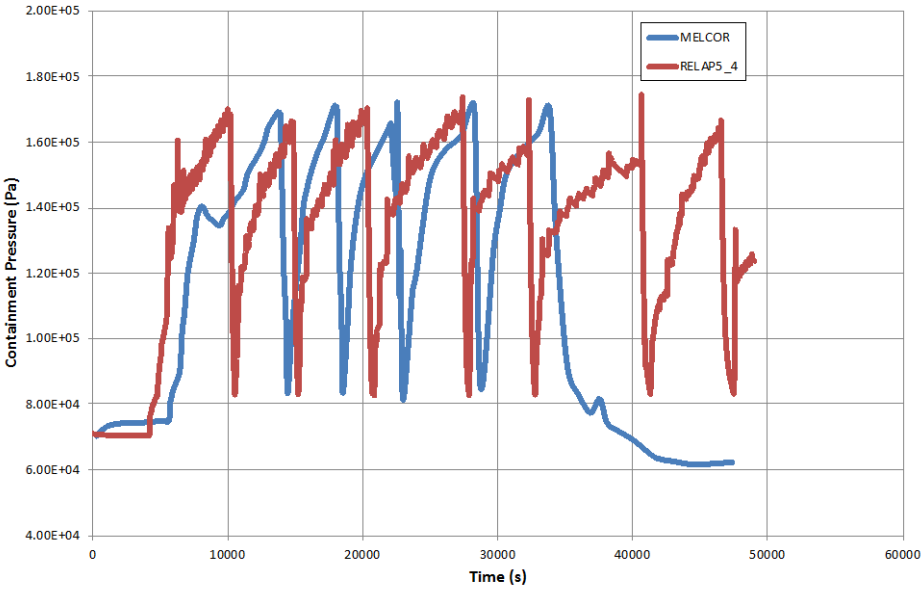

Figure 2-4. RELAP5-3D – MELCOR Containment Response Comparison.

2.1.3 LOFW RELAP5-3D Analysis

The LOFW scenarios described in Section 2.1.1 were simulated with the above revised IGPWR RELAP5-3D model. Other documents, such as the Surry Power Station FSAR (Dominion, 2007) and NUREG-1953 (NRC, 2010), were also referenced for details of the sequences.

The IE is the loss of, which was simulated by a reduction of the main feedwater flow to zero in 6.0 seconds after time t = 0.0 s. Reactor scram, which is defined as the release of the control rods, was assumed to occur 0.5 second later for those cases in which the reactor trip system was assumed to work (the 0.5 second is simulating the scram signal delays). The control rod insertion time was assumed to be equal to 1.8 seconds from the time of the reactor scram.

The main steam isolation valves (MSIVs) in the model were assumed to close 2.0 seconds after the reactor scram to simulate closure of the turbine stop valves. The SG PORVs were assumed to operate as necessary to control SG pressure. The decrease in heat removal by the SGs causes a rapid increase of pressure in the reactor coolant system that reaches the open setpoint of the pressurizer (PRZ) PORV. The PORV generally lifted a few seconds after the start of the event.

For the scenarios with available AFW (LOFW-3.0 to LOFW-4.3), only one MDAFP was assumed to be operating. The MDAFP was assumed to start 30 seconds after the reactor scram (i.e. at t = 30.5 seconds). The operators were assumed to control the SG levels to near the level of the feedwater ring (11 m). The MDAFP was terminated after the injected volume exceeded the minimum operating volume of the emergency condensate storage tank (CST), which is 96,000 gallons based on p. 10.2-29 of the Surry Power Station FSAR (Dominion, 2007). The safety injection actuation signal (SIAS) was initiated either on high containment pressure (pressure > 122 kPa [17.7 psia]) or low-low reactor pressure (12.34 MPa [1789.7 psia]) based on Page A-2 of (NRC, 2010).

The RCPs were assumed to trip when average void fraction in the vicinity of the pumps exceeded 0.1. This trip could be due to a pump failure in two-phase flow or to an operator action in response to pump vibrations.

For the LOFW-2.0 scenario in which safety injection (SI) was credited as part of the FAB procedure, one high-pressure safety injection (HPSI) pump was assumed to be available. The HPSI was terminated when the water source for the safety injection automatically switched from the reactor water storage tank (RWST) to the containment sump to simulate the failure of HPR. Containment spray and fan coolers were assumed to be available

because the containment spray uses a significant amount of RWST water and results in an earlier loss of HPSI flow.

The calculations were terminated when the maximum cladding temperature reached 2099 K for cases with Zircaloy and 1804 K for cases with FeCrAl and Cr-coated (or Chromite). The temperatures were assumed to represent significant core damage.

In the following sections, the results of these LOFW sequences calculations are provided:

- LOMFW with AFW unavailable, i.e., Loss of All Feedwater
  - LOFW-1.0, unmitigated loss of all feedwater
  - LOFW-2.0, mitigated loss of all feedwater with FAB but HPR fails
- LOMFW with AFW available and PORV LOCA/LOSC
  - LOFW-3.0, PORV LOCA
  - LOFW-4.0, loss of seal cooling with leakage rate of 182 gpm per pump
  - LOFW-4.1, loss of seal cooling with leakage rate of 182 gpm per pump, with no secondary side depressurization
  - LOFW-4.2, loss of seal cooling with leakage rate of 76 gpm per pump
  - LOFW-4.3, loss of seal cooling with leakage rate of 480 gpm per pump.

2.1.3.1 Unmitigated Loss of All Feedwater (LOFW-1.0)

This scenario assumes no AFW available. After LOFW at t = 0 second, the reactor was tripped, but AFW failed to start. The LOFW caused the closure of the MSIV, determining the isolation of the three SGs. The RCPs continued to run while power was removed from the system via the SG PORV.

The loss of all feedwater sequences was unmitigated with the failure of FAB. The only cooling mechanisms were the inventory of water stored in the SGs and the reactor coolant system (RCS) at the beginning of the transient. The calculated sequences of events are shown in Table 2-8.

On the secondary side, the water in the SG is boiled off and steam is discharged by the SG PORV into the atmosphere. On the primary side, after the total loss of inventory in the SGs (t = 55 mins), the pressure increased by the decay heat caused a loss of coolant from the PRZ PORV into the PRZ relief-tank (PRT), and after the rupture of the PRT vent disk, there was a discharge of the primary coolant into the containment. Therefore, the core quickly reached damage conditions.

Table 2-8. Sequence of Events for Scenario LOFW-1.0.

Event	Time (hr:min)		
	Zircaloy	FeCrAl	Chromite
Loss of MFW	00:00	00:00	00:00
SG PORVs open	00:01	00:01	00:01
SG dryout	00:55	00:55	00:55
PRZ PORVs open	00:55	00:55	00:55
PRT failure	01:11	01:11	01:11
RCPs tripped for high void	01:23	01:23	01:23
Core begins to uncover	01:42	01:42	01:42
0.5 kg H_2 generated	01:57	02:25	02:21
First cladding rupture	02:16	02:20	02:21
Calculation terminated	02:19	02:27	02:23

The calculations were terminated when the maximum temperature in the cladding reached a given value. The value was 2099 K for Zircaloy and 1804 K for FeCrAl and Chromite.

The differences between calculations due to the different claddings were negligible prior to the onset of core uncovery and were relatively small after the onset of core uncovery. The calculations were terminated when the hottest cladding in each reached its failure temperature. The termination times varied by less than 10 minutes (a delay of 8 minutes for FeCrAl and a delay of 4 minutes for Chromite). The calculated amount of hydrogen produced during the transients varied significantly between claddings. The amount of hydrogen produced was 1.0 kg for FeCrAl, 5.5 kg for Chromite, 51.1 kg for Zircaloy.

The following figures illustrate the effect of the cladding on various parameters. The differences between calculations are generally small prior to core uncovery as displayed in Table 2-8.

Figure 2-5 shows the collapsed liquid level in one of the three SGs (the other two SGs are behaving similarly) and Figure 2-6 shows the mass flow in one of the SG PORVs. Because of the LOMFW IE and the failure of the AFW, the SGs are dried out in about 1 hour.

The primary pressure started to increase at approximate 55 minutes (Figure 2-7) as the SGs dried out. The pressurizer PORV began cycling when the SG in the affected loop dried out (Figure 2-8).

The RCS temperature began to increase after all the SGs have dried out, which caused the level and pressure in the pressurizer to increase rapidly. After the pressurizer filled up with liquid, the first PORV was no longer able to relieve the pressure, and the pressure increased enough to open the second pressurizer PORV and the safety relief valves. The pressure fell after the pressurizer began to void. The pressurizer was depleted of liquid at 140 minutes (see Figure 2-9). The PRZ PORV steam was dumped into the PRT, leading to the PRT pressure increase, then to the PRT failure, and finally to the discharge of primary inventory in the containment (see Figure 2-10). Consequently, containment pressure increased (Figure 2-11).

The collapsed liquid level in the core and the maximum cladding temperature are shown in Figure 2-12 and Figure 2-13, respectively. The collapsed liquid level in the core began to decrease at 82 minutes, which is about the same time as the PRZ safety valves opened and the PRZ liquid level began to drop. The collapsed level began to decrease rapidly at about 102 minutes, when the top of the core began to uncover, and the maximum cladding temperature began to increase. The maximum cladding temperatures then began to diverge. The highest temperatures occurred with the Zircaloy cladding, but the difference in timing with the other claddings was relatively small.

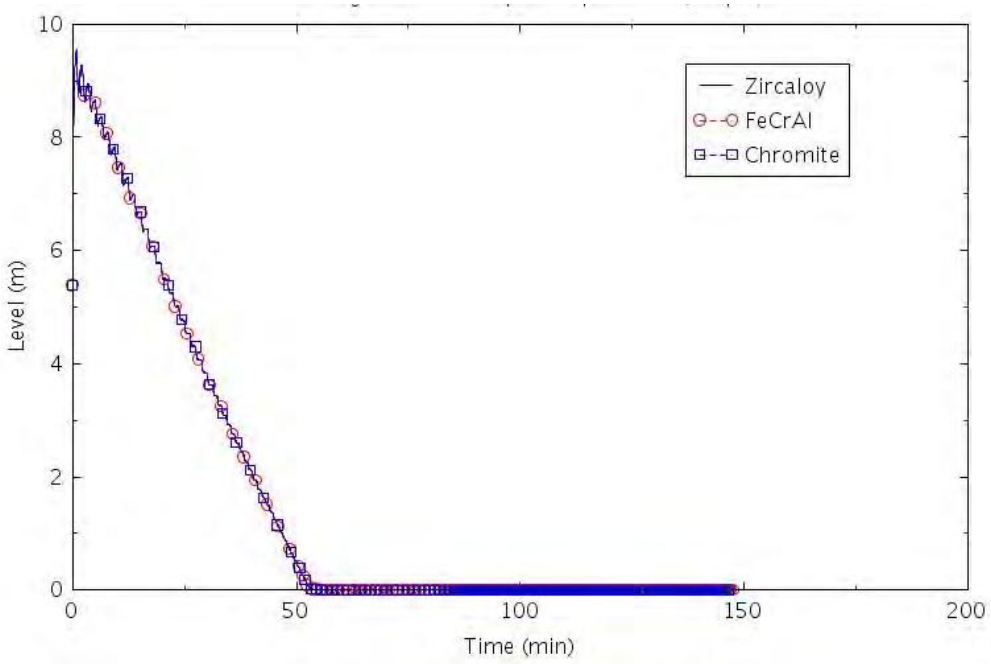

Figure 2-5. SG B Collapsed Liquid Level (LOFW-1.0).

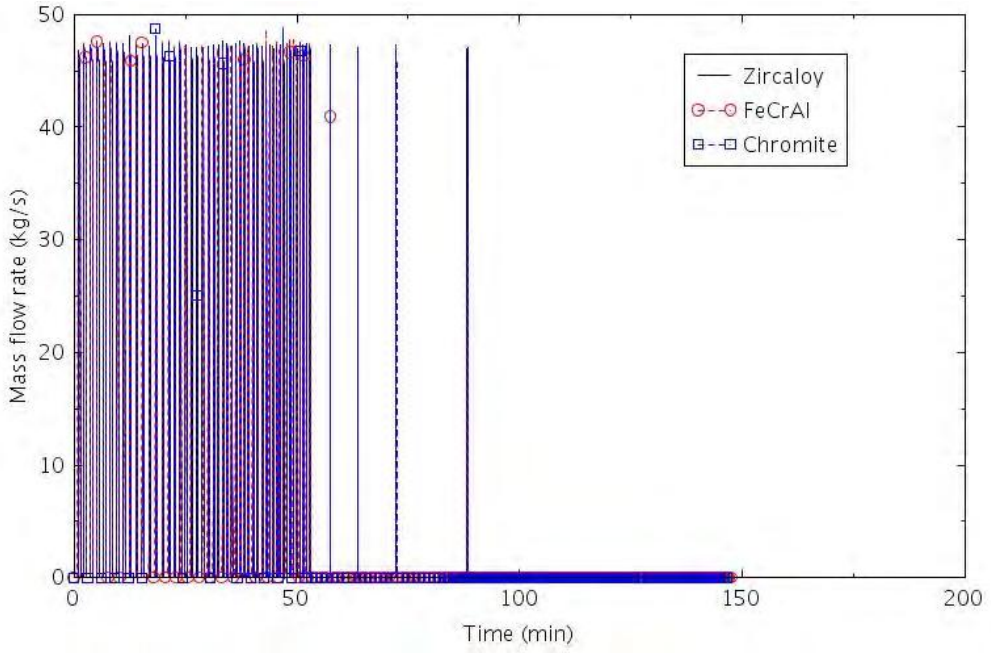

Figure 2-6. SG PORV Flow (LOFW-1.0).

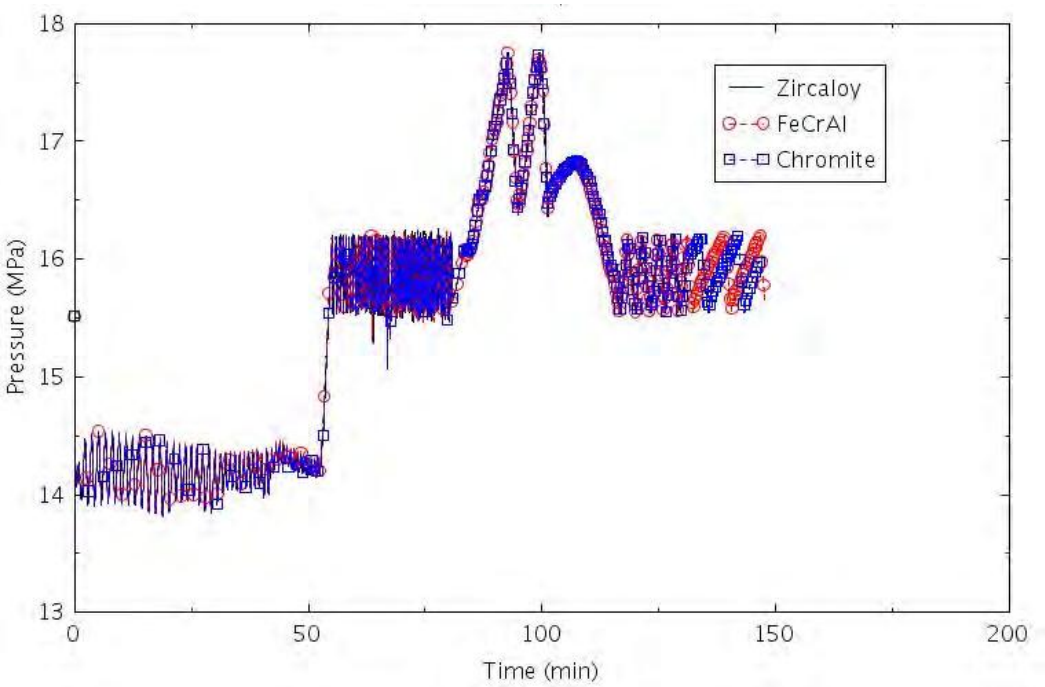

Figure 2-7. Pressurizer Pressure (LOFW-1.0).

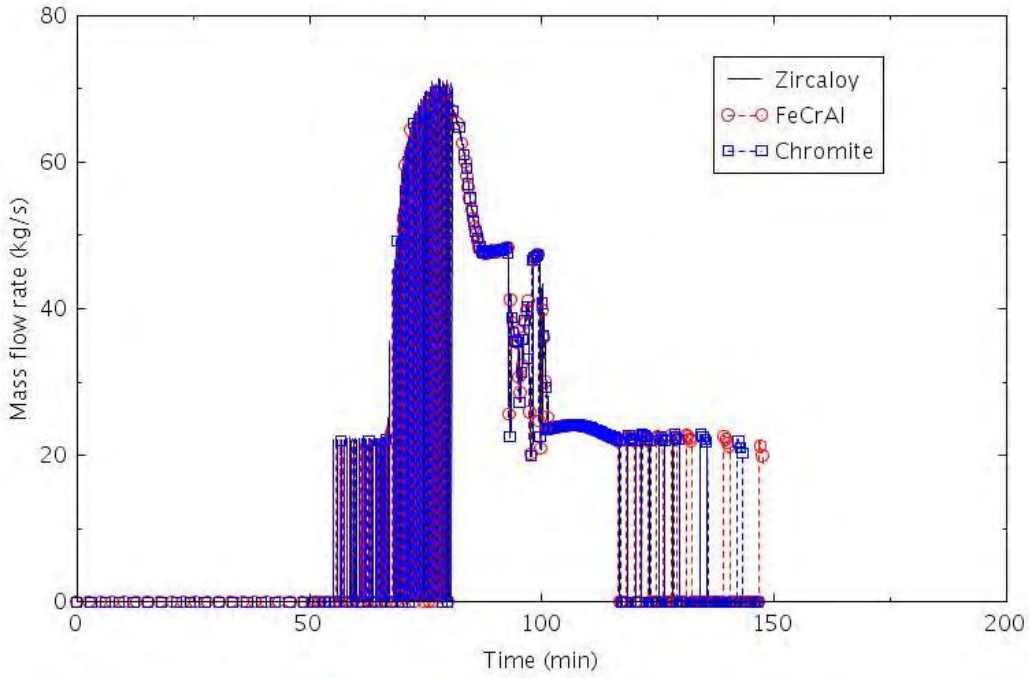

Figure 2-8. Pressurizer PORV Mass Flow (LOFW-1.0).

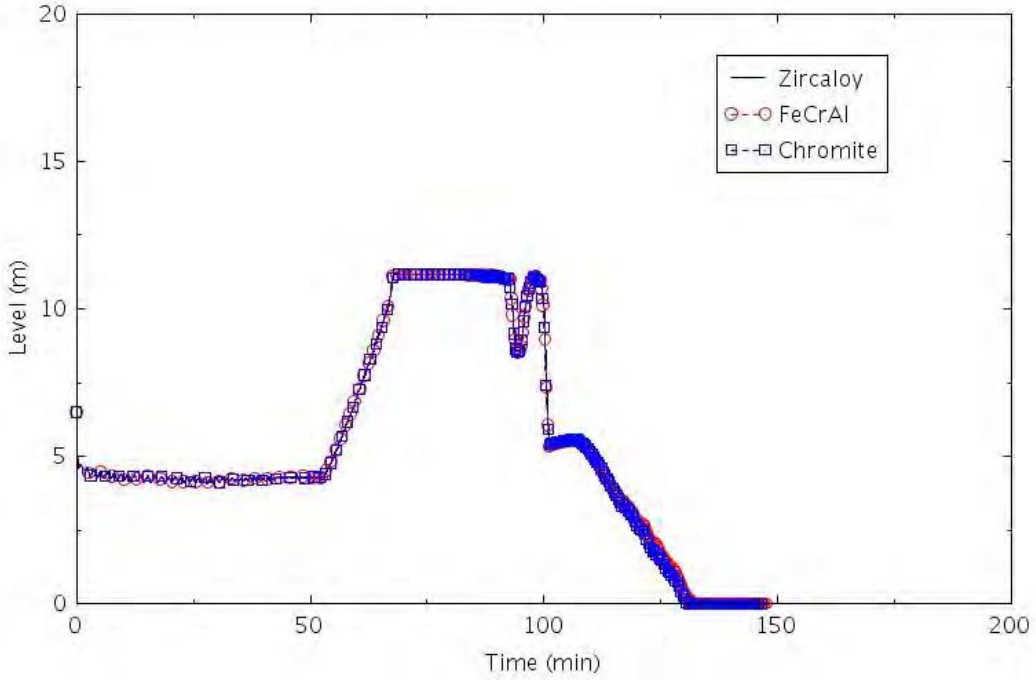

Figure 2-9. Pressurizer Collapsed Liquid Level (LOFW-1.0).

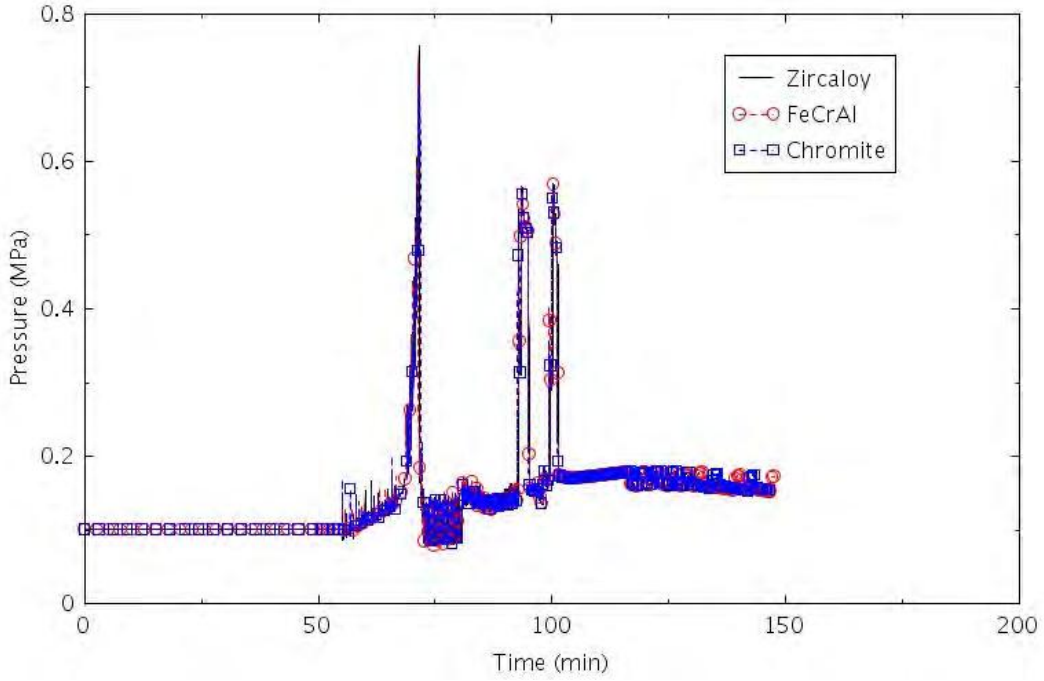

Figure 2-10. PRT Pressure (LOFW-1.0).

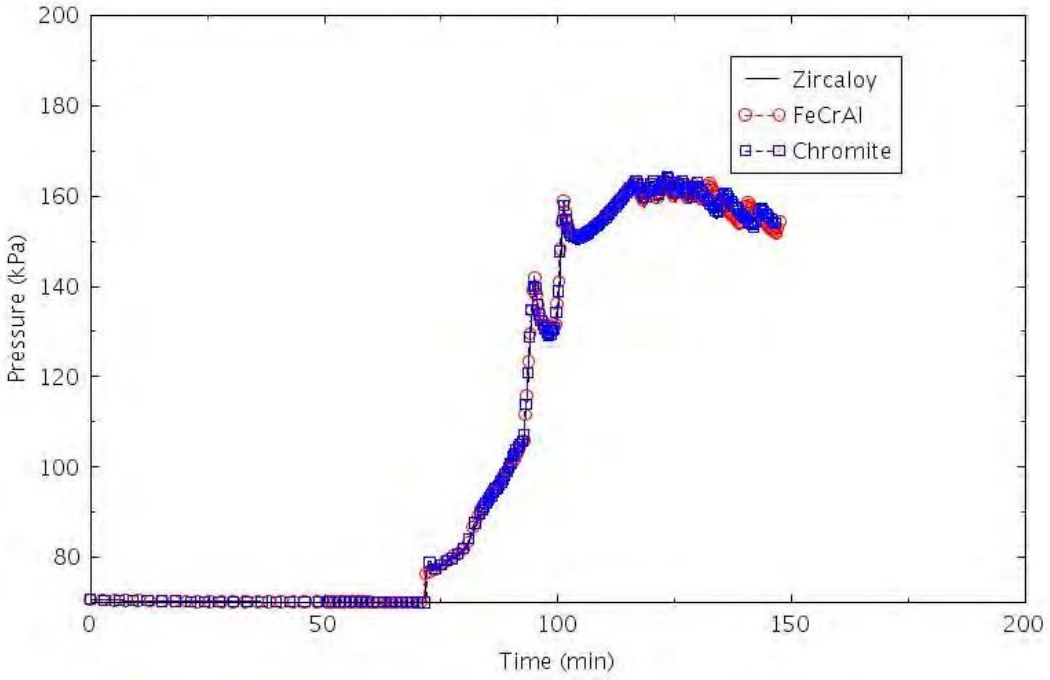

Figure 2-11. Containment Pressure (LOFW-1.0).

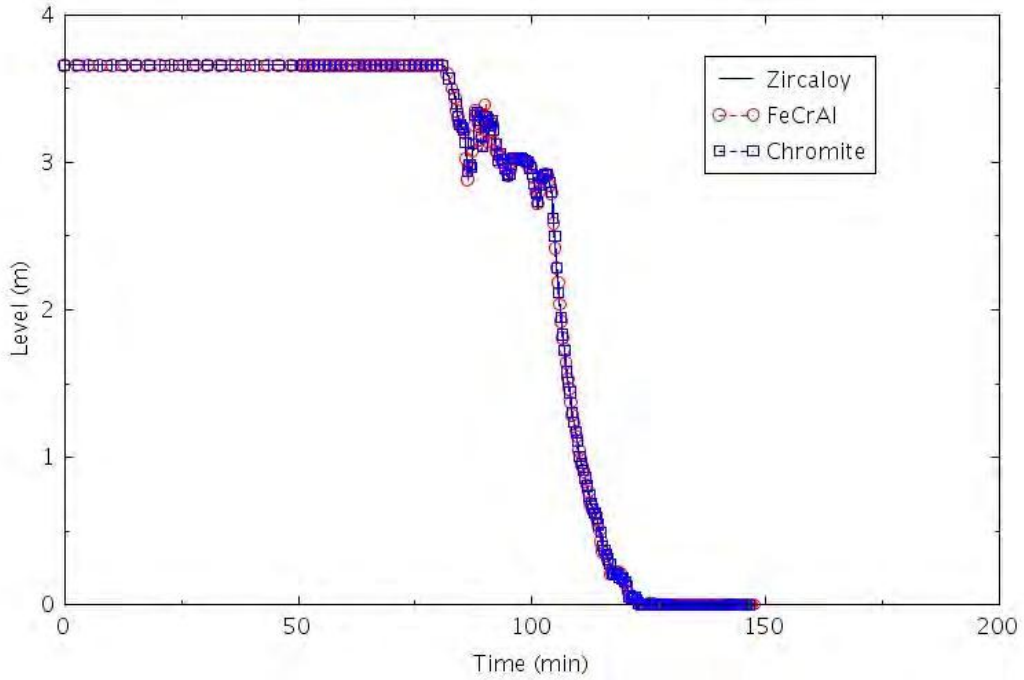

Figure 2-12. Collapsed Liquid Level in the Central Core Channel (LOFW-1.0).

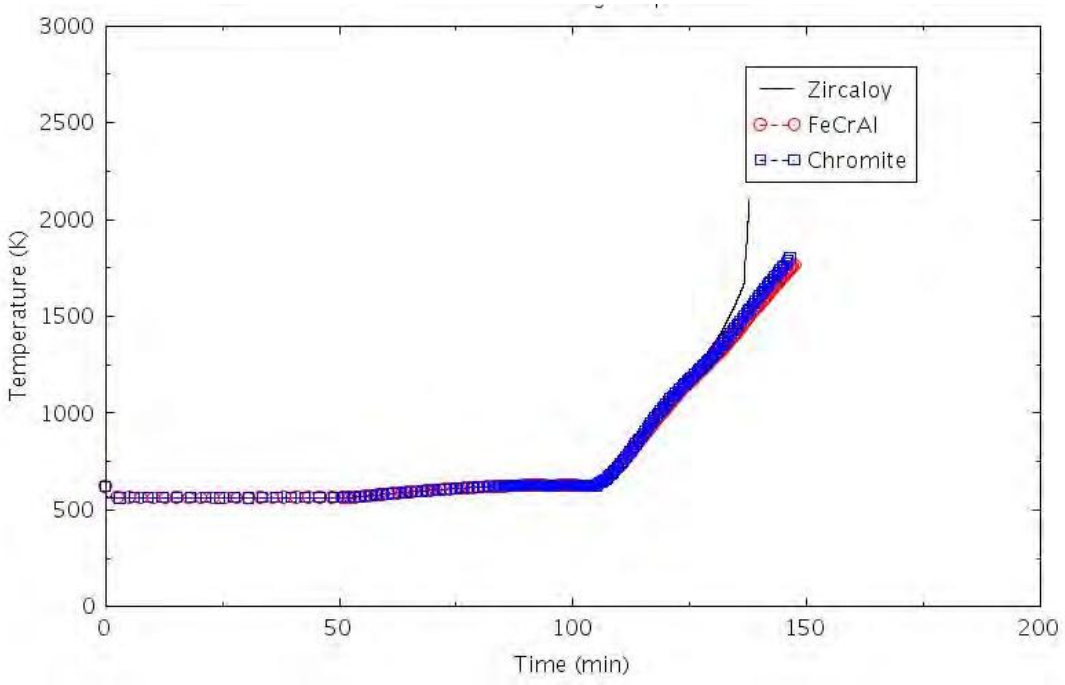

Figure 2-13. Maximum Cladding Temperature (LOFW-1.0).

2.1.3.2 Mitigated Loss of All Feedwater (LOFW-2.0)

This scenario, as in the previous one, assumes no AFW available. After the LOMFW IE occurred at t = 0 second, the reactor was tripped but AFW failed to start. The LOFW caused the closure of the MSIV, determining the isolation of the three SGs. The RCPs continued to run while power was removed from the system via the SG PORV.

This sequence was mitigated with the successful FAB procedure. On the secondary side, the water in the SG boiled off and steam was discharged by the SG PORV into the atmosphere. On the primary side, after the loss of inventory in the SGs (t = 55 mins), the pressure increased when the decay heat caused a loss of coolant from the PRZ PORV into the PRZ PRT. After the rupture of the PRT vent disk, there was a discharge of the primary coolant into the containment. The pressure peak in the containment (17.7 psia, or 0.122 MPa) generated the SI signal which actuated the high safety injection system. One HPI pump started to deliver water to the primary system, causing the opening of the PRZ PORV valve (FAB procedure).

The continuous discharge of primary inventory inside the containment, caused a further increase of the containment pressure. Containment fan coolers were activated when the containment pressure was greater than 0.114 MPa (16.6 psia). Containment sprays were instead actuated when the containment pressure reached the value of 0.172 MPa (25 psia) and turned off when the containment pressure was reduced to 0.083 MPa (12 psia).

The activation of containment sprays caused a significant consumption of the RWST water inventory. After about 11 hours, the RWST was emptied. The sequence then assumed that the high-pressure recirculation failed, therefore there were no other means for removing the decay heat from the reactor. Therefore, the core quickly reached damage conditions.

Table 2-9. Sequence of Events for Scenario LOFW-2.0.

Event	Time (hr:min)		
	Zircaloy	FeCrAl	Chromite
Loss of MFW	00:00	00:00	00:00
SG PORVs open	00:01	00:01	00:01
SG dryout	00:55	00:55	00:55
PRZ PORVs open	00:55	00:55	00:55
PRT failure	01:11	01:11	01:11
RCPs tripped for high void	01:23	01:23	01:23
FAB procedure starts, HPSI injection	01:34	01:34	01:34
Containment spray actuation	02:27	02:38	02:28
RWST empty, HPSI injection stops	10:58	11:21	11:09
Core begins to uncover	12:07	12:36	12:17
0.5 kg H_2 generated	12:41	13:58	13:42
First cladding rupture	13:17	13:52	13:42
Calculation terminated	13:21	14:10	13:42

The calculations were terminated when the maximum temperature in the cladding reached a given value. The value was 2099 K for Zircaloy and 1804 K for FeCrAl and Chromite.

The differences between calculations due to the different claddings were negligible prior to the onset of core uncovery and were mostly related to the differences in the containment pressure trends. But with the successful mitigation from the FAB operations during the HPI phase, core uncovery time was extended to about 12 hours after the event occurred, comparing with 1 hour 42 minutes if there was no FAB mitigation. With ATF designs, the times for the hottest cladding to reach the failure temperature, i.e., the termination time, were extended by 49 minutes for FeCrAl and 21 minutes for Chromite. The core uncovery times were extended by 29 minutes for FeCrAl and 10 minutes for Chromite.

The calculated amount of hydrogen produced during the transients varied significantly between claddings. The amount of hydrogen produced was 2.3 kg for FeCrAl, 4.0 kg for Chromite, 88.0 kg for Zircaloy.

The following figures illustrate the effect of the cladding on various parameters. The differences between calculations, except for the containment pressure trends, are generally small prior to core uncovery, as displayed in Table 2-9.

Figure 2-14 shows the collapsed level in one of the three SG (the other two SG are behaving similarly) and Figure 2-15 shows the mass flow in one of the SG PORVs. Because of the LOMFW IE and the failure of the AFW, the SGs are dried out in about 1 hour.

The primary pressure started to increase at approximate 55 minutes (Figure 2-16) as the SGs dried out. The pressurizer PORV began cycling when the SG in the affected loop dried out (Figure 2-17). The cycling is then continuing because of the FAB procedure actuation.

The RCS temperature began to increase after all the SGs have dried out, which caused the level and pressure in the pressurizer to increase rapidly. After the pressurizer filled up with liquid, the first PORV was no longer able to relieve the pressure, and the pressure increased enough to open the second pressurizer PORV and the safety relief valves. The pressure fell after the pressurizer began to void. The pressurizer liquid increased again at 140 minutes (see Figure 2-18) because of the FAB procedure. The FAB procedure was activated by the high pressure in the containment which was caused by the PRZ PORV steam released via the ruptured disk of the PRT (Figure 2-19). Containment pressure cycled between the spray set points actuations until the RWST inventory was depleted (Figure 2-20). RWST depletion terminated containment sprays and HPI as well (Figure 2-21 and Figure 2-22).

The collapsed liquid level in the core and the maximum cladding temperature are shown in Figure 2-23 and Figure 2-24, respectively. The collapsed liquid level in the core began to decrease at 82 minutes, reaching the minimum at 102 minutes, when the actuation of the FAB procedure brought the core level back to the normal level. The collapsed level began to decrease again at about 12 hours, when the top of the core began to uncover, and the maximum cladding temperature began to increase. The maximum cladding temperatures then began to diverge. The highest temperatures occurred with the Zircaloy cladding, but the difference in timing with the other claddings is small (from about 20 minutes for Chromite to 50 minutes for FeCrAl), considering a 14-hours transient.

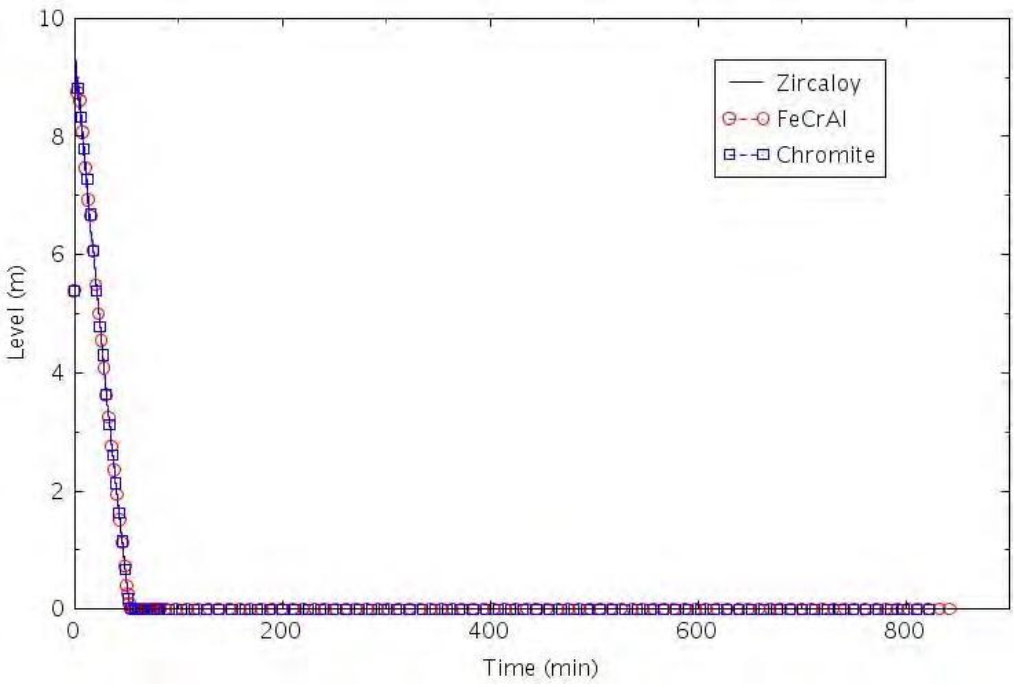

Figure 2-14. SG B Collapsed Liquid Level (LOFW-2.0).

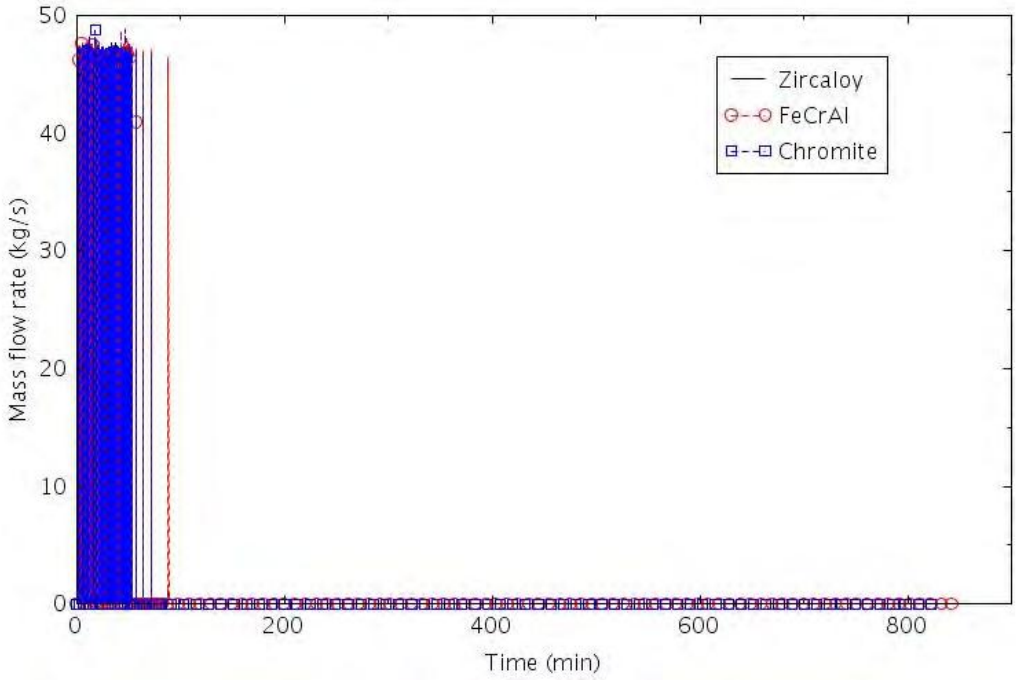

Figure 2-15. SG PORV Flow (LOFW-2.0).

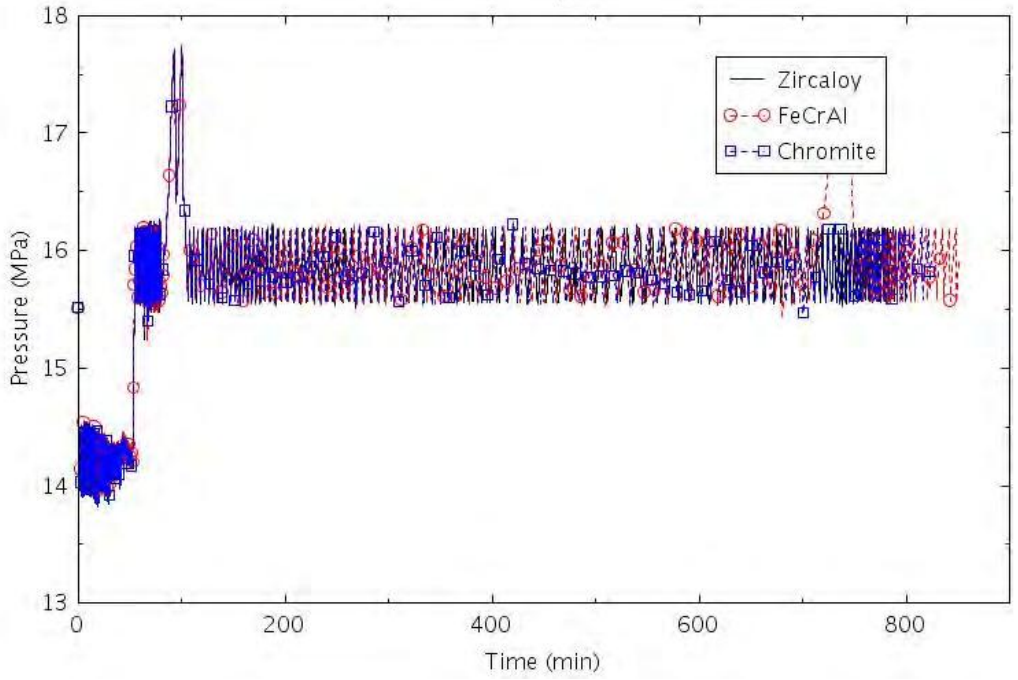

Figure 2-16. Pressurizer Pressure (LOFW-2.0).

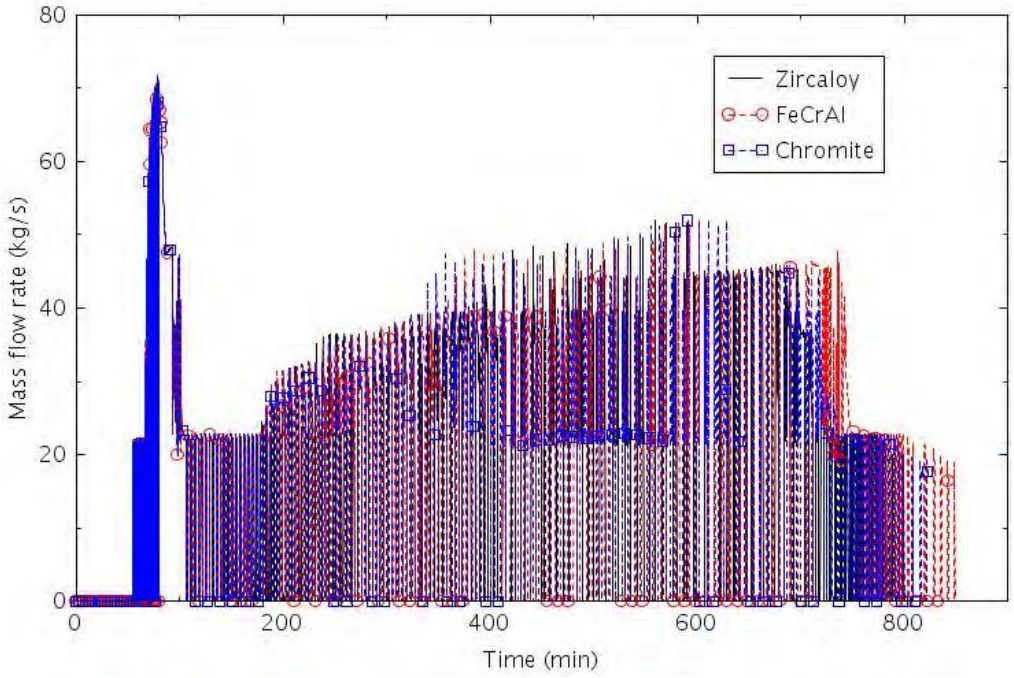

Figure 2-17. Pressurizer PORV Mass Flow (LOFW-2.0).

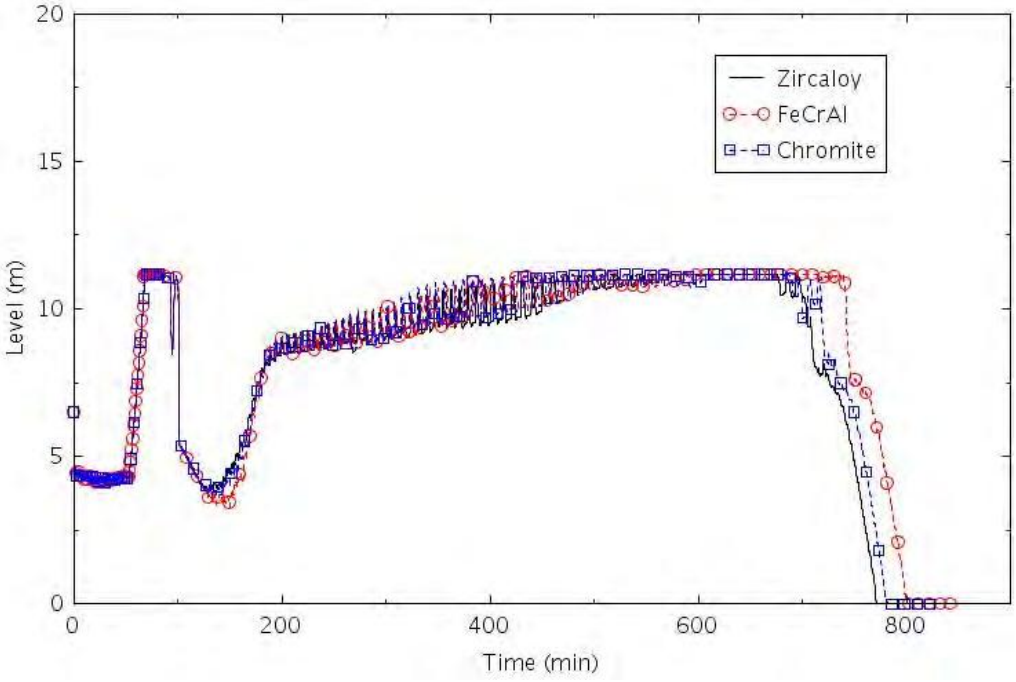

Figure 2-18. Pressurizer Collapsed Liquid Level (LOFW-2.0).

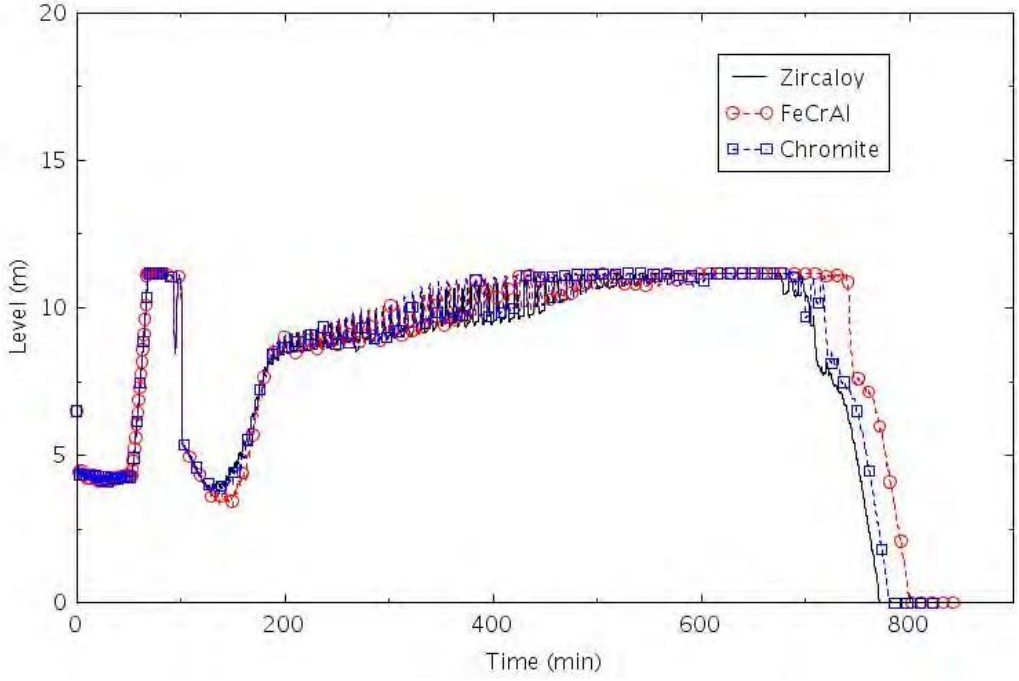

Figure 2-19. PRT Pressure (LOFW-2.0).

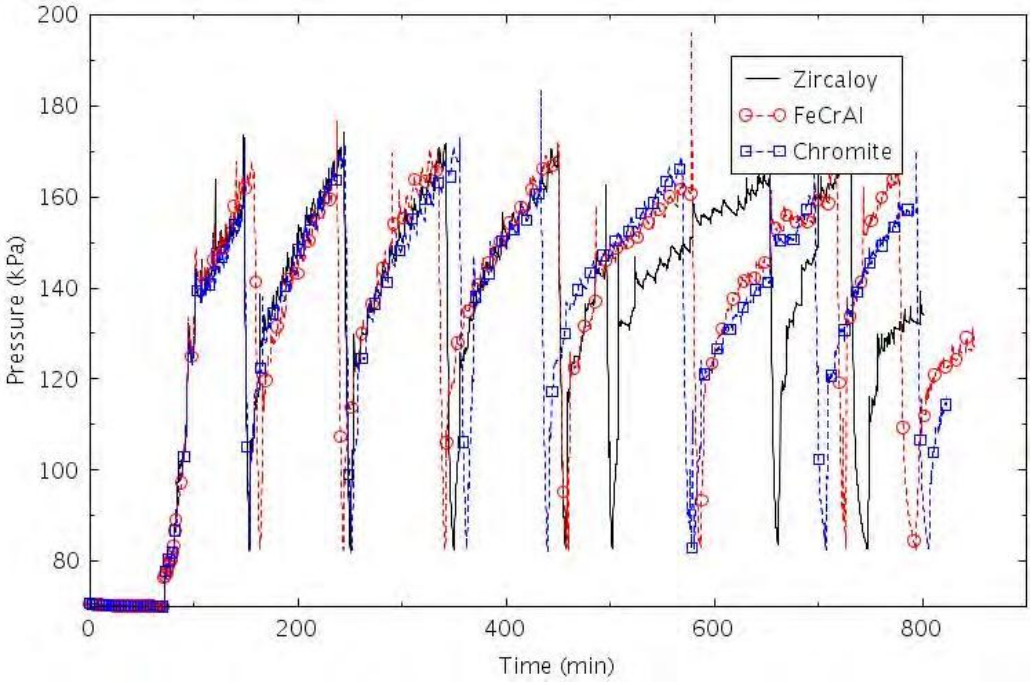

Figure 2-20. Containment Pressure (LOFW-2.0).

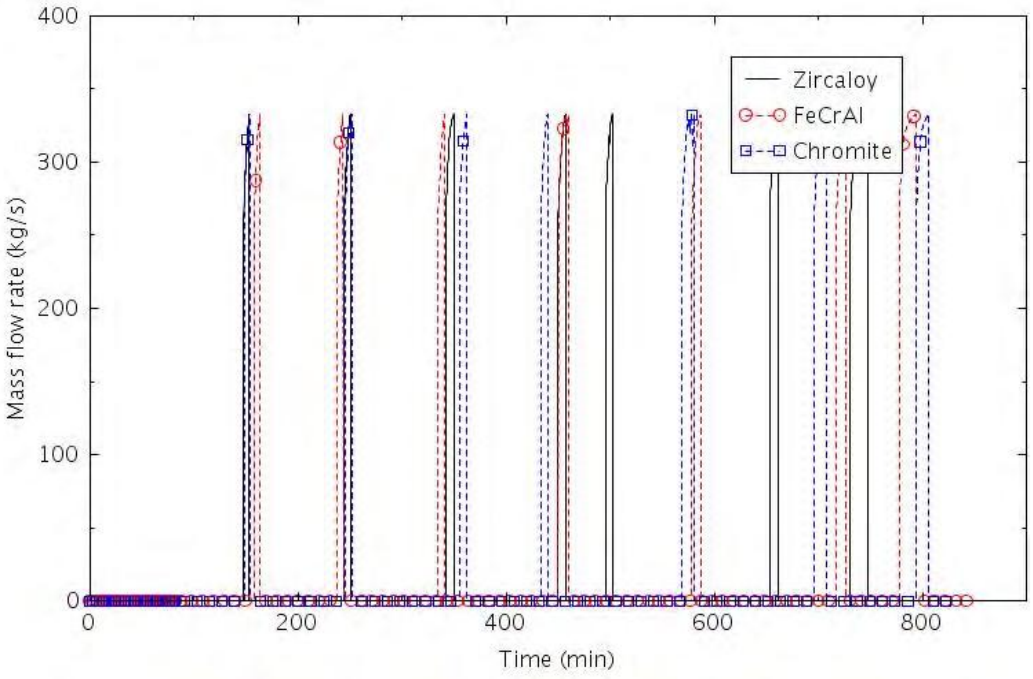

Figure 2-21. Containment Sprays Actuation (LOFW-2.0).

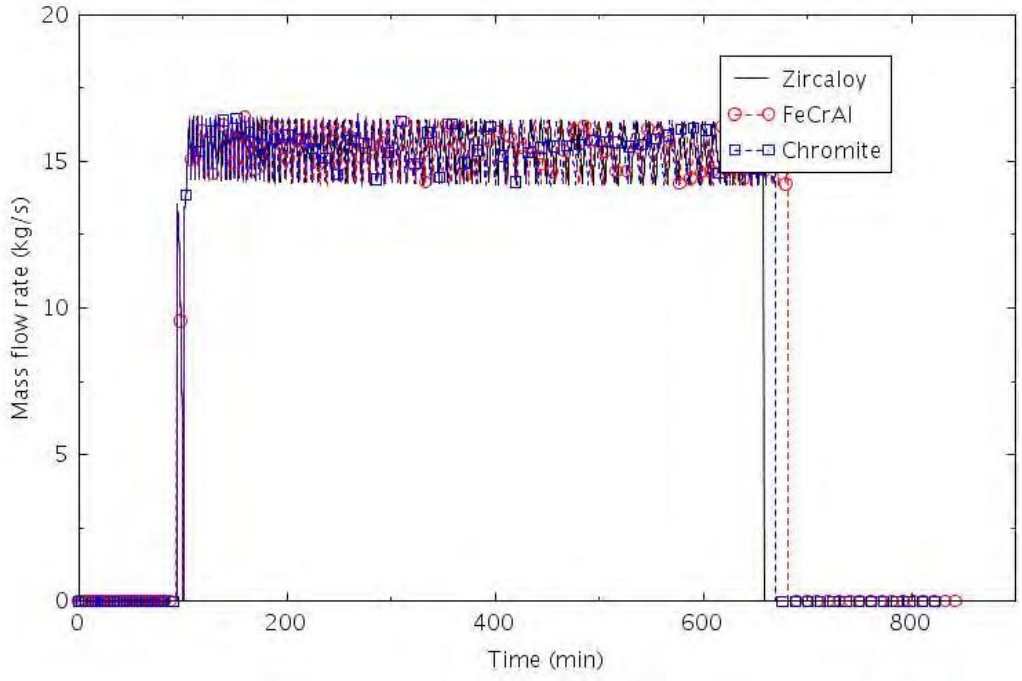

Figure 2-22. High Pressure Injection Actuation (LOFW-2.0).

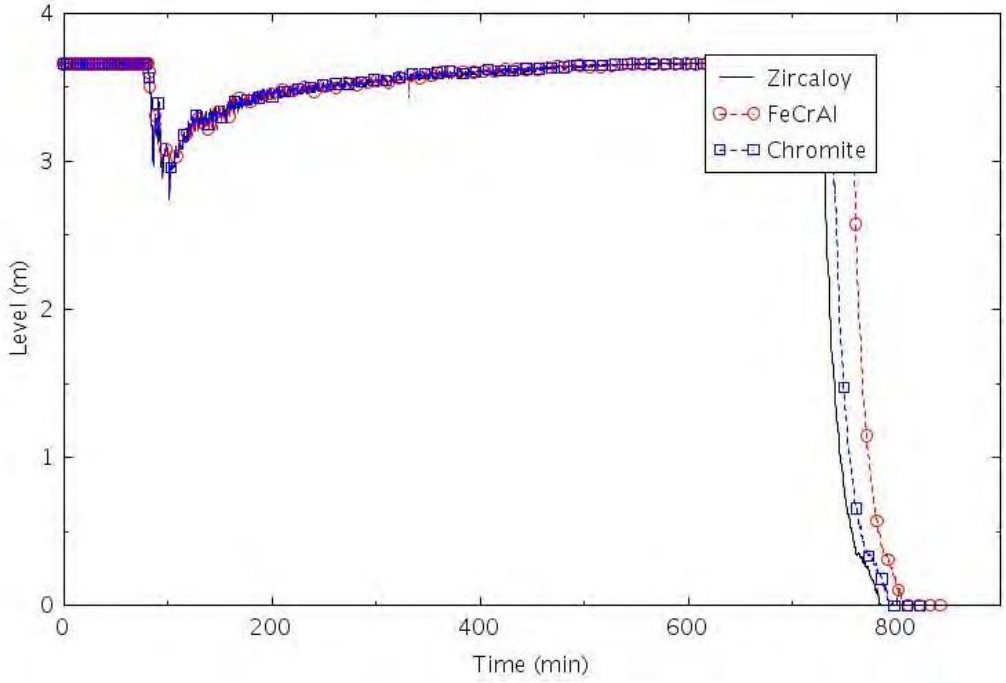

Figure 2-23. Collapsed Liquid Level in the Central Core Channel (LOFW-2.0).

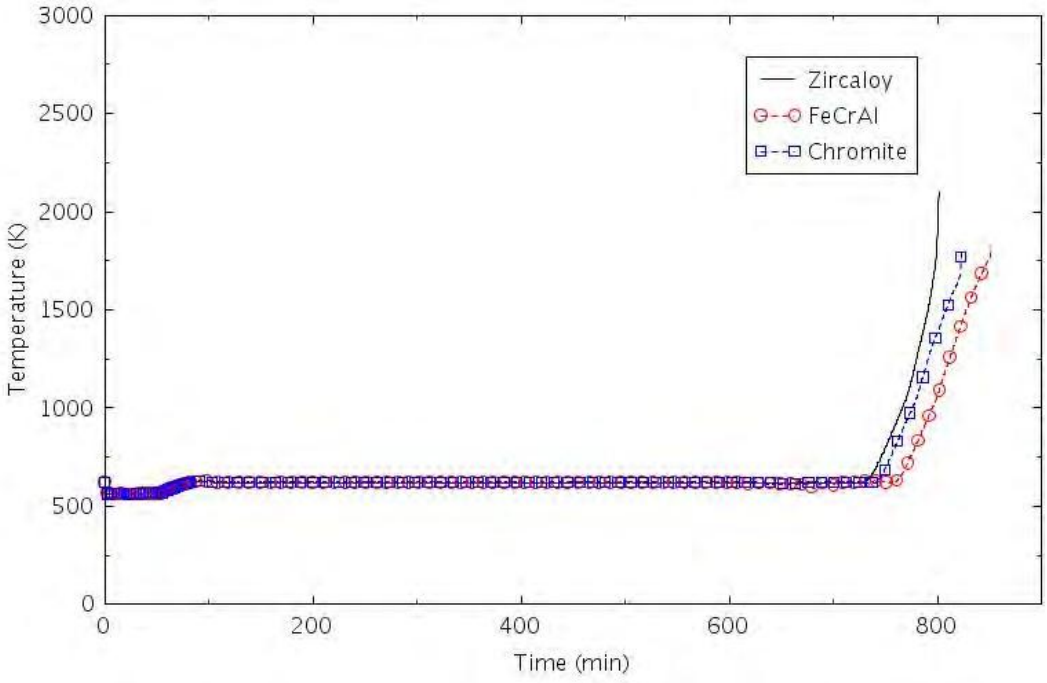

Figure 2-24. Maximum Cladding Temperature (LOFW-2.0).

2.1.3.3 LOMFW with PORV LOCA (LOFW-3.0)

This scenario assumes the availability of one AFW pump (MDAFP) after the LOMFW event occurred. The scenario also assumes that one pressurizer PORV could not re-close after opening. No actuation of HPI is credited.

After LOFW at t = 0 second, the reactor was tripped and the AFW started in 30 seconds. The LOFW caused the closure of the MSIV, determining the isolation of the three SGs. The RCPs continued to run while power was removed from the system via the SG PORV and the AFW. On the primary side, a PRZ PORV was actuated at t = 3 minutes and it stayed stuck open. The RCPs eventually stopped for high void in the primary system.

The continued loss of mass from the primary side and the unavailability of the HPI caused an increase of pressure in the PRT, which eventually failed, leading to primary coolant discharge to the containment. Pressure in the containment increased slowly while the primary pressure dropped to about 8.2 MPa. The core uncovery led to a quick core damage condition for all the three different types of clads.

Table 2-10. Sequence of Events for Scenario LOFW-3.0.

Event	Time (hr:min)		
	Zircaloy	FeCrAl	Chromite
Loss of MFW	00:00	00:00	00:00
MD-AFW start	00:01	00:01	00:01
PRZ PORV stuck open	00:03	00:03	00:03
PRT failure	00:09	00:09	00:09
RCPs tripped for high void	00:12	00:12	00:12
Core begins to uncover	01:28	01:28	01:28
0.5 kg H_2 generated	01:56	02:16	02:02
First cladding rupture	01:59	02:02	01:59
Calculation terminated	02:10	02:16	02:14

The calculations were terminated when the maximum cladding temperature reached 2099 K for Zircaloy and 1804 K for FeCrAl and Chromite.

The differences between calculations due to the different claddings were negligible prior to the onset of core uncovery and were relatively small after the onset of core uncovery. The calculations were terminated when the hottest cladding in each reached its failure temperature. The termination times varied by less than 10 minutes (a delay of 6 minutes for FeCrAl and a delay of 4 minutes for Chromite).

The calculated amount of hydrogen produced during the transients varied significantly between claddings. The amount of hydrogen produced was 1.9 kg for FeCrAl, 7.3 kg for Chromite, 28.5 kg for Zircaloy.

The following figures illustrate the effect of the cladding on various parameters. The differences between calculations are generally small prior to core uncovery, as displayed in Table 2-10.

Figure 2-25 shows the primary pressure increase as a consequence of the LOFW. The actuation of the PRZ PORV at t = 3 minutes (Figure 2-26), and because the valve stays stuck open, a small break LOCA is generated. The PORV LOCA dropped the primary pressure and caused an increase of voids in the primary circuit that led to the RCPs trip at t = 12 minutes (Figure 2-27).

With the PORV LOCA, the pressure in the PRT increased (Figure 2-28), leading to the PRT failure at t = 9 min. Consequently, the containment pressure started to increase (Figure 2-29).

The SGs level slowly increased to about 12 meters (Figure 2-30) because of the reduced energy transfer to the SG, as it can be seen by the fewer actuations of SG PORV (Figure 2-31).

Significant core uncovery started at t = 88 minutes (Figure 2-32). The core and the maximum cladding temperature are shown in Figure 2-33. The maximum cladding temperatures began to diverge immediately after the core uncovery. The highest temperatures occurred with the Zircaloy cladding, but the difference in timing with the other claddings is relatively small.

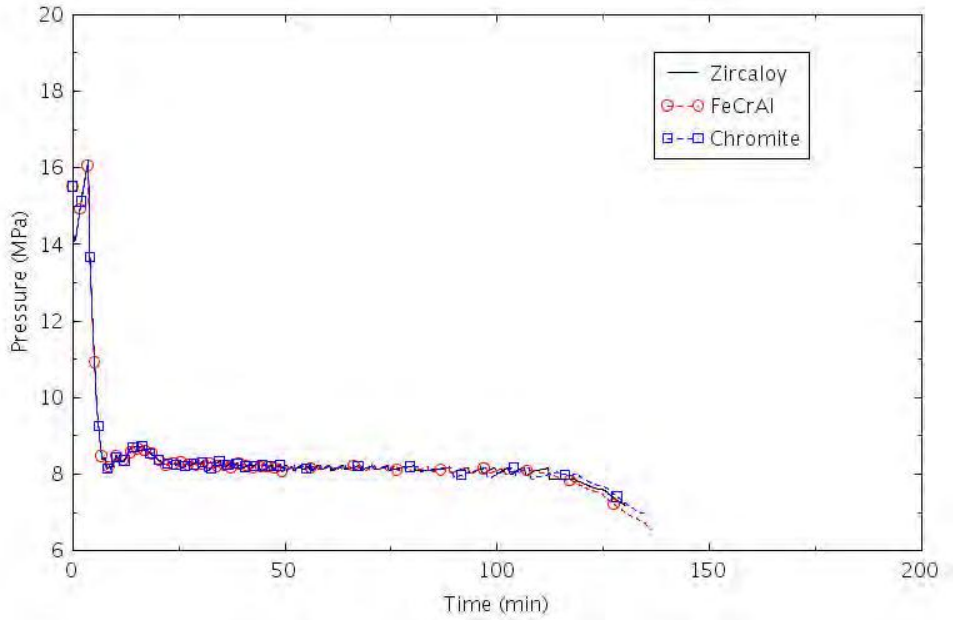

Figure 2-25. Primary Pressure (LOFW-3.0).

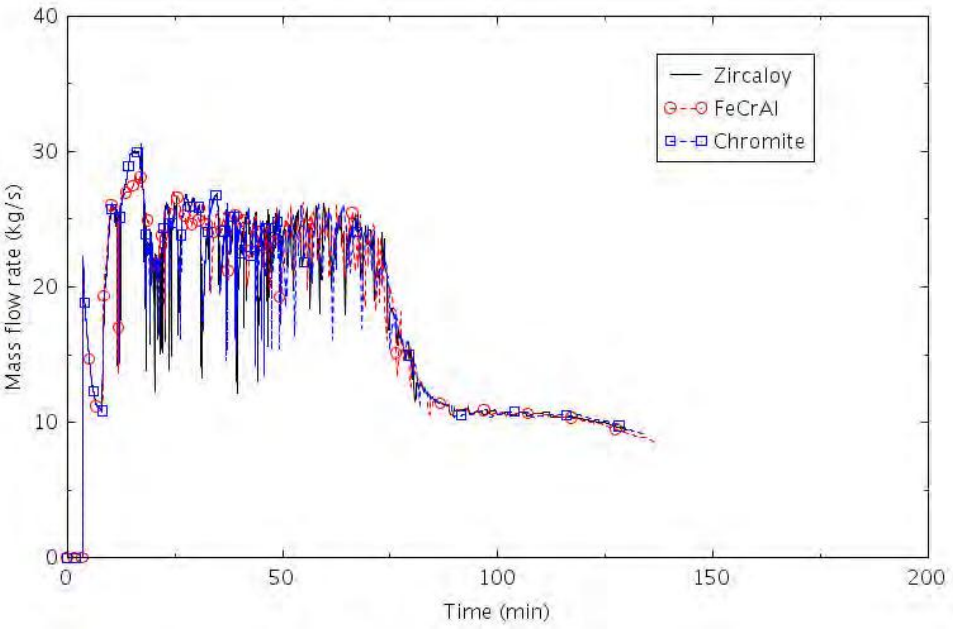

Figure 2-26. Pressurizer PORV Mass Flow (LOFW-3.0).

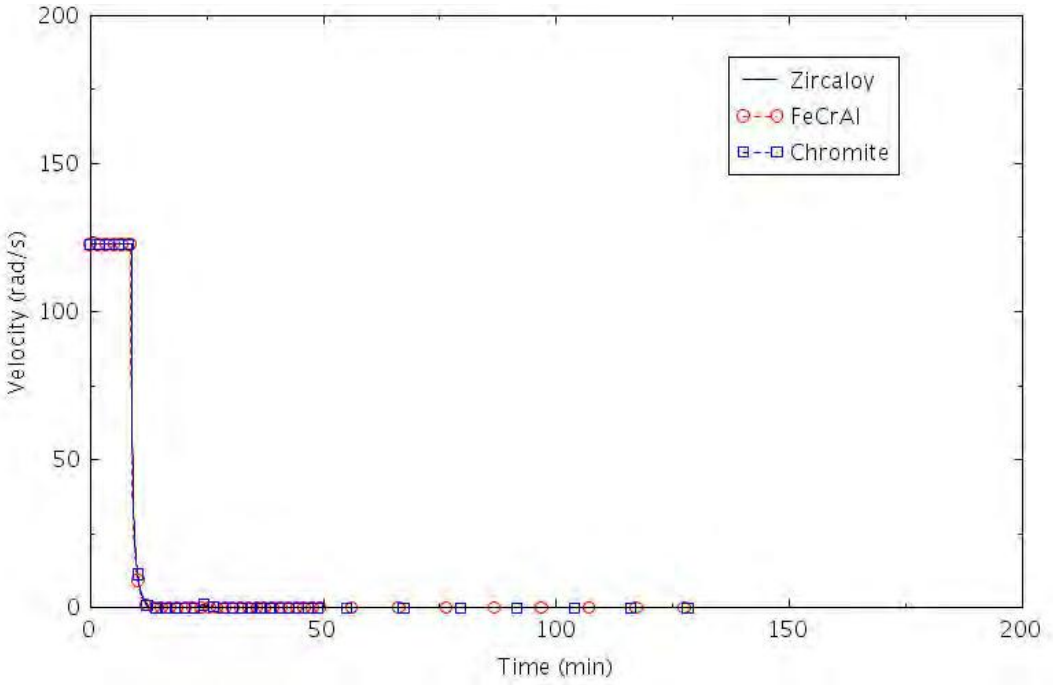

Figure 2-27. RCP B Velocity (LOFW-3.0).

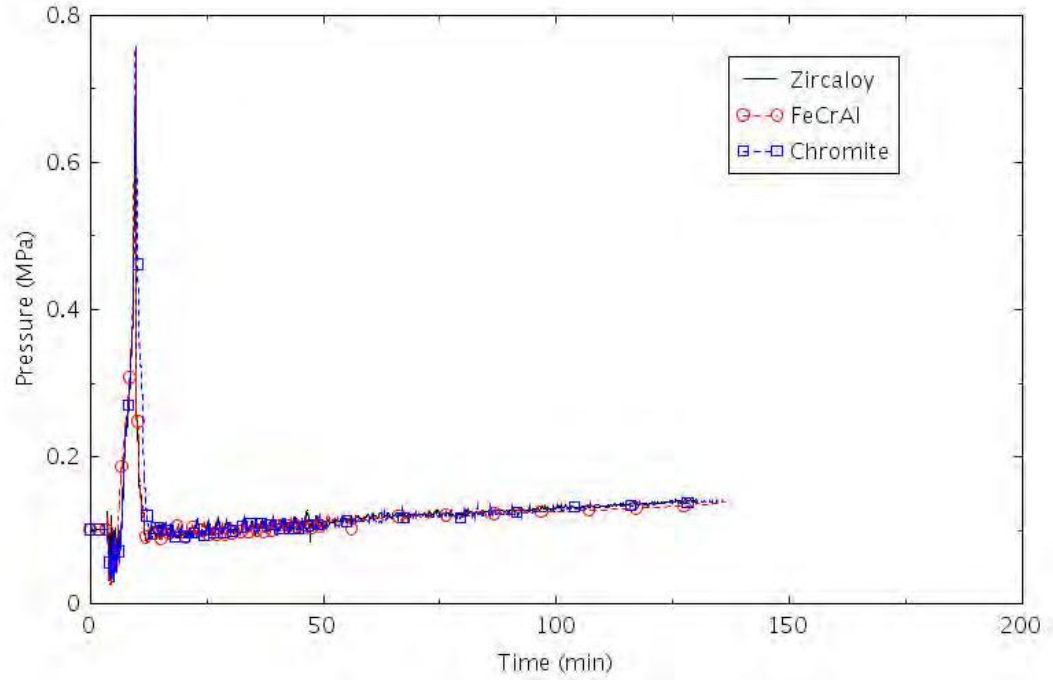

Figure 2-28. PRT Pressure (LOFW-3.0).

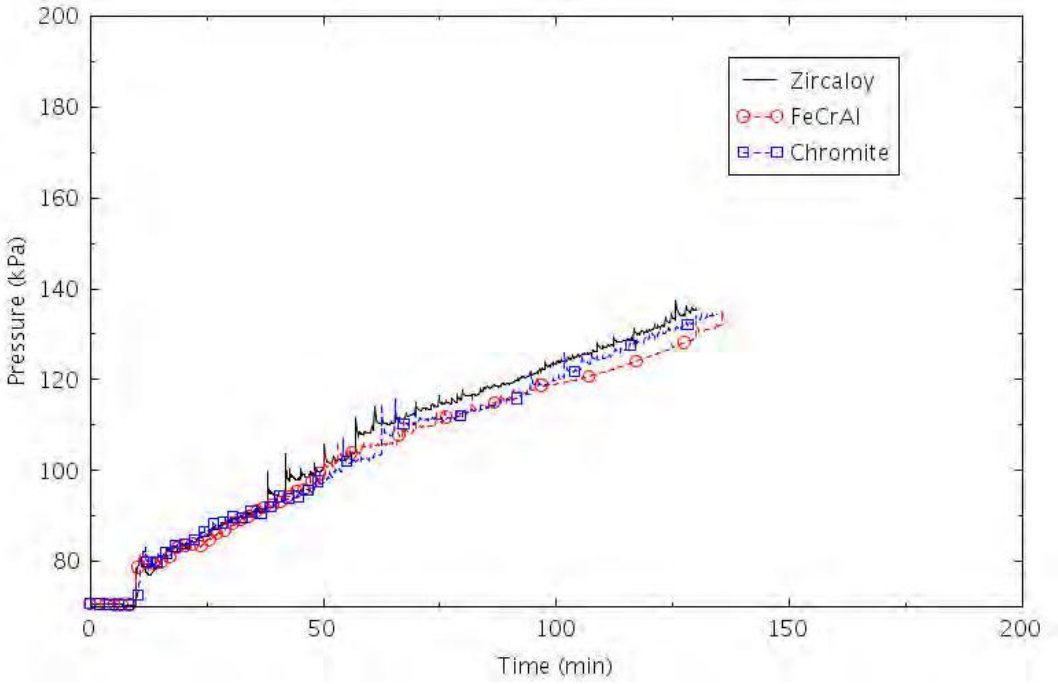

Figure 2-29. Containment Pressure (LOFW-3.0).

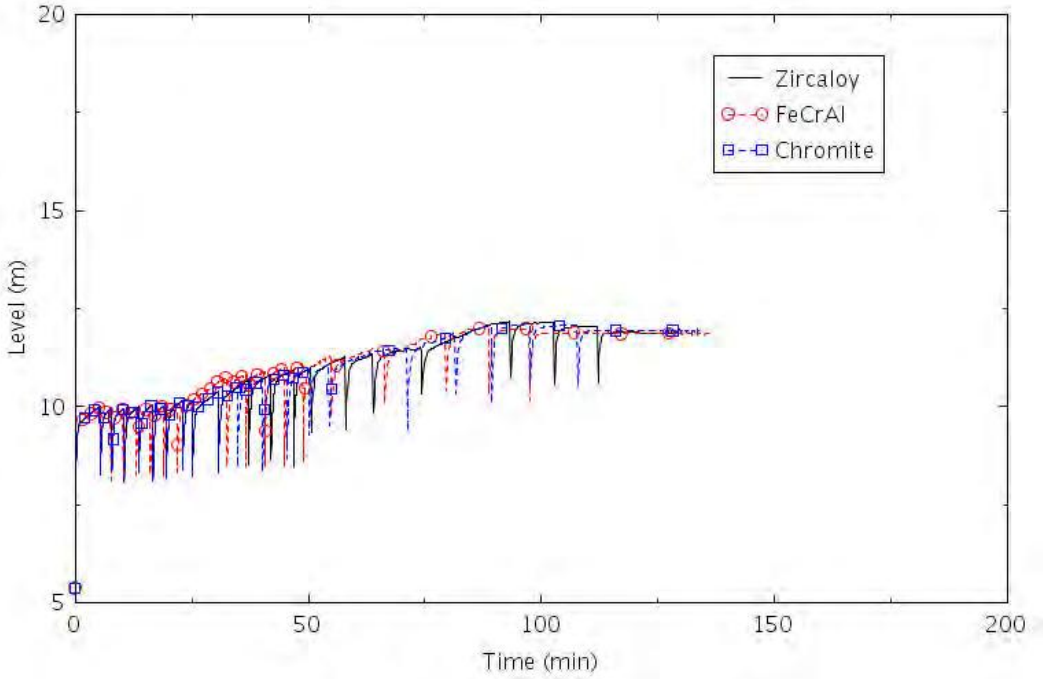

Figure 2-30. SG Level (LOFW-3.0).

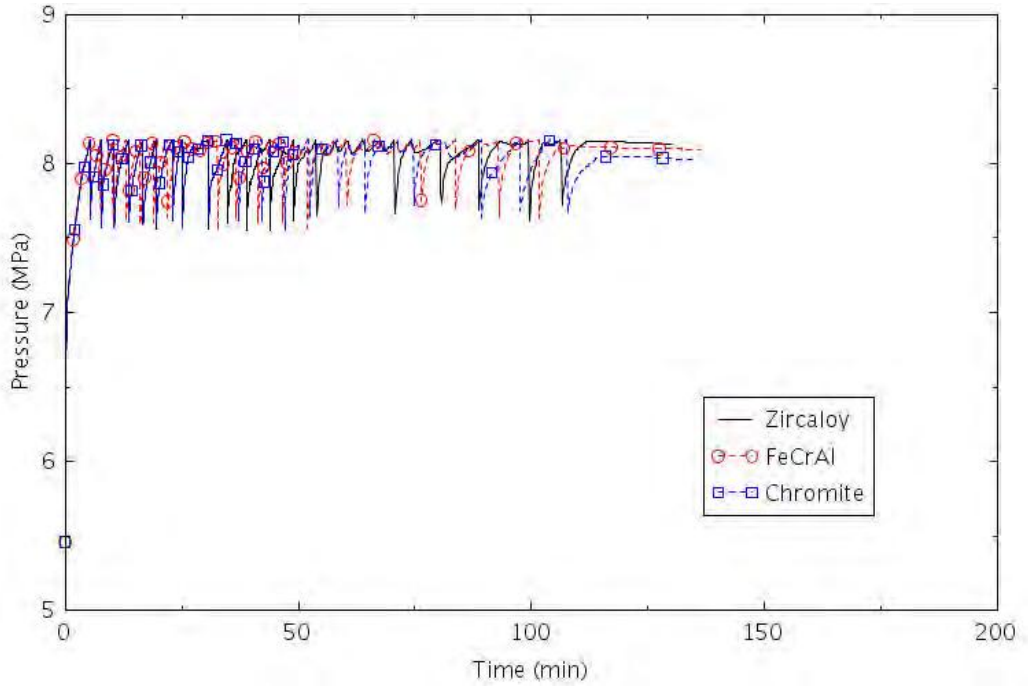

Figure 2-31. SG Pressure (LOFW-3.0).

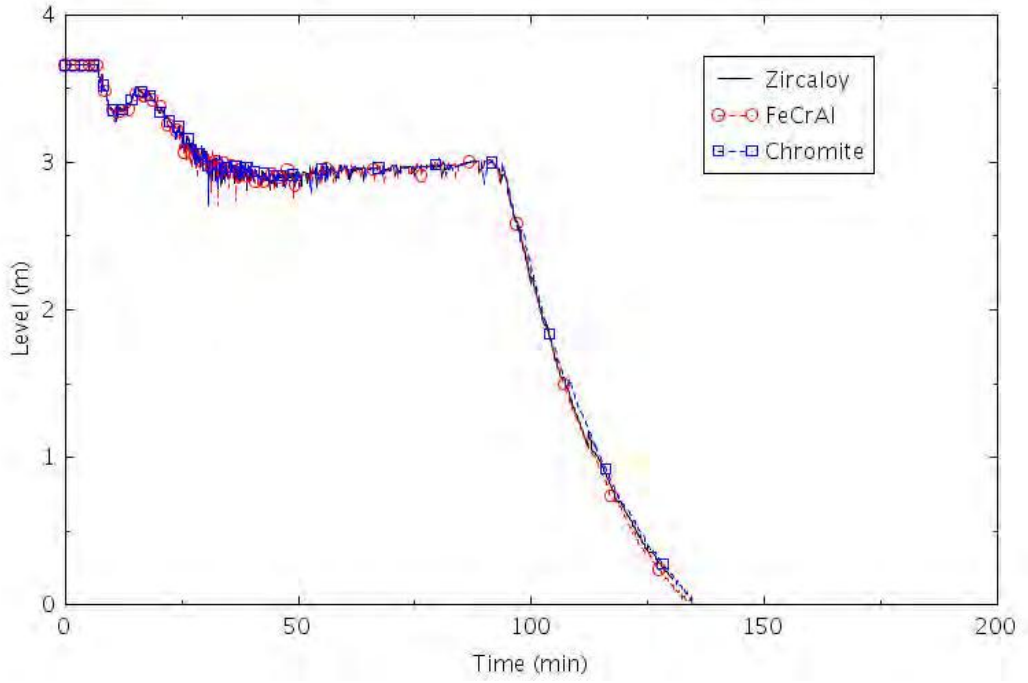

Figure 2-32. Collapsed Liquid Level in the Central Core Channel (LOFW-3.0).

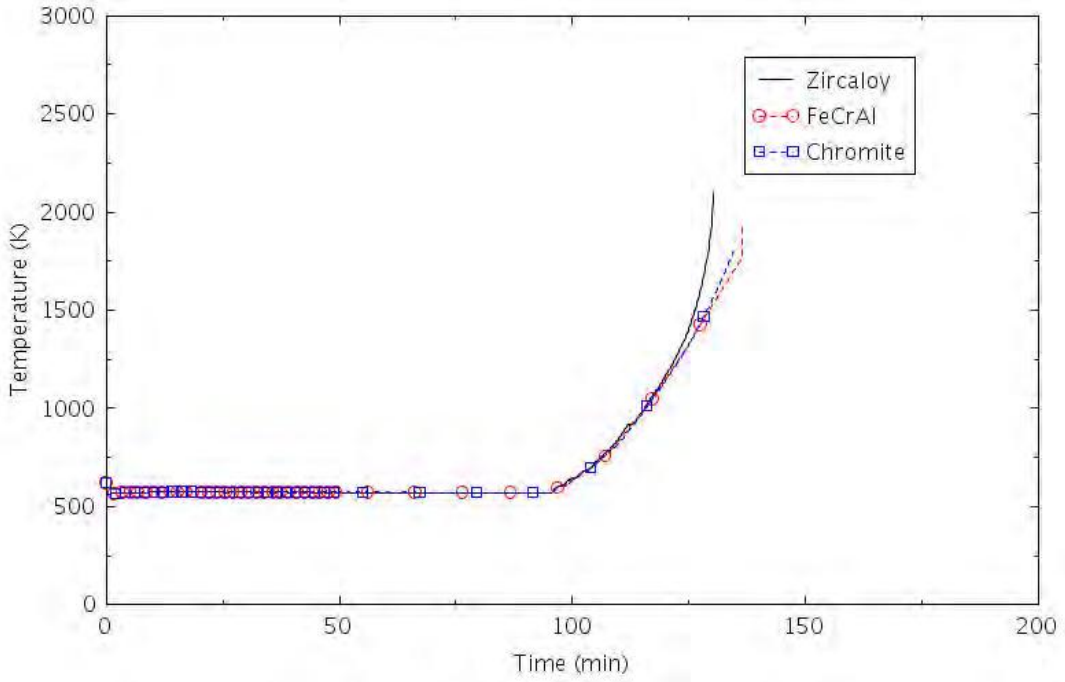

Figure 2-33. Maximum Cladding Temperature (LOFW-3.0).

2.1.3.4 LOMFW with LOSC-182 (LOFW-4.0)

This scenario assumes the availability of one MDAFP after the LOMFW event occurred. The scenario also assumes a SBLOCA due to the loss of RCP seals and a seal leakage rate of 182 gpm per pump.

After LOFW at t = 0 second, the reactor was tripped and the AFW started in 30 seconds. The LOFW caused the closure of the MSIV, determining the isolation of the three SGs. The RCPs continued to run while power was removed from the system via the SG PORV and the AFW. On the primary side, the RCP seals started to leak with a nominal leakage rate of 21 gpm, increasing to a larger leakage rate of 182 gpm at t = 13 minutes. The RCPs eventually stopped for high void in the primary system.

The continued loss of mass from the primary side and the unavailability of the safety injections prompted the operator to decide to depressurize the secondary side for reducing pressure, temperature, and leakages on the primary side. The rate of SG depressurization was about 55°C/hour(100°F/hour). Only passive injection by the accumulators was assumed (i.e., it was assumed a failure of both HPI and LPI). The injection from the accumulators allowed a temporary recovery of the liquid level in the core and a core cooling. SG levels were kept by the AFW control system, until the CST emptied at about 4h 30 min. Energy was removed from the core through loss of primary inventory via the RCP seals and through cooling with the SGs. After the MDAFP stopped, pressure in the primary side increased again. The water in the SG secondary side was boiled off and the continuous loss of primary inventory led to core damage.

The calculations were terminated when the maximum cladding temperature reached 2099 K for cases with Zircaloy and 1804 K for cases with FeCrAl and Chromite.

The differences between calculations due to the different claddings were negligible prior to the onset of core uncovery and were relatively small after the onset of core uncovery. The calculations were terminated when the hottest cladding in each reached its failure temperature. The termination times varied by about 20 minutes (a delay of 27 minutes for FeCrAl and a delay of 16 minutes for Chromite). The calculated amount of hydrogen produced during the transients varied significantly between claddings. The amount of hydrogen produced was 2.5 kg for FeCrAl, 15.6 kg for Chromite, and 55.6 kg for Zircaloy.

Table 2-11. Sequence of Events for Scenario LOFW-4.0.

Event	Time (hr:min)		
	Zircaloy	FeCrAl	Chromite
Loss of MFW	00:00	00:00	00:00
MDAFP start	00:01	00:01	00:01
RCPs seals leak at 182 gpm	00:13	00:13	00:13
RCPs tripped for high void	01:06	01:06	01:06
Operator initiate controlled cooldown of secondary side at ~100 °F/hour	01:30	01:30	01:30
Accumulator Injection	02:22	02:22	02:22
CST empty, AFP stop	04:32	04:32	04:32
SG dryout	12:24	12:24	12:24
Core begins to uncover	12:40	12:43	12:40
0.5 kg H_2 generated	13:20	14:11	13:45
First cladding rupture	13:41	13:52	13:44
Calculation terminated	13:50	14:17	14:06

The following figures illustrate the effect of the cladding on various parameters. The differences between calculations are generally small prior to core uncovery as displayed in Table 2-11.

Figure 2-34 shows the mass flow from the seals at one of the three RCPs (the other two RCPs are behaving similarly). The mass flow at the break is a function of the primary pressure, so it changes during the transient. Figure 2-35 shows the AFW mass flow, which is lasting 4 hours, 30 min, until ECST inventory is depleted.

After the RCPs trip for high void at about 1 hour, the operator is assumed to perform a secondary side depressurization. The emergency procedure is actuated at 1 hour 30 minutes (Figure 2-36). The emergency secondary side depressurization allows a reduction of RCP seal leakages and primary pressure (Figure 2-37) and the accumulators injection (Figure 2-38).

The failure to actuate of HPI and LPI did not provide any further emergency injection in the primary system, therefore the only decay heat removal mechanism was the reflux cooling in the SGs and the loss of inventory via the RCP seals. The CST was emptied at 4 hours, 30 minutes and it caused the loss of AFW. Consequently, the SG inventory was boiled off through the SG PORVs. The SGs level dropped to zero at about 12 hours, 24 minutes (Figure 2-39). The core started to uncover at about 12 hours, 40 minutes (Figure 2-40).

The core and the maximum cladding temperature are shown in Figure 2-41. The maximum cladding temperatures begin to diverge immediately after the core uncovery. The highest temperatures occurred with the Zircaloy cladding, but the difference in timing with the other claddings is relatively small.

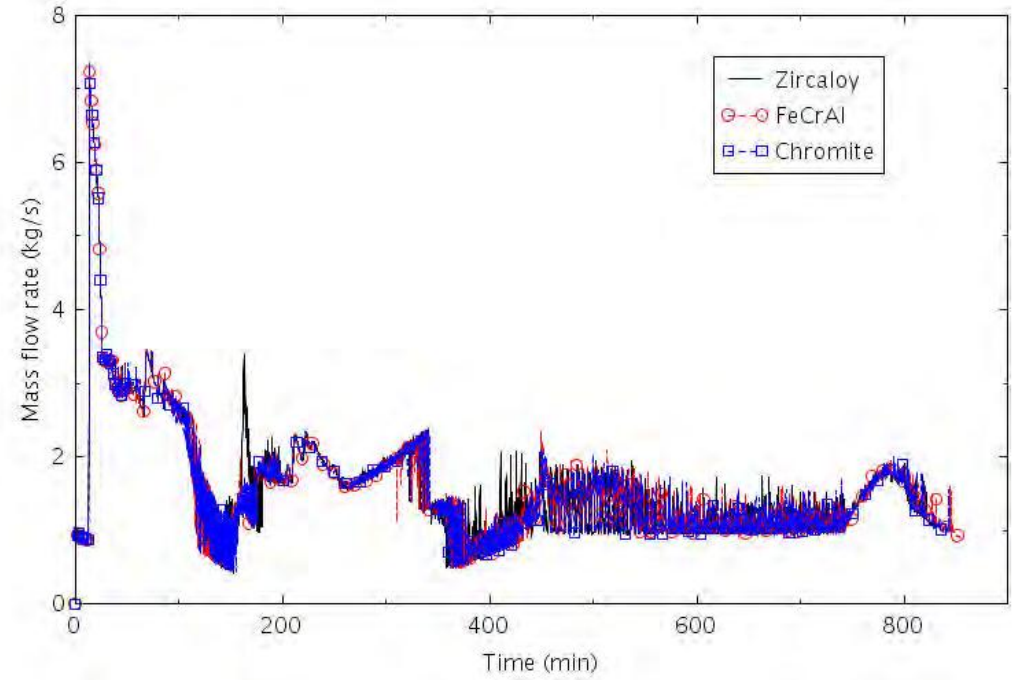

Figure 2-34. RCP Seal Leak Mass Flow (LOFW-4.0).

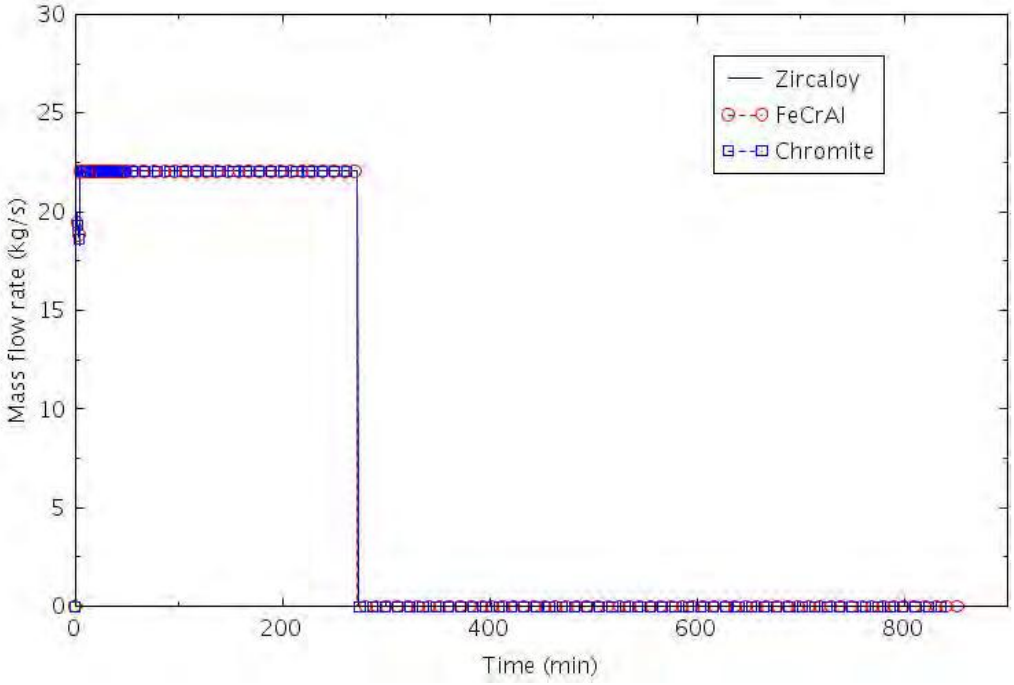

Figure 2-35. AFW Mass Flow (LOFW-4.0).

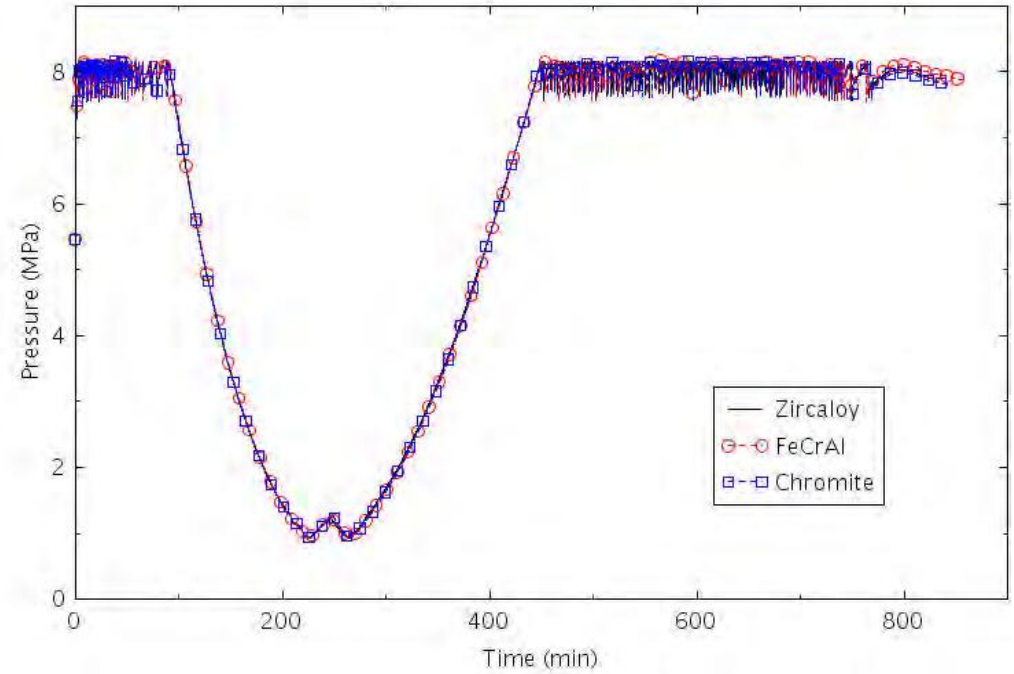

Figure 2-36. SGs Pressure (LOFW-4.0).

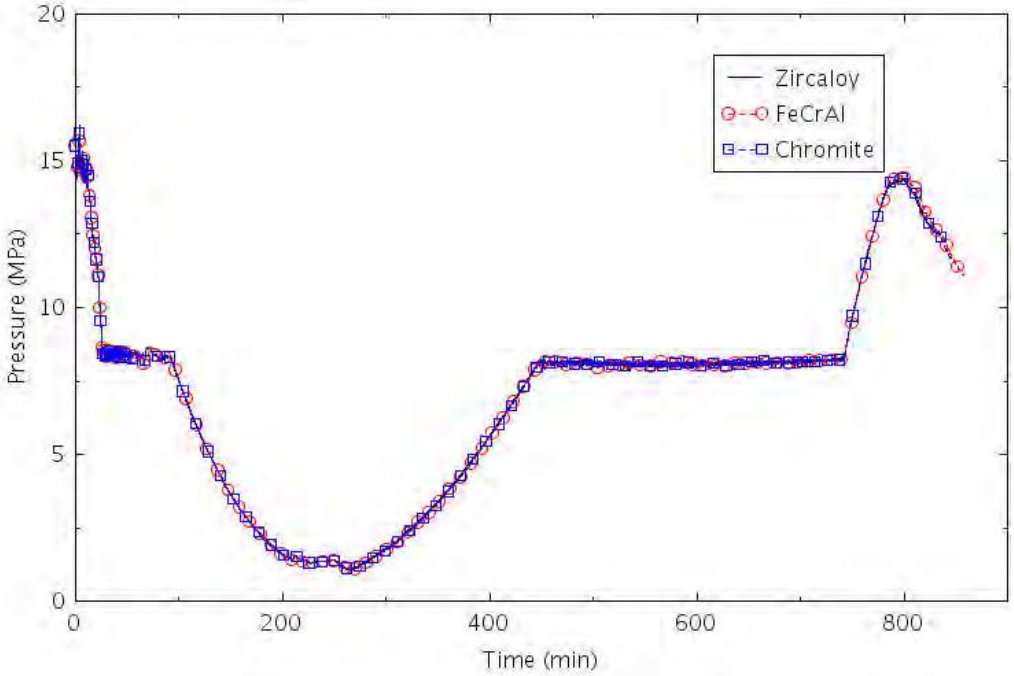

Figure 2-37. Primary Pressure (LOFW-4.0).

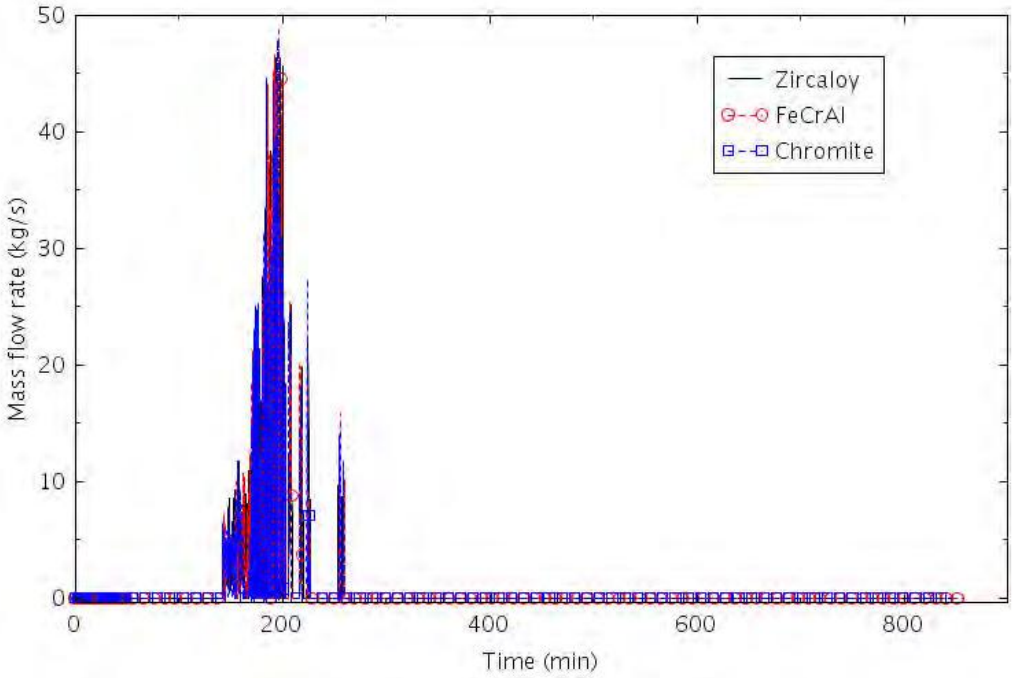

Figure 2-38. Accumulators Injection (LOFW-4.0).

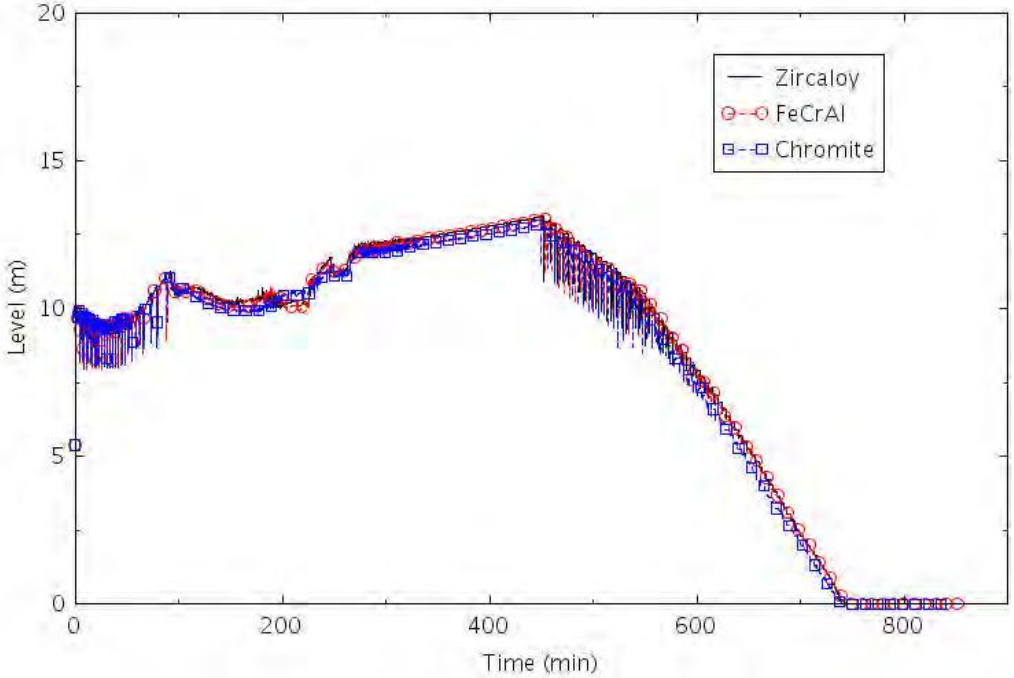

Figure 2-39. SG Level (LOFW-4.0).

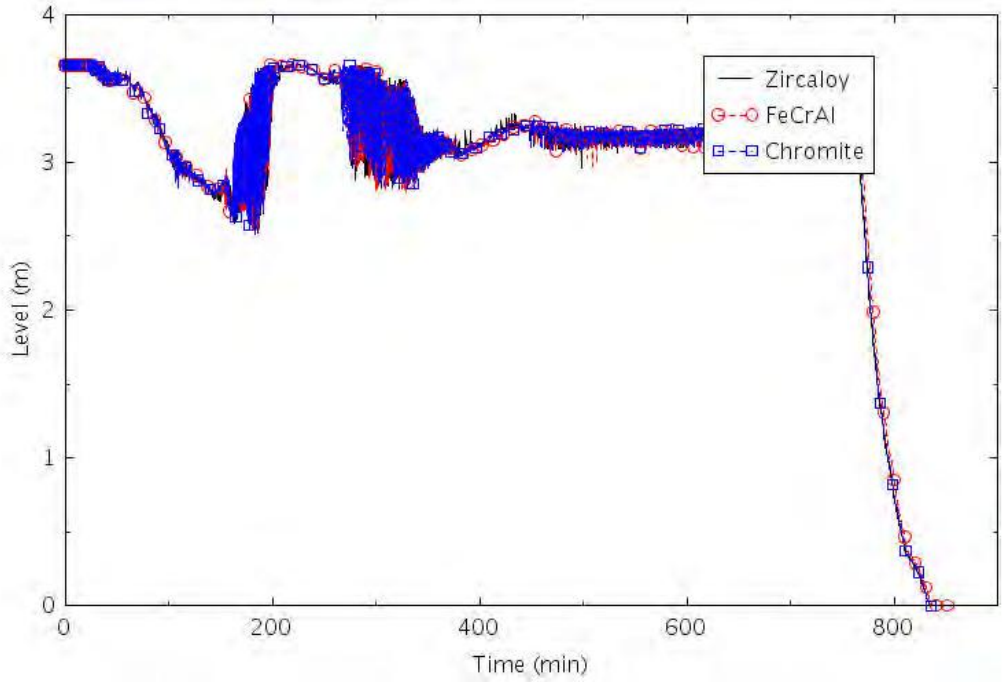

Figure 2-40. Collapsed Liquid Level in the Central Core Channel (LOFW-4.0).

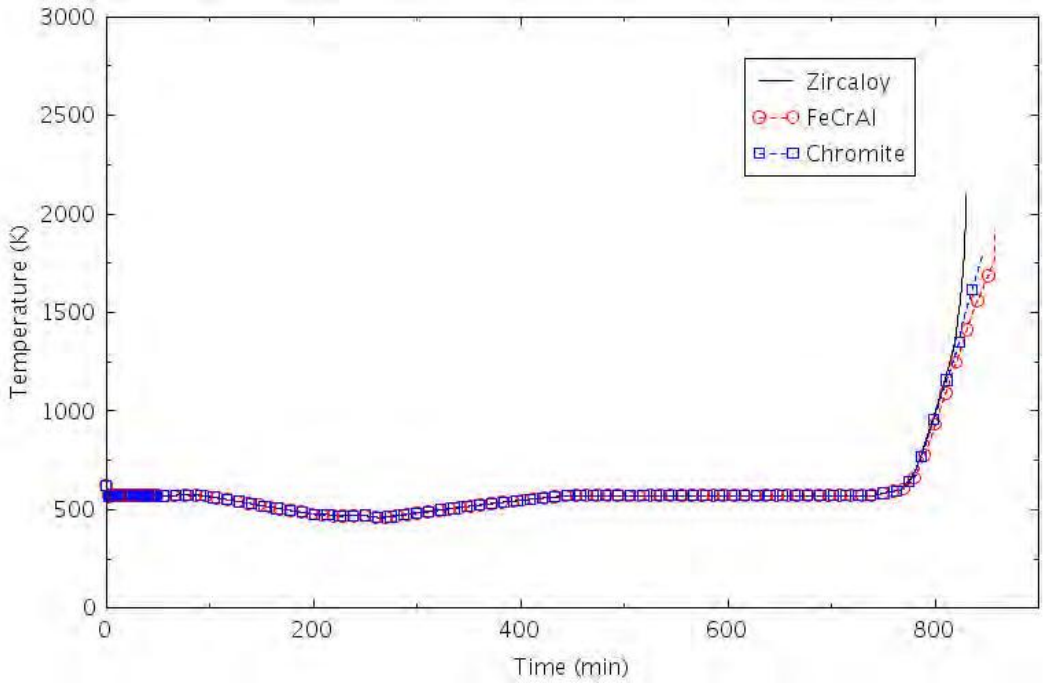

Figure 2-41. Maximum Cladding Temperature (LOFW-4.0).

2.1.3.5 LOMFW with LOSC-182 w/o Secondary Side Depressurization (LOFW-4.1)

This scenario is similar to the LOFW-4.0 scenario, but it assumes that operator fails to perform secondary side depressurization.

After LOFW at t = 0 second, the reactor was tripped and the AFW started in 30 seconds. The LOFW caused the closure of the MSIV, determining the isolation of the three SGs. The RCPs continued to run while power was removed from the system via the SG PORV and the AFW. On the primary side, the RCP seals started to leak with a nominal leakage rate of 21 gpm, increasing to a larger leakage rate of 182 gpm at t = 13 minutes. The RCPs eventually stopped for high void in the primary system.

The continued loss of mass from the primary side caused a drop of primary side pressure to about 8.2 MPa at t = 26 min. This primary side pressure then stayed constant during the whole transient, not allowing passive emergency injection by the accumulators. For mitigation, HPI and LPI were assumed to be available. Therefore, with no primary side emergency coolant injection, the continuous loss of primary inventory at the RCP seal breaks caused core damage conditions.

Table 2-12. Sequence of Events for Scenario LOFW-4.1.

Event	Time (hr:min)		
	Zircaloy	FeCrAl	Chromite
Loss of MFW	00:00	00:00	00:00
MDAFP start	00:01	00:01	00:01
RCPs seals leak at 182 gpm	00:13	00:13	00:13
Primary pressure drops at 8.2 MPa	00:26	00:26	00:26
RCPs tripped for high void	01:06	01:06	01:06
Core begins to uncover	06:48	06:48	06:47
0.5 kg H_2 generated	08:01	08:34	08:11
First cladding rupture	08:07	08:05	08:08
Calculation terminated	08:23	08:34	08:29

The calculations were terminated when the maximum cladding temperature reached 2099 K for Zircaloy and 1804 K for FeCrAl and Chromite.

The differences between calculations due to the different claddings were negligible prior to the onset of core uncovery and were relatively small after the onset of core uncovery. The calculations were terminated when the hottest cladding in each reached its failure temperature. The termination times varied by less than 10 minutes (a delay of 11 minutes for FeCrAl and a delay of 6 minutes for Chromite). The calculated amount of hydrogen produced during the transients varied significantly between claddings. The amount of hydrogen produced was 2.1 kg for FeCrAl, 9.8 kg for Chromite, 37.0 kg for Zircaloy.

The following figures illustrate the effect of the cladding on various parameters. The differences between calculations are generally small prior to core uncovery as displayed in Table 2-12.

Figure 2-42 shows the mass flow from the RCPs seals at one of the three RCPs (the other two RCPs are behaving similarly). The mass flow at the break is a function of the primary pressure, so it changes during the transient. Figure 2-43 shows the AFW mass flow, whose injection was lasting until the end of the transient.

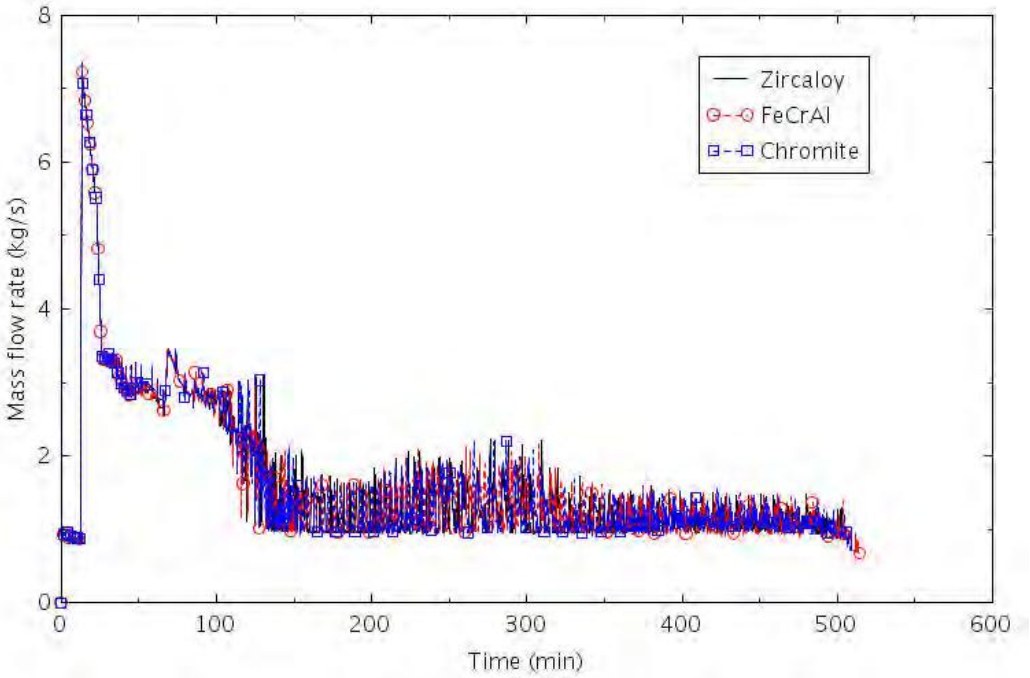

Figure 2-42. RCP Seal Leak Mass Flow (LOFW-4.1).

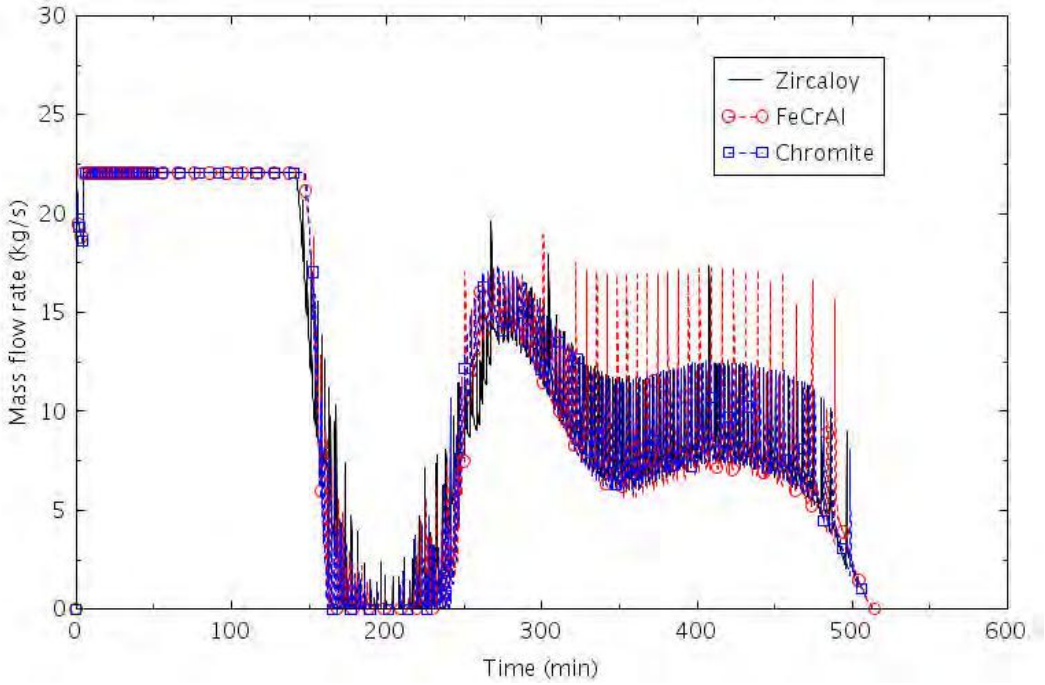

Figure 2-43. AFW Mass Flow (LOFW-4.1).

The RCPs tripped for high void at 1 hour 06 minutes. The primary and secondary pressures stayed constant at about 8.2 MPa (Figure 2-44 and Figure 2-45).

The failure to actuate the HPI and LPI, and the high value of the primary pressure did not allow any further emergency injection in the primary system, therefore the only decay heat removal mechanism was the reflux cooling in the SGs and the loss of inventory via the RCP seals. The continuous primary inventory loss through the RCPs seal break caused a core uncovery at 6 hours, 48 minutes (Figure 2-46).

The core and the maximum cladding temperature are shown in Figure 2-47. The maximum cladding temperatures began to diverge immediately after the core uncovery. The highest temperatures occurred with the Zircaloy cladding, but the difference in timing with the other claddings was relatively small.

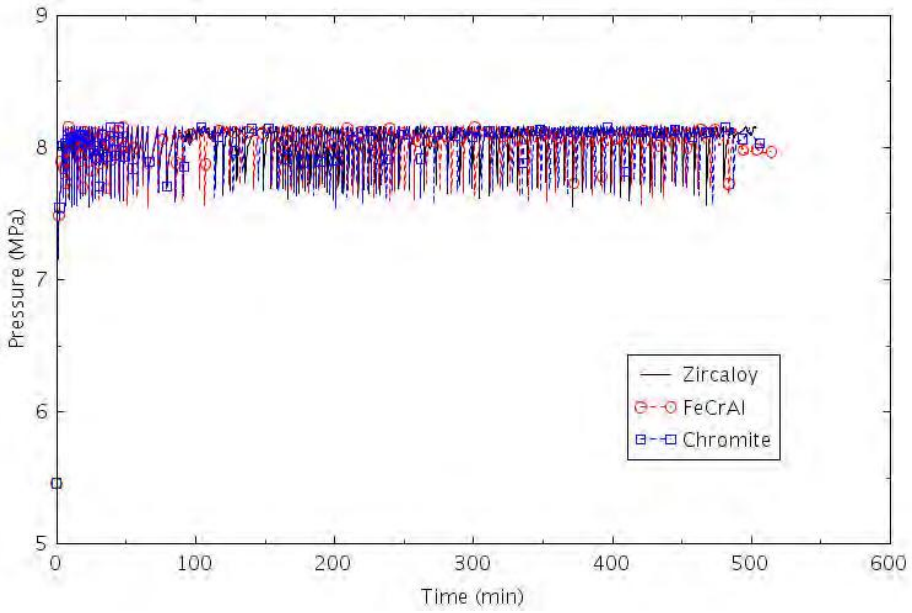

Figure 2-44. SGs Pressure (LOFW-4.1).

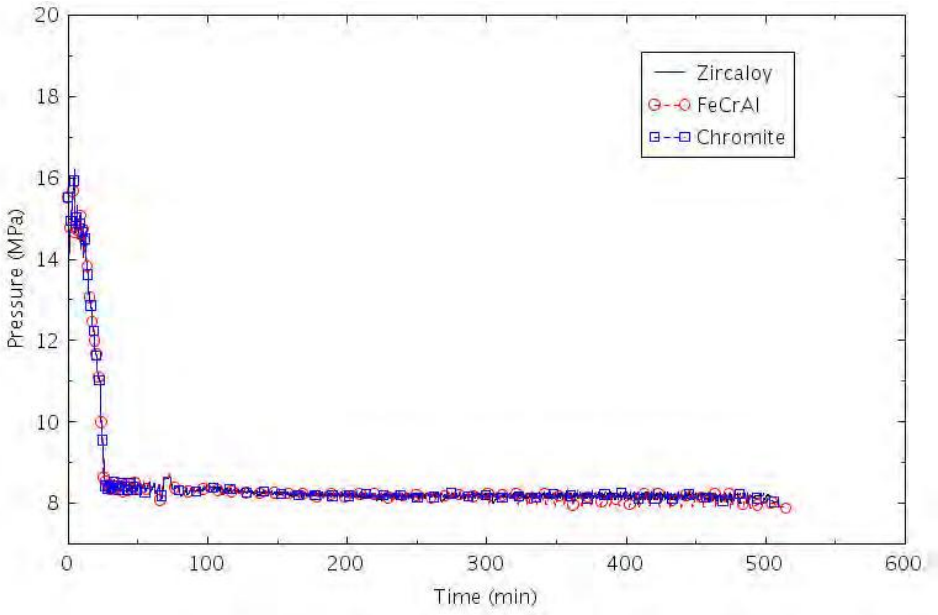

Figure 2-45. Primary Pressure (LOFW-4.1).

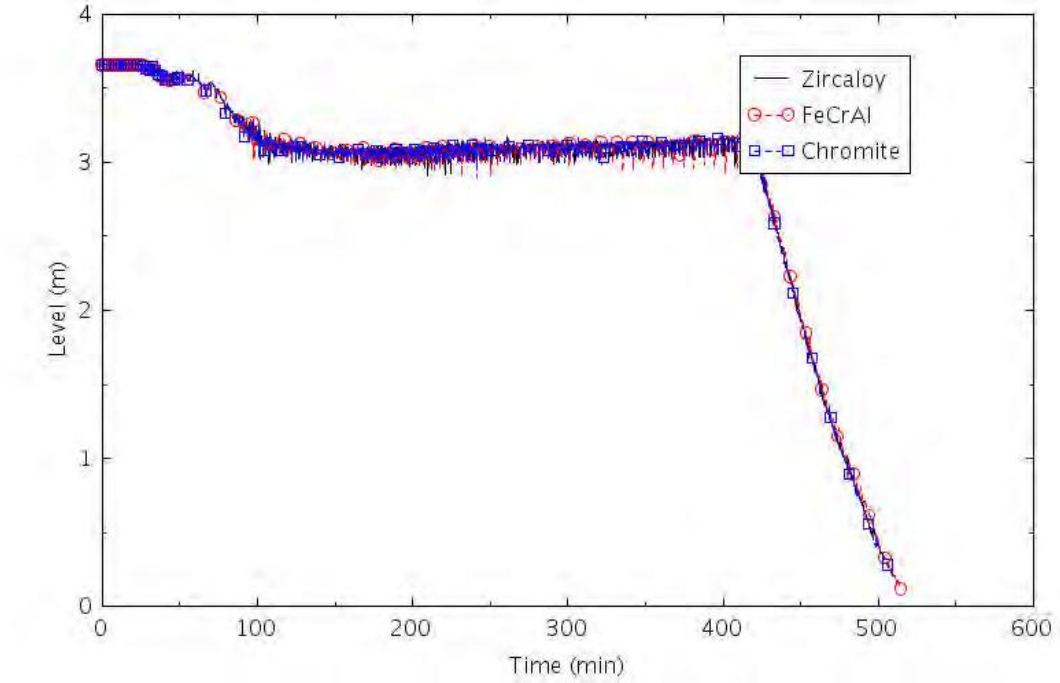

Figure 2-46. Collapsed Liquid Level in the Central Core Channel (LOFW-4.1).

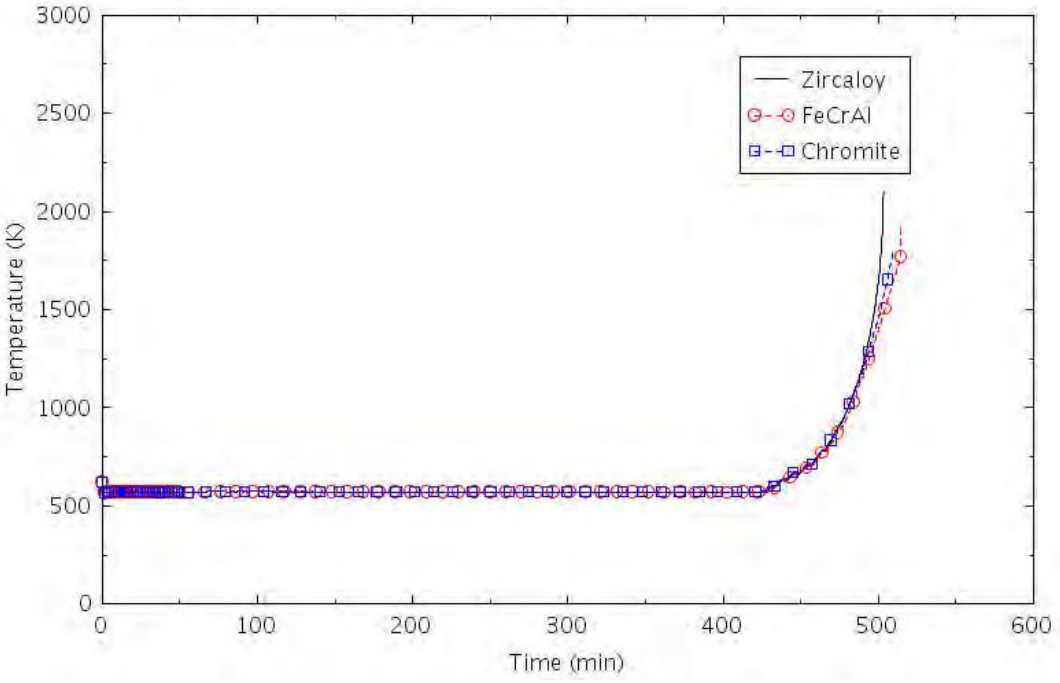

Figure 2-47. Maximum Cladding Temperature (LOFW-4.1).

2.1.3.6 LOMFW with LOSC-76 (LOFW-4.2)

This scenario is similar to the LOFW-4.0 (i.e., LOSC-182) scenario, but it assumes an RCP seal leakage rate of 76 instead of 182 gpm per pump.

After LOFW at t = 0 second, the reactor was tripped and the AFW started in 30 seconds. The LOFW caused the closure of the MSIV, determining the isolation of the three SGs. The RCPs continued to run while power was removed from the system via the SG PORV and the AFW. On the primary side, the RCP seals started to leak with a nominal leakage rate of 21 gpm, increasing to a larger leakage rate of 182 gpm at t = 13 minutes. The RCPs eventually stopped for high void in the primary system.

The continued loss of mass from the primary side and the unavailability of the safety injections prompted the operator decision to depressurize the secondary side for reducing pressure, temperature, and leakages on the primary side. The rate of SG depressurization was about 55 ºC/hour (100 ºF/hour). Only passive injection by the accumulators was assumed (i.e., it was assumed a failure of both HPI and LPI). The injection from the accumulators allowed a temporary recovery of the liquid level in the core and a core cooling. The SG levels were kept by the AFW control system until the CST emptied at about 4h 30 min. Energy was removed from the core through loss of primary inventory via the RCP seals and through cooling with the SGs. After the MDAFP stopped, pressure in the primary side increased again; the water in the SG secondary side was boiled off and the continuous loss of primary inventory led to core damage.

The calculations were terminated when the hottest cladding in each reached its failure temperature. The termination times varied by less than 20 minutes.

Table 2-13. Sequence of Events for Scenario LOFW-4.2.

Event	Time (hr:min)		
	Zircaloy	FeCrAl	Chromite
Loss of MFW	00:00	00:00	00:00
MDAFP start	00:01	00:01	00:01
RCPs seals leak at 76 gpm	00:13	00:13	00:13
RCPs tripped for high void	01:06	01:06	01:06
Operator initiate controlled cooldown of secondary side at ~100 °F/hour	01:30	01:30	01:30
Accumulator Injection	02:22	02:22	02:22
CST empty, AFW stop	04:32	04:32	04:32
SG dryout	11:06	11:06	11:06
Core begins to uncover	11:58	11:58	12:00
0.5 kg H_2 generated	12:33	13:21	13:19
First cladding rupture	13:12	13:11	13:19
Calculation terminated	13:11	13:29	13:20

Compared to the LOSC-182 case, LOSC-76 had an earlier core damage time of about 40 minutes for all the three different clad types. This earlier core damage time was caused by the smaller break area of the RCP seals. The 76 gpm leakage rate was causing a slower primary side depressurization and a smaller loss of inventory. After the SGs dried out, the primary pressure was going up faster for the LOSC-76 case because of the larger liquid inventory. This resulted in a larger loss of primary inventory through the PRZ PORVs and, as a consequence, in an anticipated core uncovery.

The differences between calculations due to the different claddings were negligible prior to the onset of core uncovery and were relatively small after the onset of core uncovery. The calculations were terminated when the hottest cladding in each reached its failure temperature. The termination times varied by less than 20 minutes (a delay of 18 minutes for FeCrAl and a delay of 9 minutes for Chromite). The calculated amount of hydrogen produced during the transients varied significantly between claddings. The amount of hydrogen produced was 2.0 kg for FeCrAl, 8.8 kg for Chromite, and 79.6 kg for Zircaloy.

The following figures illustrate the effect of the cladding on various parameters. The differences between calculations are generally small prior to core uncovery, as displayed in Table 2-13.

Figure 2-48 shows the mass flow from the seals at one of the three RCPs (the other two RCPs are behaving similarly). The mass flow at the break is a function of the primary pressure, so it changes during the transient. Figure 2-49 shows the AFW mass flow, which lasted 4 hours, 32 min, until CST was emptied.

After the RCPs tripped for high void at 1 hour 06 minutes, the operator was assumed to perform a secondary side depressurization. The emergency procedure was actuated at 1 hour 30 minutes (Figure 2-50), which allowed a reduction of RCP seals leakages and of primary pressure (Figure 2-51) and the accumulators injection (Figure 2-52).

The failures to actuate of HPI and LPI did not allow any other emergency injection in the primary system, therefore the only decay heat removal mechanism was the reflux cooling in the SGs and the loss of inventory via the RCP seals. The depletion of the CST at 4 hours, 30 minutes caused the loss of AFW and the SG inventory boiled off through the SG PORVs. The SGs level dropped to zero at about ~11 hours, 06 minutes (Figure 2-53). The core started to uncover after 12 hours, 33 minutes (Figure 2-54).

The core and the maximum cladding temperatures are shown in Figure 2-55. The maximum cladding temperatures began to diverge immediately after the core uncovery. The highest temperatures occurred with the Zircaloy cladding, but the difference in timing with the other claddings was relatively small.

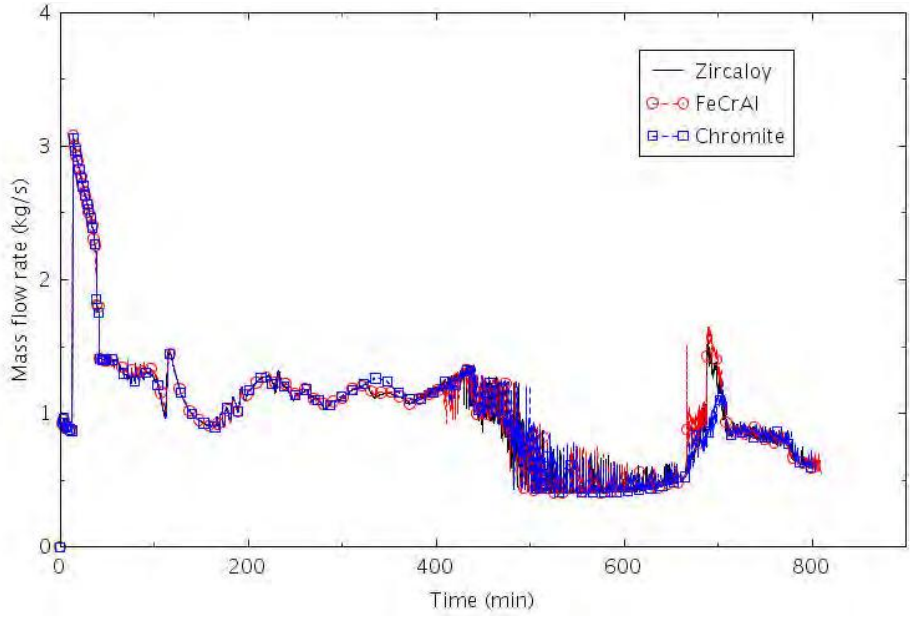

Figure 2-48. RCP Seal Leak Mass Flow (LOFW-4.2).

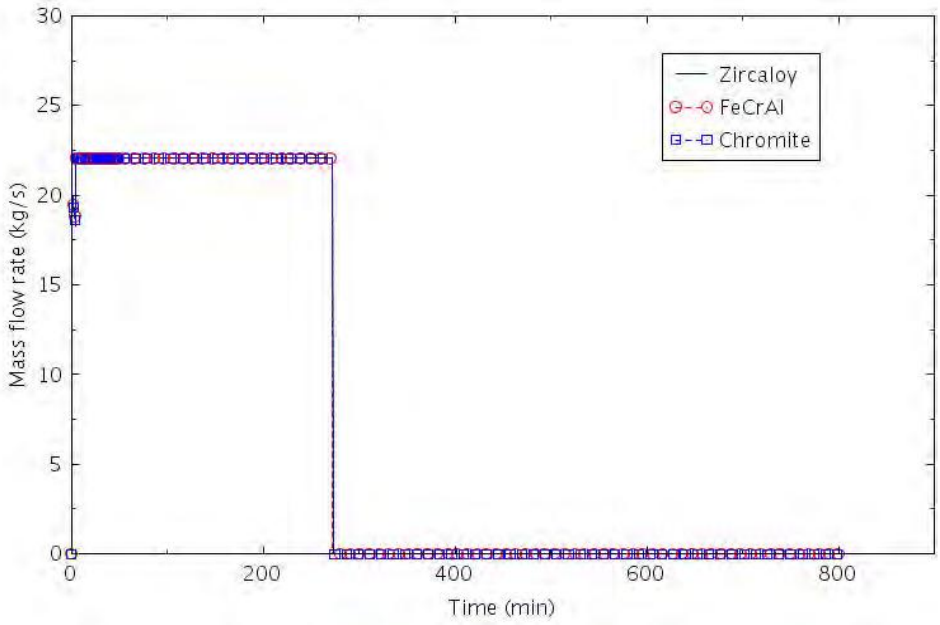

Figure 2-49. AFW Mass Flow (LOFW-4.2).

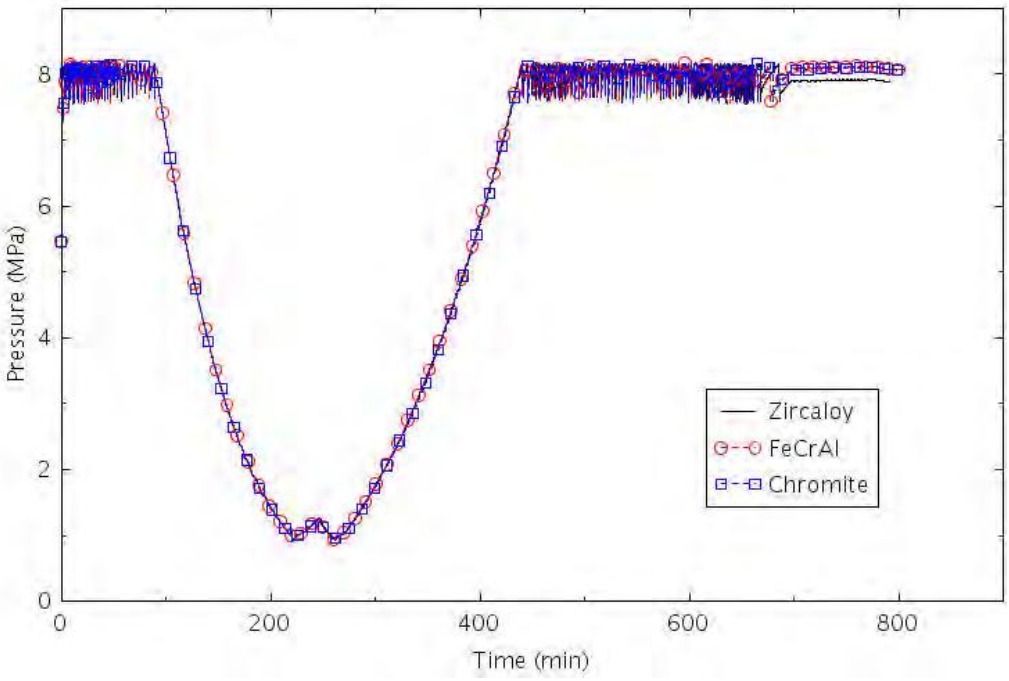

Figure 2-50. SGs Pressure (LOFW-4.2).

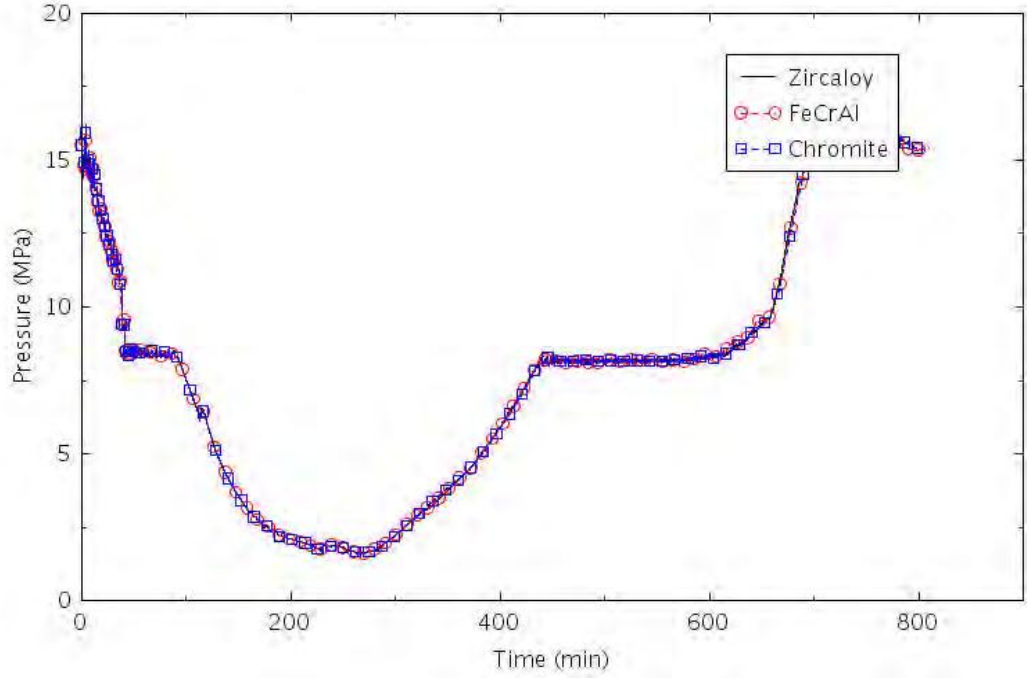

Figure 2-51. Primary Pressure (LOFW-4.2).

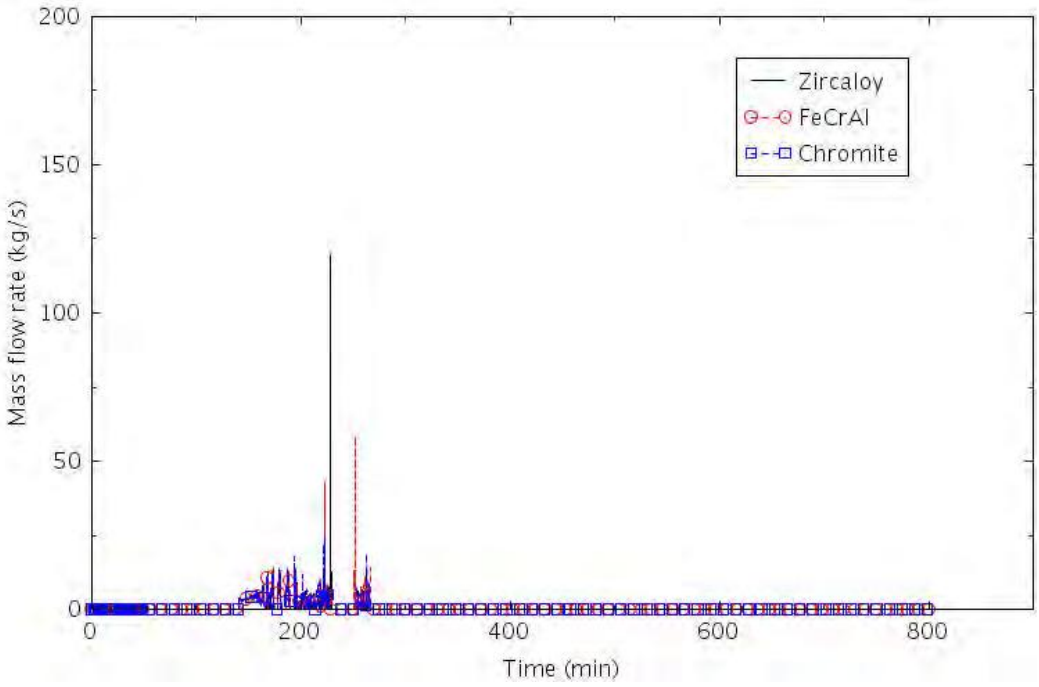

Figure 2-52. Accumulators Injection (LOFW-4.2).

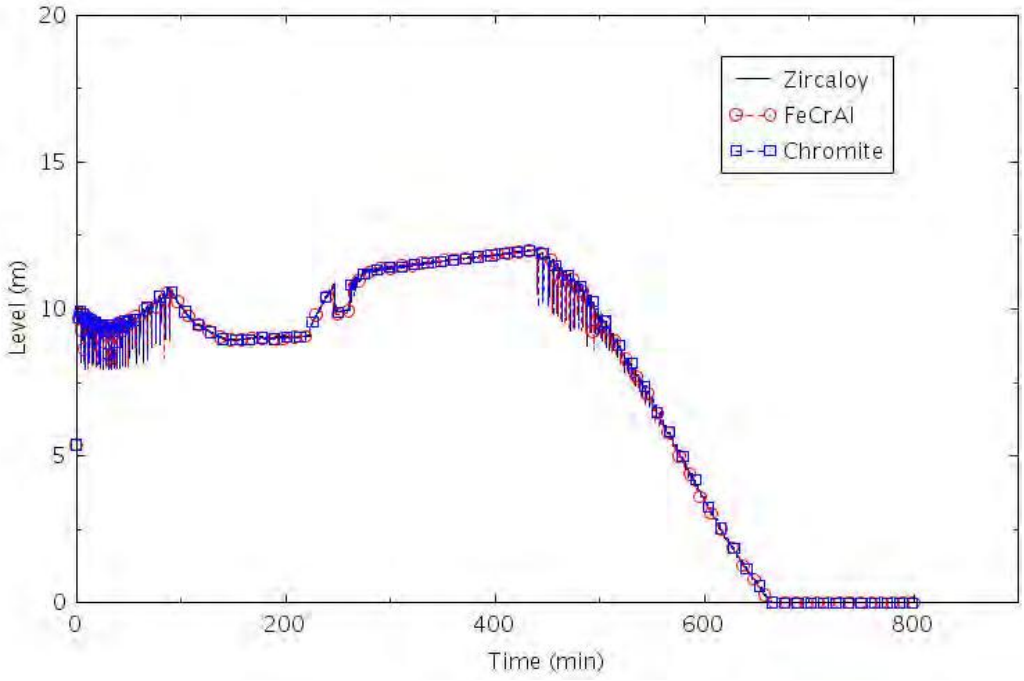

Figure 2-53. SG Level (LOFW-4.2).

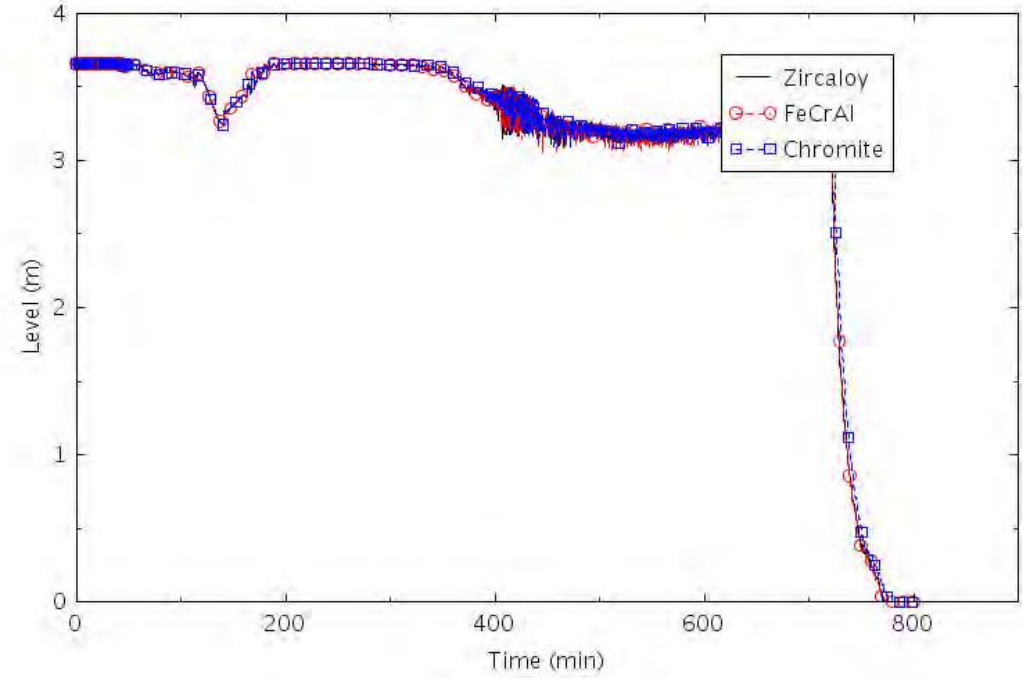

Figure 2-54. Collapsed Liquid Level in the Central Core Channel (LOFW-4.2).

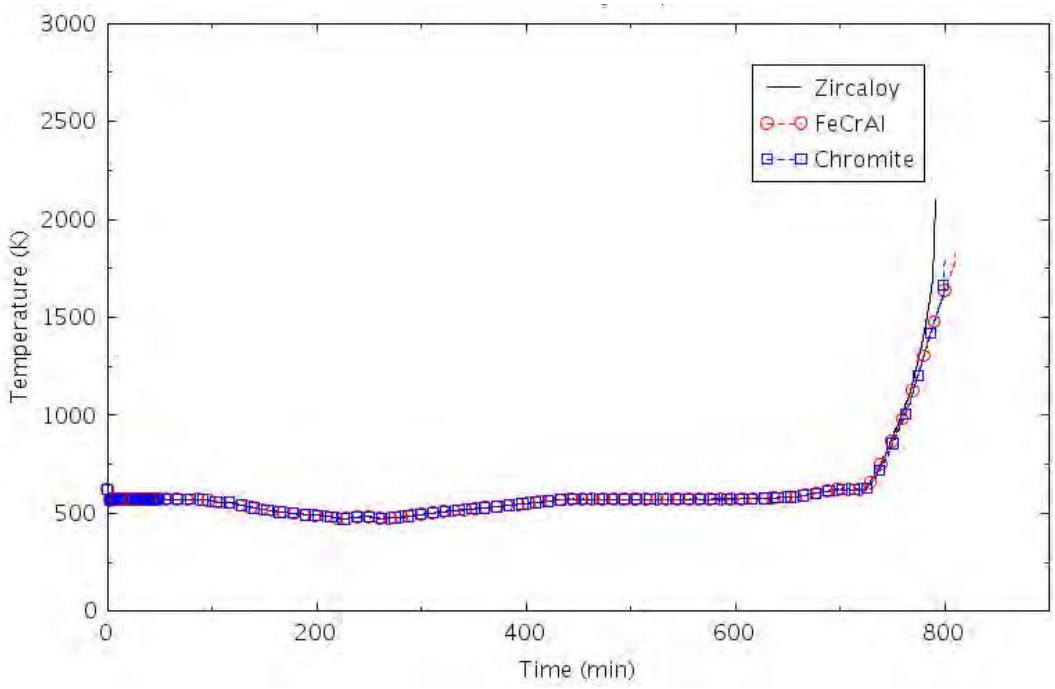

Figure 2-55. Maximum Cladding Temperature (LOFW-4.2).

2.1.3.7 LOMFW with LOSC-480 (LOFW-4.3)

This scenario is similar to the LOFW-4.0 (i.e., LOSC-182) scenario, but it assumes an RCP seal leakage rate of 480 instead of 182 gpm per pump.

After LOFW at t = 0 second, the reactor was tripped and the AFW started in 30 seconds. The LOFW caused the closure of the MSIV, determining the isolation of the three SGs. The RCPs continued to run while power was removed from the system via the SG PORV and the AFW. On the primary side, the RCP seals started to leak with a nominal leakage rate of 21 gpm, increasing to a larger leakage rate of 182 gpm at t = 13 minutes. The RCPs eventually stopped for high void in the primary system.

The continued loss of mass from the primary side and the unavailability of safety injections prompted the operator decision to depressurize the secondary side which reduced pressure, temperature, and leakages on the primary side. The rate of SG depressurization was about 55 ºC/hour (100 ºF/hour). Only passive injection by the accumulators was assumed (i.e., it was assumed a failure of both HPI and LPI). The injection from the accumulators allowed a temporary recovery of the liquid level in the core and a core cooling. SGs levels were kept by the AFW control system until the CST emptied. Energy was removed from the core through loss of primary inventory via the RCP seals and through cooling with the SGs. The continuous loss of primary inventory led to core damage.

Table 2-14. Sequence of Events for Scenario LOFW-4.3.

Event	Time (hr:min)		
	Zircaloy	FeCrAl	Chromite
Loss of MFW	00:00	00:00	00:00
MD-AFW start	00:01	00:01	00:01
RCPs seals leak at 480 gpm	00:13	00:13	00:13
RCPs tripped for high void	00:32	00:32	00:32
Operator initiate controlled cooldown of secondary side at ~100 °F/hour	01:30	01:30	01:30
Accumulator Injection	02:19	02:19	02:19
Core begins to uncover	03:51	03:54	04:14
ECST empty, MD-AFW stop	05:20	05:12	05:24
First cladding rupture	05:44	05:35	06:05
0.5 kg H_2 generated	05:48	06:19	06:13
Calculation terminated	06:05	06:19	06:27

The calculations were terminated when the maximum cladding temperature reached 2099 K for cases with Zircaloy and 1804 K for cases with FeCrAl and Chromite.

The differences between calculations due to the different claddings were negligible prior to the onset of core uncovery and were relatively small after the onset of core uncovery. The calculations were terminated when the hottest cladding in each reached its failure temperature. The termination times varied by about 20 minutes (a delay of 14 minutes for FeCrAl and a delay of 22 minutes for Chromite). The calculated amount of hydrogen produced during the transients varied significantly between claddings. The amount of hydrogen produced was 0.8 kg for FeCrAl, 7.6 kg for Chromite, and 15.2 kg for Zircaloy.

Compared to the LOSC-182 case, LOSC-480 had an anticipated core damage time of about 8 hours earlier for all three different clad types. This earlier core damage time was caused by the larger break area of the RCP seals. The 480 gpm leakage rate caused a faster primary side depressurization and a larger loss of inventory.

The following figures illustrate the effect of the cladding on various parameters. The differences between calculations are generally small prior to core uncovery, as displayed in Table 2-14.

Figure 2-56 shows the mass flow from the seals at one of the three RCPs (the other two RCPs are behaving similarly). The mass flow at the break is a function of the primary pressure, so it changes during the transient. Figure 2-57 shows the AFW mass flow. The total MD-AFW was gradually reduced by the level controller in order not to overfill the SGs.

After the RCPs tripped for high void at 32 min, the operator was assumed to perform secondary side depressurization. The emergency procedure was actuated at 1 hour 30 minutes (Figure 2-58), which allowed a reduction of RCP seal leakages, and led to a further reduction of the primary pressure (Figure 2-59) and the accumulators injection at 2 hours, 19 minutes (Figure 2-60).

The failures to actuate HPI and LPI did not provide any further emergency injection in the primary system, therefore the only decay heat removal mechanism is the reflux cooling in the SGs and the loss of inventory via the RCP seals. The SG levels were kept constant by the AFW control system (Figure 2-61). Towards the end of the transient (~5 hours, 20 min), the AFW stopped because CST was emptied. The core began to uncover at about 4 hours (Figure 2-62).

The core and the maximum cladding temperatures are shown in Figure 2-63. The maximum cladding temperatures began to diverge immediately after the core uncovery. The highest temperatures occurred with the Zircaloy cladding, but the difference in timing with the other claddings were relatively small.

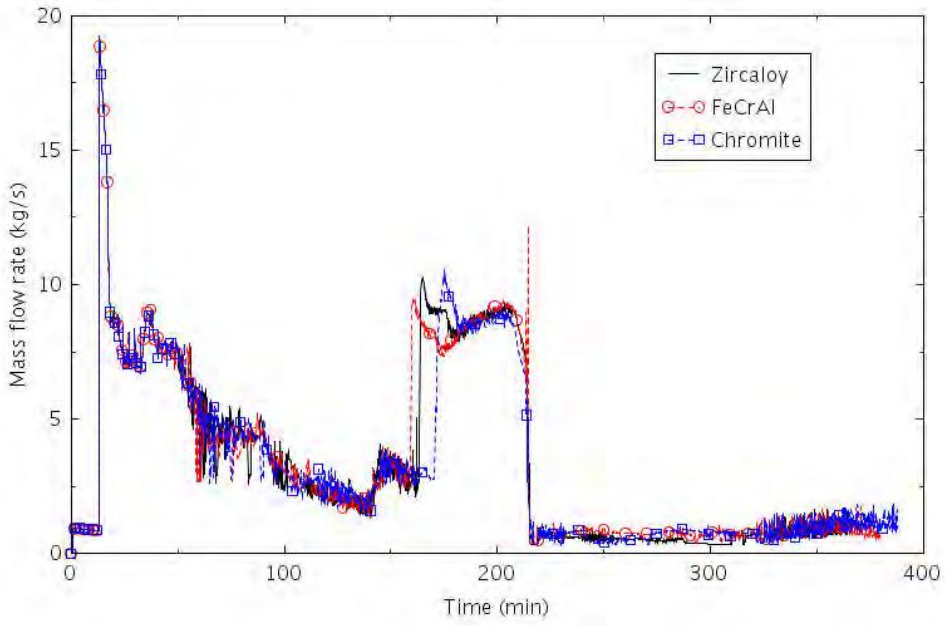

Figure 2-56. RCP Seal Leak Mass Flow (LOFW-4.3).

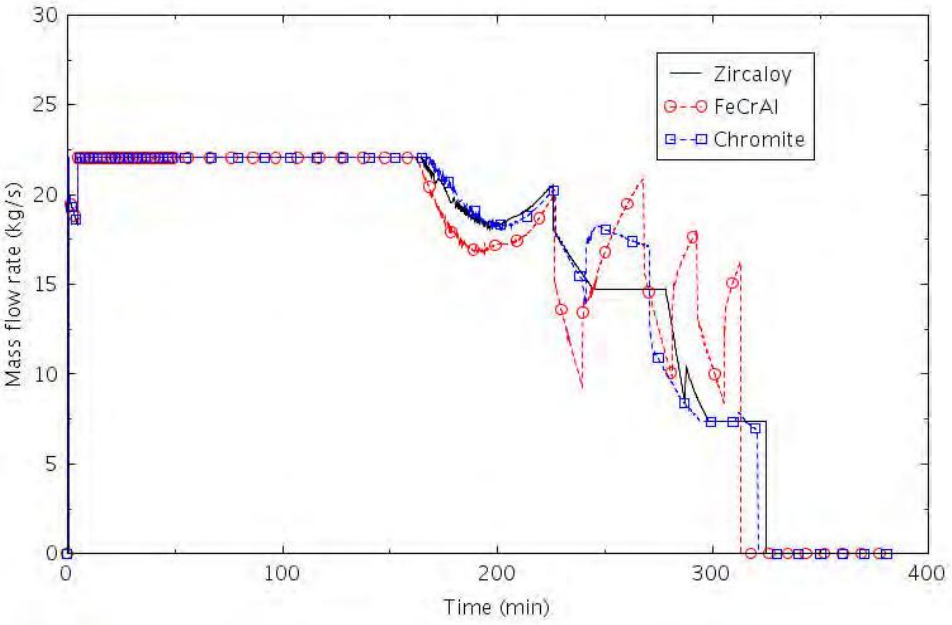

Figure 2-57. AFW Mass Flow (LOFW-4.3).

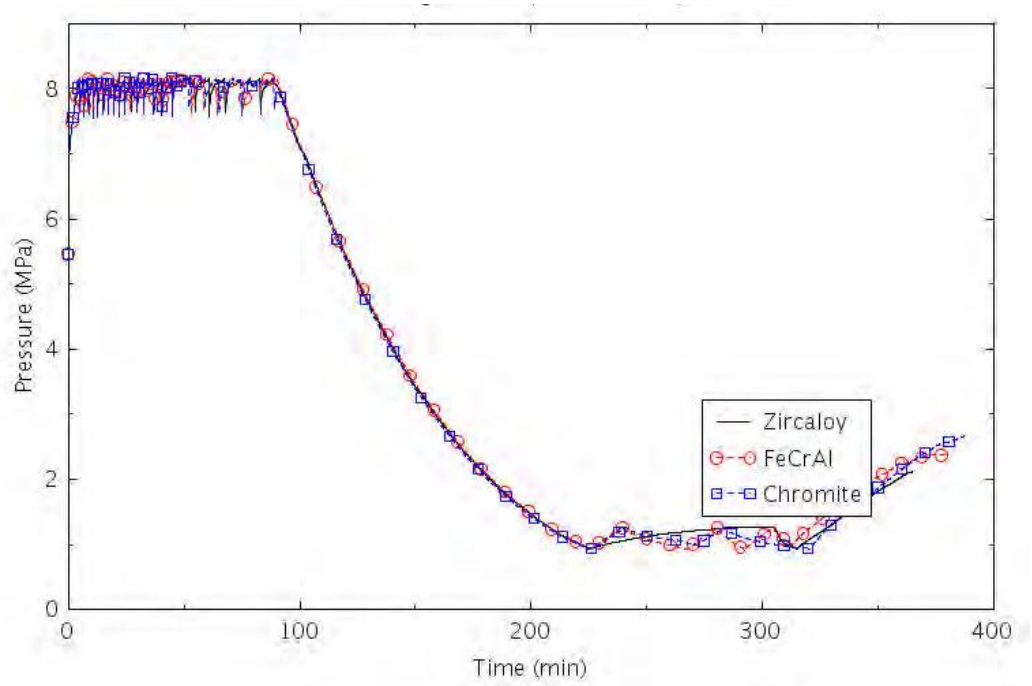

Figure 2-58. SGs Pressure (LOFW-4.3).

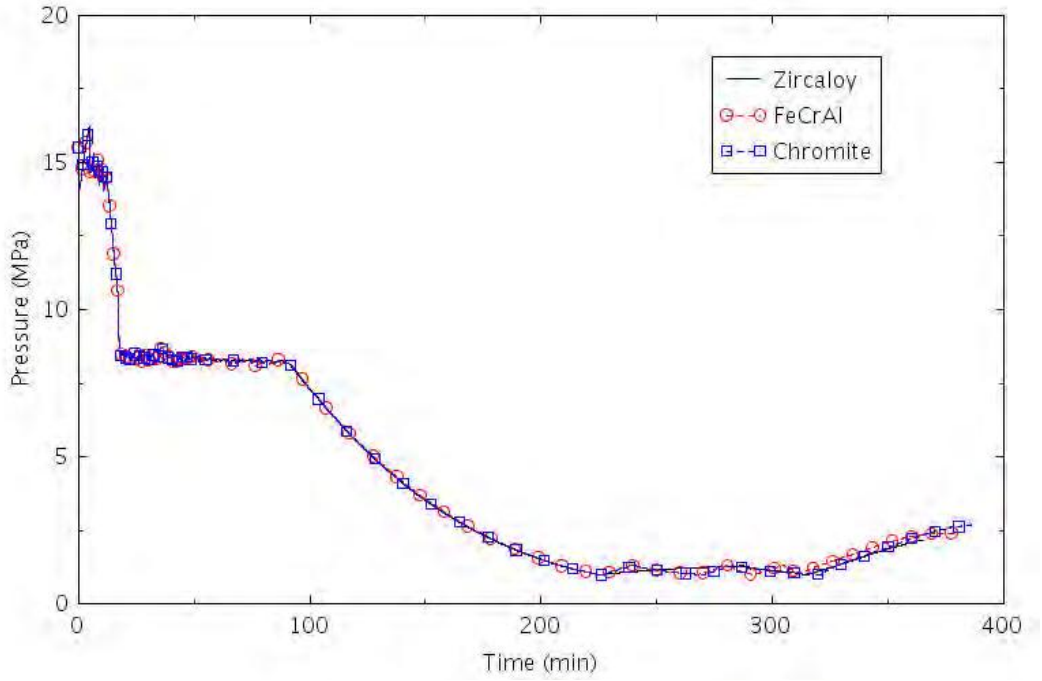

Figure 2-59. Primary Pressure (LOFW-4.3).

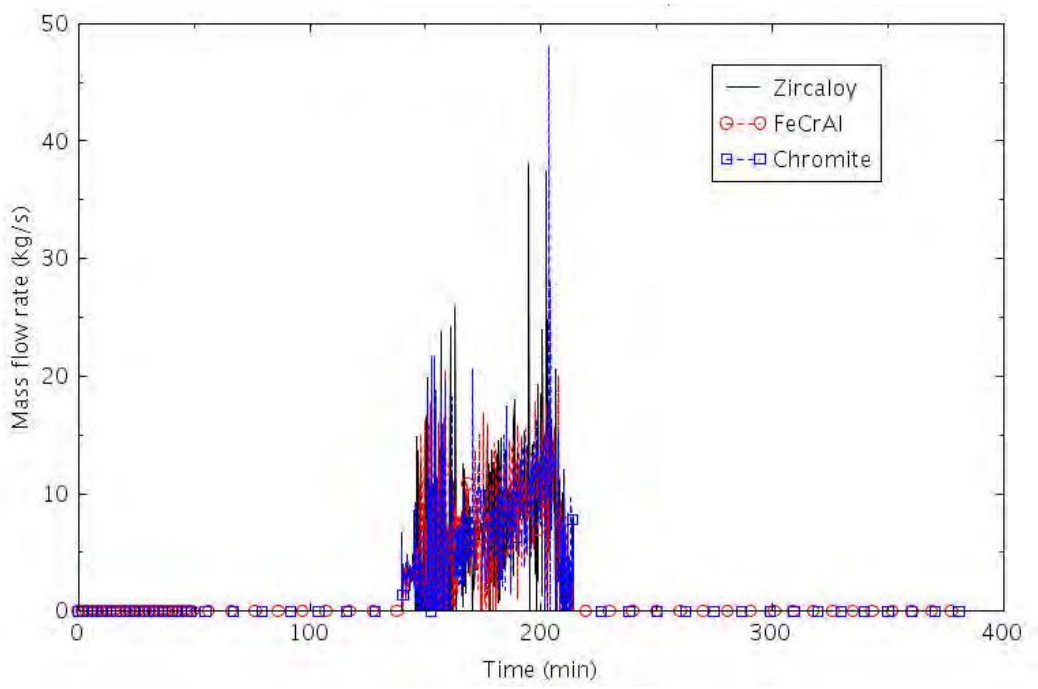

Figure 2-60. Accumulators Injection (LOFW-4.3).

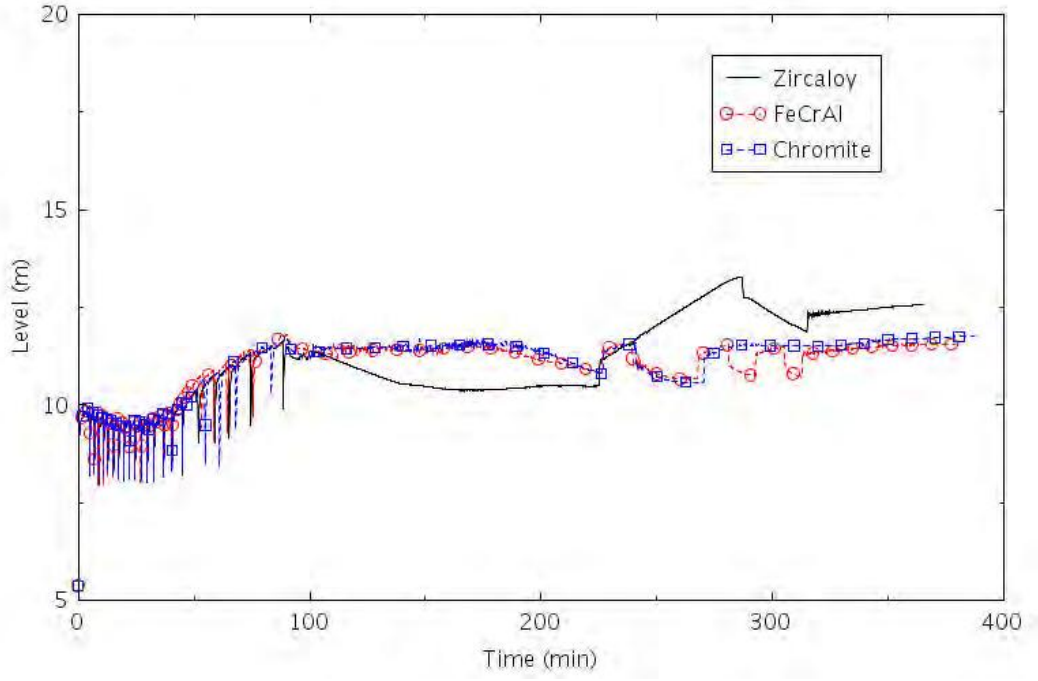

Figure 2-61. SG Level (LOFW-4.3).

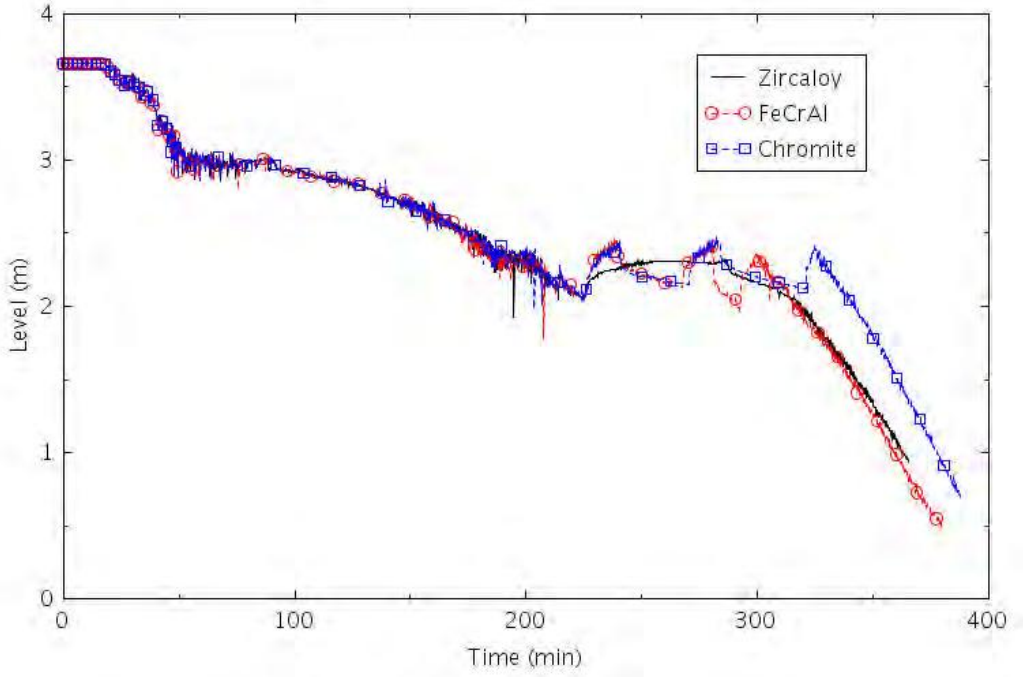

Figure 2-62. Collapsed Liquid Level in the Central Core Channel (LOFW-4.3).

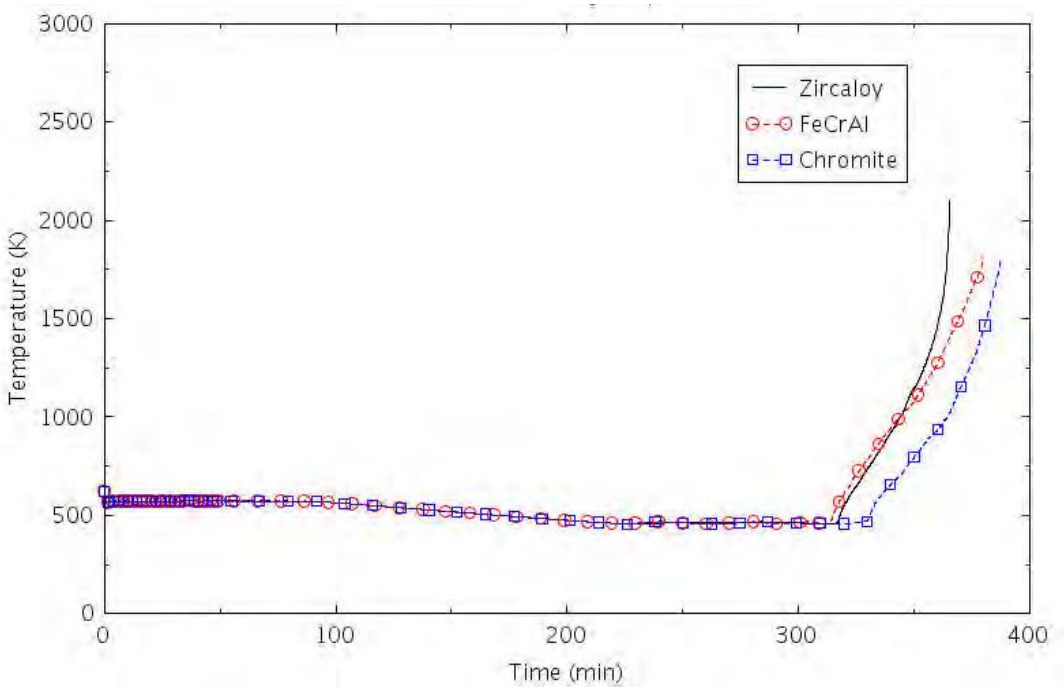

Figure 2-63. Maximum Cladding Temperature (LOFW-4.3).

2.1.4 LOFW Analysis Results

Table 2-15 presents a summary of the RELAP5-3D simulation results for time to core uncovery, time to 0.5 kg hydrogen production, and time to core damage for LOFW scenarios and for Zircaloy and ATF clads (FeCrAl and Chromite). The most severe LOFW scenarios in terms of the shortest time to reach core damage are LOFW-3.0 in which AFW is available but PORV LOCA occurs with no safety injections, and LOFW-1.0, which is the unmitigated loss of all feedwater (MFW and AFW) scenario, with no PORV LOCA or RCP seal LOCA assumed. Core damage occurs shortly after 2 hours since the LOFW IE.

Table 2-15. Summary of RELAP5-3D Time Results for LOFW Scenarios – Zircaloy and ATF Clads.

Scenario	Time to Core Uncovery (hr:min)			Time to 0.5 kg H_2 (hr:min)			Time to Core Damage (hr:min)		
	Zircaloy	FeCrAl	Chromite	Zircaloy	FeCrAl	Chromite	Zircaloy	FeCrAl	Chromite
LOFW-1.0	1:42	1:42	1:42	1:57	2:25	2:21	2:19	2:27	2:23
LOFW-2.0	12:07	12:36	12:17	12:41	13:58	13:42	13:21	14:10	13:42
LOFW-3.0	1:28	1:28	1:28	1:56	2:16	2:02	2:10	2:16	2:14
LOFW-4.0	12:40	12:43	12:40	13:20	14:11	13:45	13:50	14:17	14:06
LOFW-4.1	6:48	6:48	6:47	8:01	8:34	8:11	8:23	8:34	8:29
LOFW-4.2	11:58	11:58	12:00	12:33	13:21	13:19	13:11	13:29	13:20
LOFW-4.3	3:51	3:54	4:14	5:48	6:19	6:13	6:05	6:19	6:27

Table 2-16 compares the times to core damage for ATF designs (FeCrAl and Chromite) with those for existing Zircaloy clad design in different LOFW scenarios. The table shows that the gain of coping time, or the delay of time to core damage, is less than 20 minutes for most scenarios. For FeCrAl, four of the seven analyzed LOFW scenarios have a gain of coping time from 6 to 14 minutes. The other three scenarios have a gain of coping time from 18 to 49 minutes, which are relatively small when comparing the time to core damage with Zircaloy in the associated scenarios (about 13 hours). For Chromite, four of the seven analyzed LOFW scenarios have a gain of coping time from 4 to 9 minutes, with the other three scenarios have a gain of coping time from 16 to 22 minutes.

With the above relatively small increase of the time to core damage from the RELAP5-3D simulation results, a change to the PRA LOFW model (event tree, fault tree, success criteria, or human reliability analysis) is not warranted. The risk benefit on behalf of the CDF brought by the ATF designs would be very small and is not conducted in this analysis.

However, the RELAP5-3D simulation results show the clear benefit in adopting the ATF with much less hydrogen produced at the time of core damage. Table 2-17 compares the hydrogen production for ATF designs (FeCrAl and Chromite) with those for existing Zircaloy clad design in different LOFW scenarios. The table shows the Hydrogen production can be one or two order of magnitude lower than the Zircaloy clad cases.

Table 2-16. Time to Core Damage Comparison for LOFW Scenarios with ATF Designs.

Section	Scenario	Description	Time to Core Damage (hr:min)				
			Zircaloy	FeCrAl	Δt (FeCrAl)	Chromite	Δt (Chromite)
2.1.2.1	LOFW-1.0	Unmitigated Loss of All Feedwater	2:19	2:27	0:08	2:23	0:04
2.1.2.2	LOFW-2.0	Mitigated Loss of All Feedwater with FAB	13:21	14:10	0:49	13:42	0:21
2.1.2.3	LOFW-3.0	LOMFW with PORV LOCA	2:10	2:16	0:06	2:14	0:04
2.1.2.4	LOFW-4.0	LOMFW with LOSC-182	13:50	14:17	0:27	14:06	0:16
2.1.2.5	LOFW-4.1	LOMFW with LOSC-182 w/o Depressurization	8:23	8:34	0:11	8:29	0:06
2.1.2.6	LOFW-4.2	LOMFW with LOSC-76	13:11	13:29	0:18	13:20	0:09
2.1.2.7	LOFW-4.3	LOMFW with LOSC-480	6:05	6:19	0:14	6:27	0:22

Table 2-17. Comparing H_2 Productions for LOFW Scenarios with ATF Designs.

Section	Scenario	Description	Total H_2 (kg)				
			Zircaloy	FeCrAl	H_2% (FeCrAl)	Chromite	H_2% (Chromite)
2.1.2.1	LOFW-1.0	Unmitigated Loss of All Feedwater	51.1	1.0	2.0%	5.5	10.8%
2.1.2.2	LOFW-2.0	Mitigated Loss of All Feedwater with FAB	88.0	2.3	2.6%	4.0	4.5%
2.1.2.3	LOFW-3.0	LOMFW with PORV LOCA	28.5	1.9	6.7%	7.3	25.6%
2.1.2.4	LOFW-4.0	LOMFW with LOSC-182	55.6	2.5	4.5%	15.6	28.1%
2.1.2.5	LOFW-4.1	LOMFW with LOSC-182 w/o Depressurization	37.0	2.1	5.7%	9.8	26.5%
2.1.2.6	LOFW-4.2	LOMFW with LOSC-76	79.6	2.0	2.5%	8.8	11.1%
2.1.2.7	LOFW-4.3	LOMFW with LOSC-480	15.2	0.8	5.3%	7.6	50.0%

2.2 SGTR SCENARIO ANALYSIS

2.2.1 SGTR PRA Model and Scenarios

An SGTR is represented in the generic PRA model by the SGTR event tree (Figure 2-64). This generic SGTR event tree has the following top events:

- RPS: Success or failure of the reactor protection system to shut down the reactor
- AFW: Success or failure of the auxiliary feedwater system to provide secondary cooling to the intact steam generators to remove decay heat
- HPI: Success or failure of the high-pressure injection system to provide makeup water to the RCS. Safety injection pumps take suction from the refueling water storage tank (RWST) and provide sufficient flow to the RCS cold legs to keep the core covered
- SGI: Success or failure of operator diagnosing the loss of coolant as an SGTR event and isolating the ruptured SG
- SSC: Success or failure of primary- and secondary-side cool down by opening SG atmospheric dump valves (ADVs) or turbine bypass valves for secondary side, and pressurizer sprays or PORVs for primary side
- CSI: Success or failure of an operator to control the HPI
- FAB: Success or failure of feed-and-bleed (FAB) cooling when secondary cooling is unavailable; operator opens pressurizer PORVs or the PORV block valves to remove decay heat from the RCS while HPI pump provides makeup flow to the RCS cold legs
- REFILL: Success or failure of RWST refill for long-term makeup when operator fails to isolate the ruptured steam generator
- HPR: Success or failure of high pressure recirculation to provide long-term cooling for the reactor. Residual heat removal (RHR) pump takes water from the containment sump, provides flow to HPI pumps and delivers the water to the RCS. Operator actions are required to align the RHR pump discharge to the HPI pump suction and verify that the containment sump valves are open and the RWST suction valves are closed.
- RHR: Success or failure of residual heat removal; RHR pump provides sufficient flow through the associated heat exchanger to the RCS; operator action is required to open the RCS hot leg valves which provide the suction source for RHR pumps
- ECA: Success or failure of performance of plant emergency procedures to mitigate SGTR event; procedures require depressurization of the secondary/primary and subsequent alignment of RHR for long-term cooling.

The SGTR event tree was quantified with SAPHIRE 8 using a truncation level of 1E-12. Table 2-18 presents the quantification results. The total SGTR CDF is 2.36E-7/year. There is a total of 12 SGTR accident sequences (i.e., the sequence end state is core damage). SGTR Sequence 12 is the most risk significant sequence with a CDF of 1.60E-7/year and contributes nearly 70% of the total SGTR CDF. The SGTR Sequence 09 is the second-most risk significant sequence with a CDF of 3.43E-8/year, contributing about 15% of the total SGTR CDF.

Table 2-18. Overview of SGTR Event Trees Quantification Results.

Name	CDF	Cut Set Count	% CDF
SGTR (12 Seqs.)	2.36E-07	486	100.0%
SGTR:12	1.60E-07	19	67.9%
SGTR:09	3.43E-08	32	14.5%
SGTR:14	1.99E-08	290	8.4%
SGTR:22	1.72E-08	5	7.3%
SGTR:06	1.92E-09	2	0.8%
SGTR:19	1.58E-09	82	0.7%
SGTR:15	4.61E-10	7	0.2%
SGTR:16	2.26E-10	17	0.1%
SGTR:20	1.63E-10	19	0.1%
SGTR:21	3.38E-11	7	0.0%
SGTR:18	3.22E-11	5	0.0%
SGTR:03	3.20E-11	1	0.0%

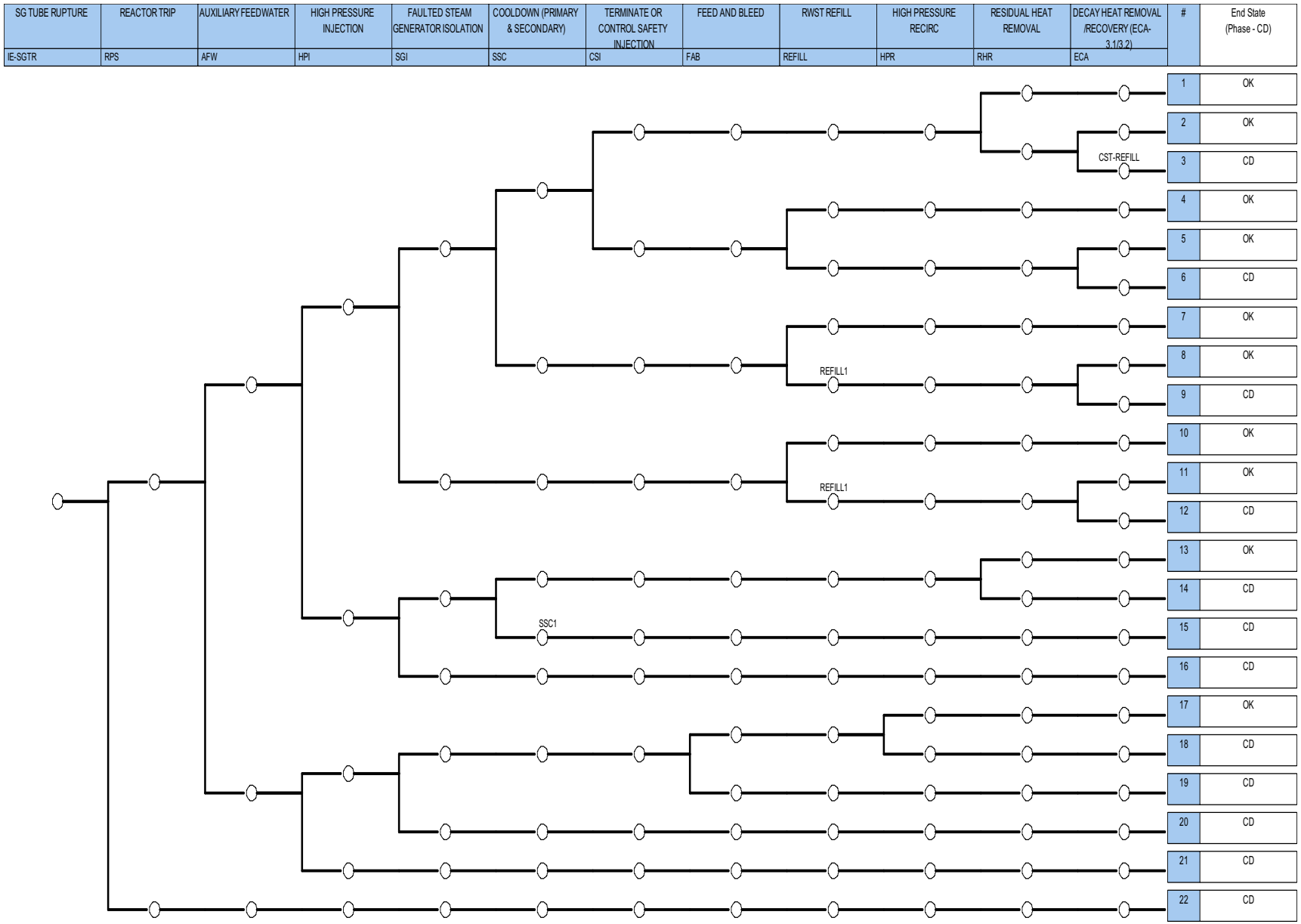

Figure 2-64. Generic PWR SGTR Event Tree.

The following SGTR scenarios were developed as input for RELAP5-3D thermal hydraulic analysis with traditional fuel design and near-term ATF designs. The scenarios can be divided into four groups: (1) without HPI scenarios; (2) with HPI scenarios; (3) without AFW scenarios; and (4) ATWS scenarios.

Without HPI Scenarios

SGTR-1: This is an SGTR with no HPI scenario. An SGTR occurs, the reactor trips, AFW is successful, there is no HPI, the isolation of a ruptured SG fails, and core damage occurs due to the loss of primary coolant without makeup.

SGTR-2: This scenario is similar with an SGTR-1 except that isolation of a ruptured is SG successful. However, primary/secondary cooldown fails. Without primary makeup from an HPI, core damage eventually occurs.

SGTR-3: This scenario is similar with an SGTR-2 except that the primary/secondary cooldowns are successful. However, an RHR system still fails to provide makeup flow to the RCS, and core damage can't be prevented.

With HPI Scenarios

SGTR-4: This is an SGTR with an HPI successful scenario. An SGTR occurs, the reactor trips, use of AFW is successful, an HPI is successful, but isolation of a ruptured SG fails, HPI finally stops when RWST depletes. Core damage occurs without continuing primary makeup.

SGTR-5: this scenario is similar with SGTR-4 except that isolation of ruptured SG is successful, however, primary/secondary cooldown fails. Without primary makeup from HPI, core damage eventually occurs.

SGTR-6: this scenario is similar with SGTR-5 other than that the primary/secondary cooldown is successful, however, there is no control of HPI, and HPI stops when the RWST depletes. Without primary makeup from HPI, core damage eventually occurs.

Without AFW Scenarios

SGTR-7: This is an SGTR with no AFW or FAB scenario. An SGTR occurs, the reactor trips, there is no AFW or FAB, and even with successful HPI, the SG is isolated. The lack of secondary cooling would lead to core damage.

ATWS Scenarios

SGTR-8: This is an SGTR and an ATWS scenario in which the RPS fails to trip the reactor when SGTR occurs. Core damage is assumed.

Table 2-19 presents an overview of the SGTR scenarios developed for RELAP5-3D analysis. All scenarios other than the ATWS would be run with RELAP5-3D, first with the current Zr-based fuel cladding design as the base case and then with the ATF design (the FeCrAl design or the Cr-coated design). Compared between different cladding designs for each scenario are the times of PCT to reach melting point, the times to generate half a kilogram of hydrogen, and the total amount of hydrogen generated when the run is terminated. The estimated time differences for PCT to reach melting point from RELAP5-3D are then considered for PRA model changes to evaluate the risk impacts from the proposed ATF design.

Table 2-19. SGTR Scenarios for RELAP5-3D Analysis.

RELAP-5 Scenario	PRA Sequence	CDF	Scenario Description	RPS	AFW	HPI	SGI	SSC	CSI	FAB	RWST	RHR	ECA
SGTR-1	S16	2.26E-10	No HPI & SGI	Trip	AFW	No HPI	No SGI						
SGTR-2	S15	4.61E-10	SGI, but No HPI & SSC	Trip	AFW	No HPI	SGI	No SSC					
SGTR-3	S14	1.99E-08	SGI & SSC, but No HPI &RHR	Trip	AFW	No HPI	SGI	SSC				No RHR	
SGTR-4	S12	1.60E-07	HPI, but No SGI & RWST Refill & ECA	Trip	AFW	HPI	No SGI				No Refill		No ECA
SGTR-5	S09	3.43E-08	HPI & SGI, but No SSC & RWST Refill & ECA	Trip	AFW	HPI	SGI	No SSC			No Refill		No ECA
SGTR-6	S06	1.92E-09	HPI & SGI & SSC, but No CSI & RWST Refill & ECA	Trip	AFW	HPI	SGI	SSC	No CSI		No Refill		No ECA
SGTR-7	S19	1.58E-09	HPI & SGI, but No AFW & FAB	Trip	No AFW	HPI	SGI			No FAB			
SGTR-8	S22	1.72E-08	ATWS	No Trip									

2.2.2 SGTR RELAP5-3D Model

Several new features were introduced in the IGPWR nodalization to properly model the SGTR transient. A summary of these features is documented in this section.

1. SG ruptured tube. Nodalization for a single tube in SG train A (SG-A) was introduced. At the same time the intact SG tubes flow and heat exchange areas were properly modified. The broken SG tube is composed of two pipes (209 and 211). The rupture is assumed at the top of the SG tube sheet (see Figure 2-65). A set of three valves (543, 544, 555) mimic the double-ended guillotine break of the SG tube, allowing primary coolant to be discharged in the SG boiler (276) after the break.

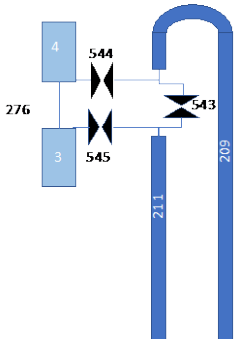

Figure 2-65. Nodalization of the Broken SG-A Tube.

2. Steam Dump (SD). The SD system was added for modeling the reactor depressurization and cooling during the early phases of the SGTR transient. A dedicated set of valves and a steam collector was added to the IGPWR nodalization (see Figure 2-66). Main SD valve characteristics are reported in Table 2-20.

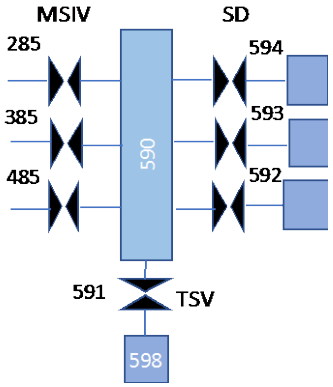

Figure 2-66. Nodalization of Steam Dump.

Table 2-20. Steam Dump Valves Characteristics.

Parameters	Value
Number of Pumps	2
Rated mass flow at the spray nozzles at -4.0 psid (lbm/second)	376.6
Rated mass flow at the spray nozzles at 26.9 psid (lbm/second)	278.9

3. PRZ spray line. Spray lines were added in order to model the operator actions for the primary system depressurization. The nodalization scheme is shown in Figure 2-67.

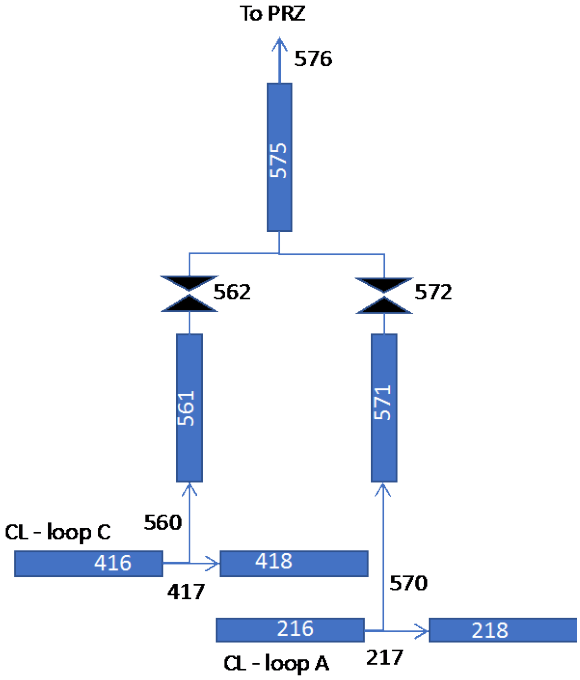

Figure 2-67. Nodalization of PRZ Spray Lines.

4. PRZ component. The component "prizer" replaced the original PRZ model in order to allow for more control options (e.g. water droplet diameter, interfacial heat transfer) during the cooldown transient calculations.

2.2.3 SGTR RELAP5-3D Analysis

The same RELAP5-3D IGPWR model was used for the simulation of the SGTR scenarios.

2.2.3.1 SGTR Base Case (SGTR-0)

Before the simulation of the SGTR sequences provided in Section 2.2.1, an SGTR base case is presented below to show the nominal plant responses to an SGTR event.

The SGTR sequence is starting with an assumed double-ended guillotine break of an SG tube near the top of the tube bundle. The analysis has been performed using a best-estimate approach, therefore choked flow models were used and no additional failures of equipment (e.g. SG PORV stuck open) were considered. As such, the set of analyses reported hereafter are not following the approach used in

the Surry Power Station FSAR (Dominion, 2007), where a set of boundary conditions were assumed for maximizing the potential loss of primary inventory and the radioactivity release into the atmosphere.

The sequence described below is based on a realistic sequence the operators would follow after an SGTR event. The information was obtained from Section 14.3 of the Surry Power Station FSAR (Dominion, 2007).

The IE is the double-ended guillotine break of a tube of SG-A. The break is assumed to happen near the top of the tube bundle. After the IE, the pressurizer pressure and levels falls. The charging pump flow immediately increases, trying to keep the level constant. However, the mass flow to the break is greater than the charging pump flow, causing a steady reduction of the RCS pressure and level.

The system pressure reduction then causes a reactor trip for pressurizer low-pressure signal (1840 psia or 12.67 MPa) and then an SI signal for pressurizer low-low pressure (1790 psia or 12.34 MPa). The reactor trip activates the closure of the Turbine Stop Valve (TSV), and the insertion of the shutdown control rods. Immediately after, the SI signal also actuates:

- The termination of the MFW
- The shutdown of the charging pumps
- The actuation of three HPSI pumps
- The startup of AFW after 30 seconds.

In a conservative analysis, generally no operator actions during the first 30 minutes are assumed. In the following analysis, as in an actual event, the operator is assumed to perform the following actions immediately after the IE:

- Understand whether the falling PRZ pressure and levels and increased charging pump flows are the symptoms of small steam-line breaks, an LOCA, or an SGTR; the identification of the SGTR accident is generally done by a condenser air ejector radiation alarm or an SG blowdown radiation alarm; eventually the level increase in an SG allows the operator to identify the faulty SG
- Ensure the actuation of SI and of AFW
- Control the RCS cooldown to maintain no-load temperature. Stop main coolant pump (MCP) pumps if SI is actuated and RCS cooling is maintained
- Isolate the ruptured SG
- Initiate RCS cooldown through intact SGs by dumping steam to the main condenser through the SD line
- Depressurize the RCS using the pressurizer spray to minimize the break flow
- Regulate the SI in order to not overfill the ruptured SG; keep the level in the pressurizer and contribute to the cooldown of the RCS.

Details of the timing of the events are reported in Table 2-21.

Table 2-21. Sequence of Events for Scenario SGTR-0.

Event	Timing (hr:min:sec)
SG tube rupture. PRZ level and pressure fall, start of charging pumps.	00:00:00
Reactor trip for PRZ low-pressure. Reactor shutdown, closure of TSV.	00:16:03
SI signal for PRZ low-low pressure. Stop of MFW.	00:16:07
Start-up of AFW pumps.	00:16:37
Operator recognizes SGTR event. Isolation of ruptured SG-A.	00:20:00
Shutdown of MCP for loop-A and B.	00:30:00
Depressurization of SG-B and C using Steam-Dump. RCS cool-down at 50 °F/hr.	00:33:20
SGTR mass flow to zero.	01:37:45
RCS reaches RHR actuation conditions (350 °F/400 psig or 450 K/3.0 MPa).	03:03:45

The following figures illustrate the details of the main analysis for SGTR-0. After the SGTR IE has occurred, the charging pumps start to inject water at 14.5 lbm/second (6.5 Kg/second) for compensating the PRZ level decrease (see Figure 2-68 and Figure 2-69). The RCS pressure starts to immediately decrease too (Figure 2-70). At time t = 16 min, the reactor trips for the PRZ low-pressure signal. Closure of the TSV is actuated and fission power is terminated by control rod insertion. Immediately after, the SI signal is generated for PRZ low-low pressure. The charging pumps are stopped and HPIS pumps and the AFW pumps are activated (see Figure 2-71 and Figure 2-72). The AFW injection is regulated in order to keep the SG level at the FW injection ring (11 m), while the HPIS injection system is regulated to refill the PRZ and to avoid the overfilling of the ruptured SG.

The operator is assumed to identify the type of accident at time t = 20 min, performing the isolation of the ruptured SG-A by closing the SG-A MSIV. The operator then stops two MCPs, one of the ruptured SGs and the MCP-B at t = 30 minutes (Figure 2-73). The MCP-C is assumed to be kept in operation for actuating the PRZ sprays at about t = 36 minutes (Figure 2-74).

At about 33 min, the operator is assumed to start the cooldown of the RCS by depressurizing the SG-B and SG-C using the SD, with a rate of 50 °F/hour, keeping enough subcooling margin (Figure 2-75).

Mass flow of the ruptured SG tube has been shown in Figure 2-71. The break mass flow rate starts to drop when the RCS pressure is reduced by the SD cooldown procedure (t = 33 minutes). The break mass flow rate becomes zero and eventually negative at t = 1 hour 37 minutes. The mass flow from the break is small and the total RCS primary coolant discharged in the SG-A is limited. Pressure and temperature of RCS are constantly reduced, reaching the RHR actuation conditions (350 °F/400 psig or 450 K/3.0 MPa) at about t = 3 hours, 03 minutes (see Figure 2-70 and Figure 2-75 for RCS pressure and average temperature, respectively).

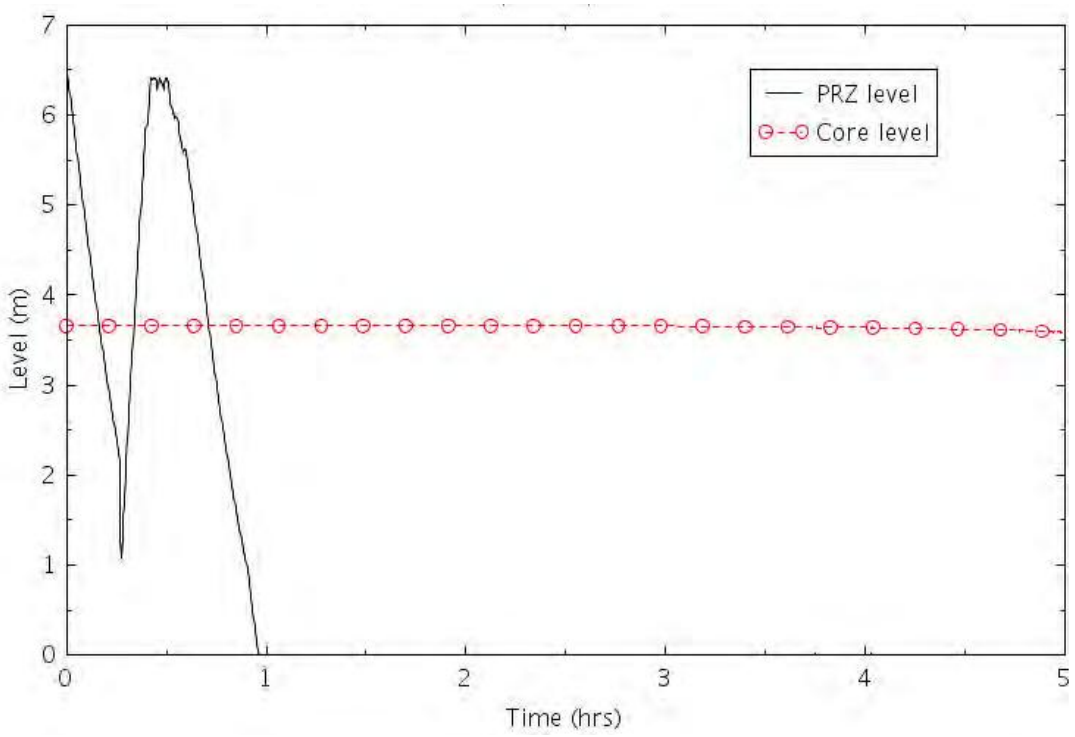

Figure 2-68. PRZ and Core Levels (SGTR-0).

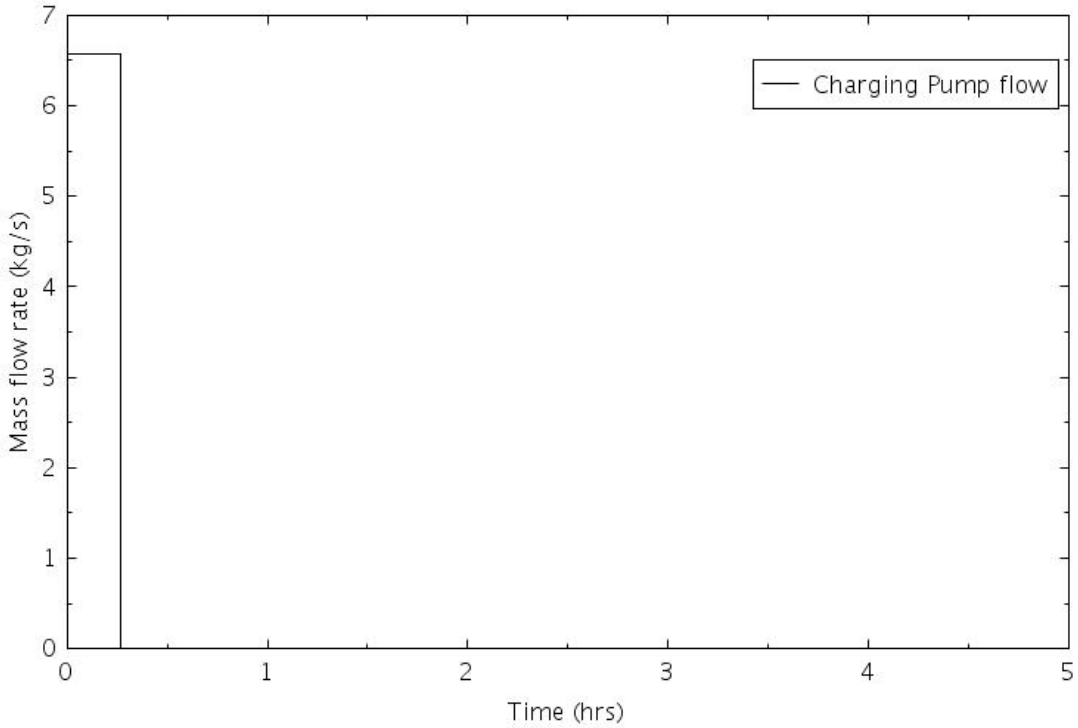

Figure 2-69. Charging Pump Flow (SGTR-0).

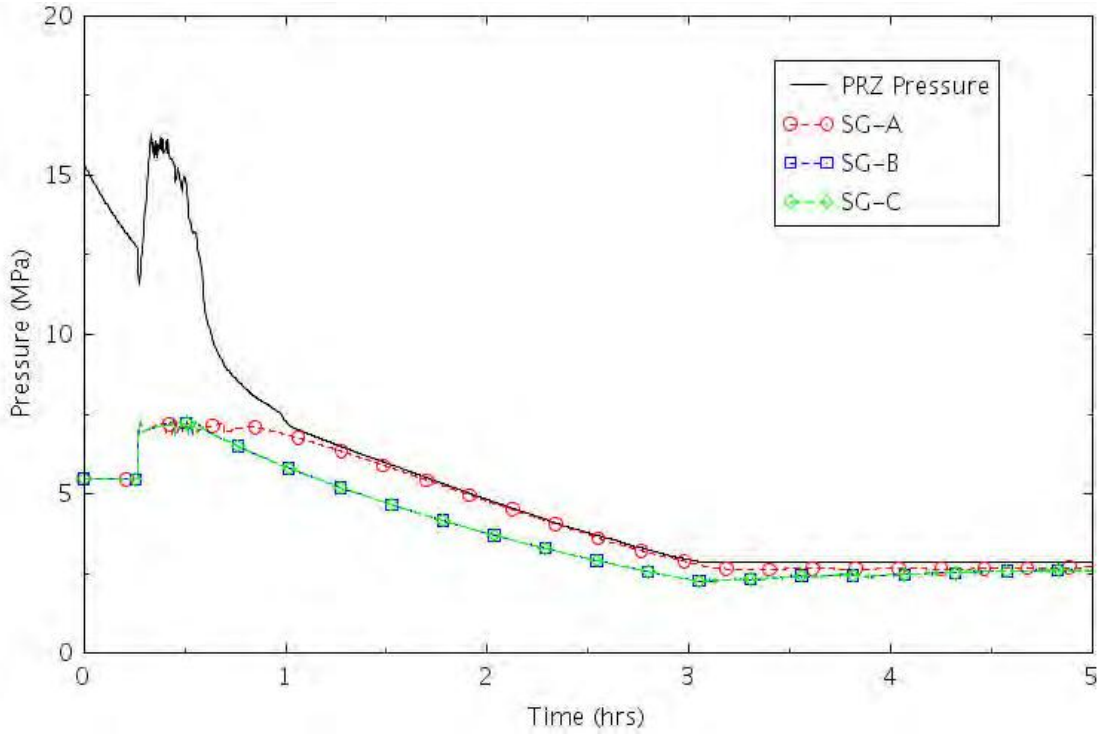

Figure 2-70. PRZ and SG Pressures (SGTR-0).

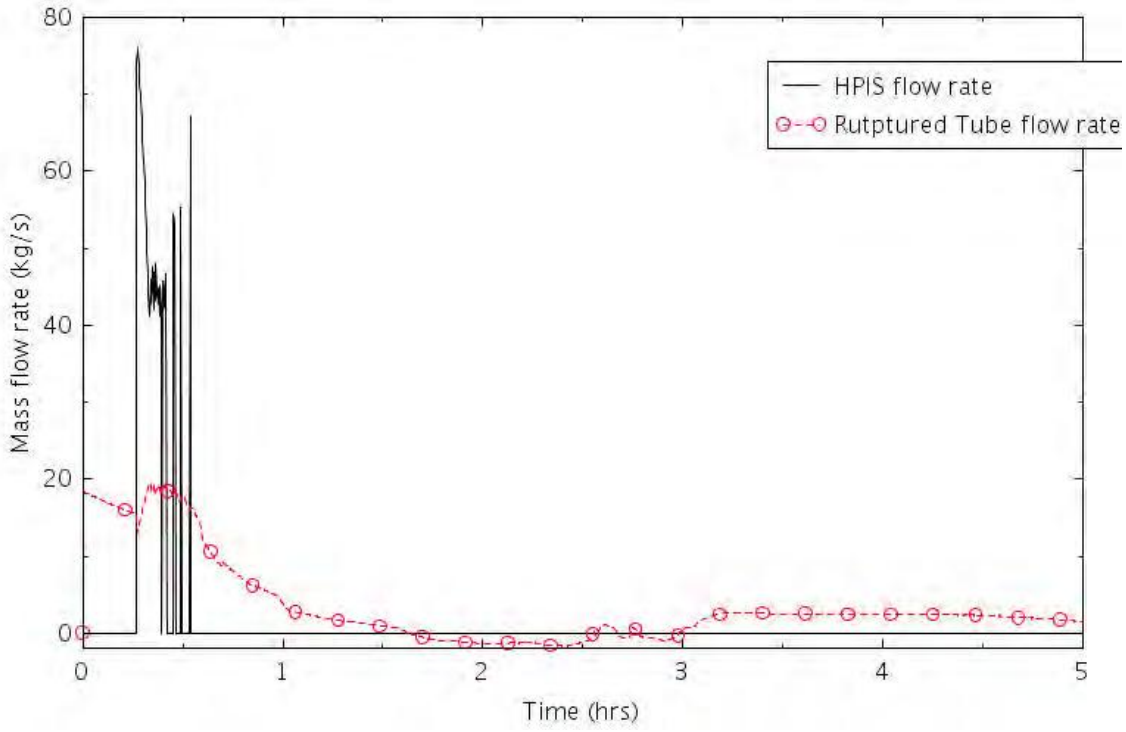

Figure 2-71. HPIS and SGTR Flow (SGTR-0).

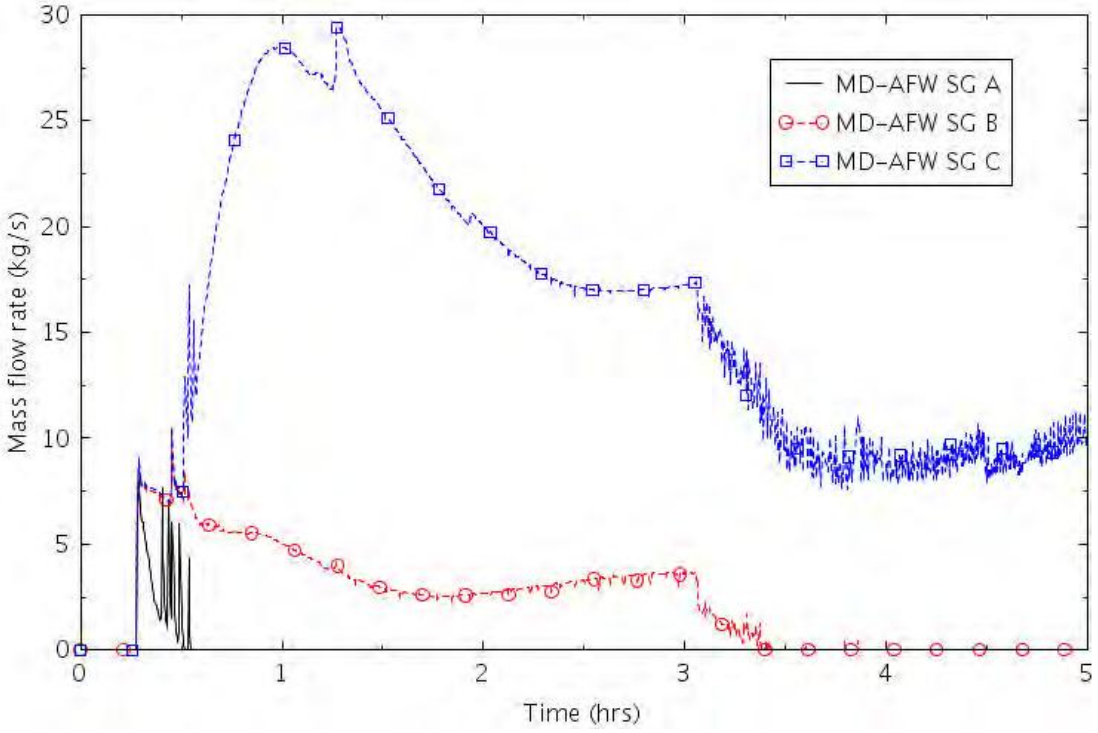

Figure 2-72. AFW Flow (SGTR-0).

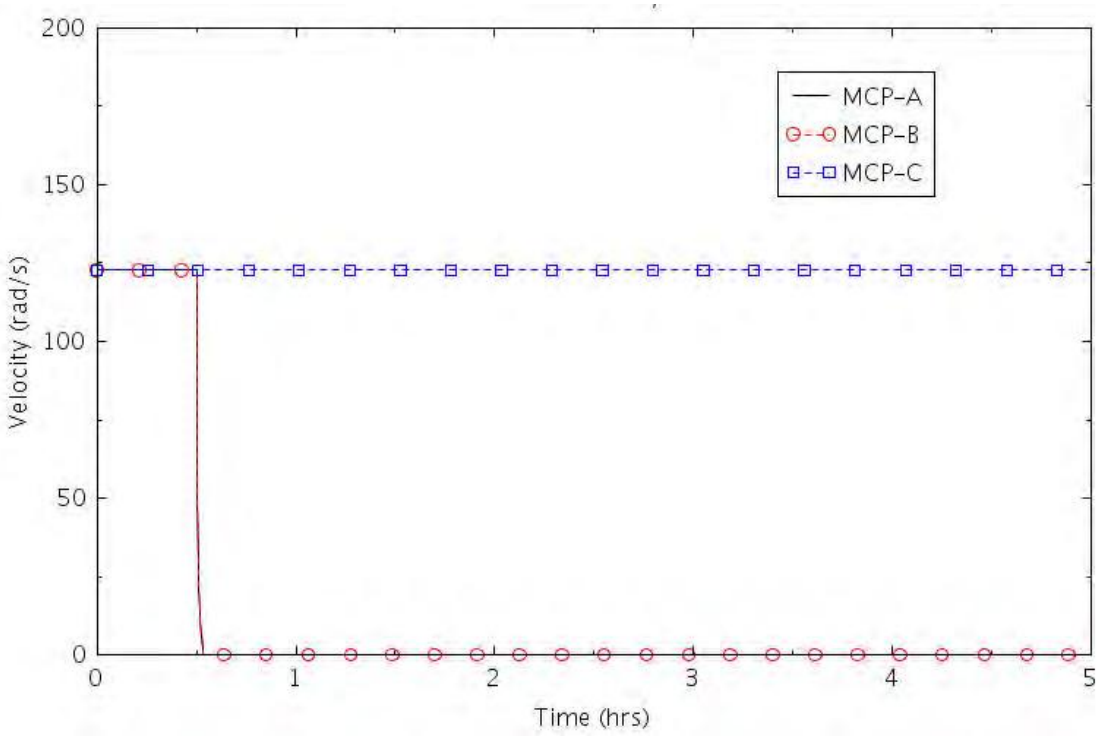

Figure 2-73. RCPs Velocity (SGTR-0).

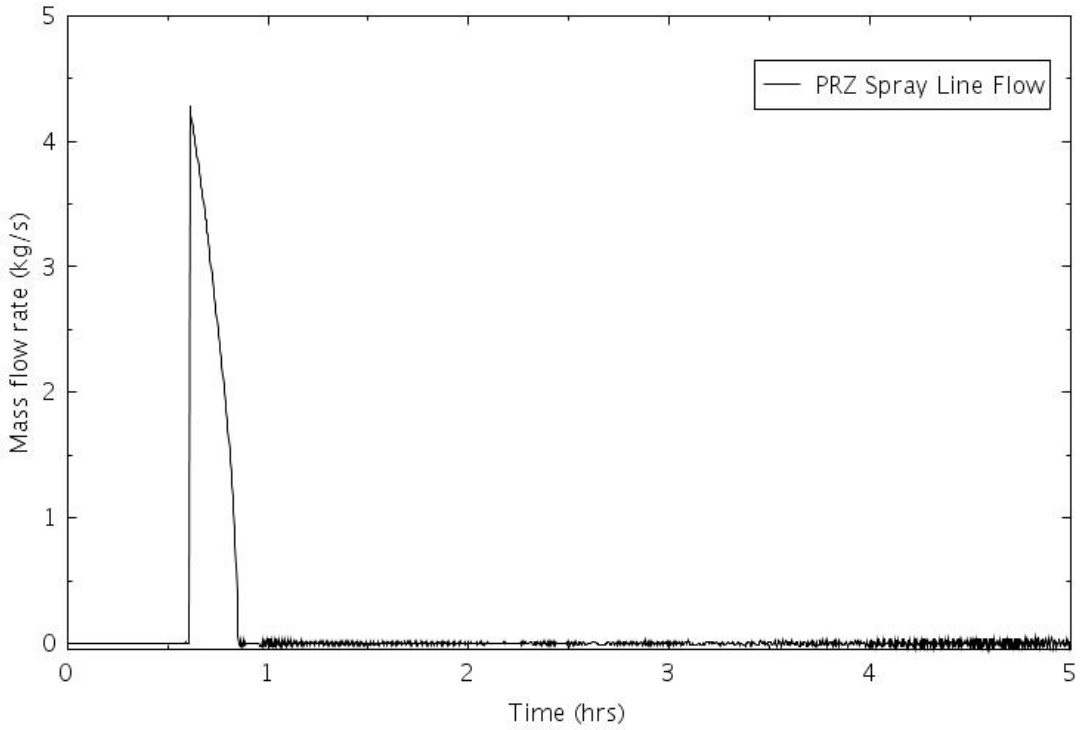

Figure 2-74. Spray Line Flow (SGTR-0).

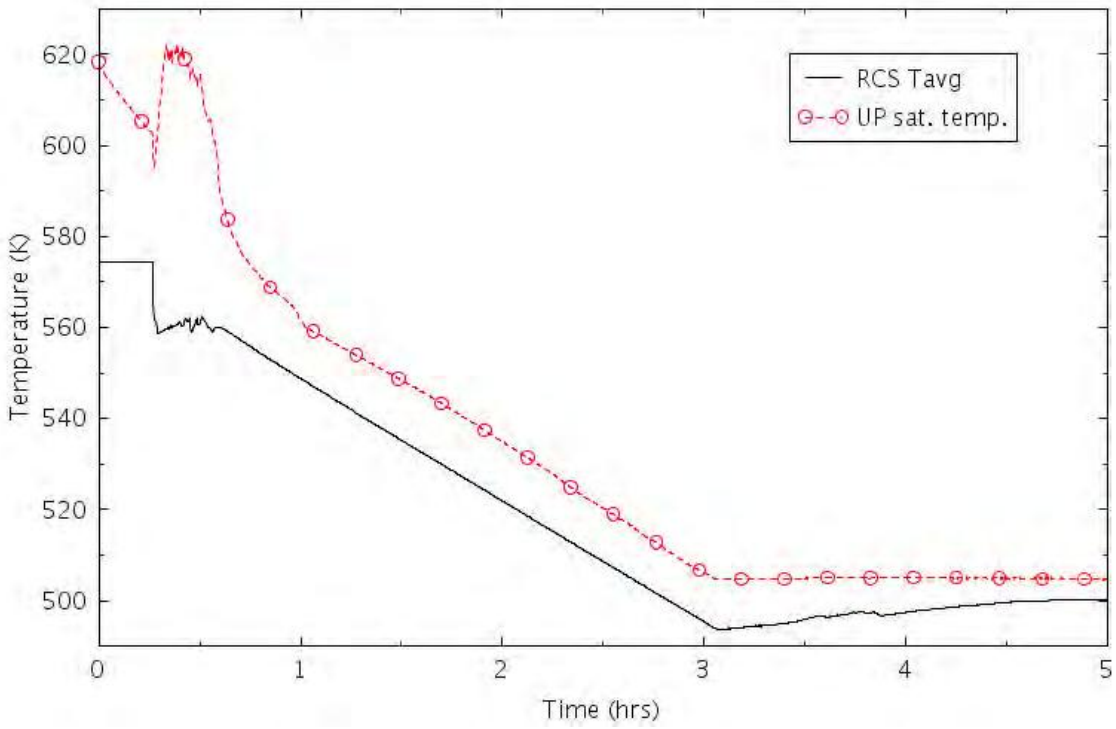

Figure 2-75. RCS Average Temperature and Upper Plenum Saturation Temperature (SGTR-0).

2.2.3.2 SGTR without HPI SGI (SGTR-1)

The first phase of SGTR-1 is similar to SGTR-0 (reactor scram for low PRZ pressure, TSV closure, termination of MFW, shutdown of charging pumps, startup of AFW after 30 seconds).

The sequence assumes that after the reactor trips and the SI signal, there are the following failures:

- No HPIS injection
- No primary/secondary cool-down
- No SG isolation.

After the operator identifies the ruptured SG, he stops MCP-A and MCP-B at t = 30 minutes and stabilizes the SG levels around the FW ring (11 meter) with the injection of AFW. Because of the energy removal from the SGs, the RCS's average temperature and pressure both decrease considerably.

The MCP-C eventually stops at t = 1 hour 46 minutes for high voids in the RCS. The RCS pressure reduction causes a decrease of the flow in the ruptured pipe of SG-A. By about 6 hours, because of the SG PORV actuation, the flow at the break oscillates allowing water ingress from the secondary to the primary side. This secondary-to-primary water ingress causes a stabilization of the core level, avoiding any core damage conditions during the first 48 hours of the transient.

Details of the timing of the events are reported in Table 2-22 and in the following figures.

Table 2-22. Sequence of Events for Scenario SGTR-1.

Event	Timing (hr:min)
SG tube rupture. PRZ level and pressure fall, start of charging pumps	00:00
Reactor trip for PRZ low-pressure. Reactor shutdown, closure of TSV	00:16
SI signal for PRZ low-low pressure. Stop of MFW	00:16
Start-up of AFW pumps	00:16
Shutdown of MCP for loop-A and B	00:30
Depressurization of SG-B and C using Steam-Dump	N/A
MCP-C stops for high voids	01:46
SGTR mass flow reversal	06:00
RCS temperature stable. End of transient simulation	48:00

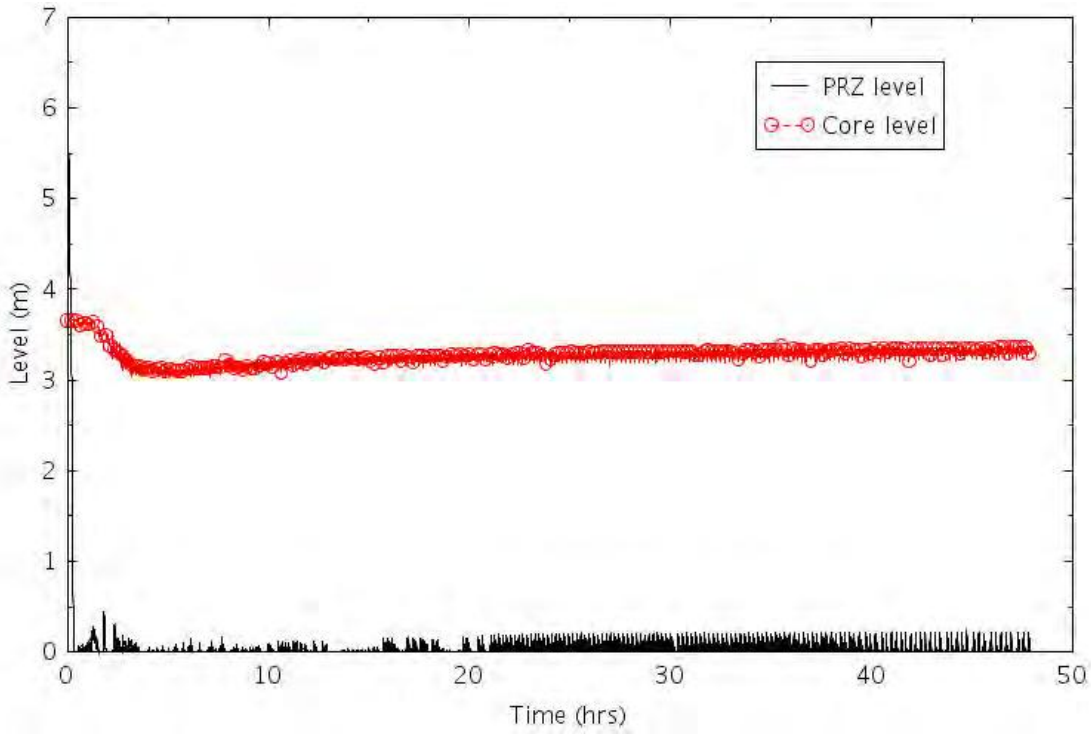

Figure 2-76. PRZ and Core Levels (SGTR-1).

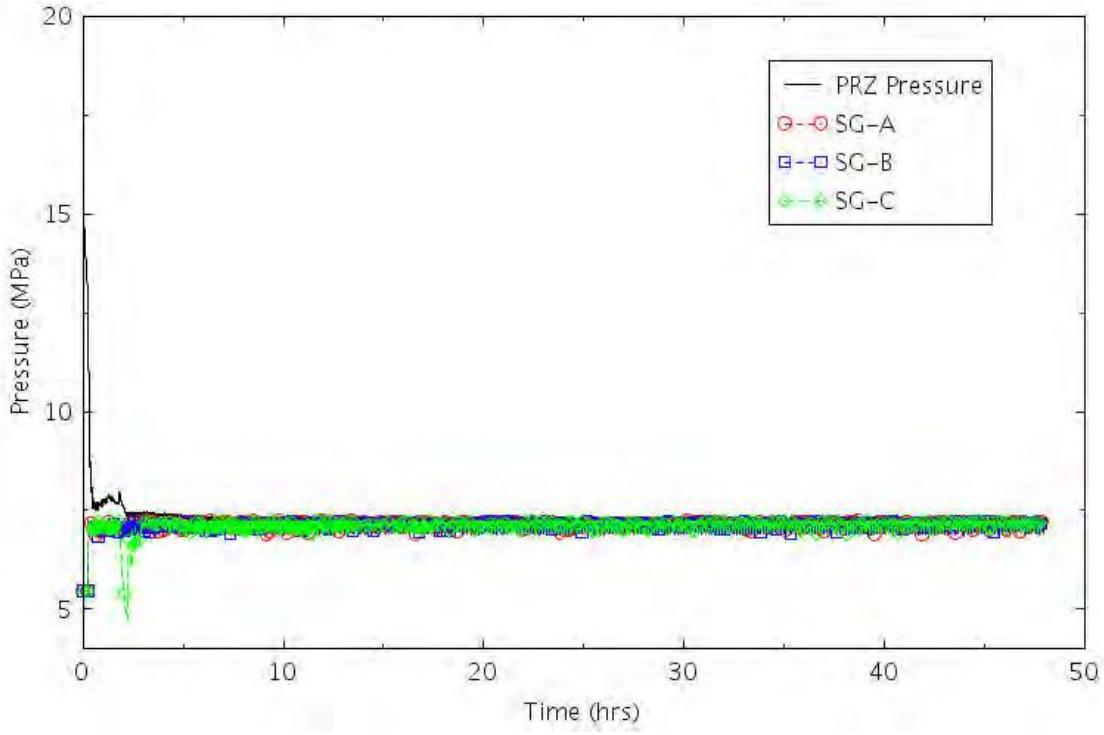

Figure 2-77. PRZ and SG Pressures (SGTR-1).

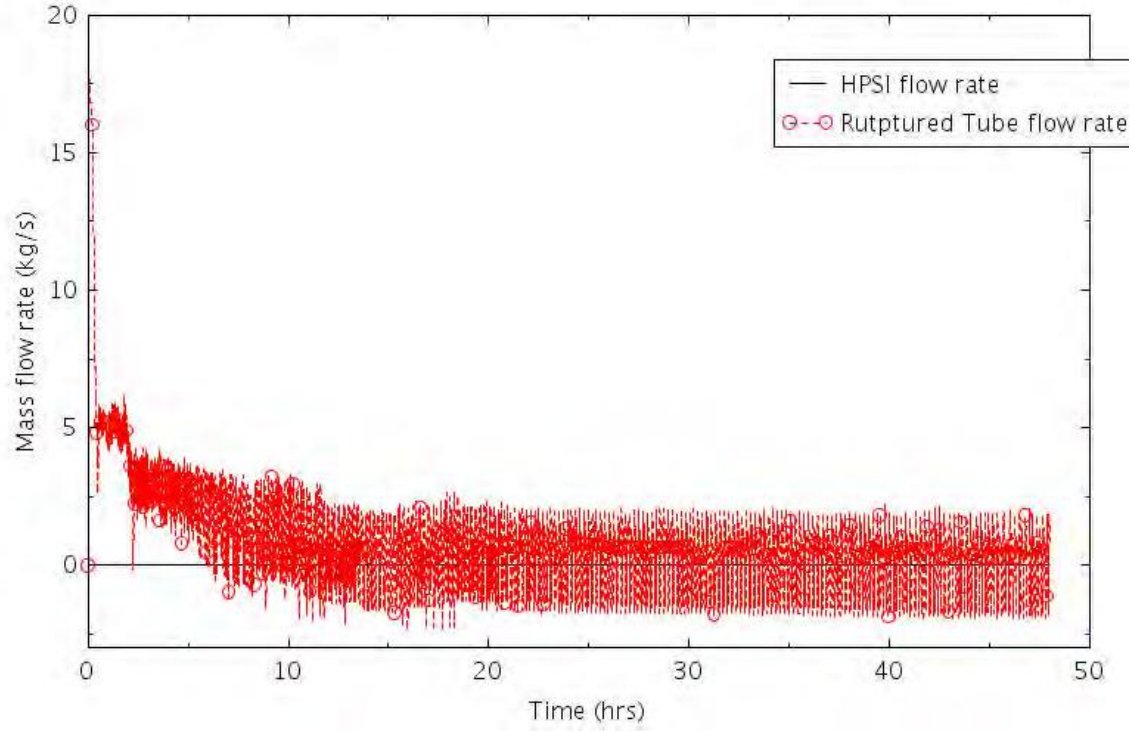

Figure 2-78. HPIS and SGTR Flow (SGTR-1).

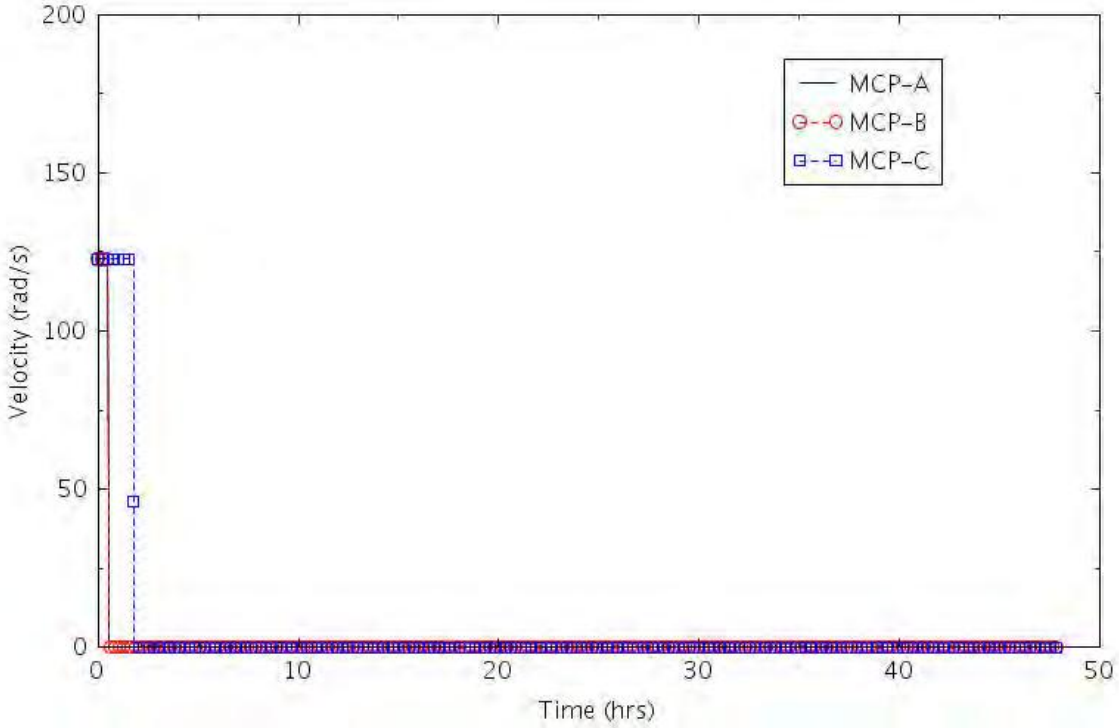

Figure 2-79. RCPs Velocity (SGTR-1).

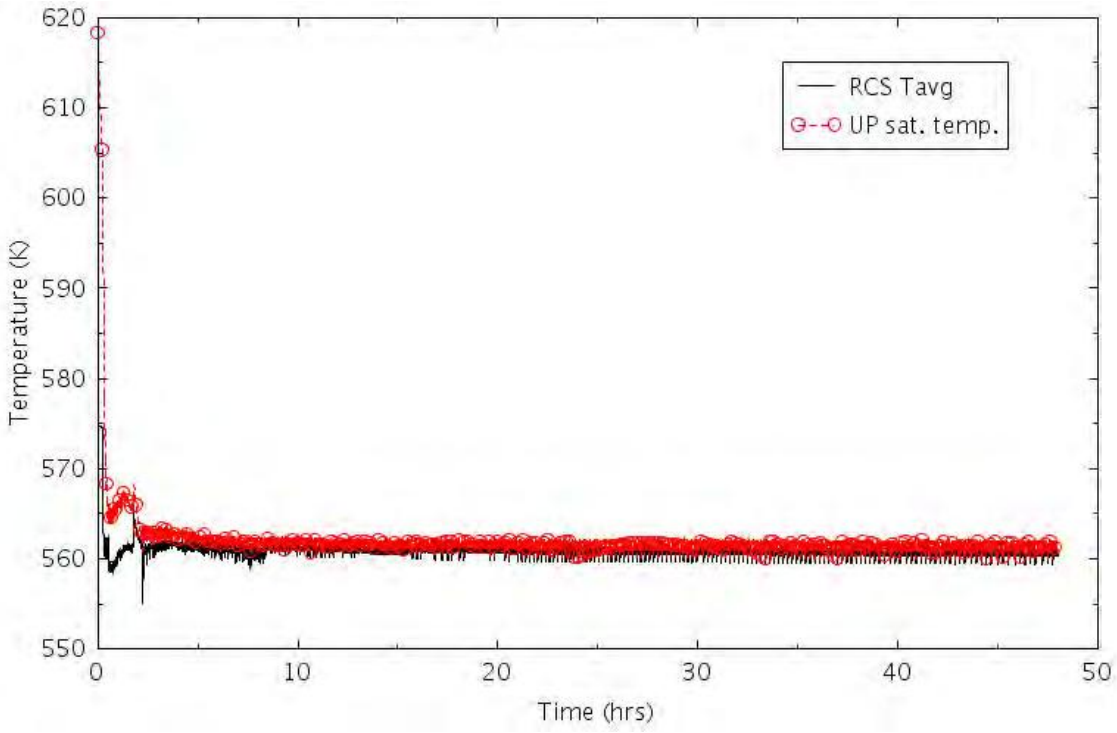

Figure 2-80. RCS Average Temperature and Upper Plenum Saturation Temperature (SGTR-1).

2.2.3.3 SGTR without HPI SSC (SGTR-2)

The first phase of SGTR-2 is similar to SGTR-0 (reactor scram for low PRZ pressure, TSV closure, termination of MFW, shutdown of charging pumps, and the startup of AFW after 30 seconds).

The sequence assumes that after the reactor trips and the SI signal, the following failures occur:

- No HPIS injection
- No primary/secondary cool-down.

The sequence is similar to SGTR-1, the only difference being the faulted SG is not isolated in SGTR-1 but it is isolated in SGTR-2. The trend of the main parameters and the timing is similar to SGTR-1, so no further information is reported.

2.2.3.4 SGTR without HPI RHR (SGTR-3)

The first phase of SGTR-3 is similar to SGTR-0 (reactor scram for low PRZ pressure, TSV closure, termination of MFW, shutdown of charging pumps, and the startup of AFW after 30 seconds).

The sequence assumes after the reactor trips and the SI signal, there are the following failures:

- No HPIS injection
- No RHR for long-term cooling.

The sequence also assumes the successful isolation of the faulted SG and the primary/secondary cooldown.

After the operator identifies the ruptured SG, he isolates it at t = 30 minutes, then he stops MCP-A and MCP-B at t = 35 minutes, and he stabilizes the SG levels around the FW ring (11 meter) with the injection of AFW. He then actuates the PRZ spray for depressurizing the RCS at about 36 minutes. He finally performs the primary/secondary cooldown at t = 40 minutes by opening the SD valves.

Because the energy removal from the SD, the RCS average temperature and pressure both decrease. The pressure differential between the RCS and the secondary side of the faulted SG is considerably reduced, so that the flow at the rupture is decreased, becoming also negative.

The MCP-C eventually stops at t = 4 hours, 4 minutes for high voids in the RCS. Provided that AFW flow continues, and also considering the additional failure of the RHR, no core damage conditions are found during the first 48 hours of the transient.

Details of the timing of the events are reported in Table 2-23 and in the following figures.

Table 2-23. Sequence of Events for Scenario SGTR-3.

Event	Timing (hr:min)
SG tube rupture. PRZ level and pressure fall, start of charging pumps.	00:00
Reactor trip for PRZ low-pressure. Reactor shutdown, closure of TSV.	00:16
SI signal for PRZ low-low pressure. Stop of MFW.	00:16
Start-up of AFW pumps.	00:16
SG-A isolation.	00:30
MCP trip for loop-A and B.	00:35
Actuation of the PRZ sprays.	00:36
Depressurization of SG-B and C using Steam-Dump.	00:40
SGTR mass flow reversal.	01:18
MCP trip for loop-C.	04:04
RCS temperature stable. End of transient simulation.	48:00

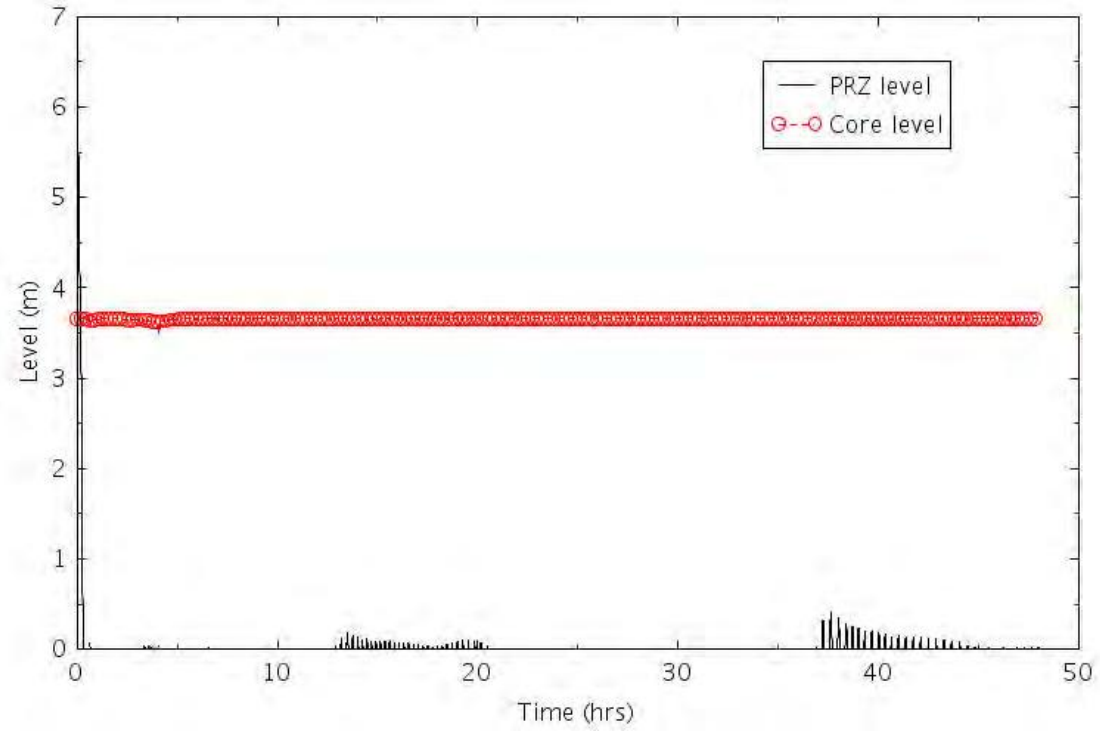

Figure 2-81. PRZ and Core Levels (SGTR-3).

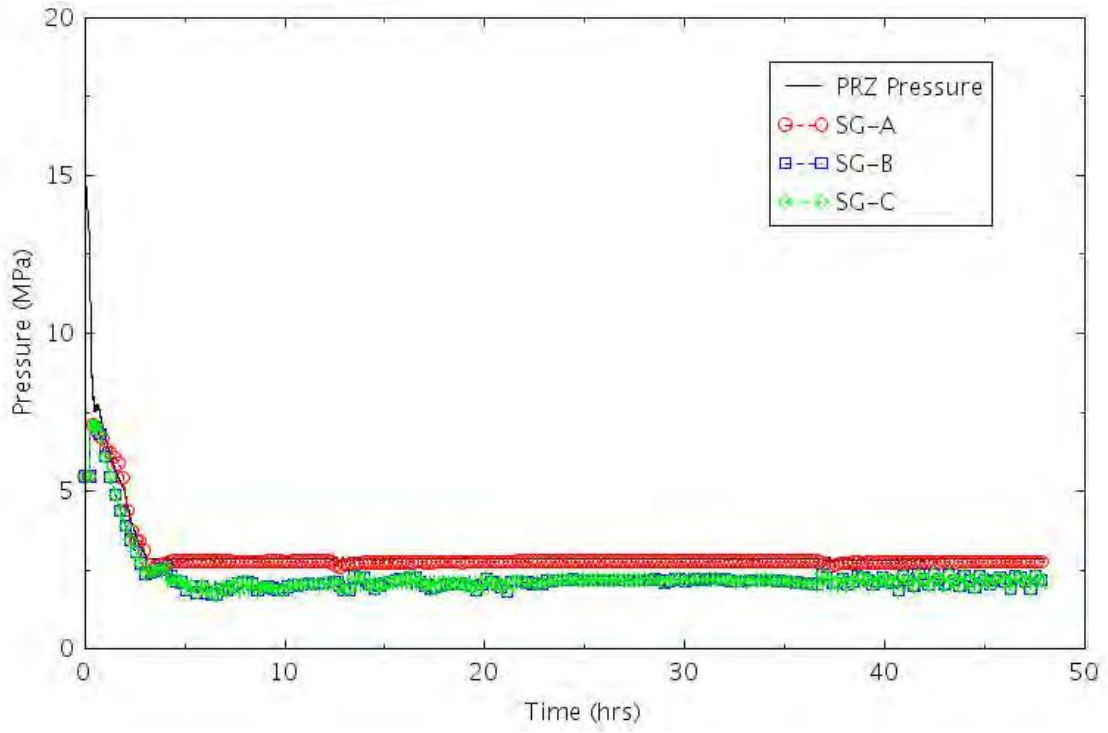

Figure 2-82. PRZ and SG Pressures (SGTR-3).

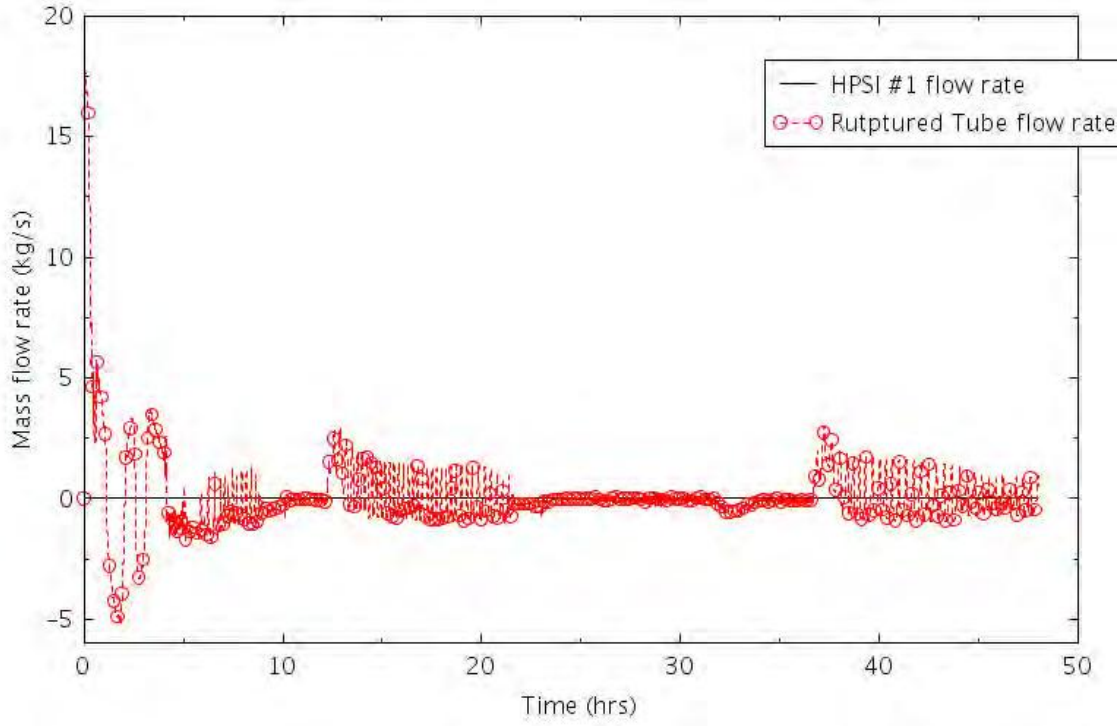

Figure 2-83. HPIS and SGTR Flow (SGTR-3).

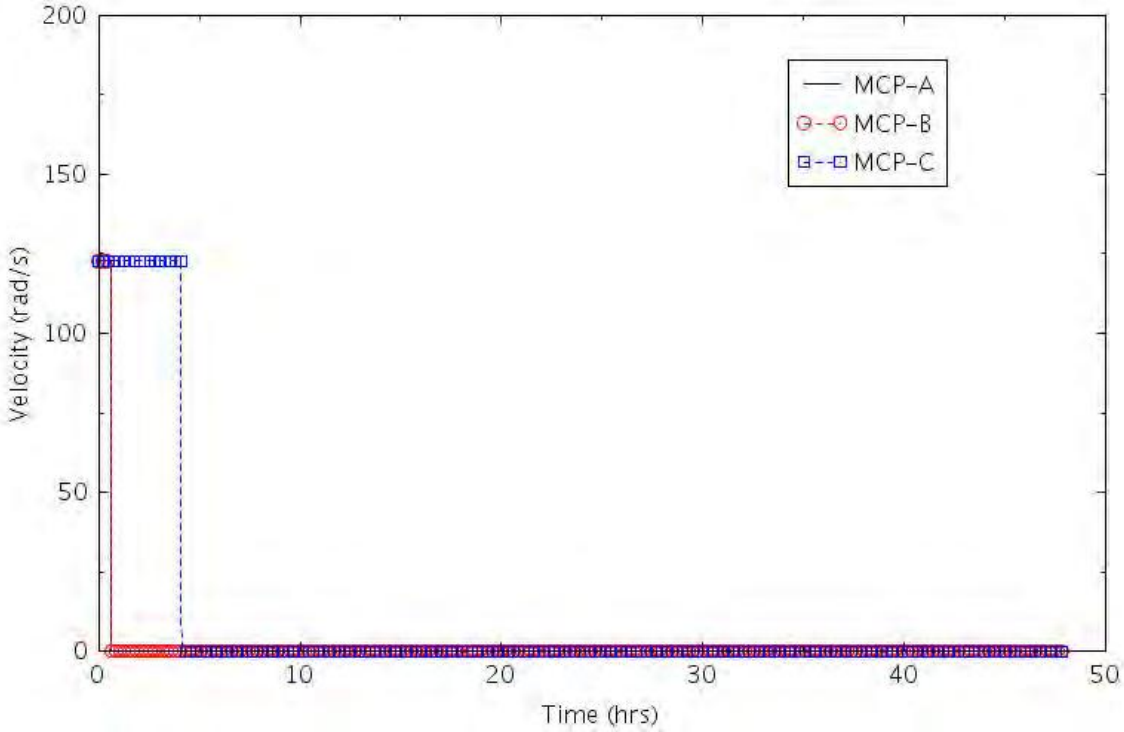

Figure 2-84. RCPs Velocity (SGTR-3).

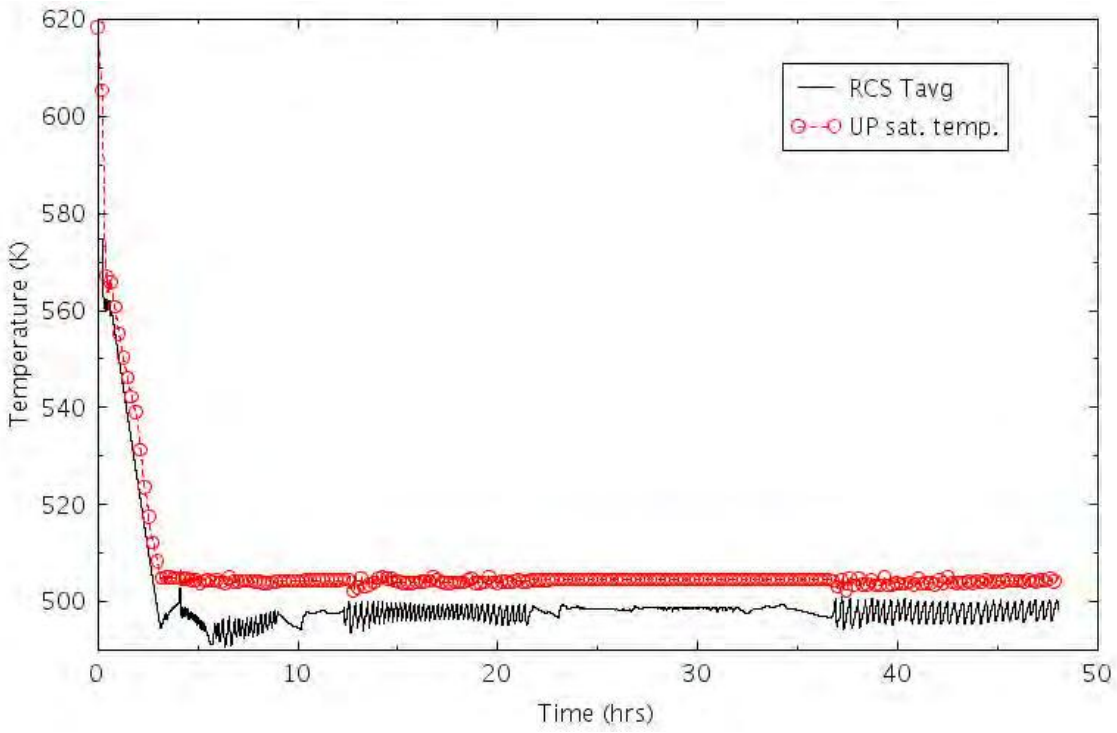

Figure 2-85. RCS Average Temperature and Upper Plenum Saturation Temperature (SGTR-3).

2.2.3.5 SGTR with HPI No SGI (SGTR-4)

The first phase of SGTR-4 is similar to SGTR-0 (reactor scram for low PRZ pressure, TSV closure, termination of MFW, shutdown of charging pumps, the startup of AFW after 30 seconds, and the startup of HPIS).

The sequence assumes that after the reactor trips and the SI signal there are the following failures:

- No SG isolation
- No RWST refilling.

The sequence also assumes the primary/secondary cooldown.

The operator fails to isolate the faulted SG. However, he stops MCP-A and MCP-C at t = 30 minutes, and he stabilizes the SGs levels around the FW ring (11 meter) with the injection of AFW. He then actuates the PRZ spray for depressurizing the RCS at t = ~36 minutes. Since there is no SG isolation, no cooldown by opening the SD valves is assumed.

The continuous injections from the HPIS and (on the secondary side) from the AFW, guarantee a stable RCS temperature and pressure. The reduced pressure differential between the RCS and the secondary side of the faulted SG allows the reduction of the flow at the rupture, which stays positive during the whole mission time.

The MCP-C eventually stops at t = 2 hours, 50 minutes for high voids in the RCS. Since RWST is not exhausted in 48 hours and the ECST is refilled, and also considering no actuation of the SD cooling, no core damage conditions are found during the first 48 hours of the transient.

Details of the timing of the events are reported in Table 2-24 and in the following figures.

Table 2-24. Sequence of Events for Scenario SGTR-4.

Event	Timing (hr:min)
SG tube rupture. PRZ level and pressure fall, start of charging pumps.	00:00
Reactor trip for PRZ low-pressure. Reactor shutdown, closure of TSV.	00:16
SI signal for PRZ low-low pressure. Stop of MFW.	00:16
Start-up of AFW pumps.	00:16
SG-A isolation.	N/A
MCP trip for loop-A and B.	00:35
Actuation of the PRZ sprays.	00:36
Depressurization of SG-B and C using Steam-Dump.	N/A
MCP trip for loop-C.	02:50
RCS temperature stable. End of transient simulation.	48:00

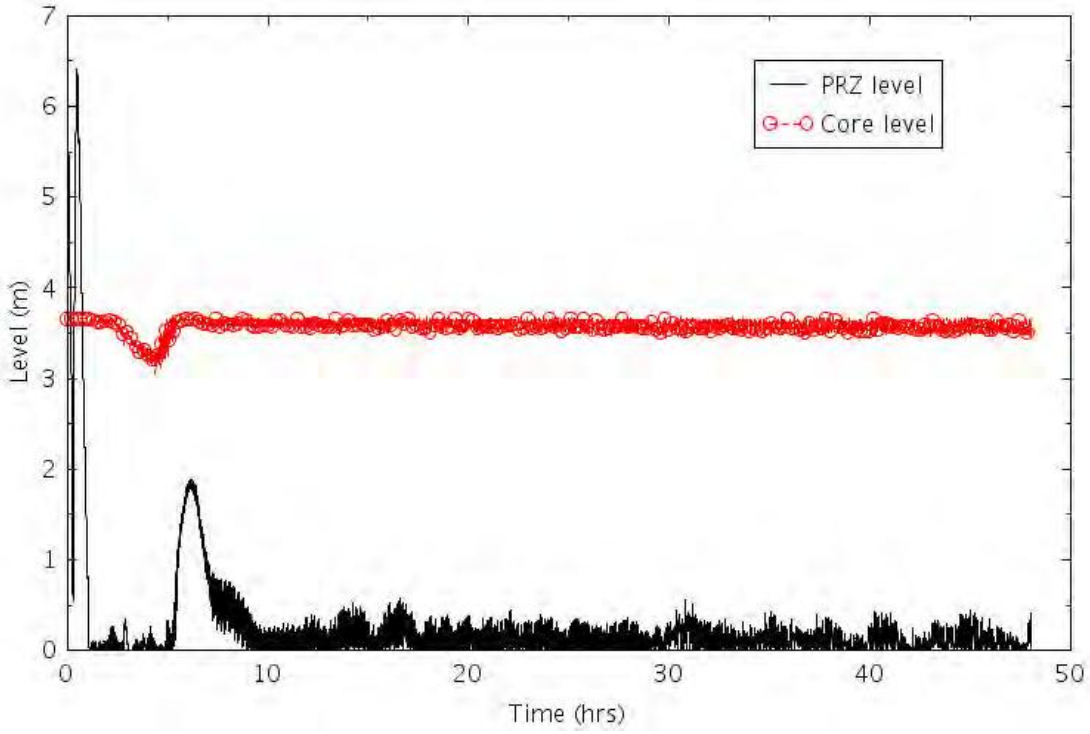

Figure 2-86. PRZ and Core Levels (SGTR-4).

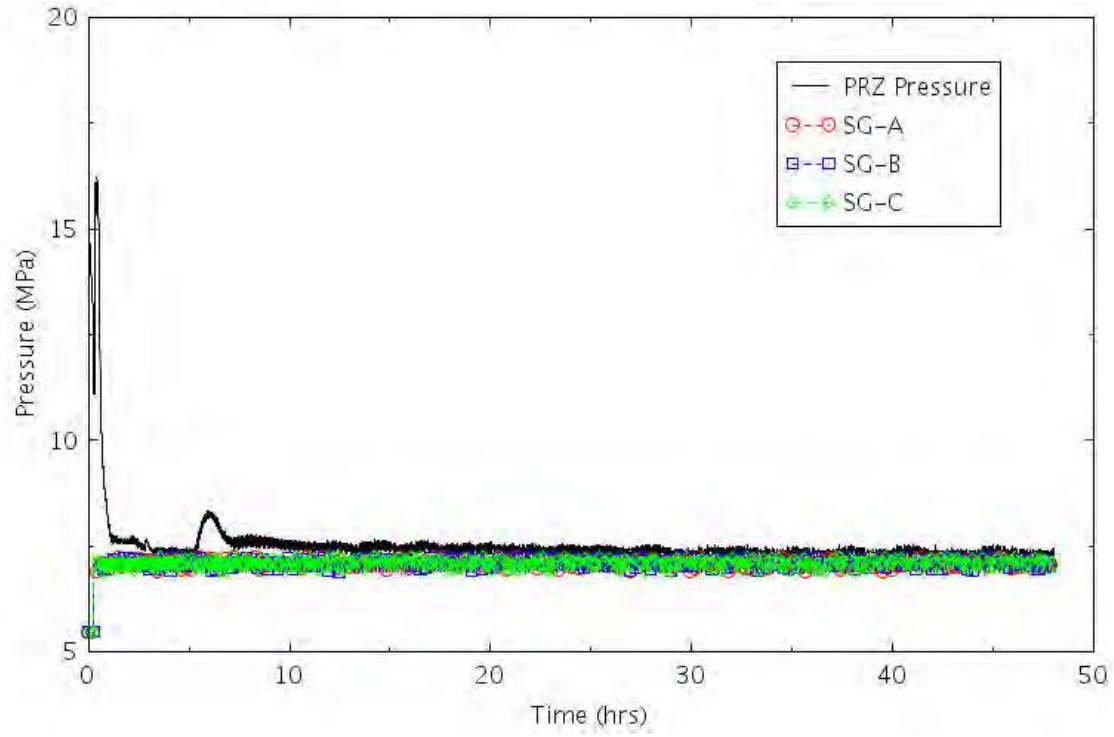

Figure 2-87. PRZ and SG Pressures (SGTR-4).

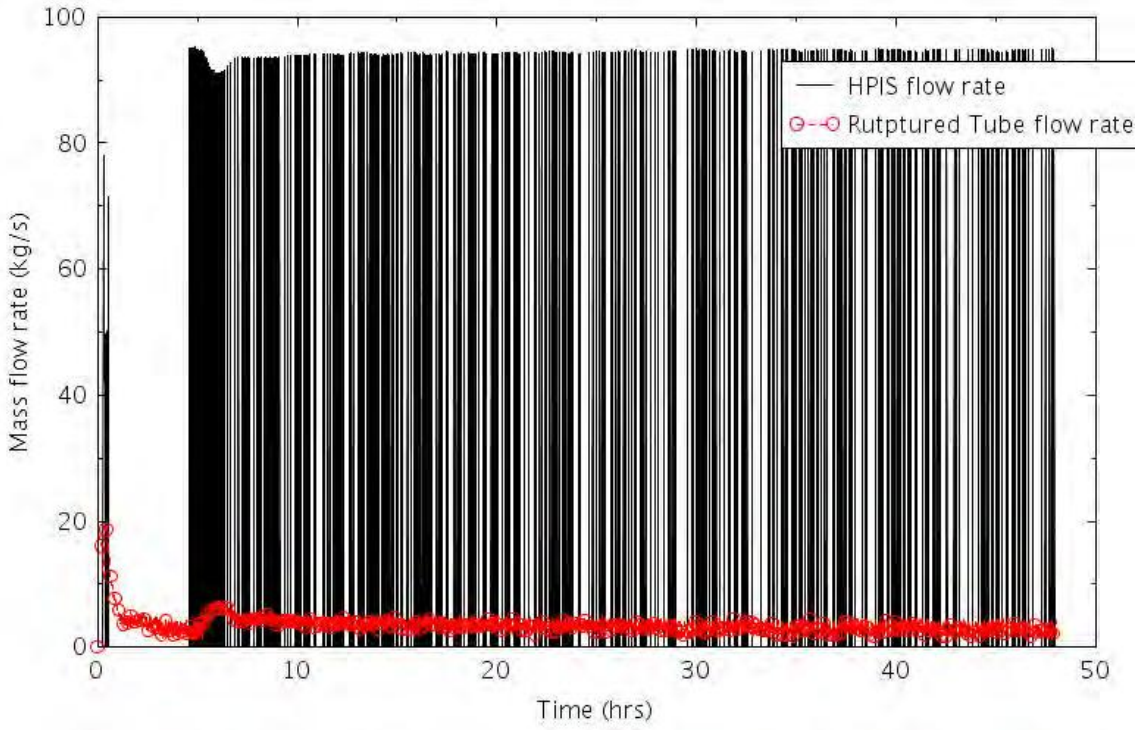

Figure 2-88. HPIS and SGTR Flow (SGTR-4).

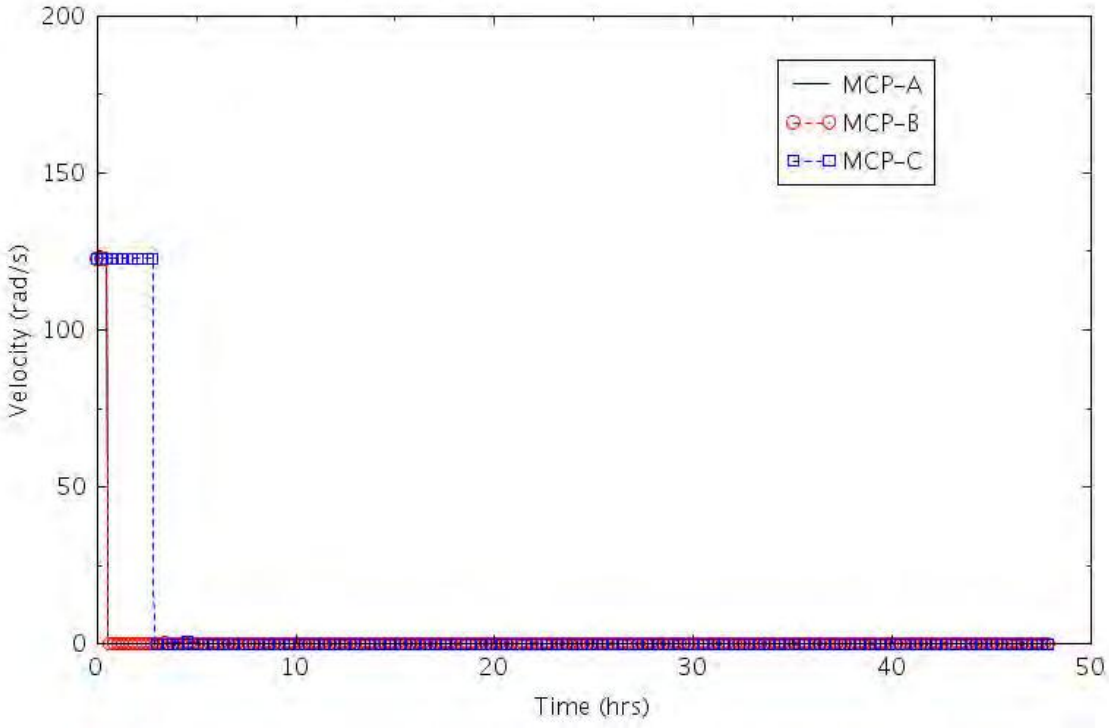

Figure 2-89. RCPs Velocity (SGTR-4).

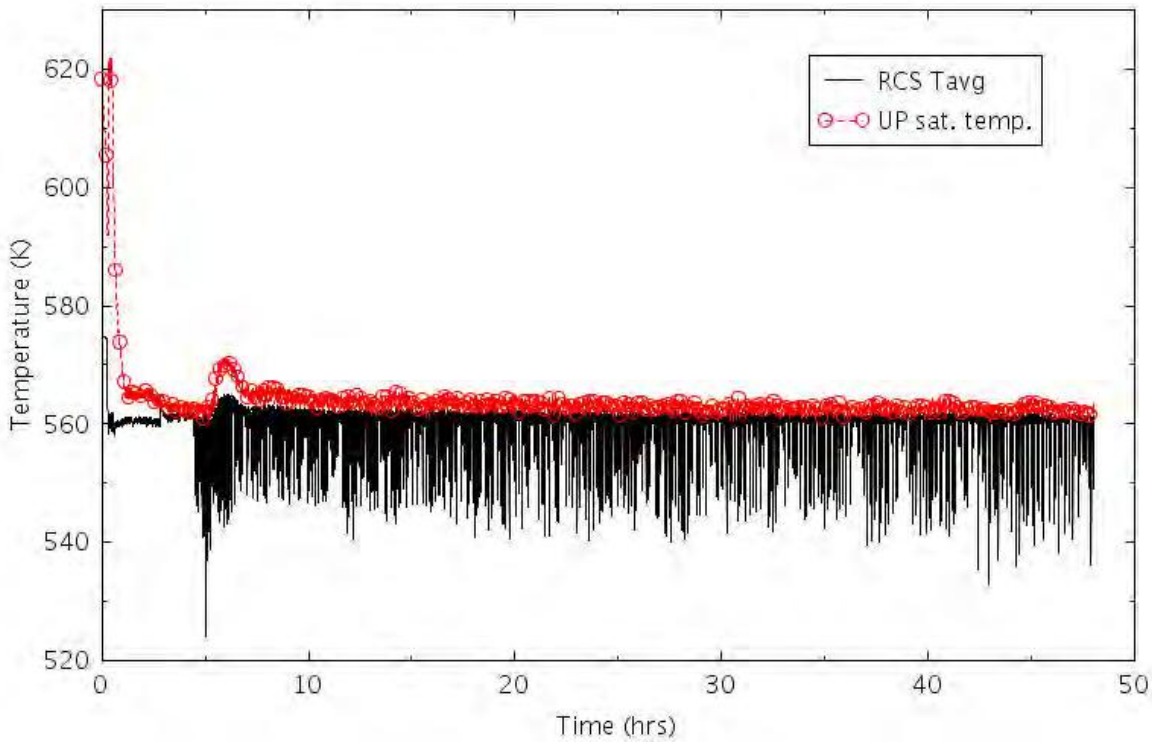

Figure 2-90. RCS Average Temperature and Upper Plenum Saturation Temperature (SGTR-4).

2.2.3.6 SGTR with HPI No SSC (SGTR-5)

The first phase of SGTR-5 is similar to SGTR-0 (reactor scram for low PRZ pressure, TSV closure, termination of MFW, shutdown of charging pumps, startup of AFW after 30 seconds, startup of HPIS pumps).

The sequence assumes that after the reactor trips and the SI signal, there are the following failures:

- No primary/secondary cooling
- No RWST refilling.

The difference with SGTR-4 is, in this case, the operator succeeds in isolating the faulted SG at t = 30 minutes, stopping at the same time MCP-A and MCP-B and stabilizing the SG levels around the FW ring (11 meter) with the injection of AFW. He then actuates the PRZ spray for depressurizing the RCS at t =~36 minutes.

The continuous injection from the HPIS and (on the secondary side) from the AFW, guarantees a stable RCS temperature and pressure. The reduced pressure differential between the RCS and the secondary side of the faulted SG allows the reduction of the flow at the rupture, which stays positive for the whole transient.

The MCP-C eventually stops at t = 2 hours, 49 minutes for high voids in the RCS. Provided that AFW flow continues, and also considering the additional failure of the RHR, no core damage conditions are found during the first 48 hours of the transient.

Details of the timing of the events are reported in Table 2-25 and in the following figures.

Table 2-25. Sequence of Events for Scenario SGTR-5.

Event	Timing (hr:min)
SG tube rupture. PRZ level and pressure fall, start of charging pumps.	00:00
Reactor trip for PRZ low-pressure. Reactor shutdown, closure of TSV.	00:16
SI signal for PRZ low-low pressure. Stop of MFW.	00:16
Start-up of AFW pumps.	00:16
SG-A isolation.	00:30
MCP trip for loop-A and B.	00:35
Actuation of the PRZ sprays.	00:36
Depressurization of SG-B and C using Steam-Dump.	N/A
MCP trip for loop-C.	02:49
RCS temperature stable. End of transient simulation.	48:00

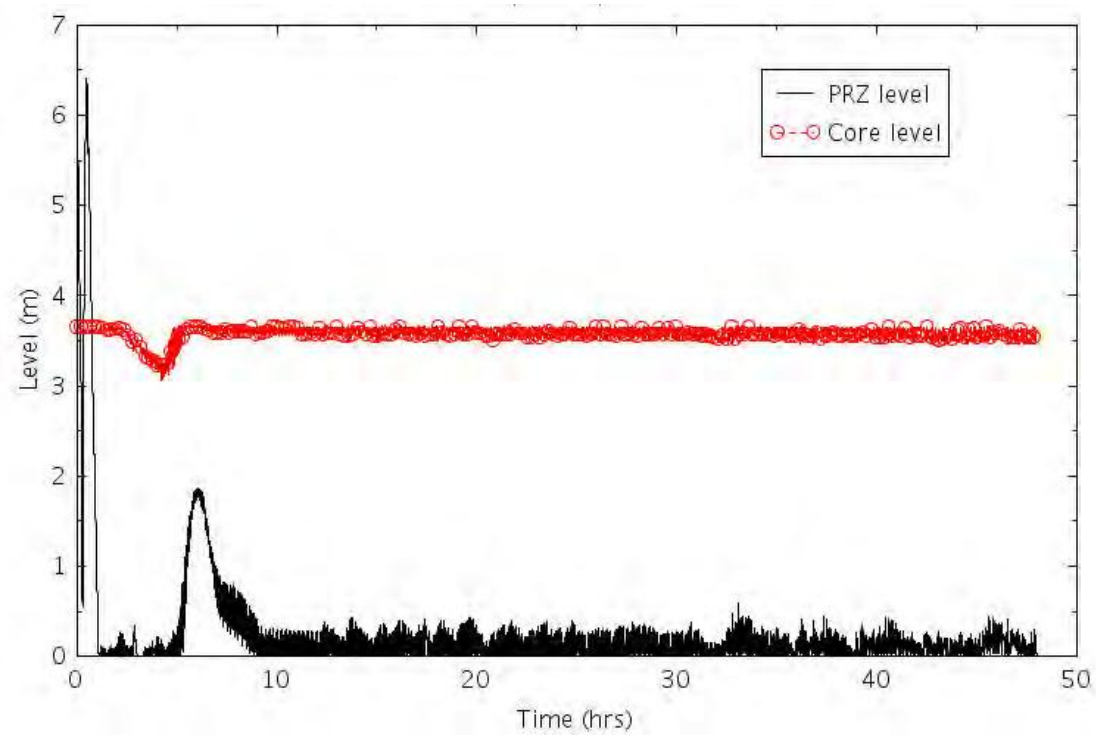

Figure 2-91. PRZ and Core Levels (SGTR-5).

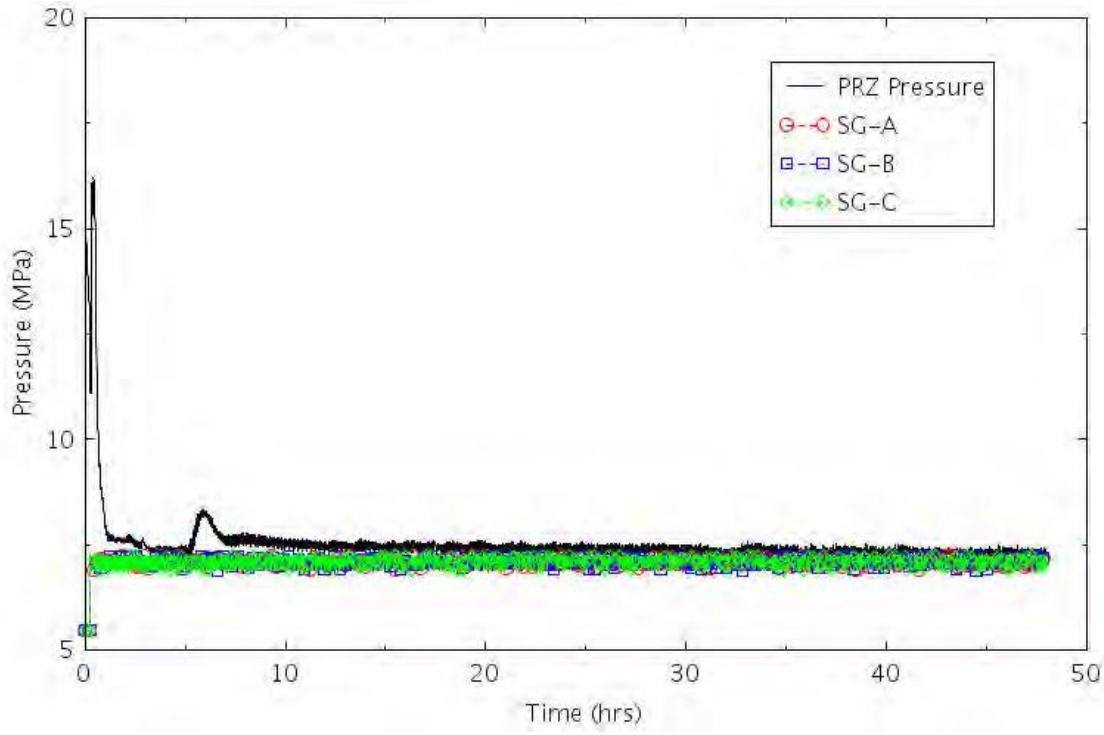

Figure 2-92. PRZ and SG Pressures (SGTR-5).

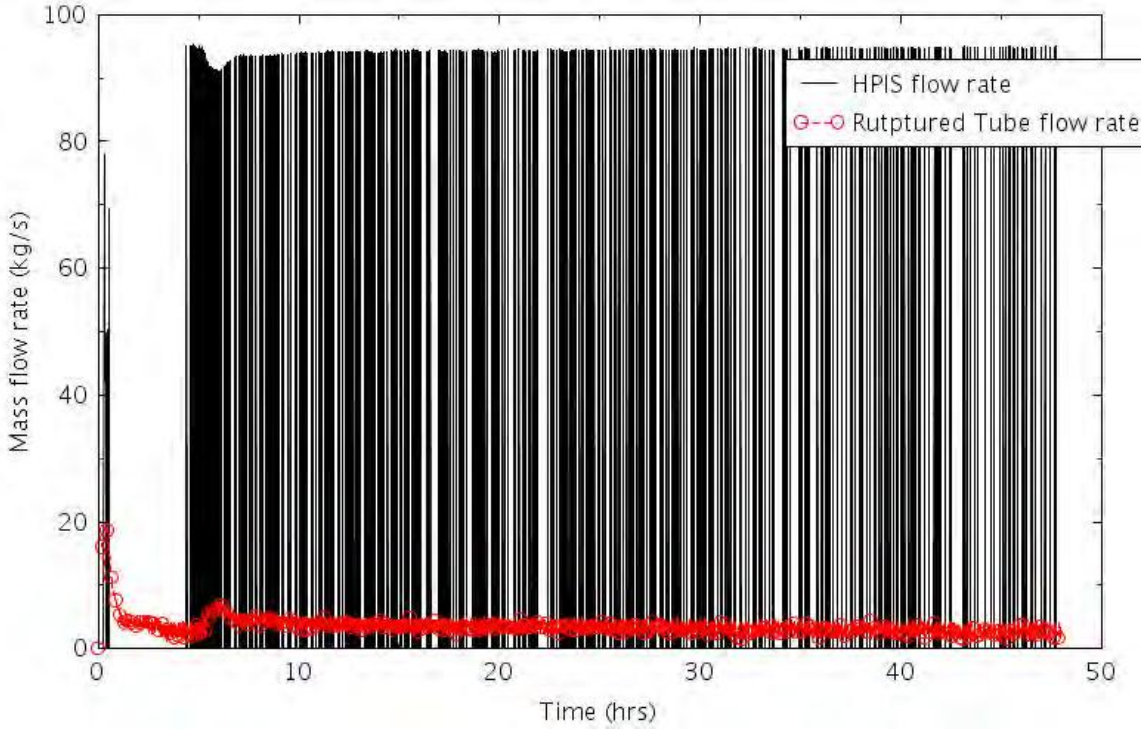

Figure 2-93. HPIS and SGTR Flow (SGTR-5).

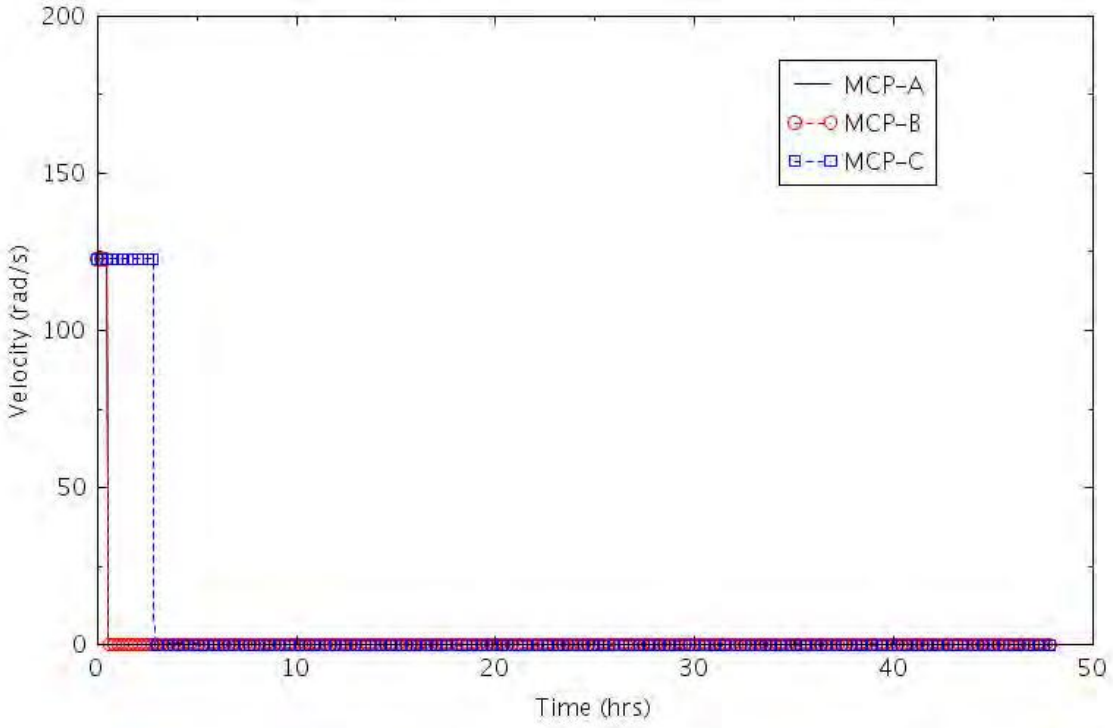

Figure 2-94. RCPs Velocity (SGTR-5).

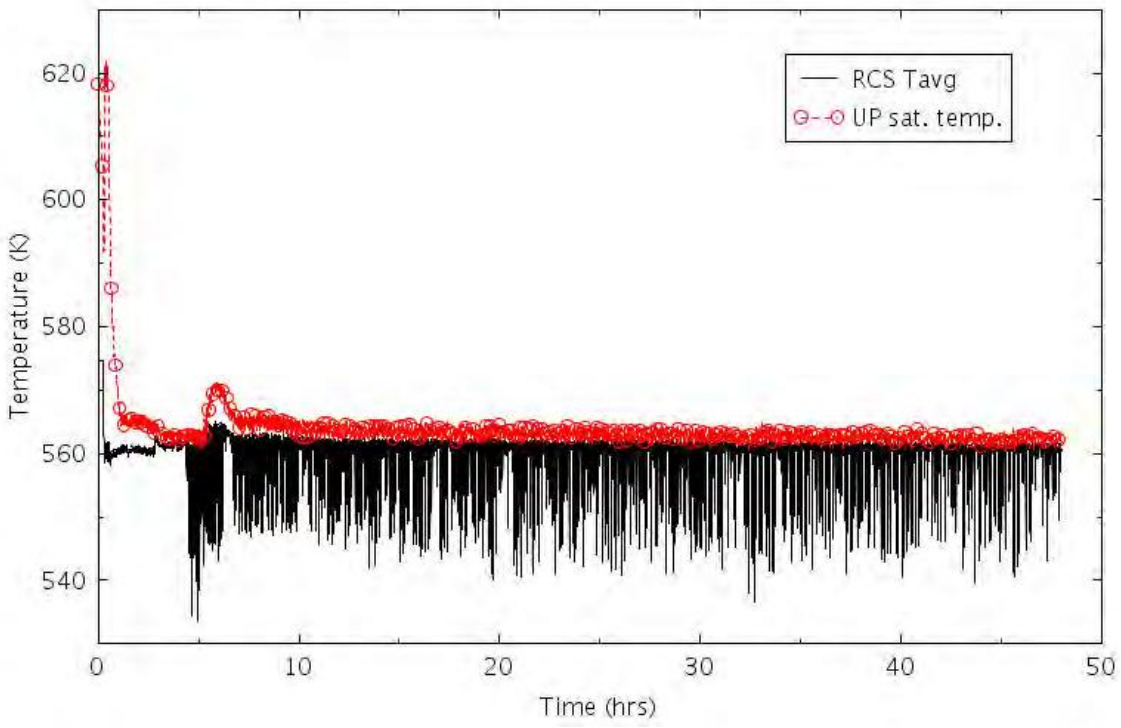

Figure 2-95. RCS Average Temperature and Upper Plenum Saturation Temperature (SGTR-5).

2.2.3.7 SGTR with HPI No CSI (SGTR-6)

The first phase of SGTR-6 is similar to SGTR-0 (reactor scram for low PRZ pressure, TSV closure, termination of MFW, shutdown of charging pumps, startup of the AFW after 30 seconds, and startup of HPIS pumps).

The sequence assumes that after the reactor trips and the SI signal, there are the following failures:

- No control of HPIS injection
- No RWST refilling.

The sequence also assumes the success of primary/secondary cooldown.

After the operator identifies the ruptured SG, he isolates it at t = 30 minutes, stopping at the same time MCP-A and MCP-B and stabilizing the SG levels around the FW ring (11 meter) with the injection of AFW. He then actuates the PRZ spray for depressurizing the RCS at t = ~36 minutes. No control of the HPIS is assumed, so the pumps are assumed to inject to their maximum flow.

Because of the energy removal from the SD, the RCS average temperature decreases, but the RCS stays high because of the HPIS injection. The non-faulted SGs are depressurized while the faulted SG stays at high pressure because of the rupture flow and the SG's isolation. The pressure differential between the RCS and the SG-A stays high, keeping a sustained flow at the ruptured tube, until there is an HPIS injection. After RWST depletion, the HPIS injection terminates and the flow in the ruptured tube goes to values close to zero.

Provided that AFW flow continues, no core damage conditions are found during the first 48 hours of the transient.

Details of the timing of the events are reported in Table 2-26 and in the following figures.

Table 2-26. Sequence of Events for Scenario SGTR-6.

Event	Timing (hr:min)
SG tube rupture. PRZ level and pressure fall, start of charging pumps.	00:00
Reactor trip for PRZ low-pressure. Reactor shutdown, closure of TSV.	00:16
SI signal for PRZ low-low pressure. Stop of MFW.	00:16
Start-up of 1 MD-AFW pumps.	00:16
SG-A isolation.	00:30
MCP trip for loop-A and B.	00:35
Actuation of the PRZ sprays.	00:36
Depressurization of SG-B and C using Steam-Dump.	00:40
RWST empty. HPIS stops. SGTR mass flow to zero.	07:46
RCS temperature stable. End of transient simulation.	48:00

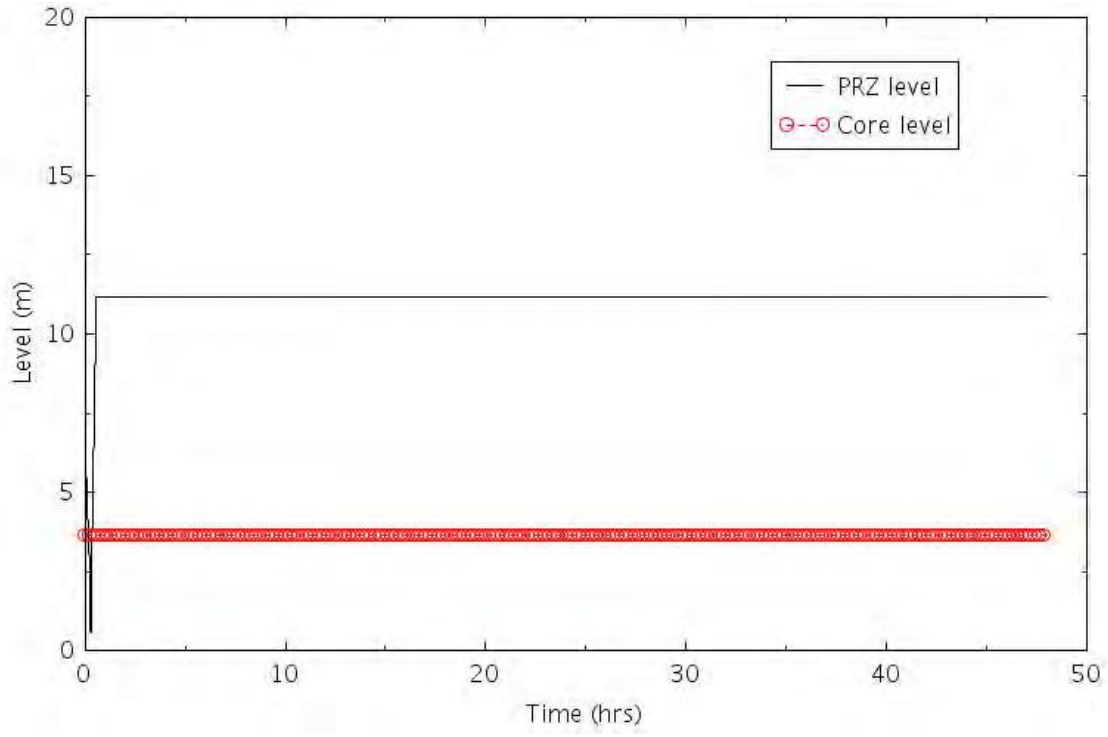

Figure 2-96. PRZ and Core Levels (SGTR-6).

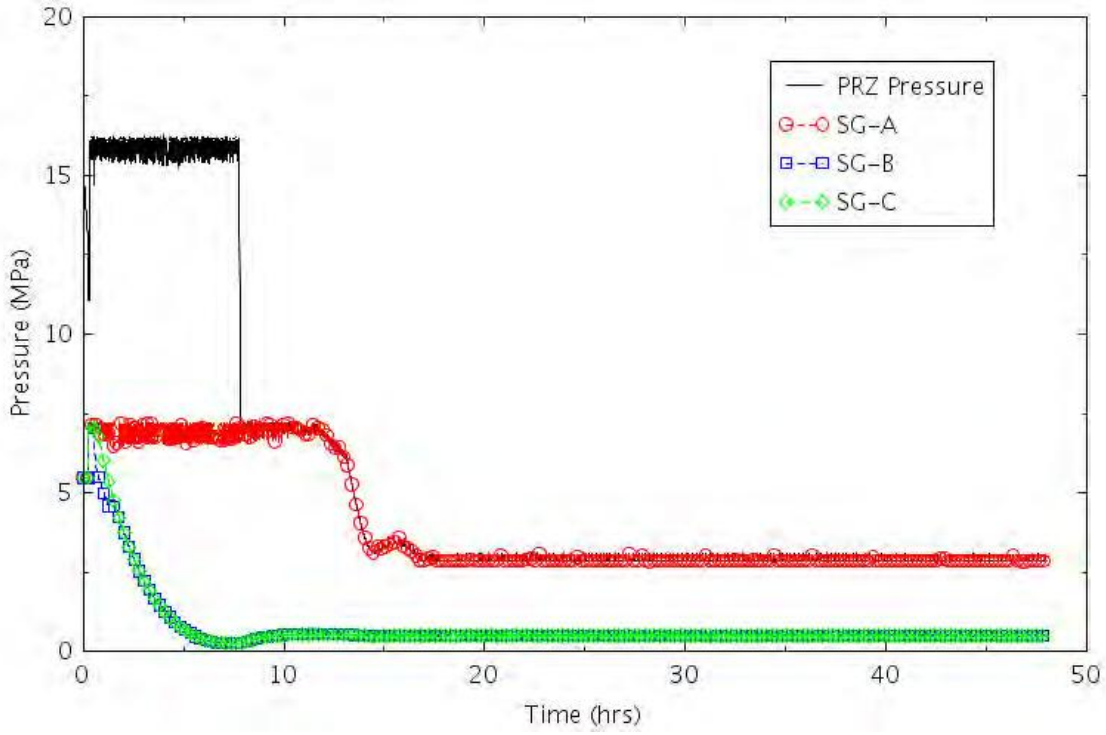

Figure 2-97. PRZ and SG Pressures (SGTR-6).

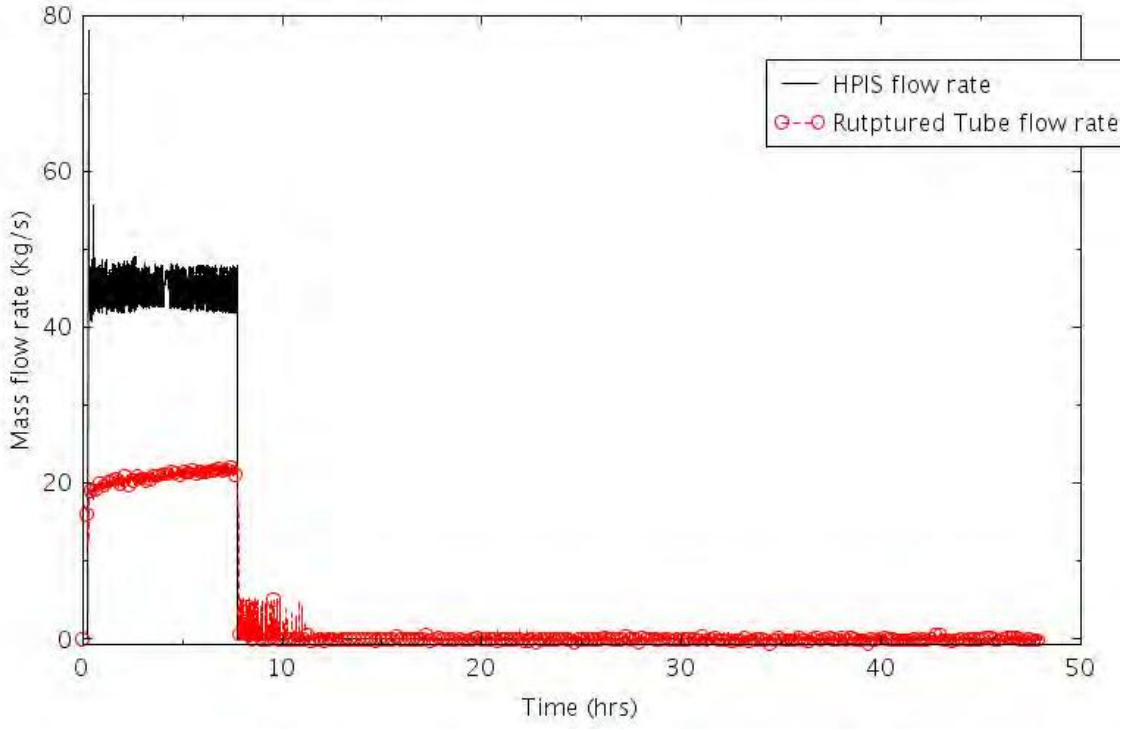

Figure 2-98. HPIS and SGTR Flow (SGTR-6).

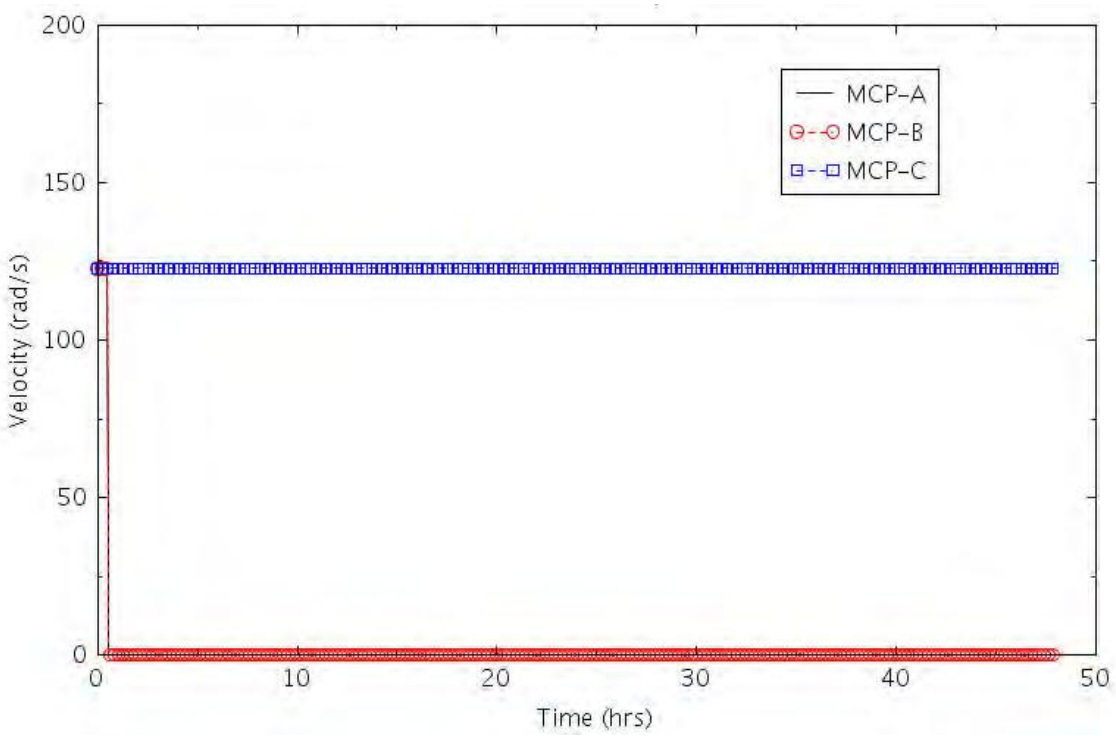

Figure 2-99. RCPs Velocity (SGTR-6).

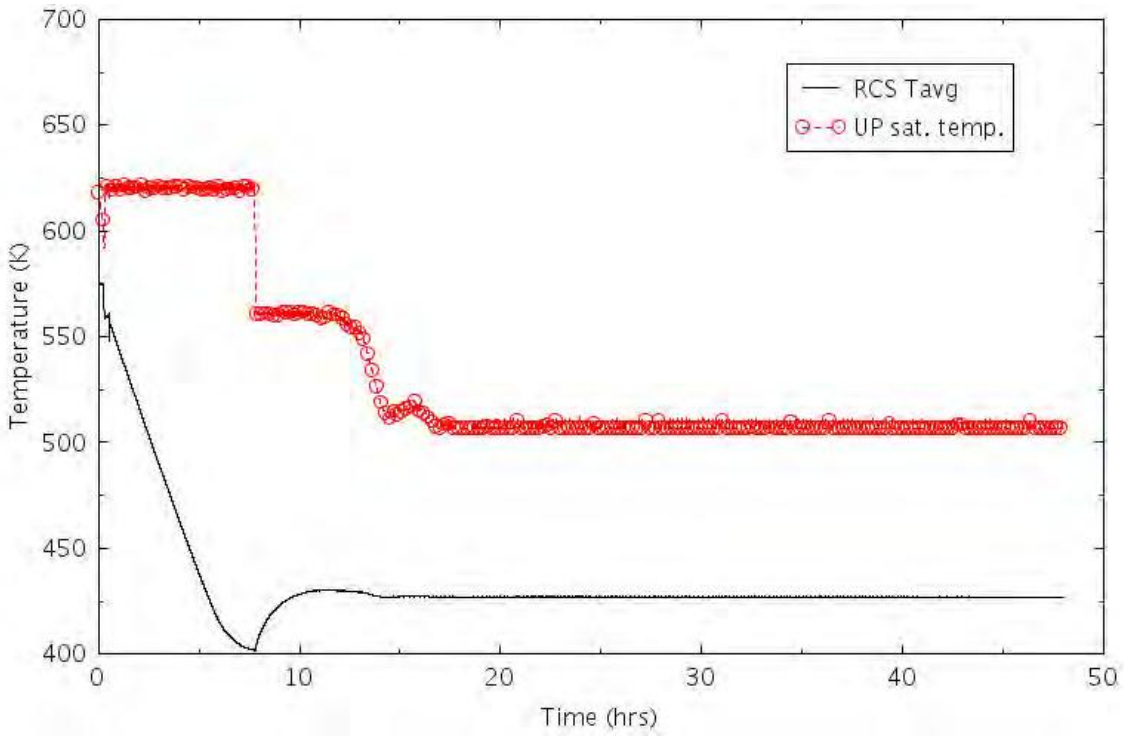

Figure 2-100. RCS Average Temperature and Upper Plenum Saturation Temperature (SGTR-6).

2.2.3.8 SGTR with HPI No AFW (SGTR-7a)

The first phase of SGTR-7a is similar to SGTR-0 (reactor scram for low PRZ pressure, TSV closure, termination of MFW, the shutdown of charging pumps, and startup of HPIS pumps).

The sequence assumes that after the reactor trips and the SI signal, there are the following failures:

- No AFW actuation
- No RWST refill.

The sequence also assumes the success of SG isolation.

Since the faultless SGs are dried out by the lack of AFW and the faulted SG is isolated, no SD-primary/secondary cool-down is possible.

The reactor is cooled down by the HPIS injection until the RWST is exhausted at t = 42 hours, 06 minutes. The stop of the HPIS injection causes an increase of the RCS average temperature, with the formation of voids that leads to the MCP-C trip at t = 42 hours, 55 minutes. Finally, the thermal inertia of the RCS avoids core damage conditions before the end of the mission time (t = 48 hours).

Details of the timing of the events are reported in Table 2-27 and in the following figures.

Table 2-27. Sequence of Events for Scenario SGTR-7.

Event	Timing (hr:min)
SG tube rupture. PRZ level and pressure fall, start of charging pumps.	00:00
Reactor trip for PRZ low-pressure. Reactor shutdown, closure of TSV.	00:16
SI signal for PRZ low-low pressure. Stop of MFW.	00:16
Start-up of 1 MD-AFW pumps.	00:16
SG-A isolation.	00:30
MCP trip for loop-A and B.	00:35
Actuation of the PRZ sprays.	00:36
Depressurization of SG-B and C using Steam-Dump.	N/A
RWST depletion. HPIS stops.	42:06
MCP trip for loop-C.	42:55
RCS temperature stable. End of transient simulation.	48:00

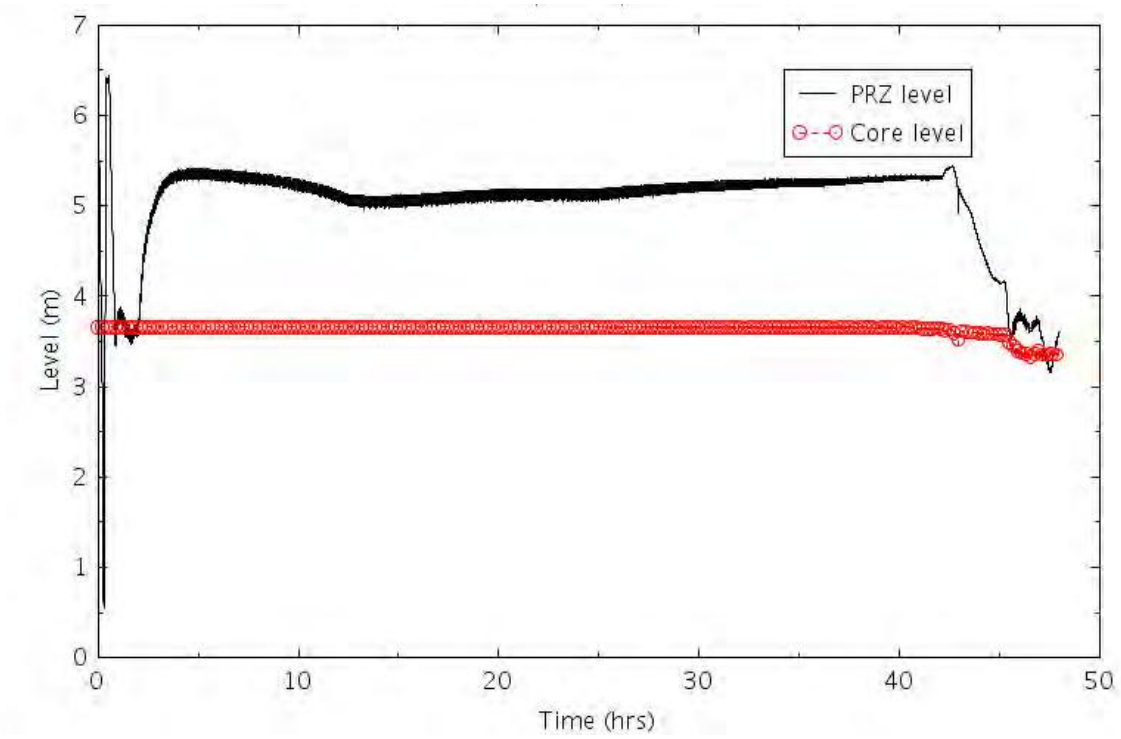

Figure 2-101. PRZ and Core Levels (SGTR-7).

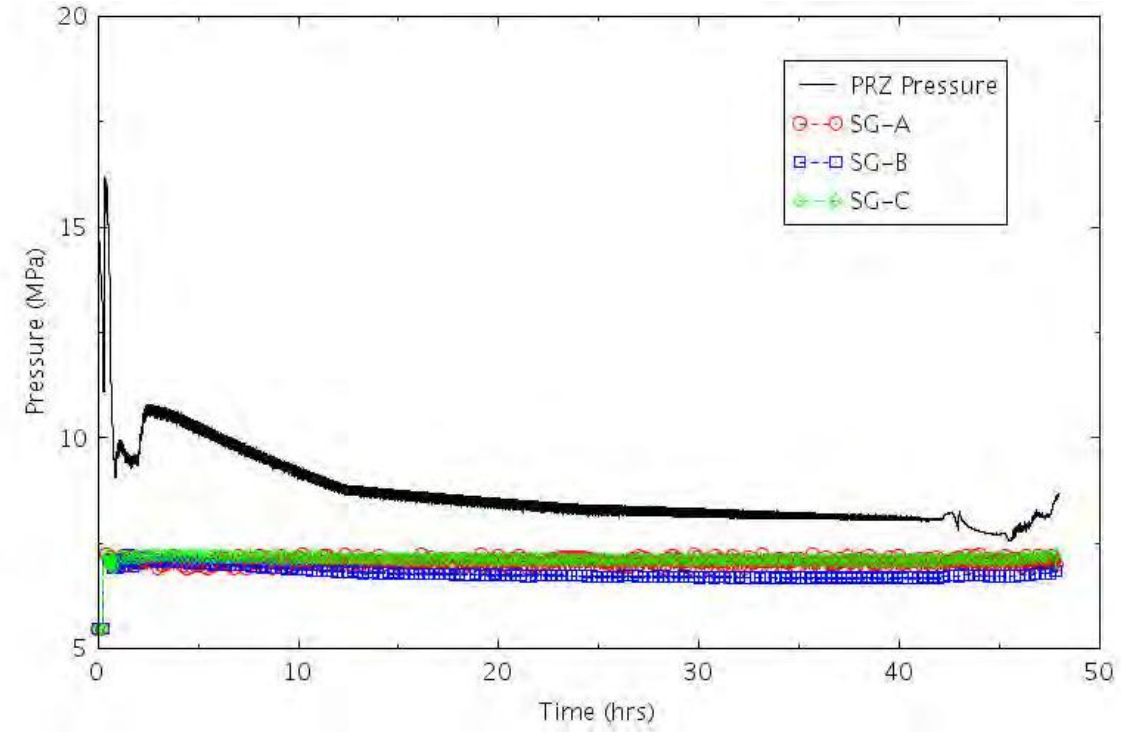

Figure 2-102. PRZ and SG Pressures (SGTR-7).

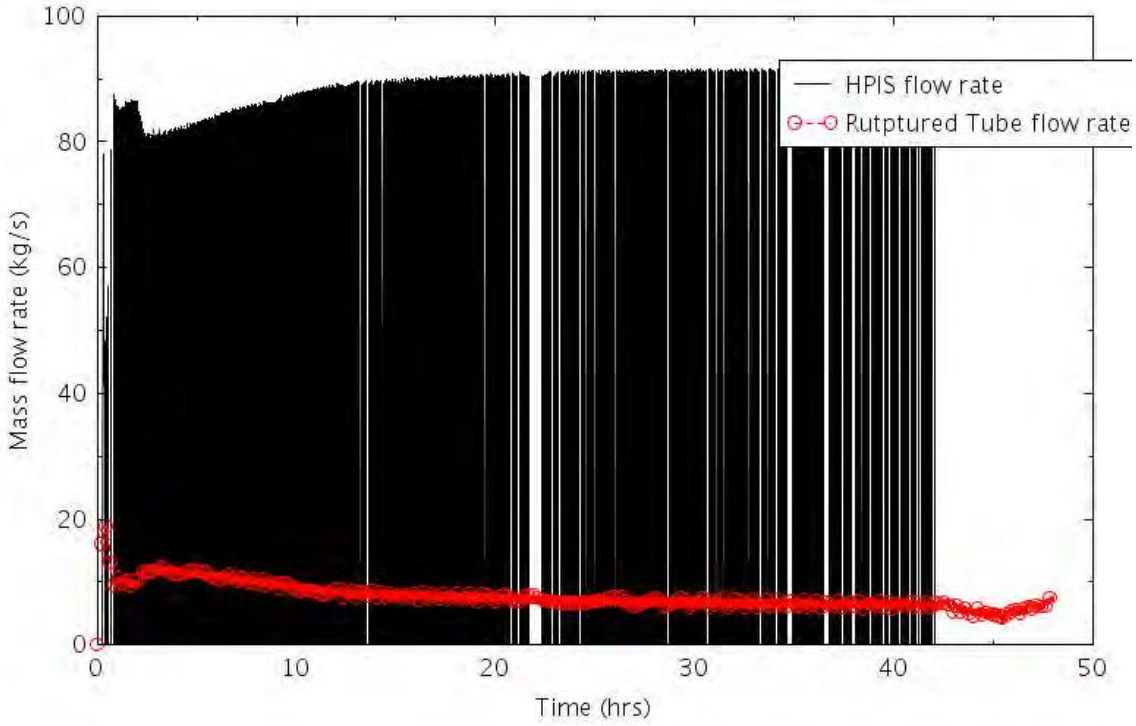

Figure 2-103. HPIS and SGTR Flow (SGTR-7).

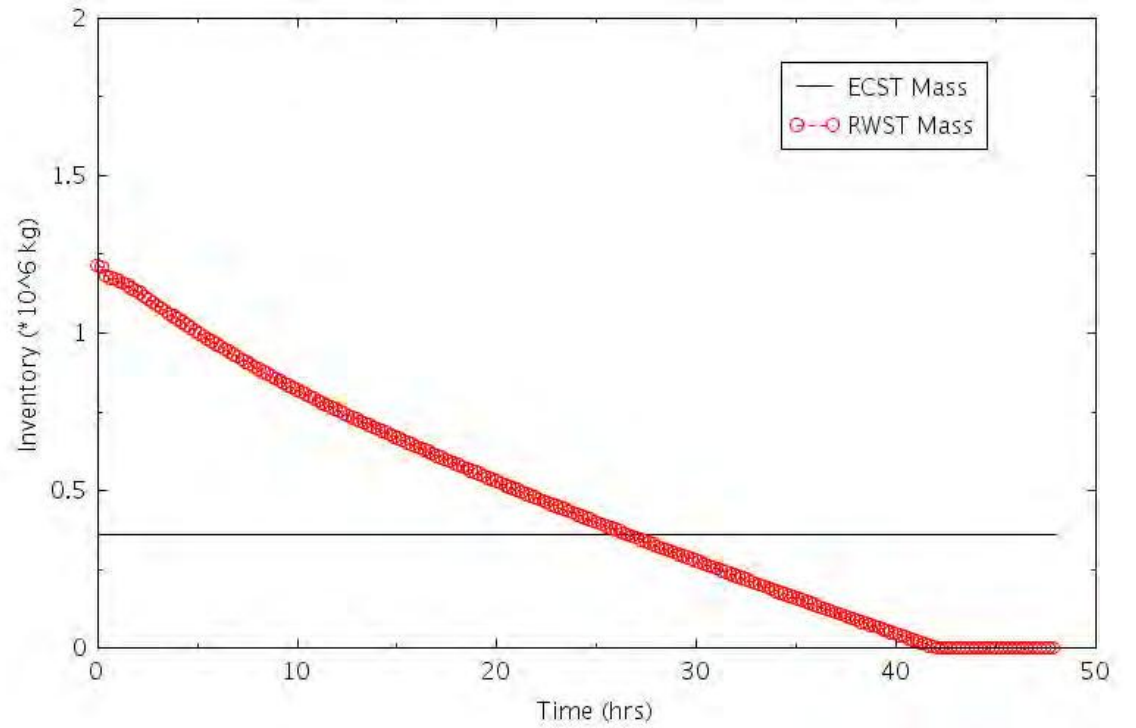

Figure 2-104. RWST and CST Inventories (SGTR-7).

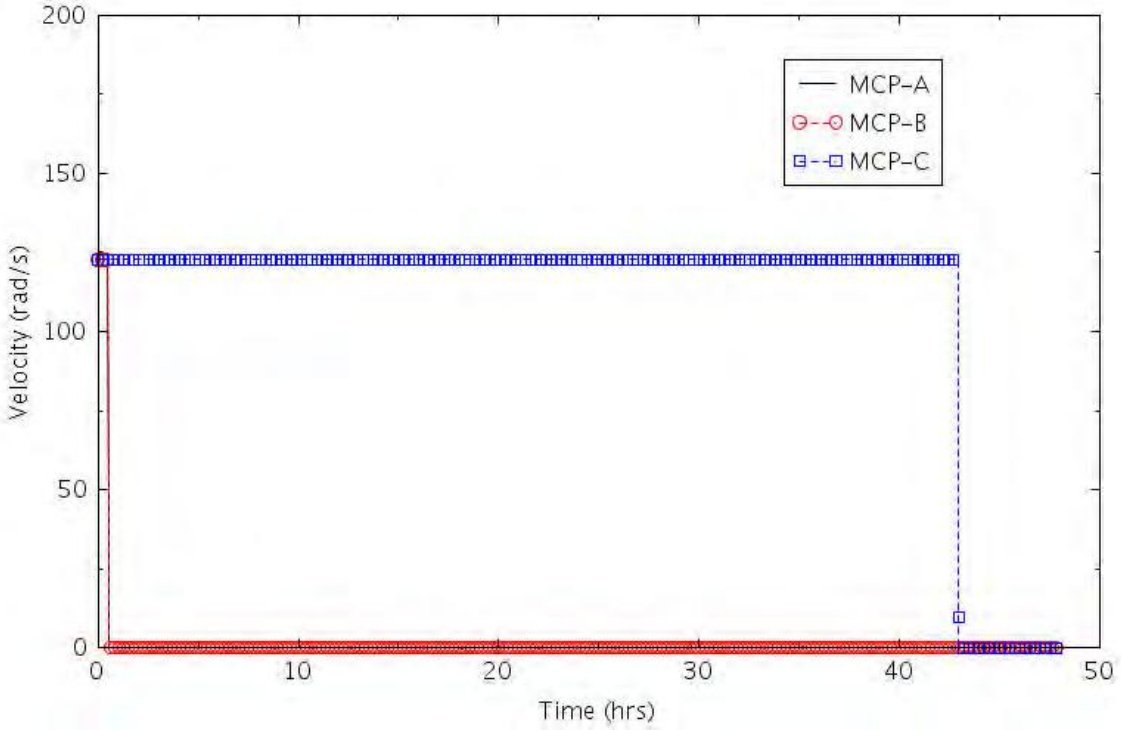

Figure 2-105. RCPs Velocity (SGTR-7).

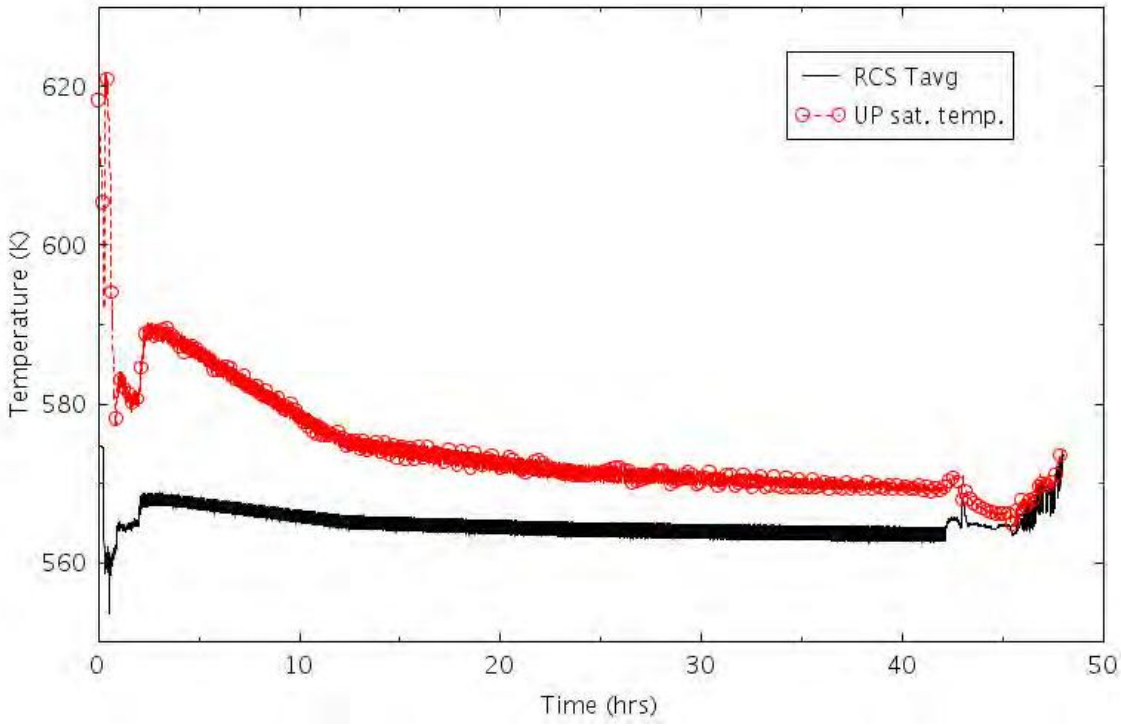

Figure 2-106. RCS Average Temperature and Upper Plenum Saturation Temperature (SGTR-7).

2.2.3.9 SGTR with HPI No AFW (SGTR-7b)

SGTR-7b is similar with SGTR-7a, with the only difference being that RWST is refilled after depletion. No core damage conditions are found before the end of the mission time, t = 48 hours.

The sequence assumes that after the reactor trips and the SI signal there are the following failures:

- No AFW actuation.

The sequence also assumes the success of SG isolation.

Since the faultless SGs are dried out by the lack of AFW and the faulted SG is isolated, no SD-primary/secondary cooldown is possible.

The reactor is cooldown by the HPIS injection. Details of the timing of the events are reported in Table 2-28 and in the following figures.

Table 2-28. Sequence of Events for Scenario SGTR-7b.

Event	Timing (hr:min)
SG tube rupture. PRZ level and pressure fall, start of charging pumps.	00:00
Reactor trip for PRZ low-pressure. Reactor shutdown, closure of TSV.	00:16
SI signal for PRZ low-low pressure. Stop of MFW.	00:16
Start-up of 1 MD-AFW pumps.	00:16
SG-A isolation.	00:30
MCP trip for loop-A and B.	00:35
Actuation of the PRZ sprays.	00:36
Depressurization of SG-B and C using Steam-Dump.	N/A
RCS temperature stable. End of transient simulation.	48:00

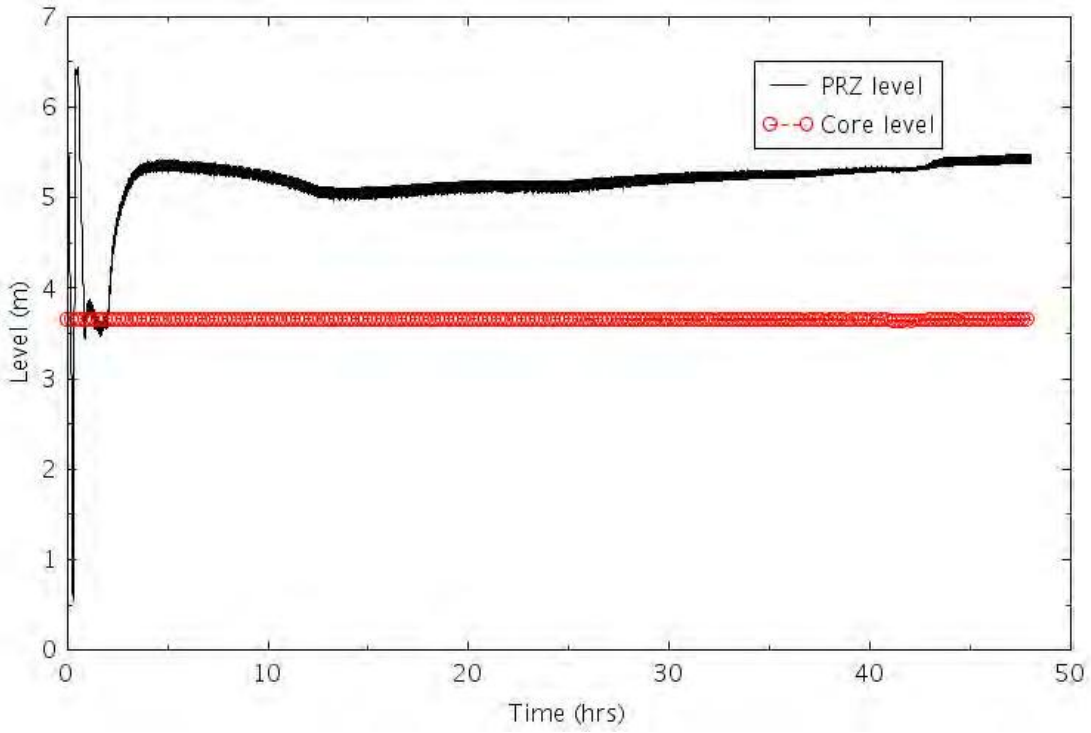

Figure 2-107. PRZ and Core Levels (SGTR-7b).

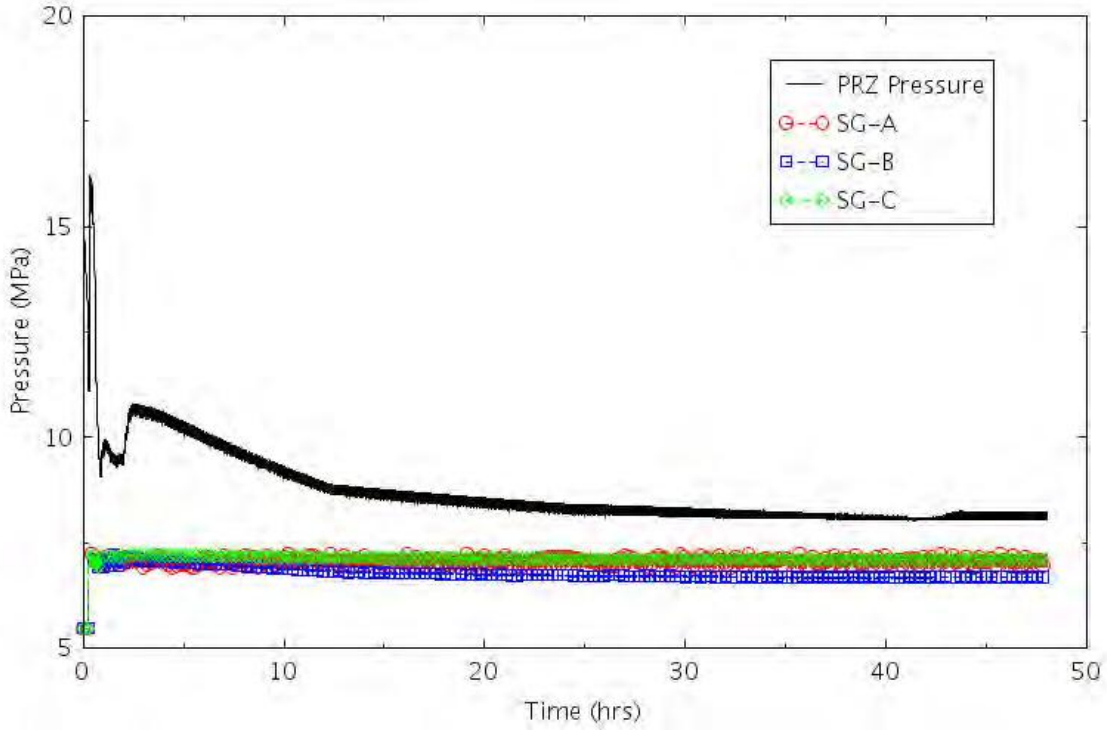

Figure 2-108. PRZ and SG Pressures (SGTR-7b).

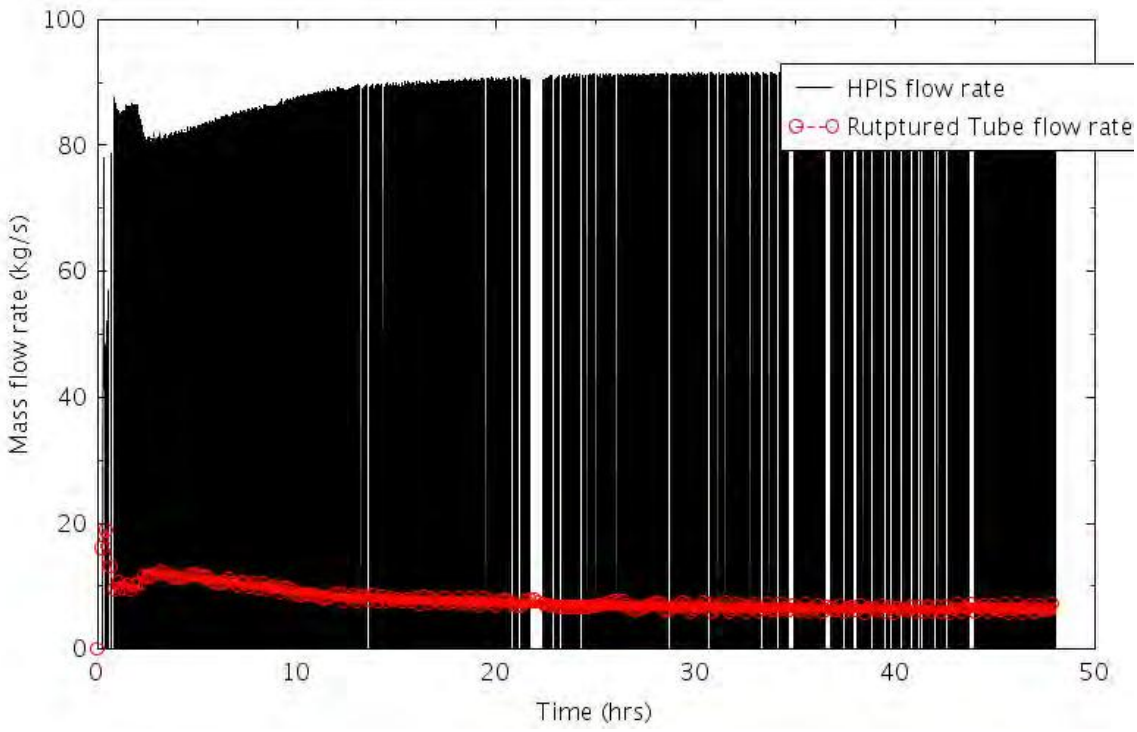

Figure 2-109. HPIS and SGTR Flow (SGTR-7b).

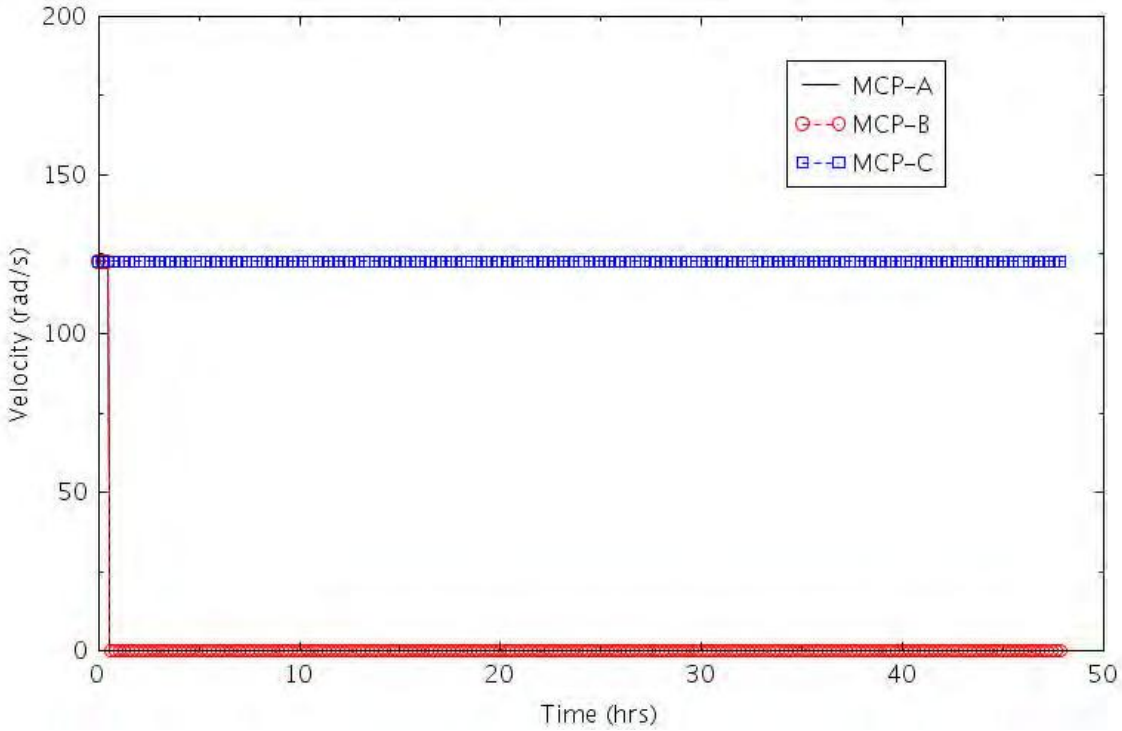

Figure 2-110. RCPs Velocity (SGTR-7b).

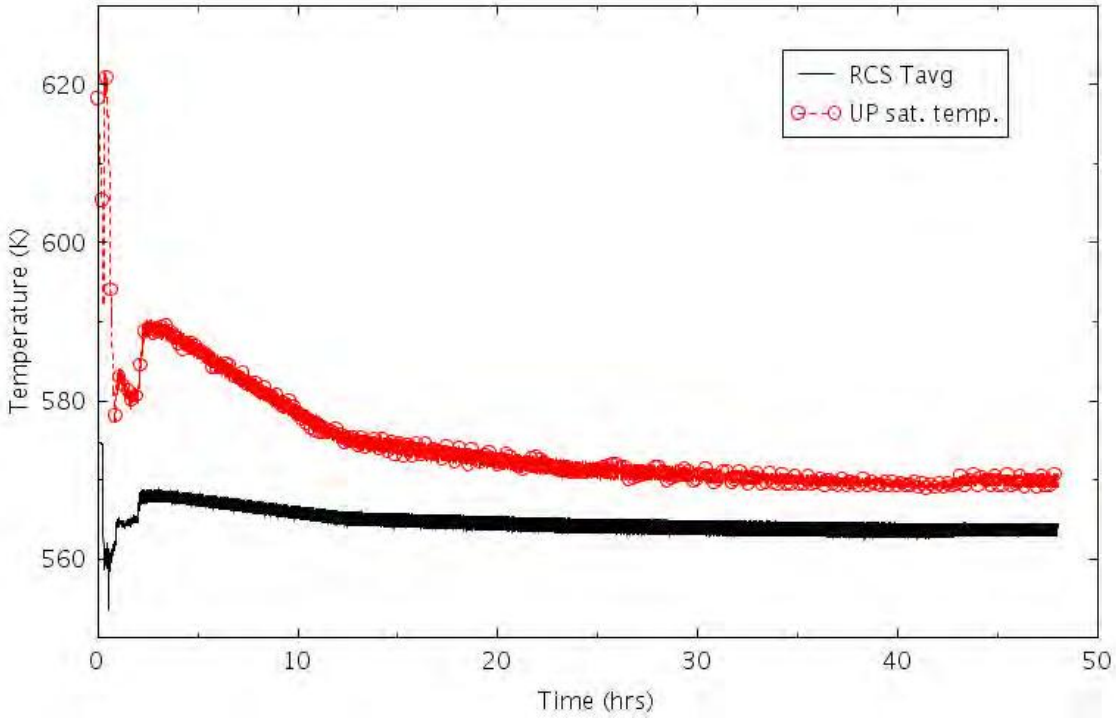

Figure 2-111. RCS Average Temperature and Upper Plenum Saturation Temperature (SGTR-7b).

2.2.3.10 SGTR Accident Sequence (SGTR-S1)

As shown from Sections 2.2.2.2 to 2.2.2.8, the SGTR sequences (SGTR-1 to SGTR-7) based on the PRA model do not reach core damage conditions within 48 hours.

In order to demonstrate the ATF impact in SGTR accident sequence, SGTR-S1 scenario was developed based on the US NRC SOARCA report (NRC, 2012), which assumes no operator actions for an extended time interval (~24 - 48 hours), and failure of steam release valves (PORVs) and of TD-AFW pump because of liquid inventory derived from the faulted SG.

The first phase of SGTR-S1 is similar to SGTR-0 (reactor scram for low PRZ pressure, TSV closure, termination of MFW, shutdown of charging pumps, actuation of three HPIS pumps, startup of AFW after 30 seconds).

However, in SGTR-S1, the SD valves are assumed to not open, therefore the secondary and the primary sides stay at high pressure, and no cooldown is executed. The operator is assumed to take control of the AFW delivery 7 minutes after the scram, as the SGs are overfilling. At t = 28 minutes, the operator is assumed to secure one of the three HPIS pump in order to reduce the flow at the break. At t = 31 minutes, the operator is assumed to have identified the faulted SG, therefore the AFW flow in the SG-A is secured. Eventually the high level in the faulted SG causes the flooding of the TD-AFW and terminates the TD-AFW water injection at the two remaining SGs at t = ~ 1 hour 37 minutes. Then the operator is assumed to not perform the following actions:

- faulted SG isolation
- stop the remaining two HPIS pumps
- stop the leakage from the faulted SG PORV
- actuate the primary side cooldown

Consequently, primary inventory is continuously lost to the secondary side via the ruptured tube and to the outside environment via the SG PORVs. The RWST is empty at t = ~12 hours, thus

terminating the HPIS injection. The high voids in the primary circuit causes the trip of the MCPs at t = ~17 hours, 34 minutes and the continuous cycling the SG PORVs leads to their failure after 119 cycles. SG PORV failure probabilities were obtained from the SOARCA report. The SG PORV failures causes a depressurization of the SG-C between t = 29 hours, 31 minutes (Zry case) and t = 25 hours, 42 minutes (FeCrAl case). SG-B PORV instead fails between t = 25 hours, 39 (Zry case) minutes and t = 29 hours, 15 minutes (FeCrAl case). The SG-B and SG-C depressurizations cause a temporary reduction of the primary pressure that allow the discharge of the accumulators.

Finally, since the ECST is not refilled, the MD-AFW injection is terminated and t = ~ 26 hours, 40 minutes. Then the core uncovery begins and the core reaches the damaged conditions.

Details of the timing of the events are reported in Table 2-29.

Table 2-29. Sequence of Events for Scenario SGTR-S1.

Event	Time (hr:min)		
	Zircaloy	FeCrAl	Chromite
Spontaneous SGTR	00:00	00:00	00:00
Reactor Scram for low PRZ pressure	00:16	00:16	00:16
Charging Pump terminated	00:16	00:16	00:16
TSV close	00:16	00:16	00:16
SD valves open/close	N/A	N/A	N/A
HPIS initiated (3 pumps)	00:16	00:16	00:16
TD-AFW and MD-AFW auto start up	00:16	00:16	00:16
Operators take control of AFW	00:23	00:23	00:23
1 of 3 HPIS pumps secured	00:28	00:28	00:28
AFW delivery to faulted SG secured	00:31	00:31	00:31
Faulted SG PORV 1st lift	00:45	00:44	00:41
TDAFW fails (faulted SG flooded)	01:37	01:35	01:39
Faulted SG isolated	N/A	N/A	N/A
HPIS secured	N/A	N/A	N/A
Leakage through faulted SG PORV stopped	N/A	N/A	N/A
RWST exhausted (HPIS delivery ends)	12:00	11:49	12:00
RCPs tripped for high void	17:34	17:55	17:34
SG-B PORV stuck open due to excessive cycling	25:39	29:15	25:49
ECST exhausted (AFW delivery ends)	26:38	26:31	26:43
First Accumulator Discharge	26:47	26:54	26:48
SG-C PORV stuck open due to excessive cycling	29:31	25:42	29:40

Core begins to uncover	33:33	33:08	33:28
0.5 kg H_2 generated	34:13	34:45	34:44
First cladding rupture	34:47	34:13	34:42
Calculation terminated	35:01	34:53	35:12

The calculations were terminated when the maximum temperature in the cladding reached a given value. The value was 2099 K for cases with Zircaloy and 1804 K for cases with FeCrAl and Chromite.

The differences between calculations due to the different claddings were negligible prior to the onset of core uncovery and were relatively small after. The calculations were terminated when the hottest cladding in each run reached its failure temperature. The termination times varied by less than 15 minutes (a negative of 8 minutes for FeCrAl and a gain of 11 minutes for Chromite). The calculated amount of hydrogen produced during the transients varied significantly between the different claddings. The amount of hydrogen produced was 1.1 kg for FeCrAl, 18.5 kg for Chromite, and 72.5 kg for Zircaloy.

The following figures illustrate the effect of the cladding on various parameters. The differences between calculations are generally small prior to core uncovery, as expected based on Table 2-22.

After the SGTR IE, the charging pumps start to inject water at 14.5 lbm/second (6.5 Kg/second) for compensating the PRZ level decrease (see Figure 2-112 and Figure 2-113). The RCS pressure starts to immediately decrease, but it eventually recovers to the PRZ PORV set-points value because of the HPIS actuation (Figure 2-114).

The operator stops the AFW to the faulted SG-A and secures one HPIS pump. However, since no other actions are assumed, the loss of primary inventory via the ruptured SG tube and the PRZ PORV is significant (Figure 2-116 and Figure 2-117).

The continuous injection of water from the HPIS leads to the RWST depletion after 12 hours (Figure 2-118.). This causes the termination of the HPSI, the consequent drop in the primary pressure, the creation of voids in the RCS, and the trip of MCPs (Figure 2-119). Also, stopping HPSI causes an increase of the primary average temperature and an increase of the faultless SGs' pressures (see Figure 2-120 and Figure 2-121).

The surge in pressure in both of the faultless SGs causes the cycling of their PORVs after 119 cycles fail as they are stuck open (see Figure 2-122). The increase of flow by the MD-AFW (Figure 2-123) leads to a depletion of the ECST by t = ~27 hours. Finally, the depletion of the SG-B and SG-C inventory causes the core uncovery and a consequential fuel damage condition (Figure 2-124 and Figure 2-125).

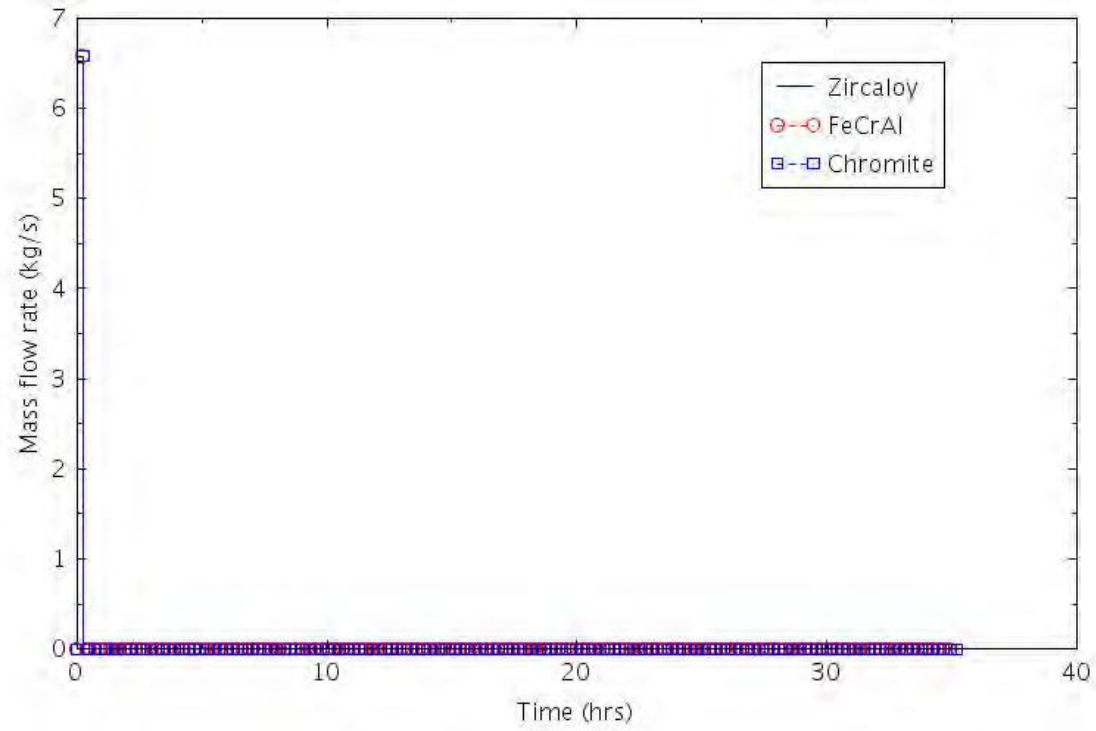

Figure 2-112. Charging Pump Flow (SGTR-S1).

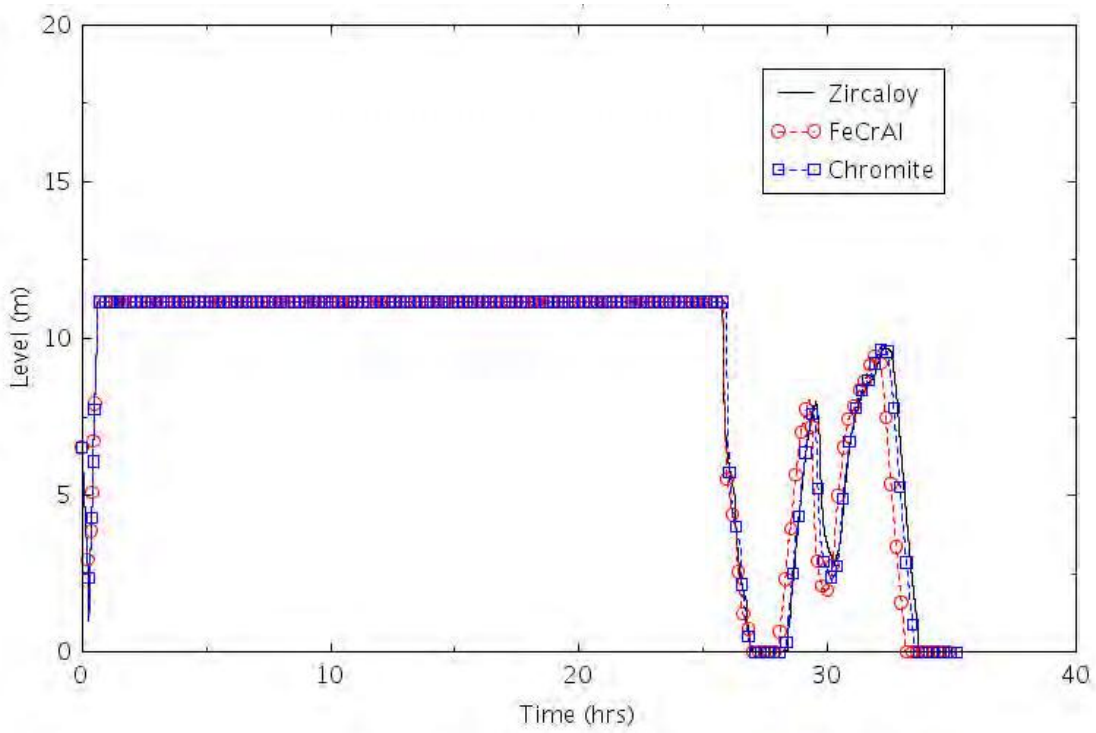

Figure 2-113. PRZ Levels (SGTR-S1).

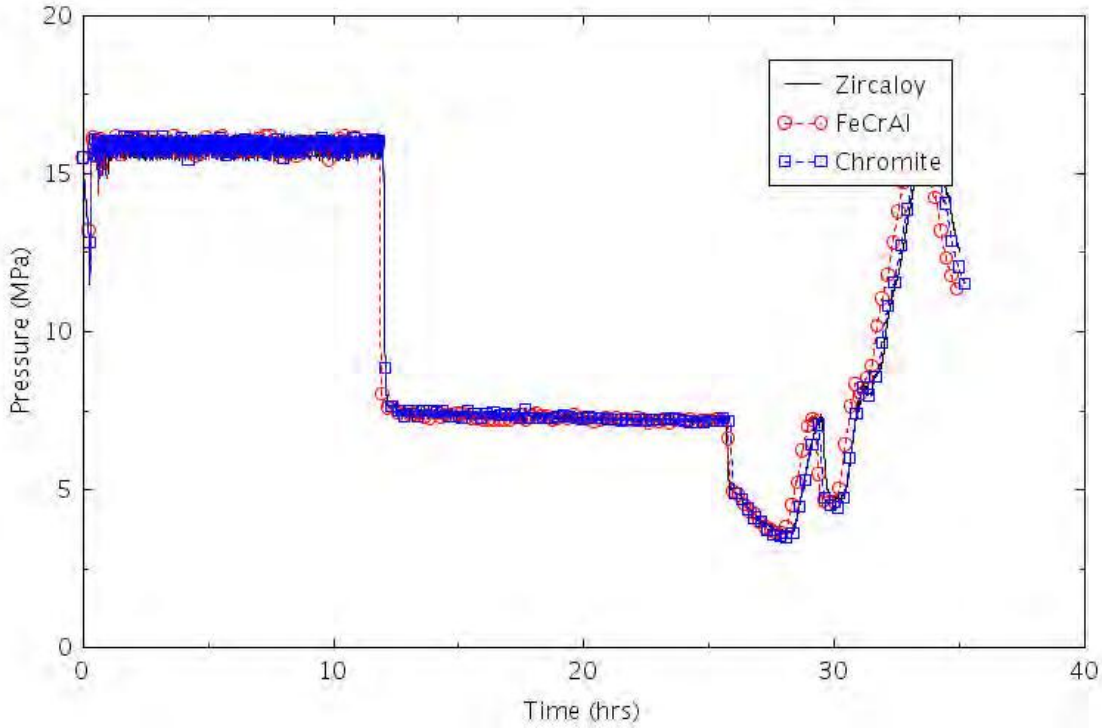

Figure 2-114. PRZ Pressure (SGTR-S1).

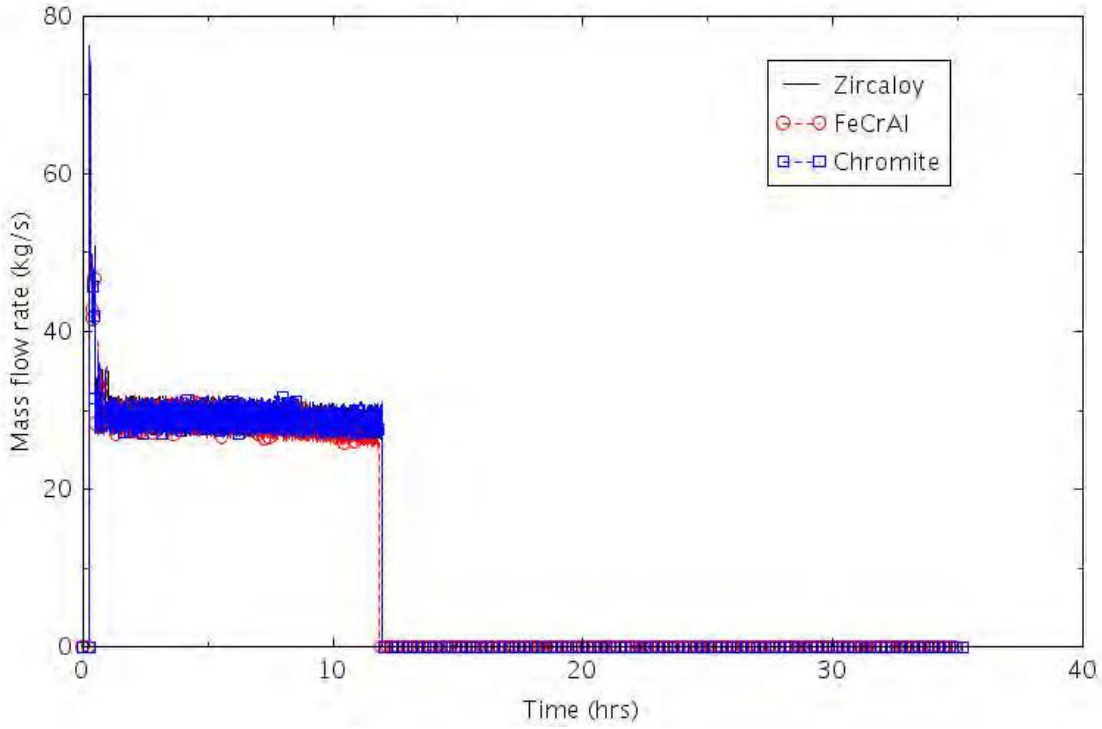

Figure 2-115. HPIS Flow (SGTR-S1).

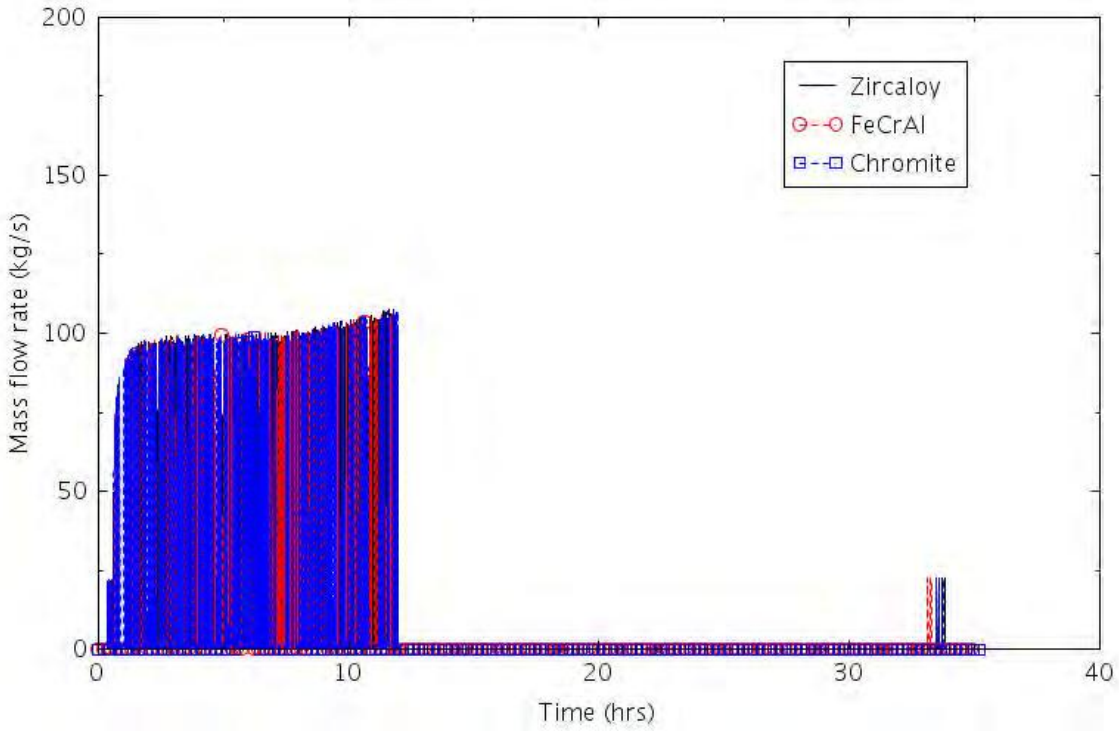

Figure 2-116. PRZ PORV Flow (SGTR-S1).

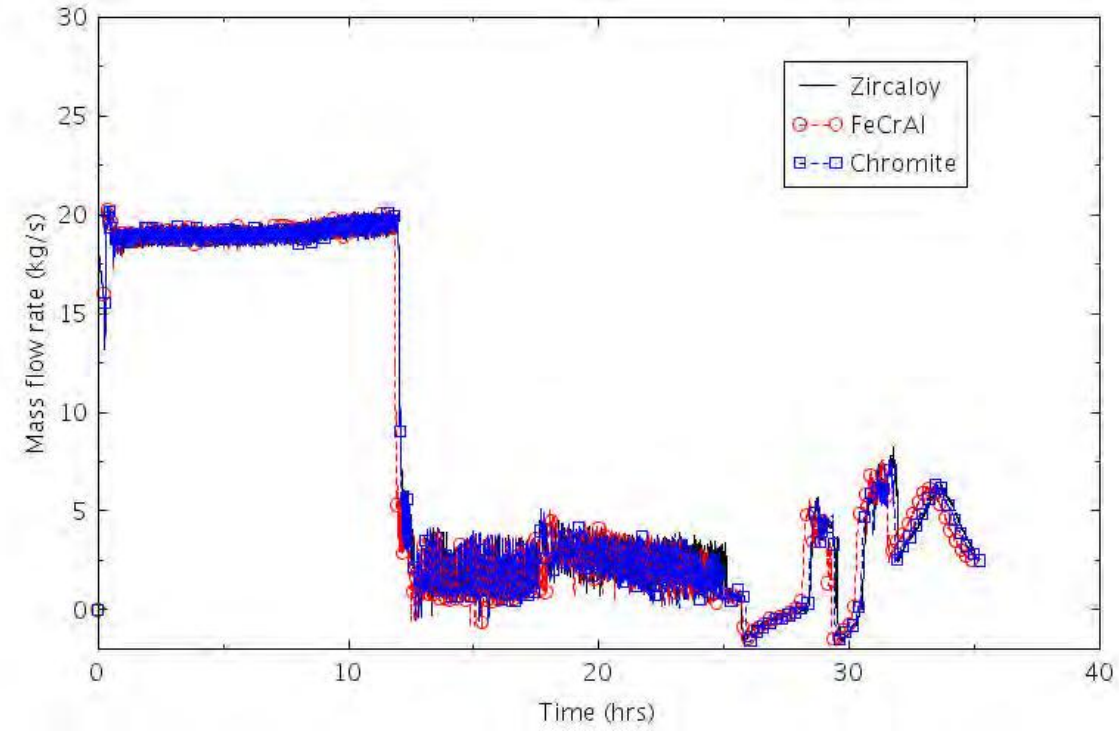

Figure 2-117. Ruptured SG-A Flow (SGTR-S1).

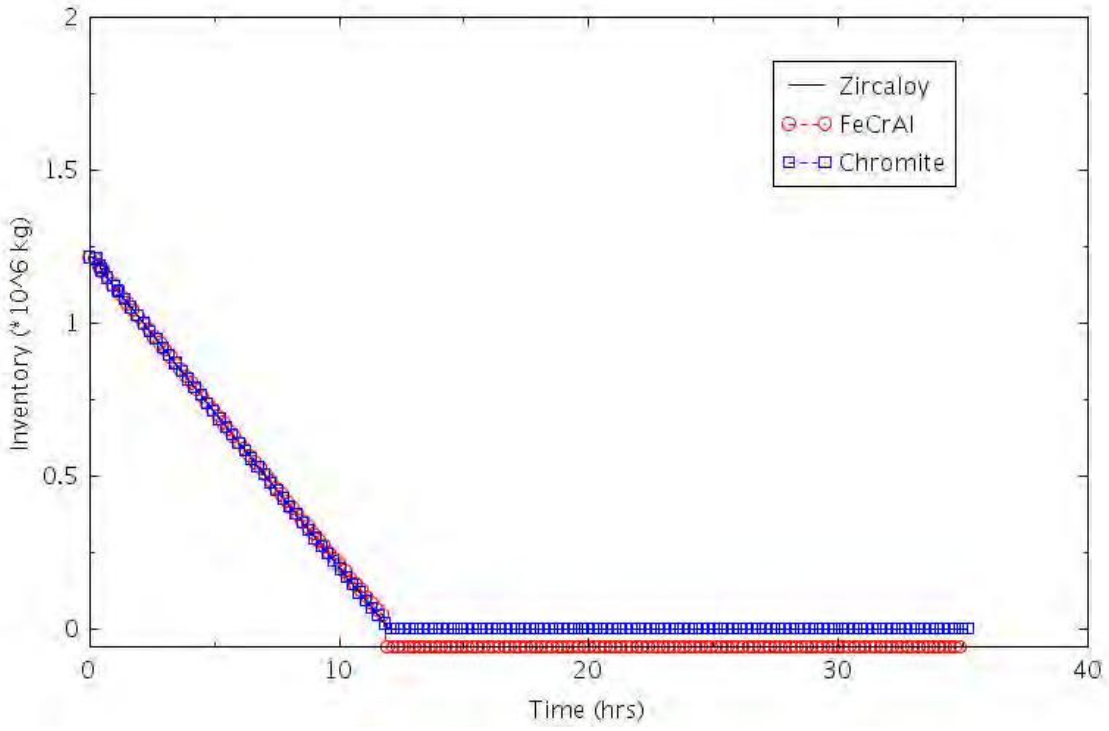

Figure 2-118. RWST Mass Inventory (SGTR-S1).

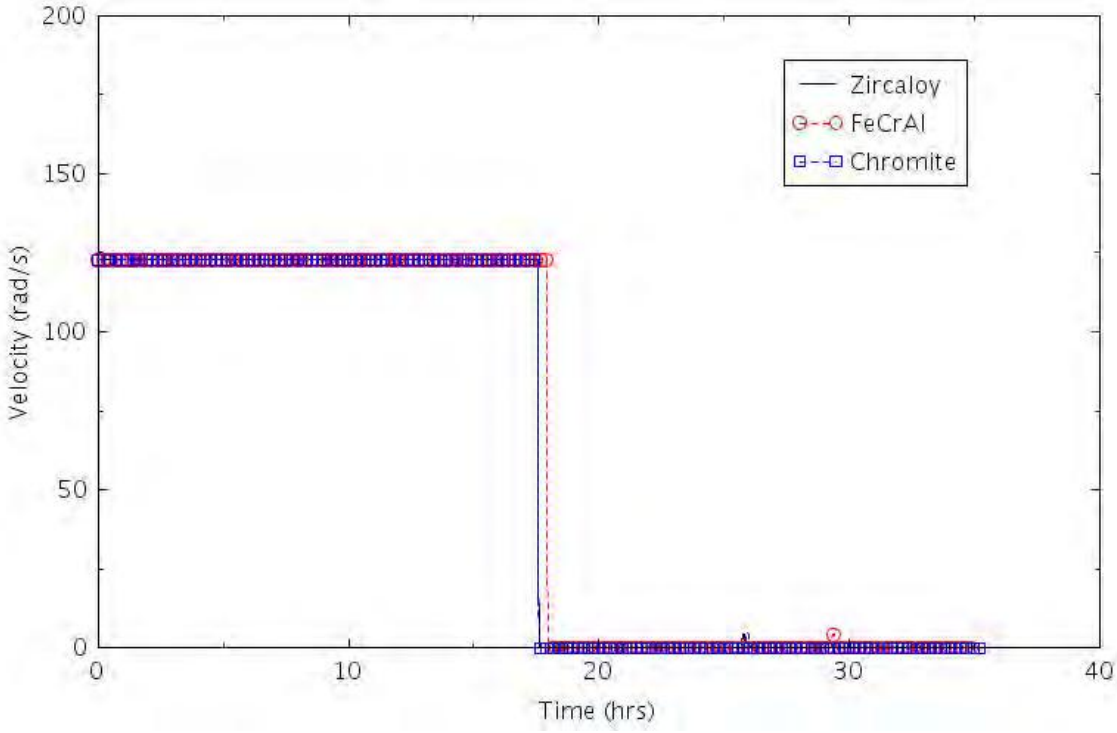

Figure 2-119. MCP-B Velocity (SGTR-S1).

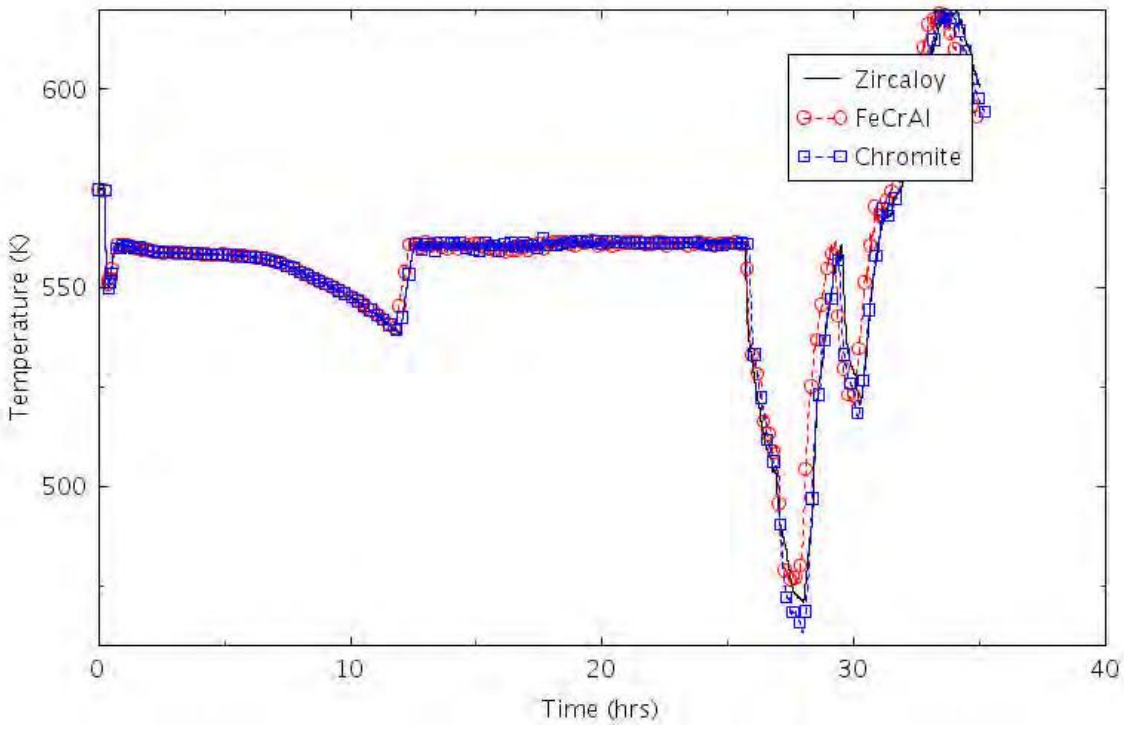

Figure 2-120. Primary Average Temperature (SGTR-S1).

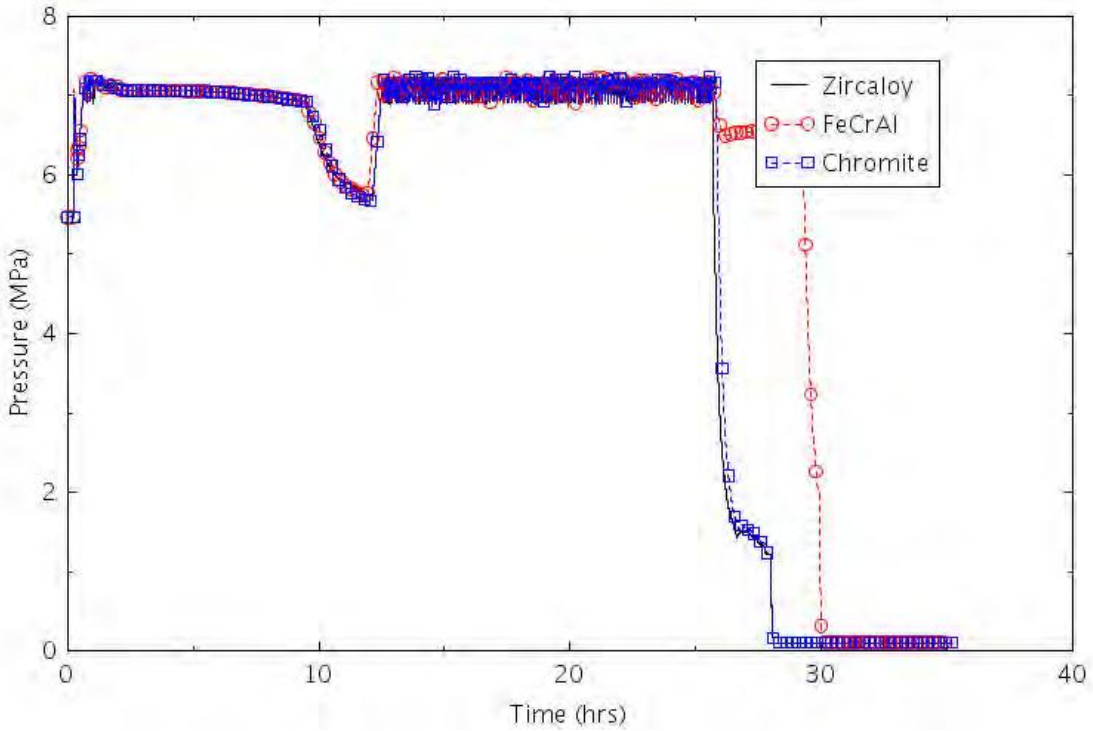

Figure 2-121. SG-B Pressure (SGTR-S1).

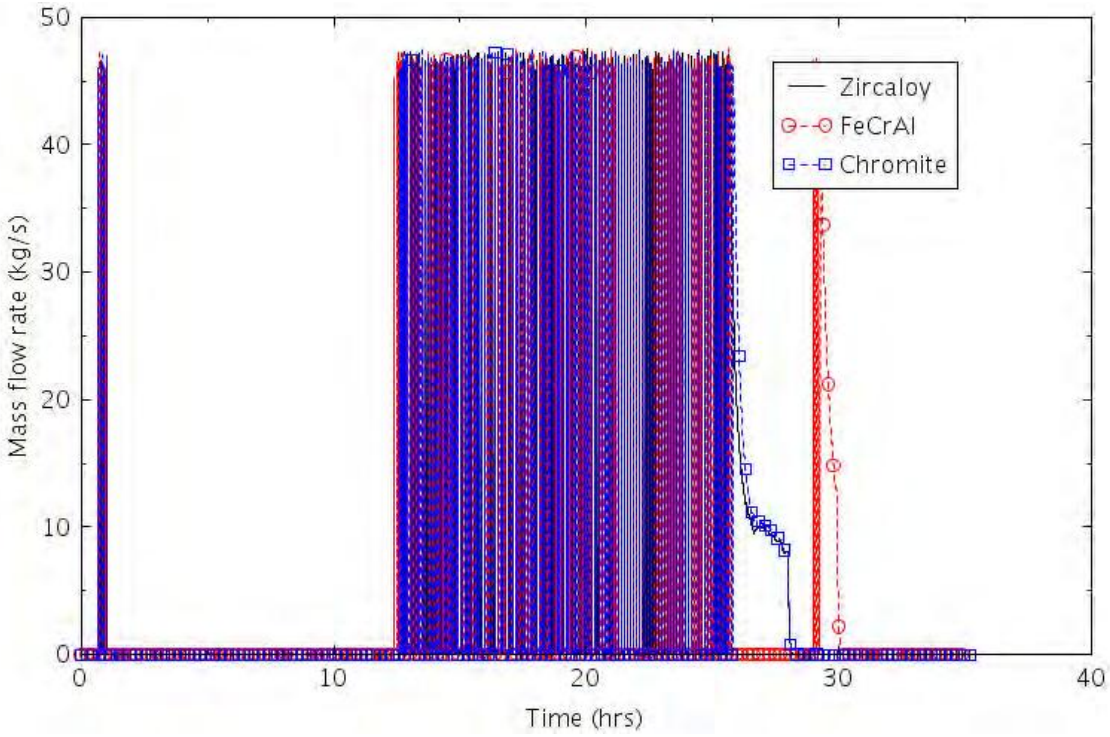

Figure 2-122. SG-B PORV Flow (SGTR-S1).

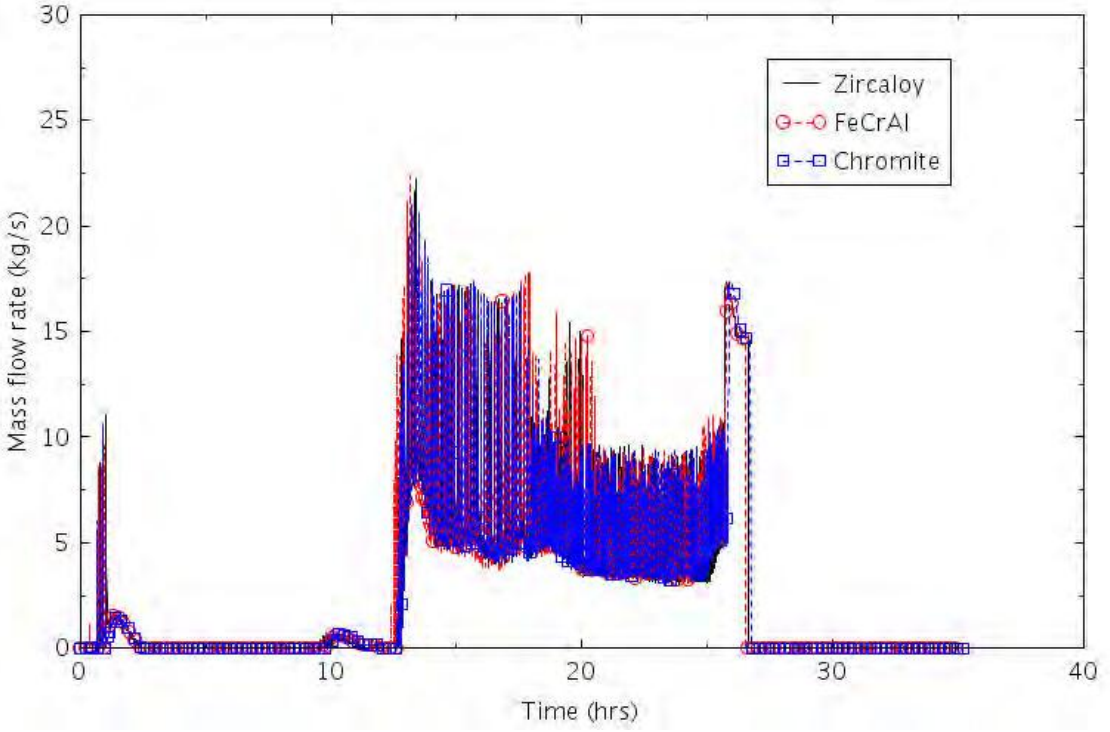

Figure 2-123. AFW Flow (SGTR-S1).

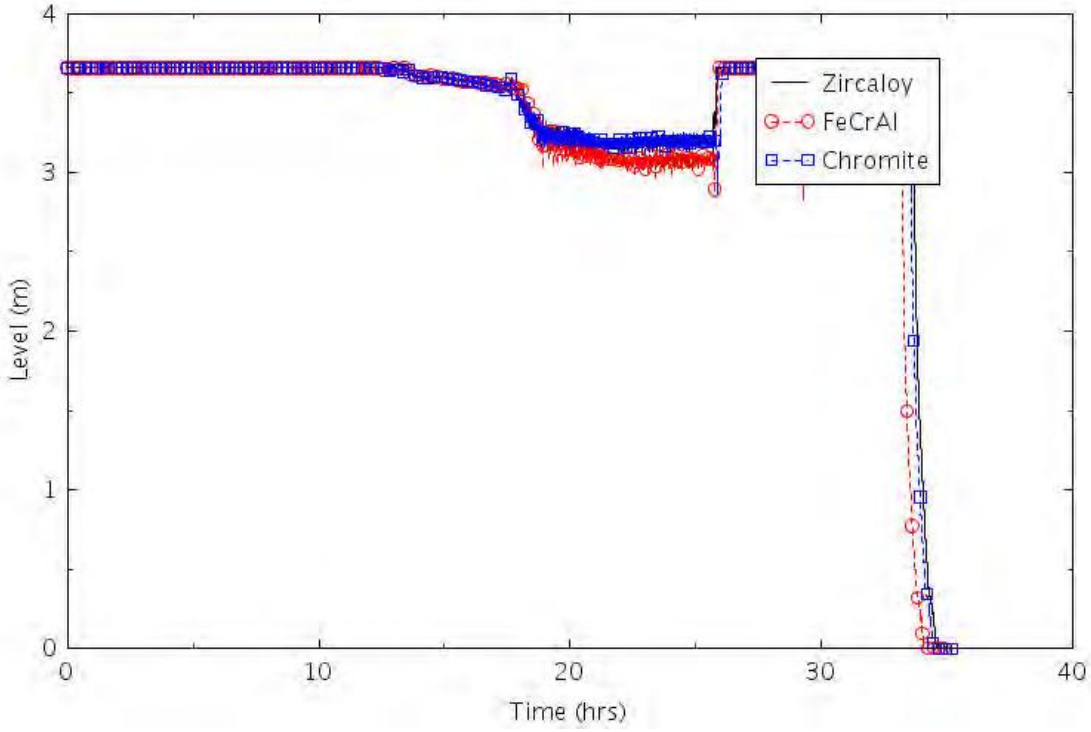

Figure 2-124. Core Collapsed Level (SGTR-S1).

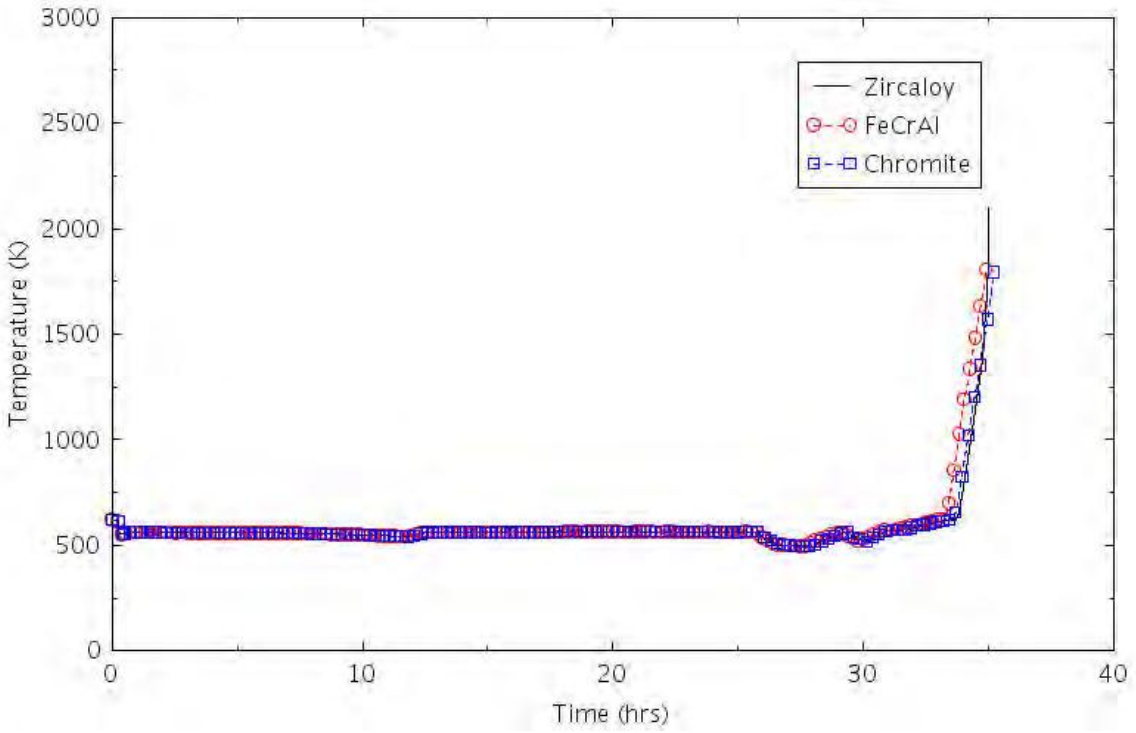

Figure 2-125. Peak Cladding Temperature (SGTR-S1).

2.2.4 SGTR Analysis Results

Based on RELAP5-3D analysis for SGTR in Section 2.2.2, the PRA accident sequences (SGTR-1 to SGTR-7) do not reach core damage conditions within 48 hours. The reasons they were defined in the PRA model with the end state of core damage are probably from the conservative and qualitative assessments when developing the PRA model. For example, in the SGTR-1 scenario that HPI is not available and the isolation of a ruptured SG fails, even though the RELAP5-3D simulations terminate with no core damage 48 hours after the IE, a qualitative assessment would argue that if SGTR continues without primary makeup from a safety injection, the plant is not in a safe, stable state and core damage will eventually occur, although the time to core damage will be longer than 24 to 48 hours with the slow progressing nature in an SGTR event.

Then, with the SGTR-S1 accident scenario developed based on the US NRC SOARCA report (NRC, 2012), which assumes no operator actions for an extended time interval, the RELAP5-3D analysis results show similar ATF impacts as those in the LOFW analysis in Section 2.1. The gain of coping time is 11 minutes for Chromite but a negative of 8 minutes (or quicker to reach core damage) for FeCrAl. So, the risk impact on behalf of the CDF brought by the ATF designs would be very small, and this scenario is not conducted for SGTR. However, the benefit in much less hydrogen produced at the time of core damage is obvious. The calculated amount of hydrogen produced during the transients for Zircaloy is 72.5 kg, but only 1.1 kg for FeCrAl (1.5% of the hydrogen production for Zircaloy), and 18.5 kg for Chromite (25% of the hydrogen production for Zircaloy).

3. RISK-INFORMED FLEX ANALYSIS

This section presents FLEX-related analysis, including an overview of FLEX, FLEX PRA modeling, FLEX risk impact, and FLEX HRA.

3.1 FLEX Overview

Flexible and diverse mitigation strategy (FLEX) is a U.S. nuclear industry initiative to increase defense-in-depth (DID) for beyond-design-basis external events such as earthquake and flood as lessons learned from the Fukushima Dai-ichi nuclear accident. NEI 12-06, first published in August 2012 with Revision 4 published in December 2016 (NEI, 2012), provides industry guidance for the implementation of FLEX. NEI 12-06 defines three FLEX associated terms: FLEX strategies, FLEX equipment, and FLEX capability. These strategies refer to those plant-specific functional approaches that a nuclear power plant (NPP) could take to maintain or restore core cooling, containment, and spent fuel pool (SFP) cooling capabilities. The term FLEX equipment refers to the equipment stored on-site or off-site with primary function to support FLEX strategies. The term FLEX capability refers to a site-specific set of equipment strategies implemented through plant-specific procedures/guidance and provide essentially indefinite coping capability through the use of plant equipment and FLEX equipment.

3.1.1 FLEX Characterizations

FLEX equipment/strategies, or FLEX in this report, can be categorized in different ways, for example, according to FLEX equipment locations and connections, according to FLEX mitigative functions and FLEX applications, or according to the accident scenarios that FLEX may mitigate.

For FLEX equipment locations and connections, FLEX equipment may be installed, pre-staged, or portable on-site and may be stored within the owner-controlled area or in close proximity to the site. Guidance on the treatment of plant mitigating strategies including FLEX and B.5.b strategies in risk-informed decision making, provided by NEI 16-06 (NEI, 2016), categorizes four different types of FLEX equipment:

- Permanently-Installed Plant Equipment, which is permanently installed in the plant but may have a different role in the mitigating strategies from its normal functions. This is called Type 1 FLEX equipment in this report.
- Onsite Portable Equipment, which is stored on or near the owner-controlled area and may need to be transferred and connected to plant systems to mitigate accidents. This is called Type 2 FLEX equipment in this report.
- Permanently-Staged Portable Equipment, which is permanently staged and needs reduced installation time to support mitigating strategies. This is called Type 3 FLEX equipment in this report.
- Offsite Portable Equipment, which is stored remotely at locations such as national response centers or other plant sites and needs longer time for transportation before supporting mitigating strategies. This is called Type 4 FLEX equipment in this report.

Figure 3-1 presents the FLEX categories base on FLEX equipment location and connection.

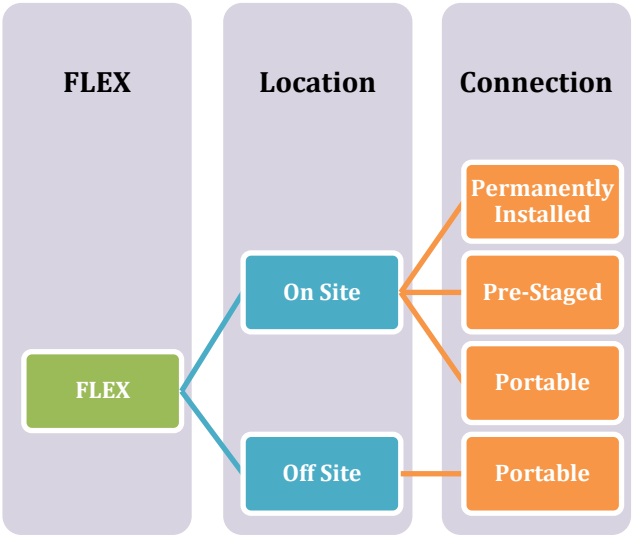

Figure 3-1. FLEX Categories based on Equipment Location and Connection.

FLEX could also be categorized based on the FLEX mitigative functions and FLEX equipment (Figure 3-2). FLEX could provide the following additional capabilities to a nuclear plant with various, plant-specific applications and equipment:

- AC Power, e.g., FLEX 4160V or 480V diesel generator (FLEX-4160, FLEX-480)
- DC Power, e.g., FLEX DC battery (FLEX-BAT) or battery charger (FLEX-CHG)
- RCS Makeup, e.g., FLEX portable diesel-driven or motor-driven pump for high pressure injection (FLEX-HPI), low pressure injection (FLEX-LPI), or RCS makeup during shutdown operations (FLEX-RCSMUP)
- SG Makeup, e.g., FLEX portable pump for secondary side injection (FLEX-SGP)
- RCP Seal Cooling, e.g., FLEX portable pump for RCP seal cooling (FLEX-RCPSCP)
- SFP Makeup, e.g., FLEX portable pump for SFP cooling (FLEX-SFPMUP).

Being originally developed and implemented to address extended loss-of-AC power (ELAP) and loss of normal access to the ultimate heat sink scenarios, FLEX is mostly credited only in SBO/ELAP scenarios in plant PRA. However, with the millions of dollars already invested in FLEX equipment, the nuclear industry should, and could, investigate various approaches to maximizing both the safety and economic benefits from the investment. For example, the industry should conduct plant-specific risk-informed plant enhancement analysis, described in Section 6 of INL/EXT-18-51436, with the FLEX equipment options in mind. With plant-specific analysis and proper development of associated procedures and training programs, FLEX could be extended for crediting in other accident scenarios (Figure 3-3).

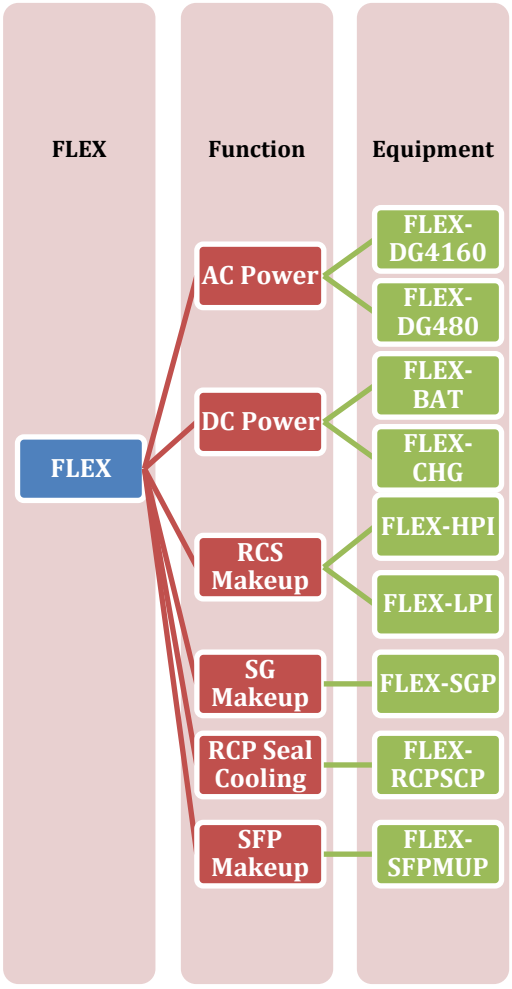

Figure 3-2. FLEX Categories based on Mitigative Function and Equipment.

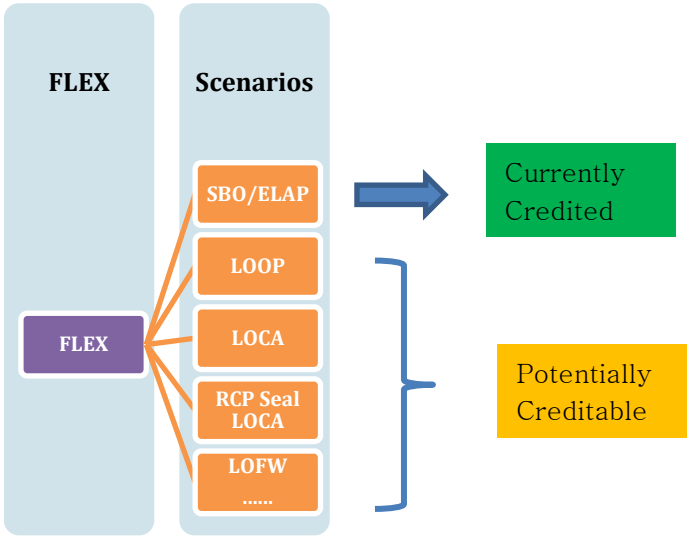

Figure 3-3. Crediting FLEX in Different Scenarios.

3.1.2 Crediting FLEX in PRA

Different types of FLEX equipment have different requirements to be credited in a PRA model. Type 1 FLEX equipment (i.e., permanently installed in the plant) could be treated like a normal plant equipment with proper data and human reliability analyses. Type 4 FLEX equipment (i.e., offsite portable equipment) is usually not credited in PRA due to the time required to transport the equipment to the site. Type 3 FLEX equipment (i.e., permanently staged portable) could be treated either like Type 1 or Type 2 depending on whether it is more similar to permanently-installed or onsite portable equipment.

To credit Type 2 FLEX equipment (i.e., onsite portable equipment) and mitigate strategies in PRA, the following evaluations should be conducted:

- **Capability and Reliability**: Whether the FLEX equipment is capable, available, and reliable to perform the mitigating function
- **Time**: Whether the time required to deploy, install, connect, and start FLEX equipment is less than the time available in order to effectively mitigate the accident
- **Procedure and Training**: Whether there are procedures/written instructions and trainings for the use of the equipment and mitigating strategies
- **Staffing and Communication**: Whether there is enough plant staffing (with the necessary skills) and external staffing (e.g., transmission dispatch operators, subcontractors for FLEX installation) to deploy, install, and connect FLEX equipment; in applying mitigating strategies, whether communications are available for the successful implementation
- **Tool**: Whether the tools (including electrical power needed for tools) required for FLEX equipment and mitigating strategies implementation are available
- **Environmental Conditions**: Whether adverse environmental conditions such as lighting, flooding, heat, radiation, and debris would challenge or prevent the deployment, timing, and implementation of the FLEX equipment and mitigating strategies

The above considerations are consistent with the ASME/ANS PRA Standard requirements (ASME and ANS, 2013) on crediting operator recovery actions and evaluating plant-specific and scenario-specific performance shaping factors. The NRC Regulatory Issue Summary (RIS) 2008-15 (NRC, 2008) allows licensees to credit B.5.b mitigating strategies in licensing actions and in significance determination process (SDP). To credit permanent or portable equipment used in these strategies, it requires the licensee to demonstrate the appropriate level of reliability and availability. Human reliability analysis must be performed to assure that adequate time is available, the procedural guidance is developed, and the plant personnel is trained.

3.2 FLEX PRA Analysis

This section presents FLEX PRA analysis that incorporates portable 480V AC DG (FLEX-DG480) and SG makeup pump (FLEX-SGP) into the generic SAPHIRE PWR model.

3.2.1 FLEX PRA Modeling

3.2.1.1 Event Tree/Fault Tree

There are two approaches to crediting FLEX equipment and mitigating strategies in a PRA model. One is to add new top events (along with associated fault trees to support the top events) to the event trees that represent the FLEX equipment and mitigating strategies. The other is to revise fault trees by incorporating the FLEX equipment and mitigating strategies into the existing logic. Caution should be given in both approaches that FLEX is credited only to those identified applicable accident sequences. The underlying logic should also be developed to ensure that FLEX equipment credit is limited to only those applicable accident sequences.

This analysis adds three new top events into the existing SAPHIRE loss of offsite power (LOOP)/SBO event tree, or more specifically, the SBO-4 event tree. Refer to (Ma & al., 2018) for the full SAPHIRE LOOP/SBO model. Figure 3-4 shows the simplified existing SBO-4 event tree. Figure 3-5 shows the revised SBO-4 event tree with the three new FLEX-related top events, FLEX-SBO-4 which is a house event for operator failing to deploy FLEX equipment for SBO-4 scenario, FLEX-DGN-480 which represents whether the FLEX 480V diesel generator (DG) could be functional, and FLEX-SGP which represents whether the SG makeup pump could provide secondary cooling to SG for the SBO-4 scenario.

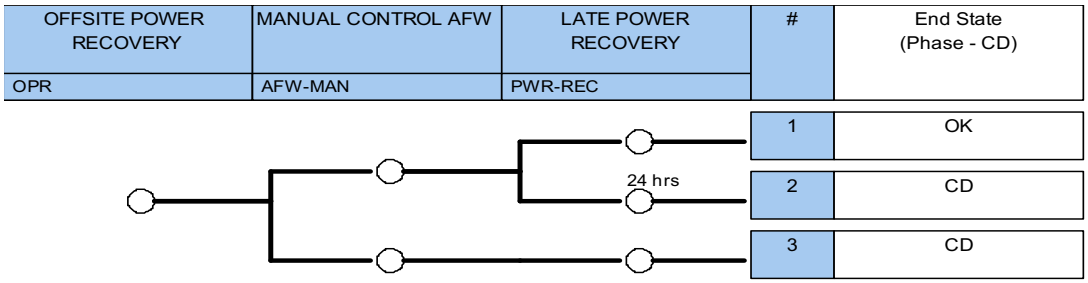

Figure 3-4. Existing SBO-4 Event Tree.

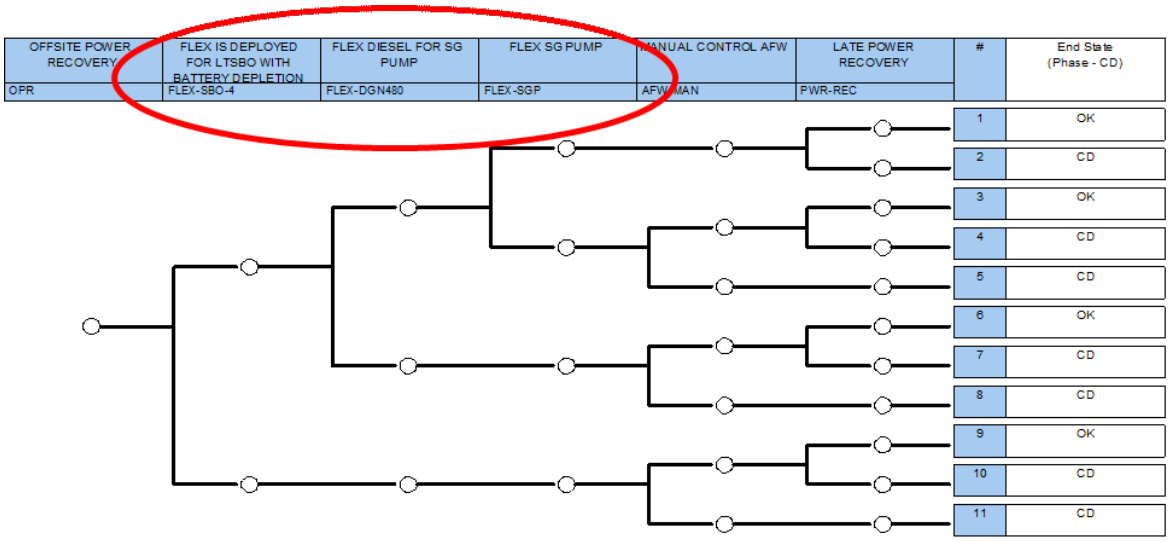

Figure 3-5. Revised SBO-4 Event Tree with New FLEX Top Events.

The logic, or fault trees, for FLEX-DGN480 and FLEX-SGP are presented in Figure 3-6 and Figure 3-7, respectively. Two redundant FLEX 480V DG trains and two redundant FLEX SG makeup pump trains are assumed in this study. Both independent and common cause failures (CCFs) for the failure modes of fail-to-start (FTS) and fail-to-run (FTR) are modeled. Equipment tests and maintenance, as well as human actions to use FLEX diesels and pumps, to refill alternative water tank for SG pumps are also modeled.

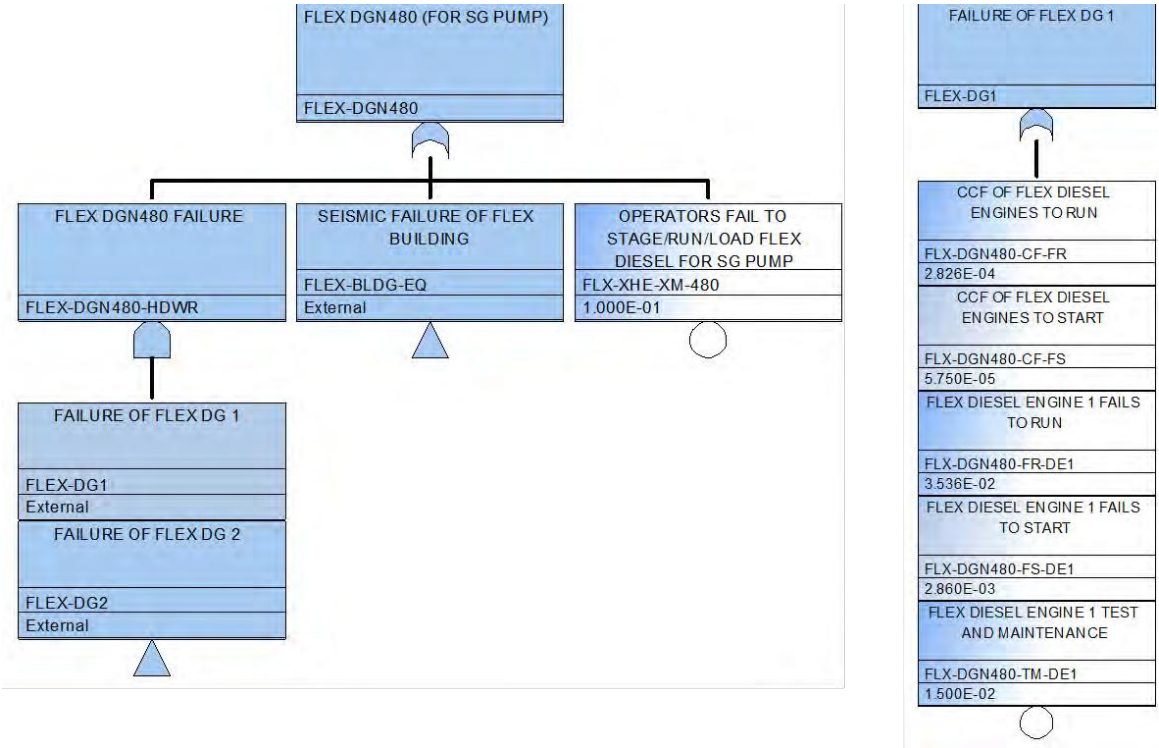

Figure 3-6. FLEX-DGN480 Fault Trees.

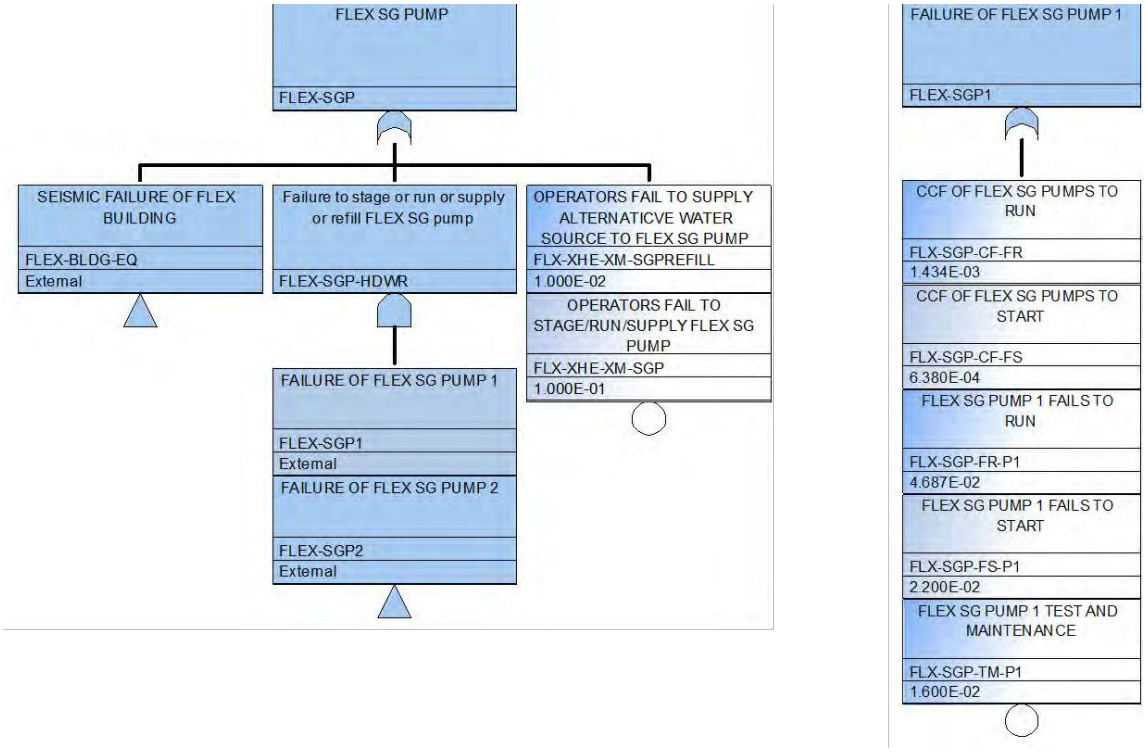

Figure 3-7. FLEX-SGP Fault Trees.

3.2.1.2 Data

For FLEX portable equipment, since there is very limited failure data available for them, generic failure rates for permanently-installed equipment as well as engineering judgments may have to be used or referred to. The NEI 16-06 cites the EPRI 3002003151 report (EPRI, 2014) that portable military equipment failure rates are higher, but are less than 10 times higher, than corresponding permanently-installed equipment failure rates assessed. In the meantime, PWR Owners Group (PWROG), with support from the boiling water reactor (BWR) Owners Group, is working to collect and analyze failure data for the most commonly-credited FLEX equipment. The preliminary results (Linthicum & Powell, 2019) from PWROG shows that, when compared with the industry average estimates for permanently installed PRA equipment as reported in NUREG/CR-6928 (Eide & al., 2007), the FTS failure probability of a portable DG and pump is more than 10 times higher than that of permanently-installed equipment, while the FTR failure rates vary against those of permanently-installed equipment (could be from three times lower to 60% higher). However, these preliminary results have large uncertainties due to limited operational time.

With insufficient industry data available to estimate portable equipment failure rates, this analysis uses the findings from above and assumes that the FLEX FTS failure probability is 10 times the industry average estimates for permanently-installed PRA equipment, and the FLEX FTR failure rate is the same of the industry average estimates for permanently-installed PRA equipment. The latest industry average estimates for permanently-installed PRA equipment can be found from the NRC Industry Average Parameter Estimates 2015 Update (NRC, 2017) on the Reactor Operational Experience Results and Database website https://nrcoe.inl.gov/resultsdb/AvgPerf/. Sensitivity studies could be conducted as needed to evaluate the impact of the data assumption on the analysis results.

For CCF, it is likely that the FLEX equipment and permanently-installed equipment is not in the same common cause group as they usually have different design characteristics, manufacturers, and operating and maintenance procedures. However, additional assessments should be conducted to make the final decision. Only the CCFs of the redundant FLEX DGs and SG pumps are currently modeled.

Table 3-1 presents the FLEX failure probabilities and failure rates used in this analysis. The template names such as EDG-SBO-FTS, EDG-FTS, EDG-TM, EDP-FTS under the Note column refer to those in the NRC Industry Average Parameter Estimates 2015 Update (NRC, 2017).

Table 3-1. FLEX Failure Probabilities/Rates.

Basic Event	Description	Failure Probability/Rate	Note
FLX-DGN480-FTS	FLEX Diesel Engine Fails to Start	3.0E-02	uses EDG-SBO-FTS which is about 10x of EDG-FTS
FLX-DGN480-FTR	FLEX Diesel Engine Fails to Run	1.5E-03	uses EDG-SBO-FTR which is about 1x of EDG-FTR
FLX-DGN480-TM	FLEX Diesel Engine Test and Maintenance	1.5E-02	uses EDG-EPS-TM
FLX-SGP-FTS	FLEX SG Makeup Pump Fails to Start	2.2E-02	uses 10x of EDP-FTS
FLX-SGP-FTR	FLEX SG Makeup Pump Fails to Run	2.0E-03	uses 1x of EDP-FTR-L
FLX-SGP-TM	FLEX SG Makeup Pump Test and Maintenance	1.6E-02	uses 1x of EDP-TM

3.2.1.3 Human Reliability Analysis

Other than FLEX data, FLEX human reliability analysis (HRA) is another big issue the industry encounters during the FLEX PRA modeling. It is recognized that existing HRA methods were

developed to evaluate and quantify human error probabilities (HEPs) associated with the operator actions taken in the control room. Yet, much of human actions in deploying, installing, and connecting FLEX equipment occur outside the control room, which may need innovative HRA methods for FLEX analysis. While Section 3.3 presents FLEX HRA for this research and the industry is actively working on new HRA methods for FLEX analysis, a scoping value of 0.1 is used as the HEP in this FLEX PRA analysis, which could certainly be revised and re-evaluate once FLEX HRA methods are developed and matured for use in the near future. Four FLEX human factor events are modeled, as shown in Table 3-2.

Table 3-2. FLEX Human Factor Events.

Basic Event	Description	Failure Probability
FLX-XHE-XE-SBO4	Operator Fails to Deploy Flex for SBO-4 Scenario	T/F
FLX-XHE-XM-480	Operators Fail to Stage/Run/Load FLEX Diesel for SG Pump	1.0E-01
FLX-XHE-XM-SGP	Operators Fail to Stage/Run/Supply FLEX SG Pump	1.0E-01
FLX-XHE-XM-SGPREFILL	Operators Fail to Supply Alternative Water Source to FLEX SG Pump	1.0E-01

3.2.2 FLEX PRA Model Quantification

The generic PWR LOOP/SBO SAPHIRE model includes four LOOP event trees: (1) LOOPGR for grid-related LOOP initiating events, (2) LOOPPC for plant-centered, (3) LOOPSC for switchyard-centered, and (4) LOOPWR for weather-related. The event tree structure is the same for all four LOOP event trees. The only differences are the initiating event frequencies and the AC power non-recovery probabilities. The above FLEX PRA model was implemented at the LOOP/SBO subtree SBO-4 level that would affect all four LOOP event trees. The four event trees were quantified with FLEX-incorporated using SAPHIRE 8. The total LOOP CDF with FLEX is 1.68E-6 per year (Table 3-3). When compared with the total LOOP CDF with no FLEX (2.28E-6 per year), the implementation of FLEX represents about 26% risk reduction.

Table 3-3. FLEX PRA Model Quantification Results.

LOOP ET	CDF No FLEX	CDF with FLEX	ΔCDF	ΔCDF%
LOOPGR	1.07E-06	8.12E-07	-2.55E-07	-23.9%
LOOPPC	6.21E-08	5.19E-08	-1.02E-08	-16.4%
LOOPSC	4.57E-07	3.58E-07	-9.85E-08	-21.6%
LOOPWR	6.89E-07	4.60E-07	-2.29E-07	-33.2%
LOOP Total	2.28E-06	1.68E-06	-5.93E-07	-26.1%

It should be noted that the above FLEX PRA analysis results represent the risk impact on a generic PWR plant. Plant-specific FLEX analysis should be conducted to evaluate plant-specific risk impact from the planned or implemented plant-specific FLEX equipment and strategies, which might be different from the results presented here due to different structure, system, and component (SSC) configurations, different plant risk profiles, and different SSC risk contributions and significance. In the meantime, FLEX reliability data and FLEX HRA included in this section could be improved with continuous industry efforts (see Section 3.3 for a preliminary FLEX HRA conducted for this research).

3.3 FLEX Human Reliability Analysis

3.3.1 Overview of an Approach to FLEX HRA[1]

This section provides a case study on how to perform human reliability analysis (HRA) for FLEX applications. Because of the availability of observational data from a South Korean stress test exercise involving the use of FLEX equipment, the case study presented in this section is centered on Korean operating experience. One characteristic of Korean NPPs is that they are multi-unit sites. As such, response to abnormal events involving FLEX equipment is inherently multi-unit. Nonetheless, the study provides a useful example of FLEX HRA that may be readily generalized to U.S. commercial plants. Of particular interest is the use of existing HRA methods to perform the analyses. While much research emphasis in the U.S. is on developing new methods and approaches to treat FLEX HRA, this section illustrates that it is in many cases possible to use existing HRA methods for FLEX. As such, this case study suggests investment and expertise U.S. plants already possess in existing HRA methods that can be applied to FLEX HRA. Of course, there is value in developing new approaches, but the successful deployment of legacy HRA methods in Korea demonstrates another possibility that should be considered for FLEX HRA.

After the accident at Fukushima Dai-ichi, a diverse and flexible coping strategy has been suggested to increase defense-in-depth for beyond-design-basis scenarios such as ELAP or loss of ultimate heat sink that could occur simultaneously at multiple units on a site (NEI, 2012). FLEX consists of four elements:

1. Both plant and FLEX equipment that provides means of obtaining power and water to maintain or restore key safety functions for all reactors at a site
2. Reasonable staging and protection of FLEX equipment from beyond-design-basis scenarios
3. Procedures and guidance to implement FLEX strategies
4. Programmatic controls that assure the continued viability and reliability of the FLEX strategies.

The addition of FLEX in existing defense-in-depth basically plays an important role in the mitigation of single-unit as well as multi-unit accidents.

Human reliability analysis is a collection of methods for analyzing human errors and providing human error probabilities (HEPs) for their application in PRAs (Pyy, 2000), (Swain & Guttmann, 1983). The main purpose of HRA in the context of a PRA is to identify, analyze, and quantify all human-related basic events in the logical structure of the PRA. These are also called human failure events (HFEs), and the error probabilities for them, i.e., HEPs, are generally estimated by HRA methods. To date, many HRA methods, such as the Technique for Human Error Rate Prediction (THERP) (Swain & Guttmann, 1983), Accident Sequence Evaluation Program (ASEP) (Swain, 1987), Cause-Based Decision Tree (CBDT) (Parry & et al., 1992), Human Cognitive Reliability (HCR) (Parry & et al., 1992), Standardized Plant Analysis Risk human reliability analysis (SPAR-H) (Gertman & et al., 2005), and Korean Standard HRA (Jung, 2005) have been developed and practically applied in a variety of complex systems, such as nuclear power plants (NPPs), military systems, aircraft, and chemical plants (Kim, Park, & Jung, 2017), (Swain, 1990).

[1] This section is adapted from "Human and organizational factors for multi-unit probabilistic safety assessment: identification and characterization for the Korean case" (Arigi, Kim, & Kim, 2019) and "Treatment of human and organizational factors for multi-unit HRA: application of SPAR-H method" (Park, Arigi, & Kim, 2019), which were published in the journals of *Nuclear Engineering and Technology 51 (2019) 104-115* and *Annals of Nuclear Energy 132 (2019) 656-678*, respectively. Because portions of those papers were developed under the LWRS, they are presented in this report to provide insights into human reliability analysis modeling for FLEX applications.

Currently-developed and -applied HRA methods generally focus on the analysis of human errors in single-unit PRAs with credit only to fixed equipment, while HRA methods for supporting FLEX strategies and multi-unit PRAs have not been well established (Arigi, Kim, & Kim, 2019). This implies that existing HRA methods may have several challenges to reflect the major characteristics for PRAs with FLEX strategies. To date, the common challenges and factors identified as important for FLEX HRA are extreme conditions, prioritization and limitation of resources, and stress level (Yalaoui & Yolande, 2018). In accidents requiring FLEX, the operational situation, as well as the human and organizational factors, could become more complex and significant than in less severe accidents.

Several reports, including (Arigi, Kim, & Kim, 2019), (CNSC, 2014), (Modarres, 2015), (Schroer & Modarres, 2013), and (St Germain & et al., 2017) indicate that the complexity of FLEX accidents depend considerably on the degree of unit-to-unit interactions for multi-unit sites. Human and organizational factors are regarded as two of the key factors that can influence these unit-to-unit interactions. If an accident occurs that influences more than one unit, the human and organizational factors due to the formation of accident management organizations, the use of shared or mobile equipment, and the influence of a severe accident on another unit (e.g., causing radiation release, increasing complexity, and causing accessibility issues) may have a critical impact on the plant safety and the PRA result. Therefore, issues have been raised regarding the analysis and evaluation of the human and organizational factors in the multi-unit HRA.

This section suggests an approach to treating the human and organizational factors for FLEX HRA. This approach is also applicable to Levels 1, 2, and 3 PRA—corresponding to design-basis accidents, beyond-design-basis accidents, and beyond-design-basis accidents with environmental release, respectively. Section 3.3.2 identifies and categorizes human and organizational factors for FLEX HRAs. This categorization is based on the review of the literature on severe accident management. Multi-unit HRA is an important consideration for FLEX because of the large number of multi-unit plants in the U.S. and internationally. Section 3.3.3 conducts a task analysis for the human task types for FLEX. Section 3.3.4 evaluates the applicability with a representative HRA method to identify the challenges of an existing HRA method for treating FLEX task types. Section 3.3.5 suggests the use of existing HRA methods to identify means for addressing these challenges while also considering a literature survey and actual practices. Again, because of the ready availability of completed FLEX implementations, this section draws heavily on experience with South Korean nuclear plants, but the lessons learned are readily generalizable to the U.S. commercial fleet of NPPs.

3.3.2 Human and Organizational Factors for FLEX HRAs

This section introduces human and organizational factors for FLEX HRAs categorized into five factors:

1. Organization
2. Task objects
3. Task
4. Performance shaping factors
5. Environmental factors.

These five factors play important roles in determining the results of HRA and highlight distinguishing features between accidents. This categorization is based on the review of literature on PRAs, literature on severe accidents management, as well as current Korean emergency response practice. Table 3-7 indicates a summary for comparison of human and organizational factors in FLEX HRA. The details are provided in (Arigi, Kim, & Kim, 2019).

Table 3-4. Comparison of Human and Organizational Factors in FLEX HRA.

Category		Single-Unit HRA with Credit Only to Fixed Equipment (Existing HRA)	Multi-Unit HRA
Organization		Main control room (MCR) operator, local operator	MCR, local operator, technical support center (TSC), emergency operating facility (EOF), Operating support center (OSC), sub-contractor
Task object		MCR board, fixed equipment, shared equipment	MCR board, fixed equipment, shared equipment, mobile equipment
Task	Task type	Available to two task types	Available to nine task types
	Collaboration & communication	MCR – local operator, MCR (Unit 1)–MCR (Unit 2)	Complex communication and collaboration occur
	Installation of mobile equipment	Not applicable	Installation of mobile equipment: sub-contractor, operation of mobile equipment: local operator
	Decision-making on priority of shared/mobile equipment	Not applicable	A standard and guideline for priorities for use of shared/mobile equipment is required.
	Situation awareness	Not explicitly considered in the current HRA	Situation awareness needs to be explicitly considered due to the insufficient information and necessity of prediction of situation.
Performance shaping factors (PSFs)		Applicable	The same PSFs are applicable, but the significance level of PSFs can be different.
Environment factors		Not applicable	Impact from radiation, debris from natural disaster, etc., need to be considered.

3.3.3 Task Analysis of FLEX Task Types

This section introduces six human task types and how they were analyzed by two task analysis approaches:

1. HRA event tree analysis suggested by THERP (Swain & Guttmann, 1983)
2. Timeline analysis.

Further details are described in the following sub-sections.

3.3.3.1 Human Task Types

Based on the human and organizational factors for the HRAs introduced in the previous section, this review defined six human task types by considering organizations and work devices for the FLEX HRA introduced in Table 3-4. Table 3-5 shows task types considered in this study. Following are the explanations for each task type. Type III and above are especially FLEX-centered because of the introduction of mobile equipment or main control room abandonment.

Table 3-5. Six Human Task Types Depending on Organizations and Work Devices.

No.	Task Type I		Task Type II		Task Type III		Task Type IV		Task Type V		Task Type VI	
	Task Sequence	Actor	Task Sequence	Actor	Task Sequence	Actor	Task Sequence	Actor	Task Sequence	Actor	Task Sequence	Actor
1	Diagnosis	MCR Operators	Diagnosis	MCR Operators	Diagnosis	MCR Operators	Diagnosis	TSC	Diagnosis	TSC	Diagnosis	TSC
2	Execution	MCR Operators	Execution (Fixed Equipment)	Local Operators	Execution (Mobile Equipment)	Local Operators	Transfer of Command	MCR Operators	Transfer of Command	MCR Operators	Transfer of Command	MCR Operators
3							Execution	MCR Operators	Execution (Fixed Equipment)	Local Operators	Execution (Mobile Equipment)	Local Operators

- Task Type I is the simplest task type. Main control room (MCR) operators diagnose plant states and execute the necessary actions on the MCR board. Task Type I is generally considered in existing HRAs. The MCR operators use emergency operating procedures (EOPs), abnormal operating procedures (AOPs), general operating procedures, system operating procedures, and Severe Accident Management Guidelines (SAMGs) to mitigate the accidents. As for an example of Task Type I, in the case that secondary heat removal using auxiliary feed water (AFW) or start-up feedwater (SFW) systems are unavailable in a transient scenario, MCR operators diagnose and perform a FAB operation on the MCR board using EOPs immediately after they recognize cues, such as an alarm for an AFW system, failure of AFW pumps, or failure of SFW pumps. In addition, when the MCR operators utilize shared equipment, such as an alternative AC diesel generator (AAC DG) or an instrument air system, this also corresponds to Task Type I. Lastly, the environmental effects for the tasks in Task Type I could be negligible as long as the MCR is not directly affected by fire or radioactivity.

- Task Type II indicates a task type in which the MCR operators make a diagnosis but give directives for the local operator to carry out vital actions on fixed equipment at the local site. EOPs, AOPs, general operating procedures, and SAMGs can be used for mitigating the accidents. For an example corresponding to Task Type II, when the MCR operators recognize that the atmospheric dumping valves (ADVs) cannot be opened on the MCR board, they communicate with the local operators and visit the local site to manually open the ADVs using hand switches. Furthermore, execution by local operators may require some time for fixed equipment access and may be affected by environmental factors, such as internal fire or debris due to seismic waves. These may block equipment routing and limit or delay access to areas (NEI, 2016).

- Task Type III is defined as a task type in which the diagnosis is performed in the MCR, and a local operator executes the mobile equipment in the NPP site. The operators who work in Task Type III can use AOPs, EOPs, and SAMGs. Especially, based on NEI 12-06 (NEI, 2012) or the multi-barrier accident coping strategy (MACST) (i.e., Korean version of FLEX) (Park & et al., 2018), FLEX support guidelines (FSGs) or MACST operating procedures (MOPs) are also considered for providing pre-planned strategies and accomplishing specific tasks, e.g., the use of mobile equipment, to support the functions of the EOPs and AOPs.

  Task Type III includes more complicated processes between the diagnosis by MCR operators and the execution by local operators. Figure 3-8 shows an example of the EOP related to the use of mobile equipment. For example, when the MCR operators diagnose that the AC power cannot be recovered within 2 hours in the situation of a station blackout, they declare an ELAP event and perform the procedures for the use of the mobile equipment according to the step in Figure 3-8, i.e., "Deployment and installation for FLEX/MACST equipment (FSG/MOP-02)." Then the MCR operators communicate with the field workers to deploy and install the mobile equipment. Lastly, the local operators utilize the mobile equipment. The actions performed in the local site could also be affected by environmental factors, such as internal fire or debris due to seismic waves.

1.0 Verify if AC power could be recovered within 2 hours	**1.0 Perform the actions below;** (1) FSG/MOP-01, "Load shed" (2) FSG/MOP-02, "Deployment and installation for FLEX/MACST equipment"

Figure 3-8. Example of the EOP Related to Use of Mobile Equipment.

- In Task Type IV, the diagnosis is made by the Technical Support Center (TSC), while the MCR operators implement the mitigating actions on the MCR board. This task also uses the procedures such as EOPs, SAMGs, and MOPs (or FSGs). The use of shared equipment could be an example of Task Type IV. The TSC carries out a strategic decision for the use of shared equipment and communicates with the MCR operators. Then, the MCR operators perform necessary actions on the MCR board based on the procedure corresponding to the decision made by the TSC. In addition, environmental effects could be negligible as long as the TSC or MCR are not directly affected by environmental factors, e.g., fire or radioactivity.

- For Task Type V, the TSC is the decision-maker and provides instructions to the MCR. The MCR operators diagnose adequate local actions based on the procedures, then the local operator executes on fixed equipment. The procedures including EOPs, SAMGs, and MOPs (or FSGs) are applied for this task type. Moreover, the execution by local operators requires some time to access the fixed equipment and is affected by environmental factors, such as internal fire or debris due to seismic waves.

- Task Type VI is the most complex task type. The TSC makes decisions and gives commands to the MCR. The MCR operators diagnose adequate actions based on the procedures and communicate with subcontractors to deploy and install the mobile equipment. The local operators then execute the mobile equipment after communicating with the MCR operators. This task employs the procedures such as EOPs, SAMGs, and MOPs (or FSGs). Additionally, deployment and installation of the mobile equipment by subcontractors or the execution by local operators could also be affected by environmental factors, such as internal fire or debris due to seismic waves.

3.3.3.2 Task Analysis for Task Types: Examples of Task Type I and V

Task analysis is the process of collecting task-related information necessary for performing HRA on the HFEs that require a detailed analysis (Ainsworth & Kirwan, 1992). Essentially, all of the detailed information related to the task is included in the task analysis together with the overall situation information about the task and the factors influencing the error occurrence. For task analysis in support of HRA, a variety of different techniques are used. Hierarchical task analysis is generally used in the process of identifying detailed task sequences, while timeline analysis identifies time-related information, such as the time window. Lastly, the results of the task analysis can be used as a direct input in the qualitative/quantitative analysis or as a technical basis for such an input.

In this section, the task analysis approach comprised the following:

1. The HRA event tree analysis suggested by THERP (Swain & Guttmann, 1983)
2. A timeline analysis.

Both of these were performed for the six task types. First, the HRA event tree analysis decomposes each task type into multiple subtasks. The task types defined by the organizations and work devices could have a relatively complex structures and are composed of several subtasks that may have different task characteristics. The tasks may also be performed by different organizations with different work devices and different communication paths. For example, the use of mobile equipment consists of a few subtasks with different organizations and task characteristics, such as the deployment and installation of mobile equipment by subcontractors and the execution by the local operator. Secondly, a timeline analysis of each task type is required for the following:

1. Investigating how the timeline is composed of the times for the subtasks involved in each task type
2. Identifying the time window that refers to the available time for the task to be completed to maintain the state of the plant successfully.

This time information is an important input for estimating HEPs in HRA (Parry & et al., 1992), (Swain & Guttmann, 1983). This study essentially analyzed the time window as defined and considered in SPAR-H.

The following sections include representative examples of the task analysis for Task Types I and V. These tree types include all the aspects of HRA discussed above and are representative tasks for FLEX deployment.

Task Analysis of Task Type I

Task Type I could be divided into two-unit tasks:

1. Diagnosis by MCR operators
2. Execution by MCR operators.

These divisions were made based on the task characteristics introduced in the previous section. Figure 3-9 and Table 3-6 show the HRA event tree and its branch explanation for Task Type I, respectively. In the HRA event tree, each of the tasks is treated as either a success or a failure. The use of x-F (where x represents a number), such as "1-F" or "2-F", in Figure 3-9 indicates a failure to perform a unit task, while S represents the success of the task. In addition, when each task fails, there are possibilities for recovery by several factors, such as self-review or reviews by others like extra crew or a shift technical advisor (Jung, 2005), (Parry & et al., 1992). The notations recovered from the failures such as "1" or "1 or 2" in Figure 3-9 indicate the possible stages that could be moved by the recovery factors. Lastly, Fx, where x is a number such as "F1" or "F2", represents an irretrievable failure of the task and the probability of each Fx is estimated by multiplication with a HEP and its recovery failure probability (RFP) of a human task. It leads to the failure of a corresponding task type. In other words, the error possibility of each task type can be calculated by the sum of all the Fx values. Therefore, the HEPs for Task Type I could be calculated by equation (1), as follows.

$$HEP\ for\ Task\ Type\ I = Probability\ of\ "F1" + Probability\ of\ "F2" = HEP\ ("A") \times RFP\ ("A") + HEP\ ("B") \times RFP\ ("B") \quad (1)$$

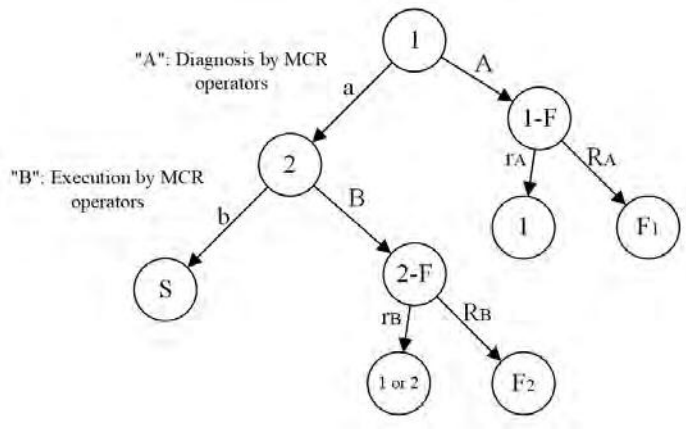

Figure 3-9. HRA Event Tree of Task Type I.

Table 3-6. Branch Explanation in HRA Event Tree of Task Type I.

Task	Potential Performance	Notation in HRA Event Tree
"A": Diagnosis by MCR operators	Success in diagnosis	a
	Failure in diagnosis	A
	Success in the recovery of A	rA
	Failure in the recovery of A	RA
"B": Execution by MCR operators	Success in execution	b
	Failure in execution	B
	Success in the recovery of B	rB
	Failure in the recovery of B	RB

Figure 3-10 shows the time window of Task Type I, T_{SW}, calculated by equation (2), below.

$$Time\ window\ for\ Task\ Type\ I = T_{Delay} + T_{Diagnosis} + T_{Execution} + Time\ margin \quad (2)$$

The equation consists of the delay time (T_{Delay}), diagnosis time by MCR operators ($T_{Diagnosis}$), execution time by MCR operators ($T_{Execution}$), and time margin. The delay time refers to the time that the MCR operators recognize a cue by alarm or disturbance noted after an initiating event, while the diagnosis and execution time indicate the time taken for the MCR operators to diagnose and execute proper actions, respectively. The time margin refers to the arithmetic difference between the sum of the time required and the time available (EPRI, 2016). The time required refers to the crew response time required for, e.g., diagnosis, execution, deployment, or installation, while the time available indicates the time available for operator actions and is estimated by subtracting T_{SW} from delayed times, such as the time taken for the operators to recognize the cue, or the time that personnel or equipment is temporally unavailable.

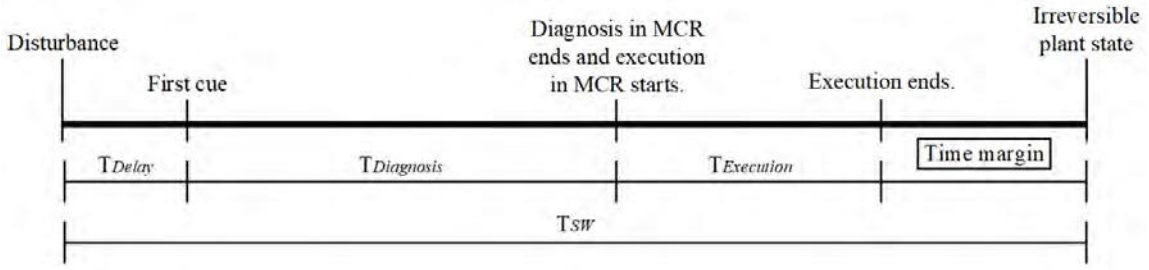

Figure 3-10. Time Window of Task Type I.

Task Analysis of Task Type V

Task Type V is comprised of five subtasks:

1. Decision-making by the TSC
2. Communication between the TSC and MCR operators
3. Procedure-following by the MCR operators,
4. Communication between the MCR and local operators
5. Access and execution of fixed equipment by local operators, based on the task characteristics introduced in the previous section.

Figure 3-11 and Table 3-7 show the HRA event tree and its branch explanation for Task Type V, respectively. The HEPs for Task Type V can be calculated by equation (3) below:

$$HEP\ for\ Task\ Type\ V = Probability\ of\ \text{"F1"} + \text{Probability of "F2"} + Probabilityof\ \text{"F3"} + \text{Probability of "}F4\text{"} + \text{Probability of "F5"} = HEP\ (\text{"}A\text{"}) \times RFP\ (\text{"}A\text{"}) + HEP\ (\text{"}B\text{"}) + HEP\ (\text{"}C\text{"}) \times RFP\ (\text{"}C\text{"}) + HEP\ (\text{"}D\text{"}) + HEP\ (\text{"}E\text{"}) \times RFP(\text{"}E\text{"}) \quad (3)$$

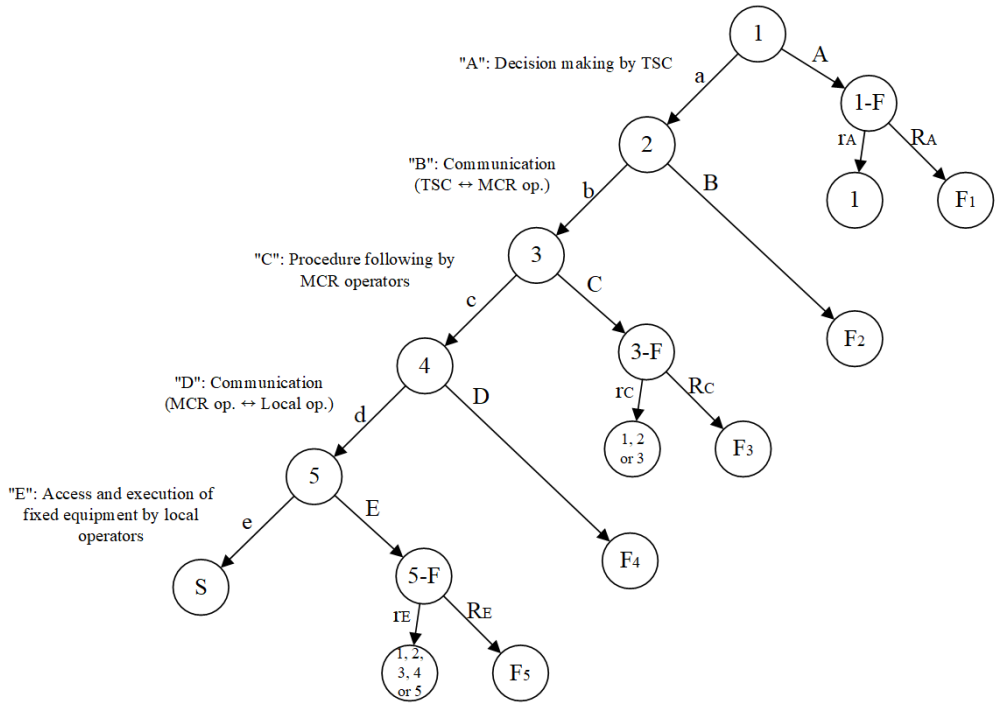

Figure 3-11. HRA Event Tree of Task Type V.

Table 3-7. Branch Explanation in HRA Event Tree of Task Type V.

Task	Potential Performance	Notation in HRA Event Tree
"A": Decision-making by TSC	Success in diagnosis	a
	Failure in diagnosis	A
	Success in recovery of A	rA
	Failure in recovery of A	RA
"B": Communication between TSC and MCR operators	Success in execution	b
	Failure in execution	B
"C": Procedure-following by MCR operators	Success in execution	c
	Failure in execution	C
	Success in recovery of C	rC
	Failure in recovery of C	RC
"D": Communication between MCR and local operators	Success in execution	d
	Failure in execution	D
"E": Access and execution of fixed equipment by local operators	Success in execution	e
	Failure in execution	E
	Success in recovery of C	rE
	Failure in recovery of C	RE

Figure 3-12 shows the time window of Task Type V, T_{SW}, calculated by equation (4).

$$Time\ window\ for\ Task\ Type\ V = T_{Delay} + T_{Decision\text{-}making} + T_{Procedure\ following} + T_{Access} + T_{Execution} + Time\ margin \quad (4)$$

It is composed of delay time (T_{Delay}), decision-making time by the TSC ($T_{Decision\text{-}making}$), time taken to follow the procedure by the MCR operators ($T_{Procedure\ following}$), access time by local operators (T_{Access}), execution time by local operators ($T_{Execution}$), and a time margin.

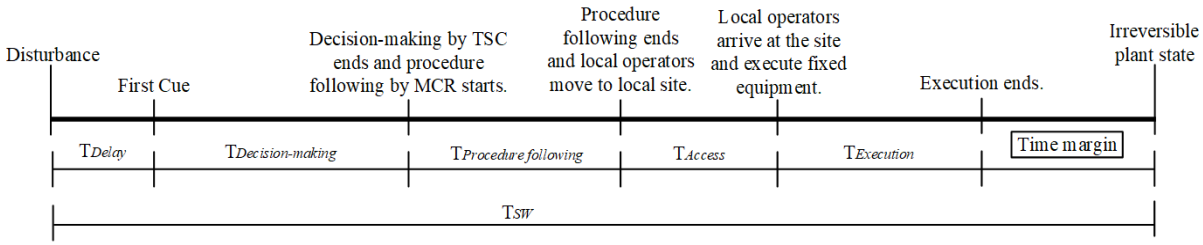

Figure 3-12. Time Window of Task Type V.

3.3.3.3 Summary of the Task Analysis Results

Table 3-8 indicates a summary of how to estimate HEPs according to the task types. The recovery failure probabilities identified by the HRA event tree analysis method of THERP are excluded from each equation. This is because this study assumed that the recovery factors in the approach being presented are reflected by following the rule in the SPAR-H method. The consideration of recovery factors in SPAR-H is quite different from that of THERP (Gertman & et al., 2005), (Swain & Guttmann, 1983). The THERP considers the error recovery possibility by the review of second checkers, supervisors, or the appearance of a second crew in situations where additional steps in procedures can cause an error, help determine the correct response, and reflect it to modify the HEPs. On the contrary, SPAR-H models restoration or reparation actions in more detail in the fault tree or adjusts the nominal HEP by assigning the appropriate positive levels to the appropriate subset of performance-shaping factors (PSFs) in order to reflect potential recovery influences on HEPs.

Table 3-8. Summary of Equations for Estimating HEPs According to Task Types.

No.	The Equations for Estimating HEPs
Task Type I	HEP (Diagnosis by MCR operators) + HEP (Execution by MCR operators)
Task Type II	HEP (Diagnosis by MCR operators) + HEP (Communication between MCR operators and local operators) + HEP (Assess and execution of fixed equipment by local operators)
Task Type III	HEP (Diagnosis by MCR operators) + HEP (Communication between MCR operators, subcontractors, and local operators) + HEP (Deployment and installation of mobile equipment by subcontractors) + HEP (Execution of mobile equipment by local operators)
Task Type IV	HEP (Decision-making by TSC) + HEP (Communication between TSC and MCR operators) + HEP (Procedure-following by MCR operators) + HEP (Execution by MCR operators)
Task Type V	HEP (Decision-making by TSC) + HEP (Communication between TSC and MCR operators) + HEP (Procedure-following by MCR operators) + HEP (Communication between MCR operators and local operators) + HEP (Assess and execution of fixed equipment by local operators)
Task Type VI	HEP (Decision-making by TSC) + HEP (Communication between TSC and MCR operators) + HEP (Procedure-following by MCR operators) + HEP (Communication between MCR operators, subcontractors, and local operators) + HEP (Deployment and installation of mobile equipment by subcontractors) + HEP (Execution of mobile equipment by local operators)

Table 3-9 shows a summary of the equations used to estimate the time windows according to task types.

Table 3-9. Summary of Equations for Estimating Time Windows According to Task Types.

No.	Equations for Estimating Time Windows
Task Type I	T (Delay) + T (Diagnosis by MCR operators) + T (Execution by MCR operators) + Time margin
Task Type II	T (Delay) + T (Diagnosis by MCR operators) + T (Access to fixed equipment by local operators) + T (Execution of fixed equipment by local operators) + Time margin
Task Type III	T (Delay) + T (Diagnosis by MCR operators) + T (Dead) + T (Deployment and installation by subcontractors) + T (Execution of mobile equipment by local operators) + Time margin
Task Type IV	T (Delay) + T (Decision-making by TSC) + T (Procedure-following by MCR operators) + T (Execution by MCR operators) + Time margin
Task Type V	T (Delay) + T (Decision-making by TSC) + T (Procedure-following by MCR operators) + T (Access to fixed equipment by local operators) + T (Execution of fixed equipment by local operators) + Time margin
Task Type VI	T (Delay) + T (Decision-making by TSC) + T (Procedure-following by MCR operators) + T (Dead) + T (Deployment and installation by subcontractors) + T (Execution of mobile equipment by local operators) + Time margin

3.3.4 Evaluation of Applicability for Existing HRAs Based on SPAR-H

This section evaluates the applicability of existing HRA methods to:

1. An analysis of FLEX task types
2. A dependence assessment between HFEs.

To demonstrate the applicability of an existing, representative HRA method for FLEX applications, we selected the SPAR-H (Gertman & et al., 2005) method, which was developed for the U.S. Nuclear Regulatory Commission by researchers at Idaho National Laboratory and has been broadly used by both industry and regulators in its intended area (i.e., NPPs in the U.S.), as well as in other industries like oil and gas (Groth & Swiler, 2012), (Petruni, et al., 2017), and (Rasmussen, Standal, & Laumann, 2015). Recently, Idaho National Laboratory also considered SPAR-H for multi-unit HRA (St Germain & et al., 2017).

In this study, SPAR-H has two major advantages to be applied as an alternative to creating new HRA methods. First, SPAR-H can be readily applied to FLEX applications by adjusting the PSF levels. Second, SPAR-H includes an approach to dependence assessment between HFEs; therefore, it could be useful to account for human and organizational dependencies, introduced as a major issue for FLEX HRA. The following sections provide further details on each evaluation.

3.3.4.1 Applicability of SPAR-H to Analysis of FLEX Task Types

This section appraises the applicability of SPAR-H for qualitative and quantitative analyses of FLEX tasks; subsequently, it identifies challenges for FLEX HRA depending on the task type. It first investigates whether SPAR-H is applicable to the qualitative analysis of HRA, such as the task, PSFs, and environmental factors. The second challenge is whether it can be applied to the quantitative aspects, i.e., nominal HEPs, PSF multipliers, and environmental factor multipliers.

To investigate the challenges of SPAR-H task types, the tasks involved in each type were evaluated and classified according to three criteria:

1. Applicable
2. Applicable, but revision required
3. Inapplicable.

Table 3-10 shows the results of the applicability evaluation for the existing SPAR-H method depending on six task types.

Tasks Evaluated as "Applicable"

FLEX tasks evaluated as "Applicable" represent existing HRAs, i.e., SPAR-H, that can be applied as developed. For example, the execution by MCR operators in Task Type IV can be analyzed by SPAR-H.

Tasks Evaluated as "Inapplicable"

"Inapplicable" tasks indicate those not covered by the existing SPAR-H method. Representatively, FLEX tasks, such as deployment and installation of mobile equipment by subcontractors or communication between TSC and MCR operators in Task Type III, have not been considered in existing SPAR-H analyses; therefore, these are evaluated as "Inapplicable."

Tasks Evaluated as "Applicable, but Revision Required"

"Applicable, but Revision Required" refers to the cases in which the existing SPAR-H method is applicable, but modification of the method is required. There are several cases for this. First, access to and execution of fixed equipment by local operators in Task Type II and execution of mobile equipment by local operators in Task Type III are similar to the execution by local operators treated in existing HRAs. A revision of the existing SPAR-H is recommended; however, the analysis of these tasks as environmental factors and the time to access the equipment is not considered in the existing SPAR-H method.

Second, procedure-following by MCR operators in Task Type IV is similar to diagnosis in the MCR with the only difference being that the decision-making critical to plant safety is already carried out by the TSC; thus, the MCR operators' diagnosis becomes relatively simple.

Third, diagnosis by the MCR operators in Task Type III and decision-making by the TSC in Task Types IV, V, and VI have different characteristics to diagnosis by the MCR operators in Task Type I or II, even though these are the diagnosis action. The diagnosis by MCR operators in Task Type III can be related to projecting the future states for the use of mobile equipment and deciding the deployment in advance and requires Level 3 Situation Awareness (SA)—projection and planning. Level 3 SA has rarely been reflected in existing HRAs, including SPAR-H.

The decision-making performed by the TSC may depend on the organizational characteristics of the TSC. The TSC has several distinguishing features compared with the MCR. For example, the TSC consists of more than 20 people and performs group decision-making, while the MCR is composed of five operators and the final decision-making is carried out by the shift supervisor.

Table 3-10. Results of Applicability Evaluation for Six Task Types.

No.	Result of Applicability Evaluation
Task Type I	• Diagnosis by MCR operators: Applicable • Execution by MCR operators: Applicable
Task Type II	• Diagnosis by MCR operators: Applicable • Communication between MCR and local operators: Inapplicable • Assess and execution of fixed equipment by local operators: Applicable, but revision required
Task Type III	• Diagnosis by MCR operators: Applicable, but revision required • Communication between MCR operators, subcontractors, and local operator: Inapplicable • Deployment and installation of mobile equipment by subcontractors: Inapplicable • Execution of mobile equipment by local operators: Applicable, but revision required

Task Type IV	• Decision-making by TSC: Applicable, but revision required • Communication between TSC and MCR operators: Inapplicable • Procedure-following by MCR operators: Applicable, but revision required • Execution by MCR operators: Applicable
Task Type V	• Decision-making by TSC: Applicable, but revision required • Communication between TSC and MCR operators: Inapplicable • Procedure-following by MCR operators: Applicable, but revision required • Communication between MCR and local operators: Inapplicable • Assess and execution of fixed equipment by local operators: Applicable, but revision required
Task Type VI	• Decision-making by TSC: Applicable, but revision required • Communication between TSC and MCR operators: Inapplicable • Procedure-following by MCR operators: Applicable, but revision required • Communication between MCR operators, subcontractors, and local operators: Inapplicable • Deployment and installation of mobile equipment by subcontractors: Inapplicable • Execution of mobile equipment by local operators: Applicable, but revision required

3.3.4.2 Applicability of SPAR-H to Dependence Assessment between HFEs

A dependency assessment of the existing SPAR-H method was conducted on single-unit HFEs, while an adequate approach to the dependency analysis between multi-unit HFEs has rarely been studied and is not yet well-established. It is not believed that this criteria for evaluating the dependency level in the existing SPAR-H can be perfectly applied in the same way to the dependency assessment between multi-unit HFEs. Therefore, it should be improved by additionally considering human and organizational dependencies important to multi-unit situations, especially in FLEX contexts.

3.3.4.3 A summary of FLEX HRA Challenges for the SPAR-H Method

Table 3-11 shows a summary of the FLEX HRA challenges for the existing SPAR-H method.

Table 3-11. Summary of FLEX Challenges for Existing SPAR-H.

	FLEX Challenges
HEP estimation for task type	• Analysis of a decision-making error by TSC • Analysis of a diagnosis error including Level 3 SA • Analysis of a procedure-following error by MCR operators • Analysis of a communication error between organizations • Analysis of an error for deploying and installing mobile equipment by subcontractors • Analysis of an error for assessing and executing fixed equipment by local operators • Analysis of an error for executing mobile equipment by local operators
Dependence assessment between HFEs	• Consideration of three human and organizational factors, i.e., human resources, radiological hazard, and use of shared/mobile equipment • Physical adjacency level between units

3.3.5 Suggestion of an Approach to HRA with FLEX Strategies

By treating the HRA challenges identified in the previous section, this section suggests how to:

1. Analyze FLEX task types
2. Evaluate dependencies between HFEs in FLEX accidents, based on the task analysis result and applicability evaluation of SPAR-H.

This approach essentially depends on the existing SPAR-H method with an additional literature survey and actual practices in Korean NPPs. For the range of uncertainty for the HEP estimated in this

approach, we assumed the SPAR-H uncertainty rule represented in Table 3-7 of NUREG/CR-6883 (Gertman & et al., 2005). The SPAR-H uncertainty follows the beta distribution, while alpha and beta values of the distribution are determined by the HEP. In addition, this section provides some examples of the analysis of FLEX tasks for the HRA.

3.3.5.1 Treatment of Challenges for the Existing SPAR-H Method

This section describes how to treat FLEX challenges for HEP estimation on task types and the dependence assessment between HFEs, which are summarized in Table 3-11.

3.3.5.1.1 Treatment of Challenges for HEP Estimation on FLEX Task Types

Analysis of a Decision-Making Error by TSC

The TSC's decision-making is similar to the diagnosis by MCR operators in existing HRAs as well as SPAR-H, but it differs in some task characteristics, including that the diagnosis actions are performed by the TSC. In this study, several SPAR-H PSFs reflecting the major characteristics of TSC's decision-making are identified for estimating the HEPs in this task. Table 3-12 shows the selected PSFs that reflect the characteristics of the TSC's decision-making. Ergonomics/HMI, available time, work process, and complexity are selected as corresponding SPAR-H PSFs, which are important to the TSC's decision-making. Subsequently, a guidance example on how to determine the PSF levels for estimate HEPs on the TSC's decision-making is suggested. Table 3-13 indicates SPAR-H PSFs and their multipliers for treating the TSC's decision-making. Lastly, the other SPAR-H PSFs, except for the PSFs included in Table 3-12 and Table 3-13, could be evaluated as identical to the existing SPAR-H.

Table 3-12. SPAR-H PSFs According to Characteristics of TSC's Decision-Making.

Characteristics of TSC	Description	Corresponding PSFs of SPAR-H
Accessibility and quality of information	• TSC indirectly obtains some information important to decision-making for mitigating the accident from the MCR and may not be equipped with the full set of systems for monitoring MCR parameters. Therefore, the TSC has relatively less quantity and accessibility of information for the plant states than the MCR.	• Ergonomics/HMI • Available time
Group decision-making	• TSC performs group decision-making with more than 20 people in Korean practice. The group decision-making may take benefit of the various strengths and expertise of its members and it is possible that the group can produce a greater number of alternatives that are of higher quality than the individual. However, it also has potential disadvantages that groups are generally slower to arrive at decisions than individuals, so sometimes it is difficult to use them adequately in situations where decisions should be made very quickly.	• Work process • Complexity • Available time

Determination of priority between units	• Third, the TSC's decision-making could affect both units simultaneously or affect the decision of other units. In Korea, when an accident influencing more than one unit occurs, a TSC is responsible for the diagnosis and control of the accident for two units. In this situation, if two units require the mobile or shared equipment simultaneously and the equipment can supply the function only for one unit, the TSC should determine the priority, i.e., which unit is more severe.	• It is not considered in PSFs, but dependence assessment will cover this in Section 3.3.5.1.2.

Table 3-13. SPAR-H PSFs and Their Multipliers for Treating TSC's Decision-Making.

SPAR-H PSF	PSF Level	Multiplier Value	Description
Complexity	Highly complex	5	• Evaluate this PSF at least more negative than "Moderately complex"
	Moderately complex	2	
Available time	Inadequate time	HEP=1.0	• This PSF depends on the relationship between the time available and the time required • Group decision-making essentially requires much more time. Evaluate available time PSF by considering the time required for decision-making, or conservatively evaluate it as at least more negative than "Time available ≥ time required"
	Time available is equal to the time required	10	
	Nominal time	1	
	Time available ≥ 5x time required	0.1	
	Time available ≥ 50x time required	0.01	
Work process	Poor	2	• Evaluate this PSF at least more negative than "Nominal"
	Nominal	1	
Ergonomics /HMI	Missing/misleading	50	• Evaluate this PSF at least more negative than "Nominal"
	Poor	10	
	Nominal	1	

In addition, there are several studies related to Level 2 (i.e., severe accident) HRA methodologies that tried to analyze decision-making errors when the TSC performs SAMG. First, (Boring, Germain, Banaseanu, Chatri, & Akl, 2015) suggested an approach to the Level 2 HRA based on SPAR-H. Several sets of SPAR-H PSFs considering the special characteristics of Level 2 PRAs were suggested in terms of HRA. Second, (Baumont, Menage, Schneiter, Spurgin, & Vogel, 2000) developed a Level 2 HRA method, i.e., the Human and Organizational Reliability Analysis in Accident Management method. It includes a decision tree for estimating the HEPs on five PSFs, such as human intervention, available time, man-machine interface, training and experience, and recovery procedures. Third, (Richner, 2006) distinguished three difficulty levels according to the difficulty of the decision-making tasks included in SAMG, then allocated the HEPs, assumed on the basis of the ASEP and THERP HRA methods. This method, especially, has experience being applied to the Beznau NPP in Switzerland.

In summary, these studies analyzed the task characteristics when the TSC performs SAMG and the way to estimate the HEPs on this task were suggested on the basis of several PSFs, i.e., available time, complexity, work process, ergonomics/HMI, experience, procedures, and stress/stressor. In particular, four PSFs—i.e., available time, complexity, work process, and ergonomics/HMI—are already identified in Table 3-12 based on the task characteristics of the TSC's decision-making.

This study also suggests a guide on how to select the SPAR-H PSF levels for the TSC's SAMG operation from the above-mentioned studies. Table 3-14 indicates the SPAR-H PSFs and their multipliers for when the TSC performs SAMG. Other SPAR-H PSFs, except for those in Table 3-14, could be evaluated as identical to standard SPAR-H analyses.

Table 3-14. SPAR-H PSFs and Their Multipliers When TSC Performs SAMG.

SPAR-H PSF	PSF Level	Multiplier Value	Description
Complexity	Highly complex	5	• Evaluate this PSF at least more negative than "Moderately complex".
	Moderately complex	2	
Available time	Inadequate time	HEP=1.0	• This PSF depends on the relationship between the time available and the time required. • Group decision-making takes much more time. Evaluate Available time PSF by considering the time required for decision-making, or conservatively evaluate it as at least more negative than "Time available ≥ time required".
	Time available is equal to the time required	10	
	Nominal time	1	
	Time available ≥ 5x time required	0.1	
	Time available ≥ 50x time required	0.01	
Work process	Poor	2	• Evaluate this PSF at least more negative than "Nominal".
	Nominal	1	
Ergonomics /HMI	Missing/misleading	50	• Evaluate this PSF at least more negative than "Nominal".
	Poor	10	
	Nominal	1	
Experience	Low	10	• Evaluate this PSF at least more negative than "Nominal".
	Nominal	1	
Procedures	Not available	50	• Evaluate this PSF at least more negative than "Available, but poor".
	Incomplete	20	
	Available, but poor	5	
Stress/stressor	Extreme	5	• Evaluate this PSF at least more negative than "High".
	High	2	

Analysis of a Diagnosis Error including Level 3 SA

Unlike the typical diagnosis by the MCR operators in Task Types I and II, it is necessary to decide the use of mobile equipment, then recall that Level 3 SA (i.e., projection and planning) is required to project the future states for the use of mobile equipment and deployment in advance. In this case, the Level 3 SA should be properly considered for estimating the HEPs, as existing HRAs, including SPAR-H, rarely reflect the Level 3 SA. However, few data are available for the evaluation of the Level 3 SA. Therefore, the best approach in this case is to select appropriate PSFs related to Level 3 SA and apply their multipliers to estimating HEPs.

First, this study identified some PSFs based on the characteristics of the Level 3 SA for the use of mobile equipment. Table 3-15 shows the SPAR-H PSFs that reflect the characteristics of Level 3 SA for the use of mobile equipment, which are categorized into accessibility of information and burden to decision-making. In total, four PSFs, i.e., complexity, stress/stressors, procedures, and experience/training, were selected as influential SPAR-H PSFs to reflect Level 3 SA for the use of mobile equipment. Table 3-16 shows the selected SPAR-H PSFs and their PSF levels with multipliers. For example, the procedure PSF may be evaluated as at least more negative than "Available, but Poor," because the procedure may not explicitly include guidelines when the operators should start to deploy the mobile equipment, as explained in Table 3-15. Lastly, other SPAR-H PSFs, except for the PSFs in Table 3-15 and Table 3-16, could be evaluated in the same way that the SPAR-H is applied to general HRA analyses.

Table 3-15. SPAR-H PSFs According to Characteristics of Level 3 SA for Use of Mobile Equipment.

Characteristics of Level 3 SA	Description	Corresponding PSFs of SPAR-H
Accessibility of the information	• Operators continuously monitor and access the information for deploying, installing, and executing the mobile equipment (not a step-by-step, but dynamic task) • Operators may not have access to all the information necessary for the decision-making, as information may be missing, unavailable, or indirectly recognized by other organizations	• Complexity • Stress/stressors
Burden of decision-making	• Operators have to be able to project the possible future state for the use of mobile equipment and decide the deployment in advance because it takes a couple of hours to deploy the mobile equipment, or there may be some unexpected delays • Operators have to make a decision in a situation in which they do not have access to all the information necessary for the decision-making and the information may be uncertain • The procedure may not include guidelines that the operators should start to deploy the mobile equipment at some point	• Procedures • Experience/training • Complexity • Stress/stressors

Table 3-16. SPAR-H PSFs and Their Multipliers for Reflecting Level 3 SA for Use of Mobile Equipment.

SPAR-H PSF	PSF Level	Multiplier Value	Description
Complexity	Highly complex	5	• Evaluate this PSF at least more negative than "Moderately Complex"
	Moderately complex	2	
Procedures	Not available	50	• Evaluate this PSF at least more negative than "Available, but Poor"
	Incomplete	20	
	Available, but poor	5	
Experience/ training	Low	10	• Evaluate this PSF to be at least more negative than "Nominal"
	Nominal	1	
Stress/stressors	Extreme	5	• Evaluate this PSF at least more negative than "High"
	High	2	

Analysis of a Procedure-Following Error by MCR Operators

This task involves the operators in the MCR performing necessary actions based on the appropriate procedures by following the decision by the TSC. It is similar to the diagnostic actions by MCR operators in Task Types I and II, but it is different as the decision critical to plant safety is already made by the TSC. Therefore, if we compare the HEPs for the procedure-following and the diagnosis by MCR operators, the former may be less than the latter in the situation when all the PSFs are evaluated at the same level. For this reason, this study recommends that this task be analyzed using the same approach as the existing SPAR-H for the typical tasks in Task Types I and II, as a conservative approach.

Analysis of a Communication Error between Organizations

Communication errors are not typically analyzed in SPAR-H, but there are several studies to estimate the error probabilities on communication errors. First, (Lee, Ha, & Seong, 2011) suggested a CREAM-based communication error analysis method (CEAM), which includes a quantitative approach to analyze the communication errors between the operators in NPPs. Based on the cognitive reliability and error analysis method CREAM (Hollnagel, 1998) and THERP, eight failure types of communication errors and nine adjustment factors to estimate the communication error probabilities are defined. Second, (Gertman & et al., 1992) developed the INTENT HRA method for estimating HEPs for decision-based errors. It defines 20 source categories for errors of intention, but only one of the error types among them includes a communication error with an execution error, as shown below.

- Error No. 17: Inadequate communication results in improper actions (Upper Bound: 2.1E-1, Lower Bound: 3.3E-3, EF: 8)

This study suggests a revised approach to estimate communication error probabilities based on the CEAM method, because it could reflect more varied and complex situations when compared with the INTENT HRA method. Further details on how to analyze communication errors are as follows:

First, identification of a failure type of communication error is required to determine a nominal error probability. The CEAM essentially defines eight failure types of communication errors according to the cognitive speaking process (CSP), which refers to the typical path from a planning process to a transmission process and is largely divided into planning and transmitting processes. Five failure types occur in the planning process that create the message, while the others originate from the transmitting process. Table 3-17 indicates eight nominal error probabilities depending on the failure types, distinguished into two categories, i.e., planning and transmitting processes.

Second, the total influence of context conditions should be determined to adjust the nominal error probability of the failure type, after determining a failure type and its nominal error probability from Table 3-17. The total influence of the context conditions is estimated by the sum of the weighting factors of the context conditions, and different context conditions were considered according to the CSP types. Table 3-18 shows the context conditions and their weighting factors according to CSP type. If a failure type is selected as the planning between CSP types, the total influence of the context conditions is calculated by the sum of the weighting factors for organization, workload, expertise level, and crew collaboration quality after the evaluation of each context condition.

In addition, the original CEAM approach considered nine context conditions for each CSP type: organization, work conditions, equipment, procedures, workload, available time, time of day, expertise level, and crew collaboration quality. However, this study considers that only four context conditions for planning and six context conditions for transmitting are moderately or highly correlated to each CSP type, as well as necessary to analyze the communication errors defined in this study.

For example, planning equipment is excluded because this context condition has a weak correlation with the planning process, as shown by Lee and colleagues (Lee, Ha, & Seong, 2011). Moreover, procedures among the context conditions in the original CEAM are excluded, as those for communication are nonexistent in situations where the operators communicate with other organizations.

Finally, the communication error probabilities are estimated by multiplying the nominal error probability of the failure types with the total influence of the context conditions. In addition, the communication error probabilities could differ depending on which organizations participate in the communication because failure types or the context conditions could be different. For example, the communication error probability between MCR and local operators could be positively assumed, as both the MCR and local operators typically work and train together. It may also have a lower error probability than the communication between the TSC and MCR operators.

Table 3-17. Nominal Error Probabilities According to Failure Type (Lee, Ha, & Seong, 2011).

CSP Type	Failure Type	Description	Nominal Error Probability
Planning	P1	Message is delivered to the wrong place or person	1.0e-3
	P2	Message transmission is inadequate	1.0e-3
	P3	Message production is inadequate	3.0e-3
	P4	Message content is wrong	5.0e-4
	P5	Message content is inappropriate for the receiver	1.0e-3
Transmitting	T1	Message is delivered at the wrong time	3.0e-3
	T2	Message is not delivered at all	3.0e-2
	T3	Message content is inconsistent content with other information	3.0e-3

Table 3-18. Context Conditions and Their Weighting Factors According to CSP Type (Lee, Ha, & Seong, 2011).

CSP Type	Context Condition	Context Condition Level	Weighting Factor
Planning	Organization	Very efficient	0.5
		Efficient	1
		Inefficient	1.5
		Deficient	5
	Workload	Nominal	1
		High	5
	Expertise level	High	0.5
		Nominal	1
		Low	5
	Crew collaboration quality	High	0.5
		Nominal	1
		Low	5
Transmitting	Organization	Very efficient	0.8
		Efficient	1
		Inefficient	1.2
		Deficient	2
	Equipment	Supportive	0.5
		Adequate	1
		Tolerable	1.5
	Working conditions	Good	0.8
		Nominal	1
		Bad	2
	Workload	Nominal	1

		High	2
	Expertise level	High	0.8
		Nominal	1
		Low	2
	Crew collaboration quality	High	0.8
		Nominal	1
		Low	2

Analysis of an Error for Deploying and Installing Mobile Equipment by Subcontractors

The deployment and installation of mobile equipment has not been considered and analyzed in existing HRAs, including SPAR-H, but several studies have tried treating FLEX/MACST actions related to the use of mobile equipment. Representatively, the NEI-16-06 (NEI, 2016) report provides guidance for analyzing FLEX/MACST actions based on the CBDT and THERP, while Kim et al. (2018a, 2018b) performed a preliminary HRA, including a detailed task analysis, qualitative analysis of error modes and PSFs with recovery potentials, and estimation of HEPs in association with deploying portable equipment, based on an EPRI external event HRA method, i.e., CBDT/HCR+THERP (EPRI, 2016). These approaches are similar as they analyze the tasks based on existing HRA methods.

This study suggests an approach to estimate the HEP of the deployment and installation of mobile equipment based on the above studies, the task characteristics, and the observation in the stress test. Figure 3-13 shows a flow chart for determining the HEP for the deployment and installation of mobile equipment. First, the task is classified into two states: (1) impossible to perform deployment and installation, and (2) possible to perform deployment and installation, according to whether the mobile equipment is available or not. When it is impossible to perform the deployment and installation, it is evaluated as a guaranteed failure (i.e., the HEP is 1.0). Case examples are provided below:

- *Case 1:* All the mobile equipment is already being used on other units in situations where the number of units is more than the amount of mobile equipment.
- *Case 2:* The route for mobile equipment is fully blocked and unavailable due to environmental factors, such as debris.
- *Case 3:* Qualified personnel is not available to drive the vehicle carrying the mobile equipment.

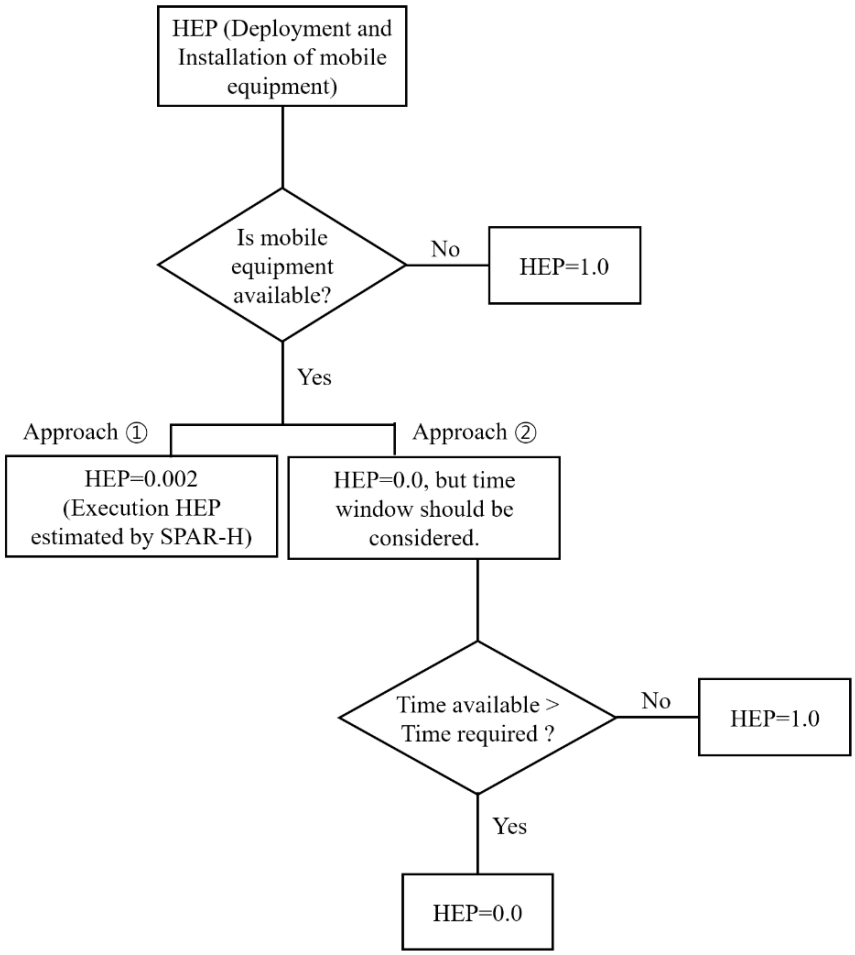

Figure 3-13. Flow Chart to Determine HEP for Deployment and Installation of Mobile Equipment.

Situations when it is possible to deploy and install the mobile equipment could be evaluated in two ways. The first is to analyze this task based on the existing SPAR-H. Table 3-19 indicates an estimation of the HEPs for the deployment and installation of mobile equipment using SPAR-H. The PSF levels and multiplier values are assumed based on the task characteristics and the observation in the stress test for Korean NPPs, and the HEP is estimated as 2.0e-3. In addition, this value has a similar range of the HEPs available to the THERP data, as follows.

- HEP=3.0e-3 (THERP Table 20-12, Select wrong controllers identified only labels) (Swain & Guttmann, Handbook of human-reliability analysis with emphasis on nuclear power plant applications, 1983)

Table 3-19. Estimation of HEPs for Deployment and Installation of Mobile Equipment using SPAR-H.

SPAR-H PSF	PSF Level	Multiplier Value	Estimated HEP
Available time	Nominal time	1	2.0e-3
Stress/stressor	High	2	
Complexity	Nominal	1	
Experience/training	Nominal	1	
Procedures	Nominal	1	
Ergonomics/HMI	Nominal	1	
Fitness for duty	Nominal	1	
Work process	Nominal	1	
Nominal execution HEP		1.0e-3	
Total influence of PSFs		2	
HEP (Deployment and installation of mobile equipment) = 2.0e-3			

The second approach is to set the HEP as 0.0 after evaluating the feasibility of the total time window, i.e., identifying whether the task is possible before the plant state becomes irreversible. This task comprises relatively simple physical actions that are not critical to the failure of the mobile equipment; however, it takes a lot of time to finish. Therefore, in this approach, if the time available for the system is sufficiently long for the operators to finish the task, the HEP should be evaluated as a success (HEP=0.0). The following aspects should be considered in applying this approach.

- *Required time for preparing deployment of mobile equipment:* The time for the subcontractors to prepare for deployment of the mobile equipment should be considered in T_{Dead} of the time window.
- *The number of units for which the subcontractors are responsible:* When the subcontractors are responsible for two units, and if they are working on the other unit, the deployment and installation for this unit can be delayed, allowing time to finish work on the other unit. This delay time should be considered in T_{Dead} in the time window.
- *The number of subcontractor personnel required for deployment and installation:* The number of personnel may affect the time required for deployment and installation, i.e., $T_{Deployment\ \&\ Installation}$ of the time window.
- *Clearing the path of debris:* More time may be required for deploying the mobile equipment due to debris. This should be considered in $T_{Deployment\ \&\ Installation}$ of the time window.

Analysis of an error for assessing and executing fixed equipment by local operators

This task is similar to that of execution by MCR operators, which has been considered in the scope of existing HRAs. In this case, the existing SPAR-H method could be used, but the access time and environmental factors could also be considered for reasonably estimating the HEPs in FLEX accidents.

First, access time refers to the time taken for local operators or subcontractor personnel to access the work device in a local place, such as fixed equipment or mobile equipment. It is recommended to consider this access time when estimating the execution HEP by applying SPAR-H.

Second, environmental factors (e.g., debris, radiation, and high temperature) that restrict operators from accessing the work device should be considered as a PSF. The NEI-16-06 includes details regarding how to reflect environmental factors on estimating the HEPs. Table 3-20 shows the multiplier values depending on the environmental factor levels, suggested by NEI-16-06.

Table 3-20. Multiplier Values According to Environmental Factor Levels (NEI, 2016).

Environmental Factor Level	Multiplier Value	Description
Nominal	x1	• Environmental factors are in nominal conditions
Adverse	x2	• Environmental factors are in adverse conditions that will not preclude the task (e.g., partial fire or a little debris)
Precludes	HEP=1.0	• Environmental factors preclude the task (e.g., completely blocking the path to work device)

Analysis of an error for executing mobile equipment by local operators

If the preceding task, i.e., deployment and installation of mobile equipment by subcontractors, fails, this task is evaluated as a guaranteed failure (HEP=1.0). If it succeeds, this task is analyzed in the same way to assess the error for assessing and executing fixed equipment by local operators. Environmental factors, as well as the access time, also need to be considered for reasonably estimating the HEPs in accident scenarios.

3.3.5.1.2 Treatment of FLEX Challenges on Dependence Assessment between HFEs

As noted, because many FLEX activities involve multiple units, it is important to consider actions that span units during FLEX. One challenge is that multi-unit dependence cannot be assessed adequately using the existing SPAR-H method. This study suggests a way to evaluate and treat dependencies between HFEs in the cut sets from the multi-unit PRA model. Figure 3-14 shows a decision tree for determining the dependency levels for the HFEs in multi-unit cut sets. It basically assumes that a TSC manages up to two units according to the Korean case. The dependency levels suggested in Figure 3-14 (i.e., Complete Dependence [CD], High Dependence [HD], Moderate Dependence [MD], Low Dependence [LD], and Zero Dependence [ZD]) essentially depend on the levels suggested in the approach of the existing SPAR-H and the experience in the stress test. Further details follow on the four evaluation factors considered for the dependence assessment: (1) type of cut set; (2) physical adjacent level; (3) human resource; and (4) work device.

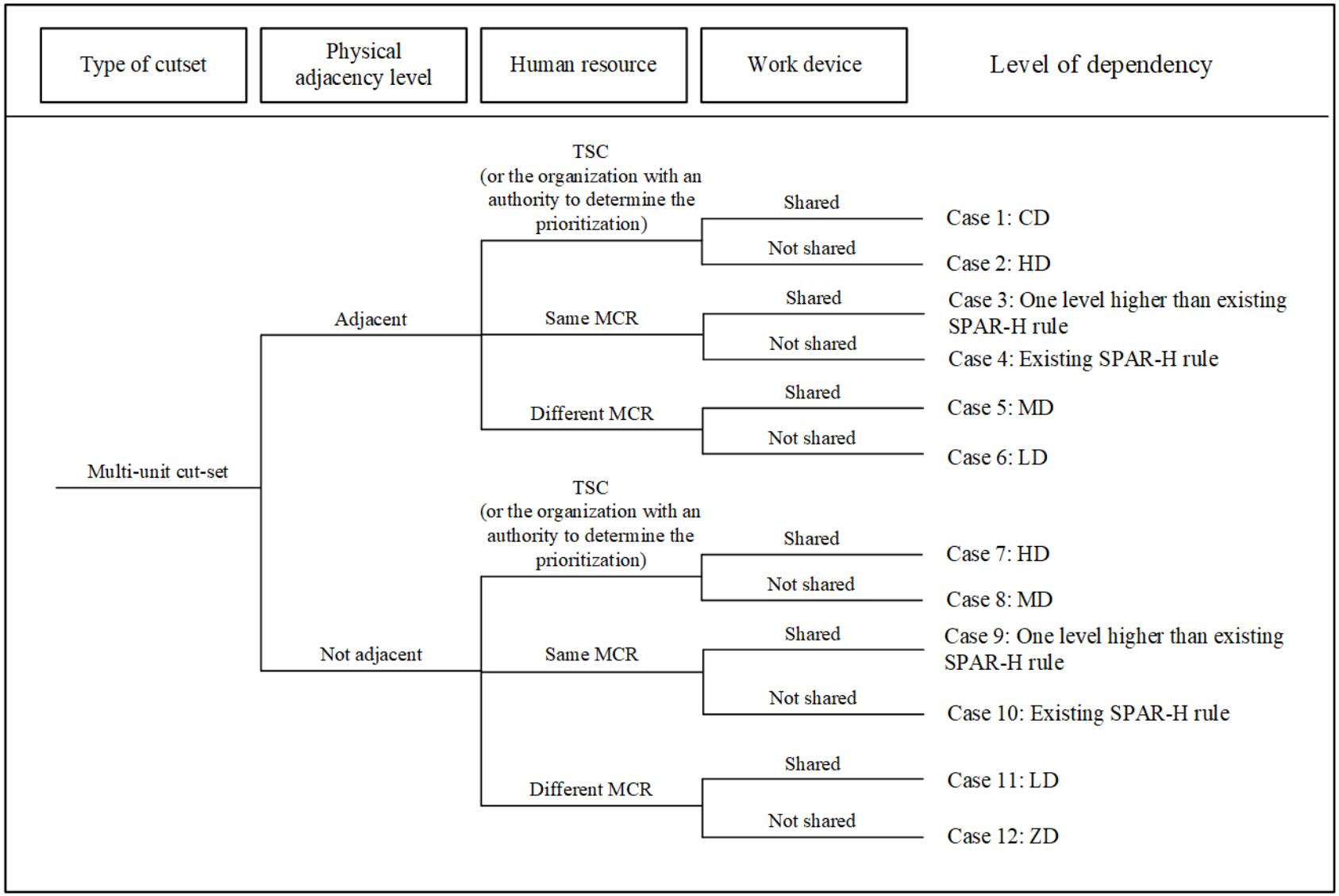

Figure 3-14. Decision Tree to Determine Dependency Levels for HFEs in FLEX Cut Sets.

First, the "Type of cut set" determines whether the cut set is generated from the multi-unit PRA model. The "Multi-unit cut set" in the branch of "Type of cut set" indicates the case that two HFEs are carried out in a single unit or different units. In addition, there are several exceptions that may not follow the existing rule. For example, a failure of the load shedding, which is a preceding action for the use of mobile equipment, can cause a guaranteed failure of the mobile equipment. If an HFE performing load shedding and another including the use of mobile equipment for the same unit are involved in a single-unit cut set, the dependency level between them should be evaluated as CD.

Second, the "Physical adjacency level" refers to whether the units where two HFEs occur are adjacent or not. "Adjacent" in the branch of "Physical adjacency level" corresponds to the cases that two units share mobile/shared equipment or auxiliary building, while "Not adjacent" shows the HFEs are not adjacent. The former may have higher dependency levels than the latter. For example, the closer the unit that the accident occurs is, the more likely it will be affected by, for example, radiological hazard or fire. In the case that two units share the equipment, use of the equipment for a unit may affect the use of the other.

Third, "Human resource" represents whether the previous HFE includes the failure of organization that has a higher authority for determining the priority of corresponding equipment, or whether the decision-making in the previous HFE is performed by the same MCR with the current HFE. The decision-making of this higher organization could highly affect the next HFE. Representatively, the TSC's decision-making errors may affect both units at the same time or affect the decision of other units via shared/mobile equipment, while MCR operators' decision-making is only dedicated to the corresponding unit. Therefore, the TSC's decision-making could have a higher dependency level than the MCR operators' decision-making. In addition, when the decision-making is performed by the same MCR in the previous and current HFEs, it may have a higher dependency level than the case that the decision-makings are carried out by the different MCR.

Lastly, "Work device" distinguishes the shared type of equipment, such as shared equipment or mobile equipment, and non-shared type of equipment, such as MCR board or fixed equipment. This factor asks whether the work device in the previous HFE is shared or not. The biggest difference between shared and not-shared equipment depends on the impact scope of the equipment. If the shared or mobile equipment is free from determining the priority between units, it could be selected as the non-shared type.

3.3.5.2 Examples of HEP Estimation for FLEX Task Types

Task Type III analysis example

This section introduces how to estimate HEPs of FLEX tasks for PRAs. Table 3-21 provides an example of an HFE corresponding to Task Type III. Table 3-22 shows the calculation sheet of the HFE for Task Type III. All the information in this example, such as timing information, PSF conditions, context conditions, and environmental factors, are assumed based on the experience in the stress test and NEI-16-06 (NEI, 2016). Finally, the HEP of the HFE for Task Type III was estimated as 7.3e-2.

Table 3-21. An Example of an HFE and Its Information for Task Type III.

Contents		Description
HFE		• Operators fail to operate the 1 MW mobile diesel generator early in a seismic event.
Details		• Due to a seismic event, a station blackout occurs and is extended to an ELAP situation. After the operators in the MCR declare ELAP under the condition that the TSC is not organized yet, they make a request to the subcontractors to deploy and install the 1 MW mobile diesel generator. Then, the subcontractor personnel move a vehicle carrying the diesel generator, a forklift for changing cable positions, and a vehicle carrying the cables to a designated place (i.e., deployment). After this, the subcontractors install the cable and connect it to the electric system of the corresponding unit. Finally, the local operators move to the local place that the mobile diesel generator is installed and start the equipment. • The electric power supplied from a 1 MW diesel generator is used for operating charging pumps in the early stage of an accident. Charging pumps play a role in the recovery of an accidental loss of coolant, due to the leak of the seal in the reactor coolant pumps. • The following are assumptions considered in this scenario. It is assumed that the subcontractor personnel are responsible for two units and they are already working on the other unit affected by the seismic event, while the mobile equipment is available to the unit requiring the mobile equipment. It takes 1 hour to begin deploying the equipment in the corresponding unit, after finishing the work on the other unit. Moreover, a fallen water tank is blocking the path for deploying the equipment. It also takes 1 hour to remove it and use the path.
Cue		AC power is not restored to the safety busses from the loss of all AC power.
Procedures		EOPs and FSG/MOPs
Personnel		MCR operators, subcontractors and local operators
Work device		Mobile equipment
Task type		Task Type III
FLEX tasks		Diagnosis by MCR operators, communication between MCR operators, subcontractors, and local operators, deployment and installation of mobile equipment by subcontractors, and execution of mobile equipment by local operators
Timing information	T_{SW}	8 hours
	T_{Delay}	90 minutes
	$T_{Diagnosis}$	5 minutes
	T_{Dead}	1 hour (Time to start deploying the equipment after the work is complete on the other unit)
	$T_{Deployment\ \&\ installation}$	1 hour (Time to remove the debris) + 2.5 hours (Time to deploy and install the equipment)
	$T_{Execution}$	30 minutes

Table 3-22. Calculation Sheet of HFE for Task Type III.

FLEX Tasks in Task Type III	SPAR-H PSF / Context Condition / Environmental Factor	PSF Level / Context Condition Level	Multiplier Value / Weighting Factor	Estimated HEP
Diagnosis by MCR operators	Available time	Expansive time	0.01	4.8e-2
	Stress/stressor	Extreme	5	
	Complexity	Moderately complex	2	
	Experience/training	Low	10	
	Procedures	Available, but poor	5	
	Ergonomics/HMI	Good	0.5	
	Fitness for duty	Nominal	1	
	Work process	Poor	2	
	Nominal diagnosis HEP		1.0e-2	
	Total influence of PSFs		5	
Communication between MCR operators and subcontractors	Organization	Efficient	1	8.0e-3
	Workload	High	5	
	Expertise level	Nominal	1	
	Crew collaboration quality	Nominal	1	
	Nominal error probability (Failure type: P2)		1.0e-3	
	Total influence of context conditions		8	
Communication between MCR operators and local operators	Organization	Very efficient	0.5	2.5e-3
	Workload	Nominal	1	
	Expertise level	High	0.5	
	Crew collaboration quality	High	0.5	
	Nominal error probability (Failure type: P2)		1.0e-3	
	Total influence of context conditions		2.5	
Deployment and installation of mobile equipment by subcontractors	Is mobile equipment available?	Yes	HEP=0.002	2.0e-3
	Selection of an approach	Approach ①		
Execution of mobile equipment by local operators	Available time	Time available >=5x the time required	0.1	1.2e-2
	Stress/stressor	High	2	
	Complexity	High	2	
	Experience/training	Low	3	
	Procedures	Available, but poor	5	
	Ergonomics/HMI	Nominal	1	
	Fitness for duty	Nominal	1	
	Work process	Nominal	1	
	Environmental factor	Adverse	2	
	Nominal execution HEP		1.0e-3	
	Total influence of PSFs		12	
∴ HEP of the HFE for Task Type III = 4.8e-2 + 8.0e-3 + 2.5e-3 + 2.0e-3 + 1.2e-2 = 7.3e-2				

Task Type V analysis example

Table 3-23 shows an example of an HFE corresponding to Task Type V. Table 3-24 shows the calculation sheet of the HFE for Task Type V. All the information in this example, such as the timing information, PSF conditions, context conditions, and environmental factors, are assumed based on the experience in the stress test and NEI-16-06 (NEI, 2016). The HEP of the HFE for Task Type V is estimated as 8.3e-1.

Table 3-23. Example of an HFE and Its Information for Task Type V.

Contents		Description
HFE		• Operators fail to depressurize pressure of the secondary side by manually opening ADVs in local site after the TSC is organized and performs SAMG.
Details		• When the TSC is organized and SAMG has been performed, operators in the MCR could try to cool the reactor coolant system via a steam generator, if possible. For the secondary heat removal using a stream generator, maintaining the inventory of the secondary side is important. In the case that the auxiliary or main feed water systems are unavailable, if the mobile pumps are ready to be executed for external injection, operators should depressurize the secondary side. This is done by manually opening ADVs in the local site to reduce the pressure of the steam generator to less than that of Shutoff Head. • After the TSC determines depressurization of the steam generator using ADVs among the catalog of available equipment, the MCR operators command the local operators to open the ADVs based on the procedures. Then, local operators access and execute the ADVs.
Cue		• The success of deployment and installation of the mobile pumps for external injection to the steam generator.
Procedures		SAMGs
Personnel		TSC, MCR operators, and local operators
Work device		Fixed equipment in local site
Task type		Task Type V
FLEX tasks		Decision-making by TSC, communication between TSC and MCR operators, procedure-following by MCR operators, communication between MCR and local operators, and access and execution of fixed equipment by local operators
Timing information	T_{SW}	8 h
	T_{Delay}	90 min
	$T_{Decision\ making}$	15 min
	$T_{Procedure\ following}$	5 min
	T_{Access}	10 min
	$T_{Execution}$	30 min

Table 3-24. Calculation Sheet of HFE for Task Type V.

FLEX Tasks in Task Type V	SPAR-H PSF / Context Condition / Environmental Factor	PSF Level / Context Condition Level	Multiplier Value / Weighting Factor	Estimated HEP
Decision-making by TSC	Available time	Time available ≥ 5x time required	0.1	8.0e-1
	Stress/stressor	High	2	
	Complexity	High	2	
	Experience/training	Low	10	
	Procedures	Available, but poor	5	
	Ergonomics/HMI	Poor	10	
	Fitness for duty	Nominal	1	
	Work process	Poor	2	
	Nominal diagnosis HEP		1.0e-2	
	Total influence of PSFs		400	
Communication between TSC and MCR operators	Organization	Inefficient	1.5	1.3e-2
	Workload	High	5	
	Expertise level	Nominal	1	
	Crew collaboration quality	Low	5	
	Nominal error probability (Failure type: P2)		1.0e-3	
	Total influence of context conditions		12.5	
Procedure-following by MCR operators	Available time	Nominal time	1	2.5e-3
	Stress/stressor	Nominal	1	
	Complexity	Nominal	1	
	Experience/training	High	0.5	
	Procedures	Nominal	1	
	Ergonomics/HMI	Good	0.5	
	Fitness for duty	Nominal	1	
	Work process	Nominal	1	
	Nominal diagnosis HEP		1.0e-2	
	Total influence of PSFs		0.25	
Communication between MCR and local operators	Organization	Very efficient	0.5	6.5e-3
	Workload	High	5	
	Expertise level	High	0.5	
	Crew collaboration quality	High	0.5	
	Nominal error probability (Failure type: P2)		1.0e-3	
	Total influence of context conditions		6.5	
Access and execution of fixed equipment by local operators	Available time	Nominal time	1	4.0e-3
	Stress/stressor	Extreme	5	
	Complexity	Moderately complex	2	
	Experience/training	High	0.5	
	Procedures	Nominal	1	
	Ergonomics/HMI	Nominal	1	

	Fitness for duty	Nominal	1	
	Work process	Nominal	1	
	Environmental factor	Adverse	2	
	Nominal execution HEP		1.0e-3	
	Total influence of PSFs		4	
∴ HEP of the HFE for Task Type V = 8.1e-1 + 1.3e-2 + 2.5e-3 + 6.5e-3 + 4.0e-3 = 8.3e-1				

3.3.5.3 Examples of Dependence Assessment between HFEs in FLEX cut sets

Table 3-25 includes two examples of cut sets from a multi-unit PRA model. In the cut sets, "#UNITS1" and "#UNITS2" are tag events indicating how many units failed, while "1#LOOP-07," "1#SBO-08," and "2#SBO-08" represent sequence tag events of the seventh sequence in a LOOP event in Unit 1, the eighth sequence of a SBO event in Unit 1, and the eighth sequence of an SBO event in Unit 2. The rules regarding these cut sets are further described in (Han, Oh, Lim, & Yang, 2018).

The underlying events in Table 3-25 represent the HFEs that are the subjects of the dependence assessment. The following sections include how to evaluate the dependence levels between HFEs in each cut set.

Dependence Assessment between HFEs in Cut Set #1

The first cut set in Table 3-25 includes two HFEs, i.e., "1AFOPHALTWT" and "1EGOPHDG01E." As the scenario unfolds, "1EGOPHDG01E" occurs first, and then "1AFOPHALTWT" is performed (the cut set order does not correspond to the scenario order of events). Table 3-26 represents detailed information on the HFEs in the first cut set. Table 3-27 provides the results of the evaluation of the HFEs in the first cut set, dependent on the dependence evaluation factors shown in Figure 3-14. As a result, according to Figure 3-14 and Table 3-27, the dependency level between these HFEs is evaluated as "Case 3: One level higher than existing SPAR-H rule."

Dependence Assessment between HFEs in Cut Set #2

The second cut set in Table 3-25 has two HFEs, i.e., "1EGOPHDG01E" and "2EGOPH-FLEX-TSC," which occur in different units, i.e., Units 1 and 2, respectively. Table 3-28 shows detailed information on the HFEs in the second cut set. Table 3-29 provides the results of the evaluation of the HFEs in the second cut set, dependent on the dependence evaluation factors shown in Figure 3-14. As can be seen in Figure 3-14 and Table 3-29, the dependency level between these HFEs is evaluated as "Case 5: MD."

Table 3-25. Cut Sets from Multi-Unit PRA Model.

No.	Basic Event #1	Basic Event #2	Basic Event #3	Basic Event #4	Basic Event #5	Basic Event #6	Basic Event #7	Basic Event #8	Basic Event #9	Basic Event #10
#1	%LOOP	#1UNITS	1#LOOP-07	1AFOPHALTWT	1EGDGR01A	1EGDGR01B	1EGOPHDG01E			
#2	%LOOP	#2UNITS	1#SBO-08	2#SBO-08	1EGDGS01A	1EGDGS01B	1EGOPHDG01E	2EGDGW01AB	2EGOPH-FLEX-TSC	NR-AC11HR

Table 3-26. Detailed Information on HFEs in the First Cut Set.

	1EGOPHDG01E	1AFOPHALTWT
Description	Operator fails to start AAC DG and connect to 4.16 kV bus (Task Type I).	Operator fails to arrange an alternate water source (Task Type II).
Unit that an HFE occurred	Unit #1	Unit # 1
Decision maker	MCR operators	MCR operators
Work device	Shared equipment (AAC DG)	Fixed equipment at the local site

Table 3-27. Evaluation Result of HFEs in the First Cut Set.

	Evaluation result
Type of cut set	• These HFEs included in a multi-unit cut set occur in the same unit (i.e., Unit #1). The type of cut set is evaluated as a "multi-unit cut set."
Physical adjacency level	• The HFEs occur in the same unit. Therefore, the physical adjacency level is evaluated as "Adjacent."
Human resource	• Decision maker for two HFEs is the same operators. It is evaluated as "Same MCR."
Work device	• The work device of the former HFE is a shared equipment, i.e., AAC DG. The work device is evaluated as "Shared."

Table 3-28. Detailed Information on HFEs in the Second Cut Set.

	1EGOPHDG01E	2EGOPH-FLEX-TSC
Description	Operator fails to start AAC DG and connect to 4.16 kV bus (Task Type I).	Operator fails to operate 1 MW mobile diesel generator (Task Type VI).
Unit that an HFE occurred	Unit #1 (Close to the unit #2)	Unit #2 (Close to the unit #1)
Decision maker	MCR operators	TSC
Work device	Shared equipment (AAC DG)	Mobile equipment (It is assumed that the number of mobile diesel generators is less than the number of units.)

Table 3-29. Evaluation Result of HFEs in the Second Cut Set.

	Evaluation Result
Type of cut set	• These HFEs included in a multi-unit cut set occur in different units (i.e., Unit #1 and #2). The type of cut set is evaluated as a "multi-unit cut set."
Physical adjacency level	• Units 1 and 2 are close together. Therefore, the physical adjacency level is evaluated as "Adjacent."
Human resource	• The subject for decision-making in the former HFE is MCR operators. It is evaluated as "Different MCR."
Work device	• The work device of the former HFE is a shared equipment, i.e., AAC DG. The work device is evaluated as "Shared."

3.3.6 Summary

This section has provided lessons learned on conducting FLEX HRA in South Korea. The example case study detailed different human task types relevant to FLEX analyses and demonstrated analyses using the SPAR-H HRA method. Special considerations were also explored for the case of multi-unit HRA and the impact on dependence calculations. This work is significant in that it illustrates the value of retaining existing HRA methods for FLEX applications. Of equal importance, while the case study provided is international, it is generalizable to U.S. commercial applications. Performing FLEX HRA can help identify the types of human errors that might be associated with different severities of accident and corresponding FLEX deployments. It can also ultimately help utilities take appropriate credit for successful FLEX deployment during accident scenarios.

4. RISK-INFORMED PASSIVE COOLING SYSTEM ANALYSIS

This section presents risk-informed analysis on a passive cooling systems, specifically the dynamic natural convection (DNC) system designed by DYNAC Systems. An overview of the DNC system and the RELAP5-3D modeling is presented in Section 4.1. The RELAP5-3D simulations of the DNC system in selected station blackout (SBO) scenarios are described in Section 4.2. Finally, the evaluation of the DNC system risk impact using the generic PRA model is conducted in Section 4.3.

4.1 DNC System RELAP5-3D Model

The DOE recently funded a proof-of-concept, bench-scale (~100 kW) DNC system test that was being conducted by a company called NuVision Engineering in association with its partner, DYNAC Systems. The DNC system relies on a passive condensing jet ejector that generates a pumping action (pressure differential) via condensation of saturated steam through the ejector that subsequently draws secondary cooling water into the steam mixture downstream of the ejector nozzle. This results in a continuous return flow to the steam generator.

While the design of the DNC system is proprietary to DYNAC Systems and the design details cannot be presented, this section presents an overview of the system scheme. Figure 4-1 shows an illustration of the DNC system. The system takes steam from the main steam line and mixes it with cooling water from a heat exchanger (HX) in a passive jet ejector to supply water to the feedwater line of a steam generator (SG). The passive jet ejector can generate sufficient head to cause natural circulation for mixed steam and water flow through the system. The heat exchanger is connected to a water pool or tank that contains water to remove decay heat for several days.

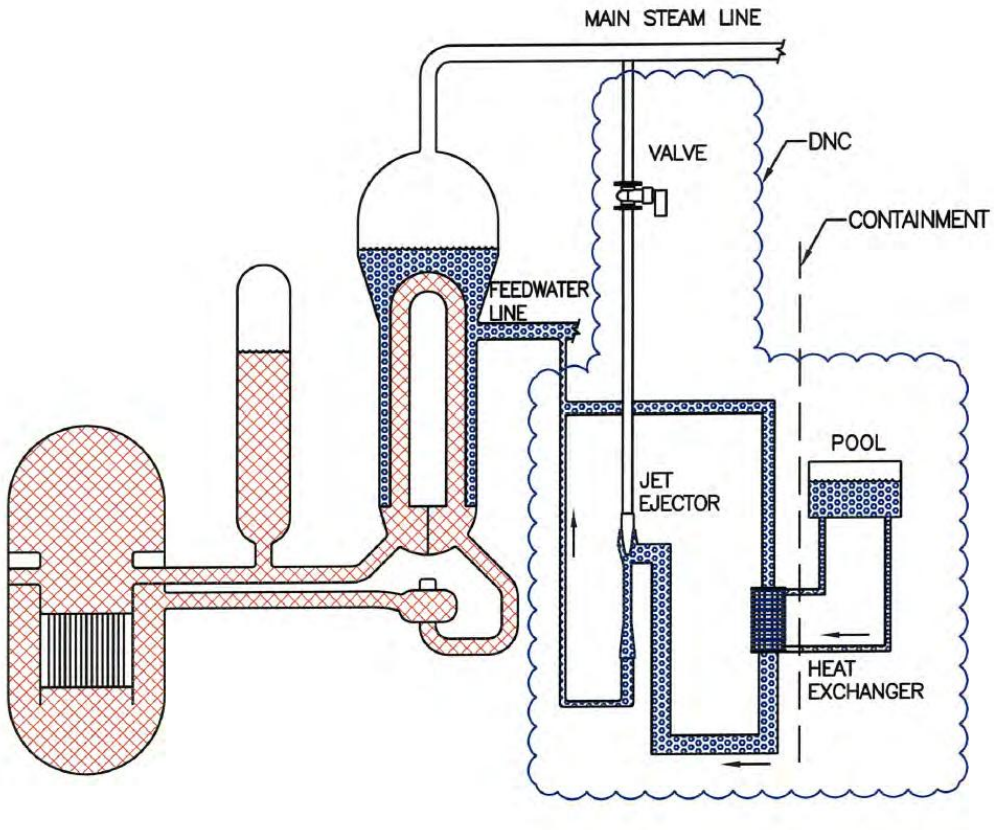

Figure 4-1. Schematic of the DNC System.

Previously, INL conducted an evaluation of the DNC system using RELAP5-3D (Davis, 2017). Although this report is not publicly available as it contains proprietary information, the same DNC system RELAP5-3D model

is used in this analysis after concurrence from DYNAC Systems. One difference from the 2017 model was the increased heat exchanger capability in this analysis in order to provide more typical values for the subcooling of the feedwater delivered to the SGs by the DNC system. Each DNC HX was sized to remove 24 MW of core power at a pressure of 8.16 MPa (1184 psia) in the current analysis, while the heat exchangers used in (Davis, 2017) were sized to remove 22 MW at the same pressure.

Figure 4-2 shows the nodalization of the model for the DNC system connected to the steam generator in Loop A. The system takes steam from the steam line (Component 284) and mixes it with cool water from a heat exchanger (Component 255) in the jet ejector, which is hereafter referred to as a conjector. The flow downstream of the conjector divides into two streams in Component 264. Most of the flow recirculates through Component 253 to the HX, while the remainder goes towards the steam generator downcomer (Component 272). The recirculating fluid flows inside the tubes of an HX that is immersed in a large pool, which is represented by Component 560. The mixing of the steam and the water in the conjector causes a pressure rise that induces natural circulation through the system. The models of the DNC systems attached to SG-B and SG-C are similar to those shown in Figure 4-2 for SG-A.

All three DNC HXs are connected to the same water pool. The flow through the DNC system was terminated when the collapsed pool level reached 67% of the height of the HX tubes. The actual performance of the DNC system with partially uncovered HX tubes is not known, but it seems reasonable to assume that the system can still operate normally when the tubes are mostly covered. The amount of time that the DNC system can remove decay heat can be easily extended by increasing the initial liquid inventory in the pool.

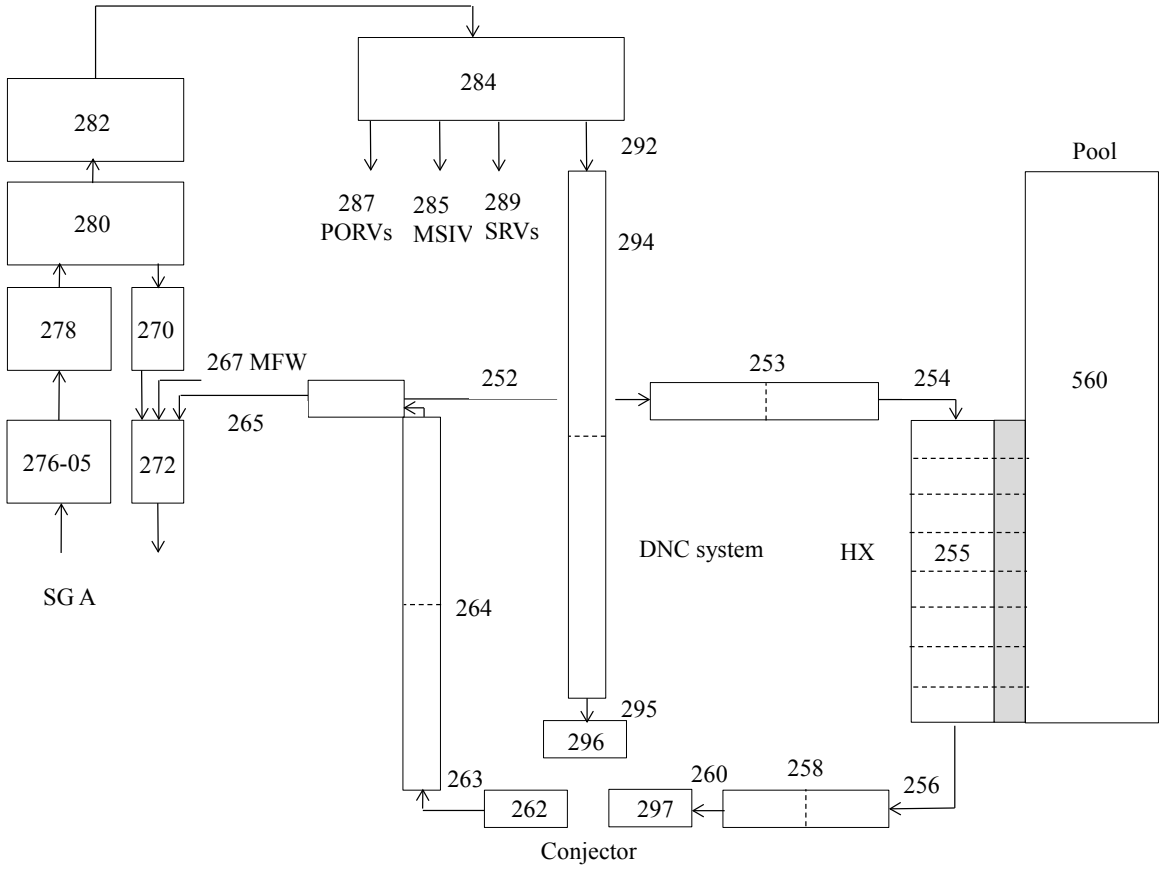

Figure 4-2. Nodalization of the DNC System Connected to SG-A.

RELAP5-3D does not have an explicit model of a conjector. Furthermore, the lengths and sizes of the pipes represented by Components 253, 258, 264, and 294 and the liquid volume of the pool are preliminary. Therefore, it is not possible to perform a mechanistic simulation of the DNC system at this time. The performance of the system is simulated using boundary conditions applied at Time-Dependent Volumes 262, 296, and 297 and Time-Dependent Junctions 252 and 292. These boundary conditions are based on correlations derived from the 100kW scaled experiments.

4.2 SBO Scenario Analysis with DNC and ATF

Three SBO scenarios from (Ma & al., 2018) were selected for DNC system RELAP5-3D analysis. The SBO event is initiated by a loss of offsite power and failure of both emergency diesel generators. Station batteries are assumed to be available for 4 hours. The event is similar to that described in (Ma & al., 2018) except that passive cooling due to the operation of the DNC system designed by DYNAC Systems was simulated.

The early responses of all three SBO scenarios (SBO-1.0, SBO-4.0, and SBO-6.0) were similar. The SBO was initiated by a loss of offsite power which was assumed to cause a reactor scram, a trip of the RCPs, an instantaneous loss of main feedwater (MFW), and a normal closure of the turbine stop valves. The loss of offsite power resulted in an instantaneous release of the control rods and a reactor scram. The loss of offsite power was also assumed to cause an instantaneous loss of MFW and a trip of all three RCPs. The MSIVs in the model were assumed to close 1 second after the loss of offsite power to simulate closure of the turbine stop valves. The motor-driven and turbine-driven AFW systems were assumed to be unavailable. A valve supplying steam flow to the DNC system opened at 15 second for each SG in which the DNC system was assumed to be available. Operation of the DNC systems resulted in controlled cooldowns of the primary and secondary systems. Leakage through the RCP seals was assumed to start 13 minutes after the beginning of the SBO based on Section 6.4 of (NRC, 2010). The nominal leakage varied between 21 and 480 gpm per RCP depending on the severity of the assumed failures in the seals.

The SIAS was initiated on low-low reactor pressure (12.34 MPa [1789.7 psia]) based on Page A-2 of (NRC, 2010), but the SIAS had no impact on the calculated results as the pumped safety injection systems were assumed to be unavailable.

The calculations were terminated when the maximum cladding temperature reached 2099 K for cases with Zircaloy and 1804 K for cases with FeCrAl and Chromite. These temperatures were assumed to represent significant core damage.

4.2.1 SBO-1.0

This scenario assumed that the MFW, AFW, and HPSI systems were not available during the SBO. All three DNC systems were assumed to be available. The only cooling mechanisms present were due to the inventory of water stored in the DNC pool, SGs, and RCS.

The calculated sequences of events are shown in Table 4-1. The reactor scram, RCP pump trip, termination of MFW, and the closure of the turbine stop valves all occurred within the first second of the event. The DNC systems began to operate at 15 seconds. RCP seal leakage began at 13 minutes. The nominal leakage was 21 gpm per pump. The cooling due to the DNC and the depressurization resulted in the SIAS at 38 minutes, but the HPSI pumps were assumed to fail. Accumulator injection began at 3 hours and 16 minutes. The station batteries were assumed to be depleted at 4 hours, but their failure had no impact on the passive DNC systems. The accumulators emptied after 56 hours. The operation of the DNC system was terminated near 62 hours because of a low pool level. Core decay heat was then removed by the boiling of the liquid in the SGs, which emptied near 72 hours. The RCS began to pressurize and the pressurizer SRVs began to cycle near 73 hours. Note that the pressurizer PORVs were assumed to not be available due to the loss of the station batteries at 4 hours. The core began to uncover near 74 hours. The differences between calculations due to the different claddings were negligible before the core began to uncover. The calculations were terminated when the hottest cladding reached its maximum

temperature. The termination times varied by up to 34 minutes. The calculated amount of hydrogen produced during the transients varied significantly between claddings. The amount of hydrogen produced was 0.0 kg for Chromite, 2.0 kg for FeCrAl, and 134.1 kg for Zircaloy. No hydrogen was produced for the case with Chromite coating because rupture was not calculated to occur. This prevented steam from reacting with the Zircaloy beneath the coating. A sensitivity calculation with Chromite that was run until a failure temperature of 2099 K showed the cladding ruptured about 4 minutes after the initial calculation was terminated.

Table 4-1. Sequence of Events for Scenario SBO-1.0.

Event	Time (hr:min)		
	Zircaloy	FeCrAl	Chromite
SBO occurs	0:00	0:00	0:00
RCP leakage begins	0:13	0:13	0:13
SIAS	0:38	0:38	0:38
Accumulator flow initiated	3:16	3:16	3:16
Batteries depleted	4:00	4:00	4:00
Accumulator flow terminated	56:25	56:24	56:26
DNC feedwater flow terminated	61:36	61:35	61:36
SG SRVs begin to cycle	66:56	66:56	66:56
All SGs empty	71:30	71:31	71:30
Pressurizer SRVs begin to cycle	73:02	73:00	73:03
PRT rupture disk opens	73:03	73:01	73:04
Core begins to uncover	73:38	73:43	73:46
0.5 kg H_2 generation	74:32	75:52	NA
First cladding rupture	75:32	75:59	NA
Core damage	75:36	76:10	76:10

The following figures illustrate the effects of the cladding on various parameters. Results are presented for SG-B, but all three SGs responded similarly in this scenario. The steam flow into the DNC system in SG-B is shown in Figure 4-3. The liquid flow delivered to the SG from the DNC system was approximately the same as the steam flow, so the liquid level was maintained at a high value (see Figure 4-4) until the operation of the DNC system was terminated near 62 hours because of a low level in the pool.

The calculated pressure in SG-B is illustrated in Figure 4-5. The pressure increased initially in response to the closure of the turbine stop valves and then decreased due to the opening of the DNC steam valves. The DNC automatically depressurized and cooled the SG. The maximum cooldown rate was about 20 K/h based on the change in the pressure. The pressure decreased until about 62 hours when the DNC was assumed to stop working. The pressure then increased until reaching the opening setpoint of the SG SRVs. The pressure cycled between the opening and closing setpoints until the liquid inventory was depleted near 72 hours. The SG PORVs were unavailable because the station batteries were assumed to be depleted at 4 hours.

The temperature of the feedwater delivered to SG-B by the DNC system is shown in Figure 4-6. The subcooling was greater than 20 K while the DNC system was operating.

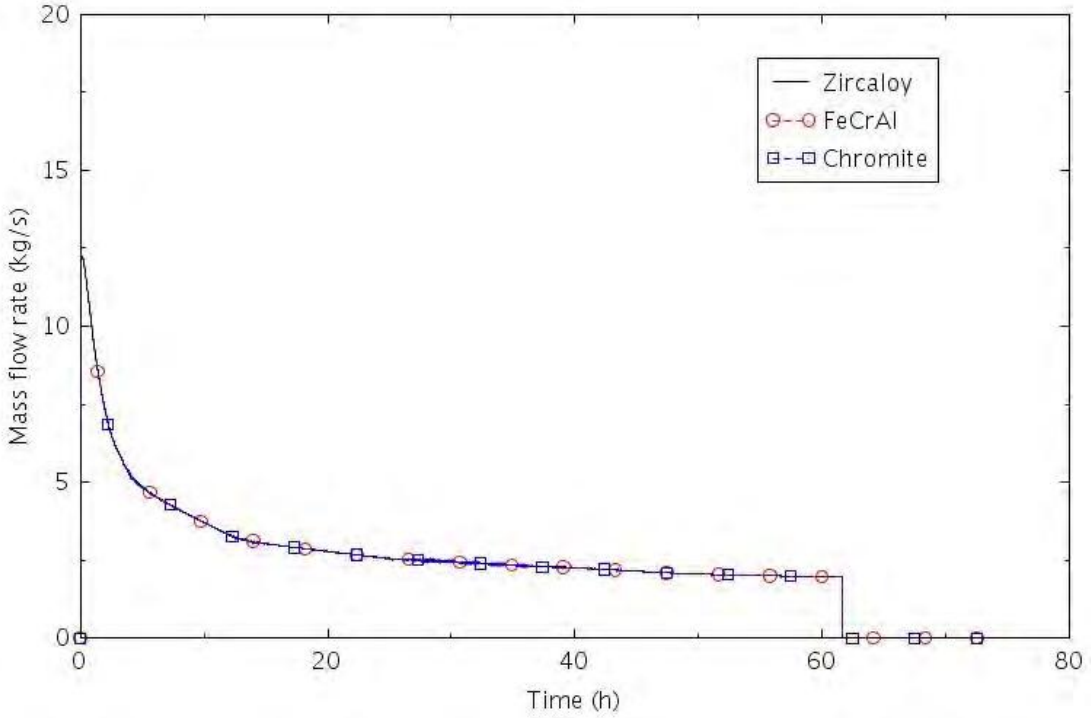

Figure 4-3. Steam Flow to the DNC System in SG-B (SBO-1.0).

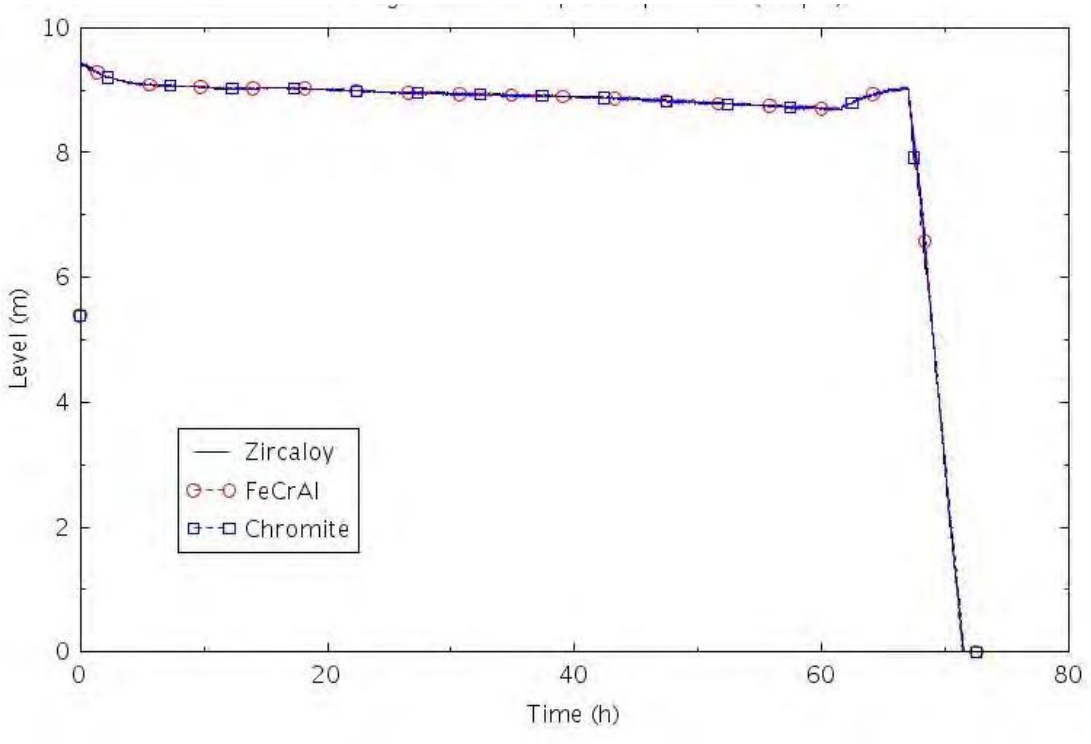

Figure 4-4.Collapsed Liquid Level in SG-B (SBO-1.0).

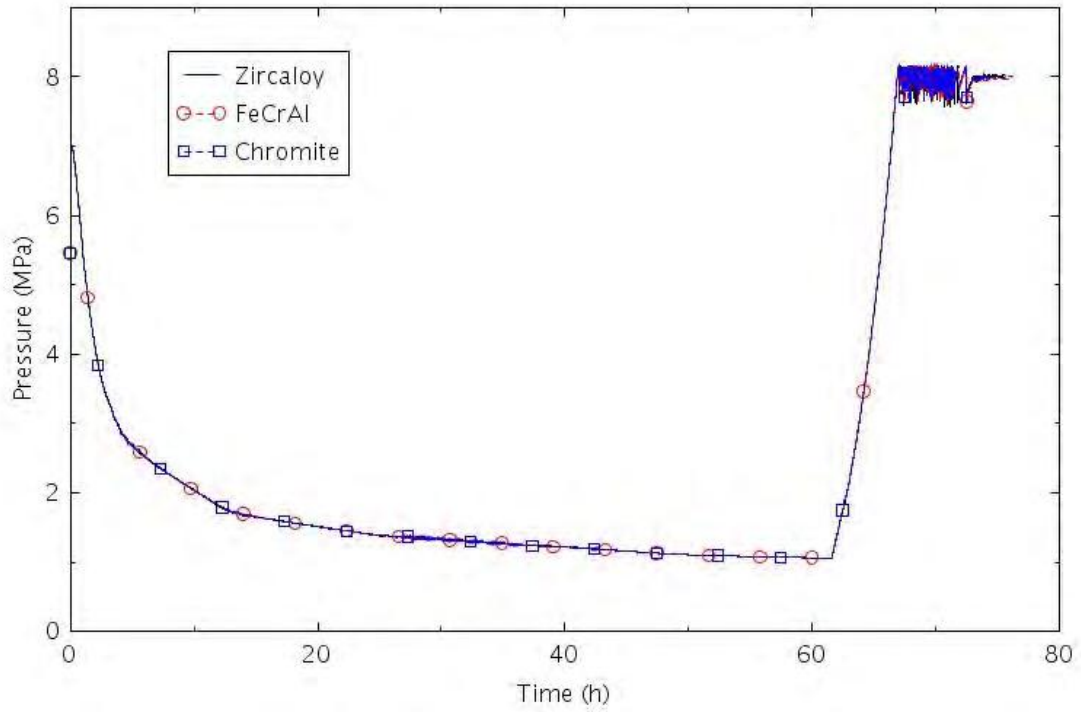

Figure 4-5. Pressure in SG-B (SBO-1.0).

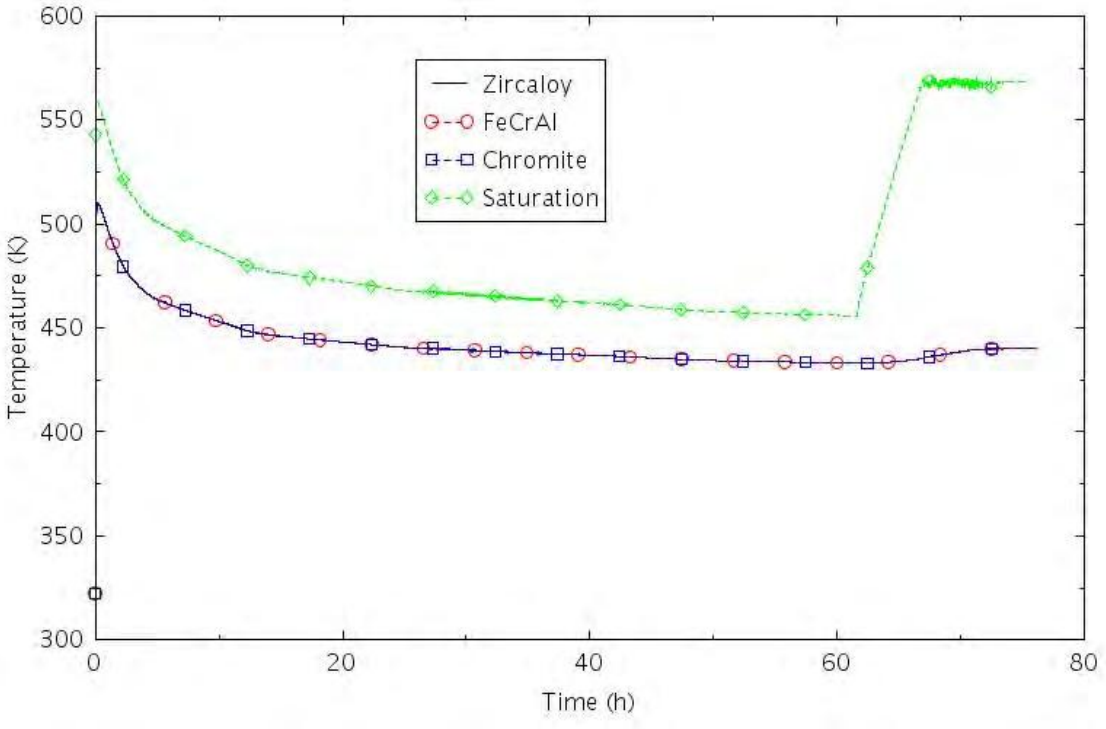

Figure 4-6. Feedwater Temperature Supplied to SG-B (SBO-1.0).

The mass flow through the seals in RCP B is illustrated in Figure 4-7. The flow area of the leakage path provides a flow rate of 21 gpm per pump at normal operating conditions. The combined leakage area for all three pumps corresponds to a 0.58 cm (0.23 inch) break. The leakage was small enough that mostly liquid passed through the seals until about 46 hours. Thereafter, mostly steam passed through the seals.

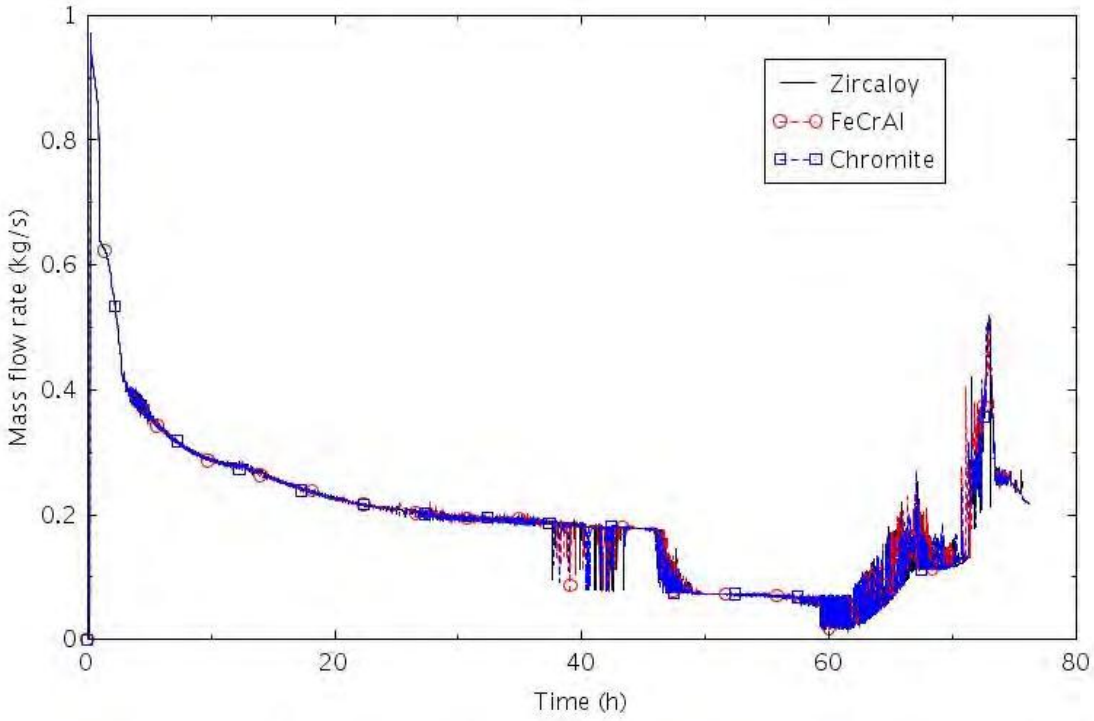

Figure 4-7. Mass Flow Rate through the Seals of RCP B (SBO-1.0).

The calculated pressurizer pressure is shown in Figure 4-8. The combination of the cooling provided by the DNC system and the LOCA created by leakage of the pump seals caused the RCS to depressurize enough to initiate accumulator injection near 3 hours. The accumulators emptied near 56 hours. The RCS pressure increased along with the SG pressures after DNC system was assumed to stop operating near 62 hours. The RCS pressure leveled out near the SG pressure when the SG SRVs began cycling near 67 hours, but then increased again before the SGs emptied near 72 hours. The pressurizer pressure reached the open setpoint of the pressurizer SRVs near 73 hours and stayed near there for the remainder of the calculation. The SRVs opened because the pressurizer PORVs were assumed to be unavailable following the depletion of the station batteries at 4 hours.

The calculated response of the pressurizer level is shown in Figure 4-9. The combination of the cooling by the DNC system and the leakage through the pump seals caused the pressurizer to empty early in the transient. The pressurizer remained empty until the DNC system was assumed to stop operating near 62 hours. The pressurizer then refilled, but emptied shortly after the SRVs began cycling.

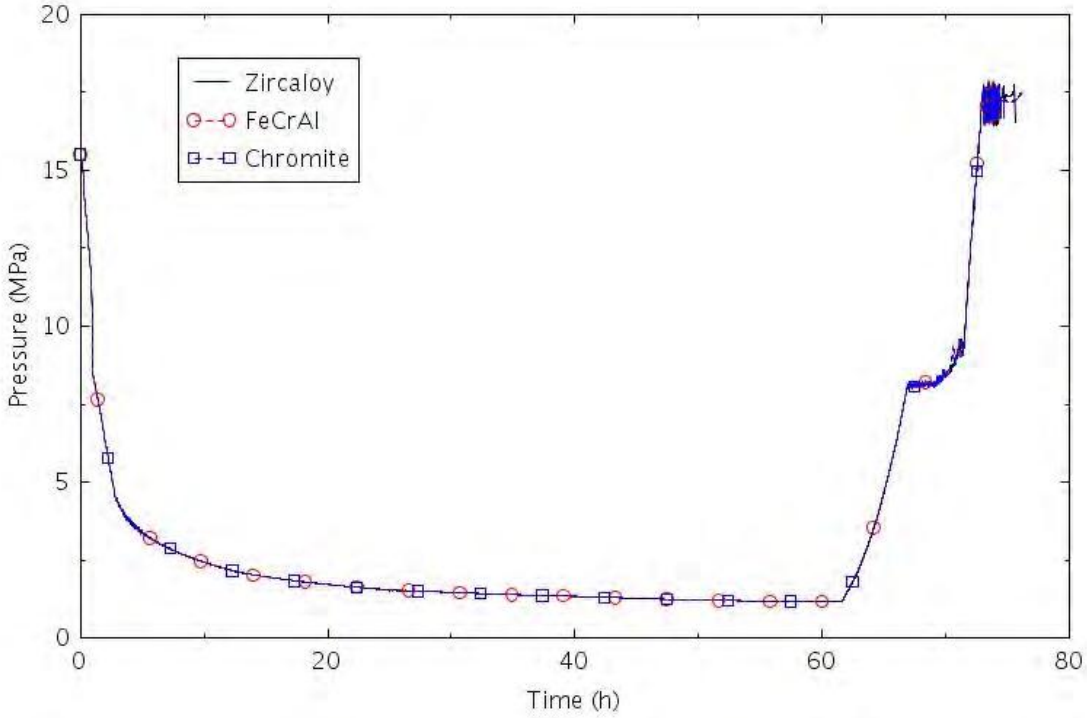

Figure 4-8. Pressure in the Pressurizer (SBO-1.0).

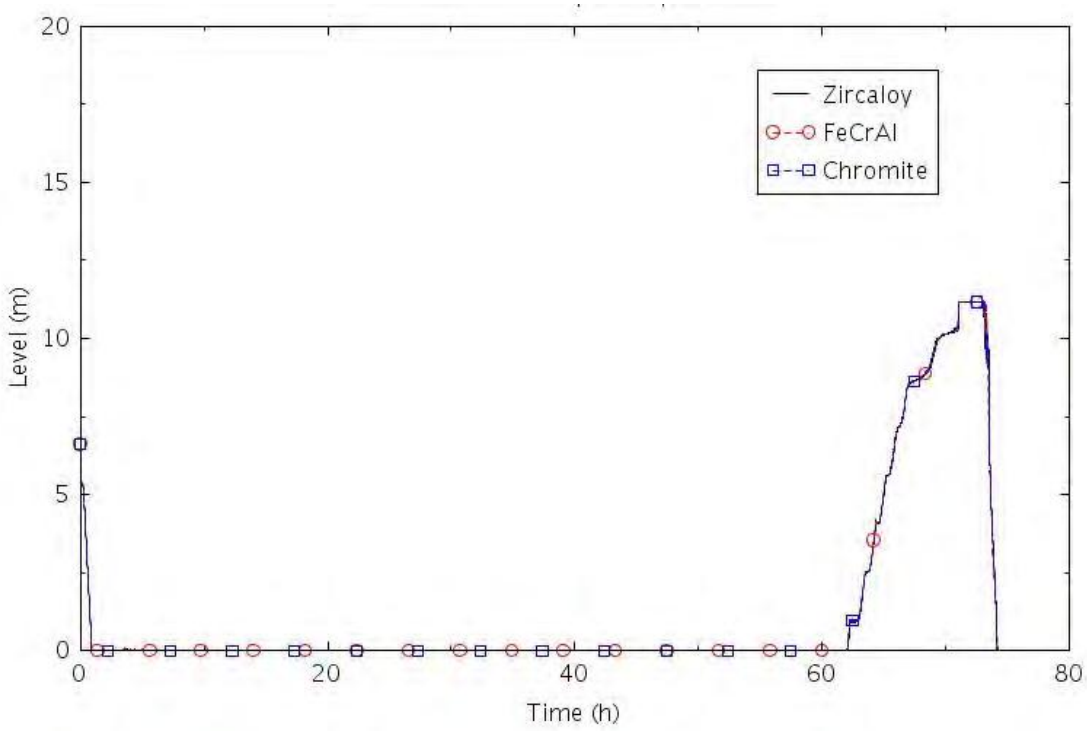

Figure 4-9. Collapsed Liquid Level in the Pressurizer (SBO-1.0).

The collapsed liquid level in the core and the maximum cladding temperature are shown in Figure 4-10 and Figure 4-11, respectively. The collapsed liquid level in the core began to decrease slightly near 3 hours due to boiling in the core, but the core was adequately cooled until about 74 hours when the collapsed level began to decrease rapidly, and the maximum cladding temperature began to increase. The maximum cladding temperatures then began to diverge with the different claddings. The time between when the core began to uncover and the onset of core damage was 118 minutes with Zircaloy, 147 minutes with FeCrAl, and 144 minutes with Chromite.

The onset of core damage could be delayed by increasing the initial liquid volume of the DNC pool or by adding water to the pool during the transient.

The SBO-1.0 calculation described previously assumed that all three DNC systems were available. Sensitivity calculations were performed with two DNC systems available and with one system available. These sensitivity calculations were performed with Zircaloy cladding.

The effect of the number of DNC systems available on the pressurizer pressure is shown in Figure 4-12. The pressure was not reduced enough to fully empty the accumulators with two DNC systems available, but otherwise the results were similar to the case with three systems available. When only one DNC system was available, the pressure was not low enough to initiate any accumulator flow. The sequences of events for all three cases were surprisingly similar as shown in Table 4-2. The time of core damage was reduced by only 5 minutes with the number of DNC systems was reduced from three to two or by 19 minutes when reduced from three to one.

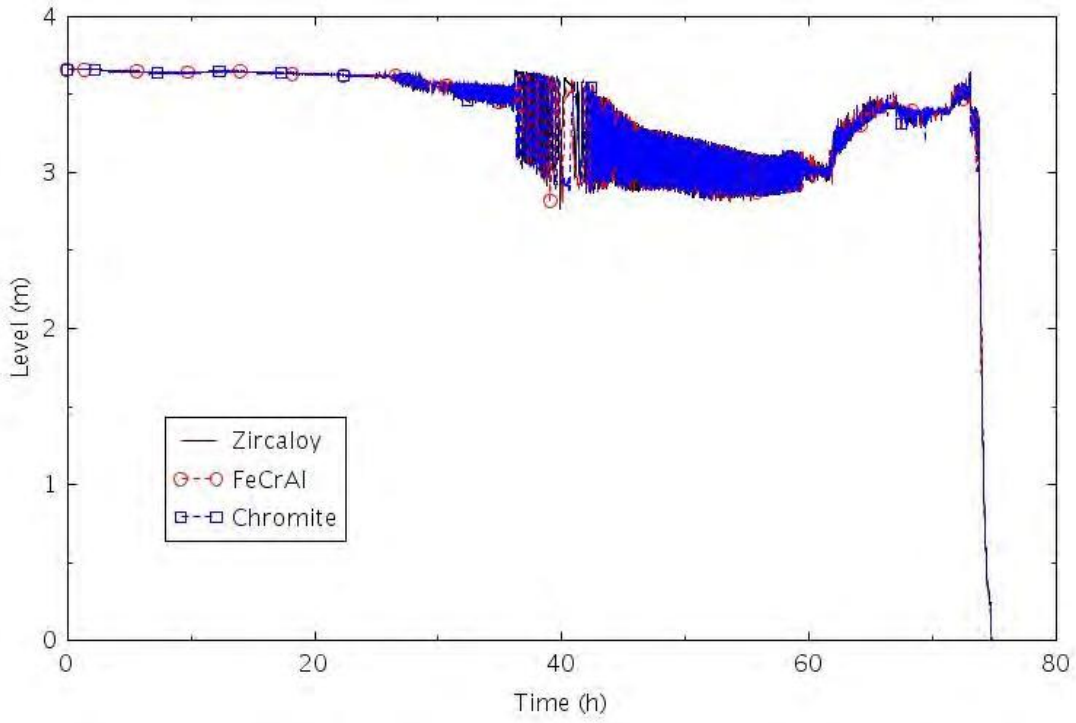

Figure 4-10. Collapsed Liquid Level in the Central Core Channel (SBO-1.0).

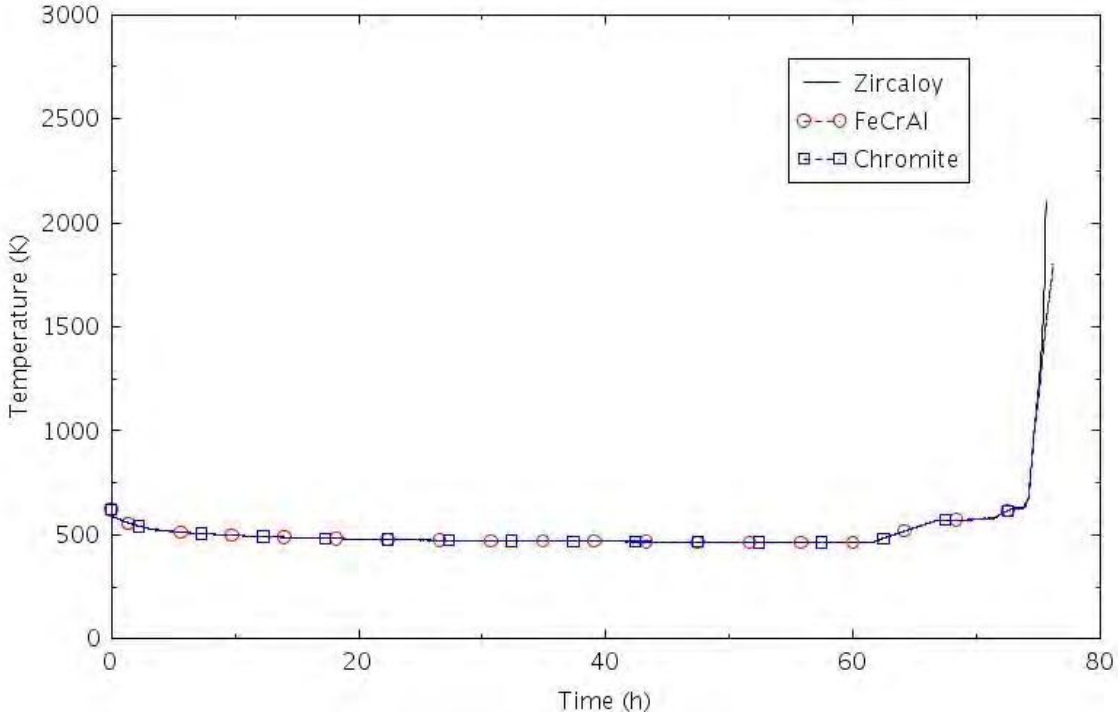

Figure 4-11. Maximum Cladding Temperature (SBO-1.0).

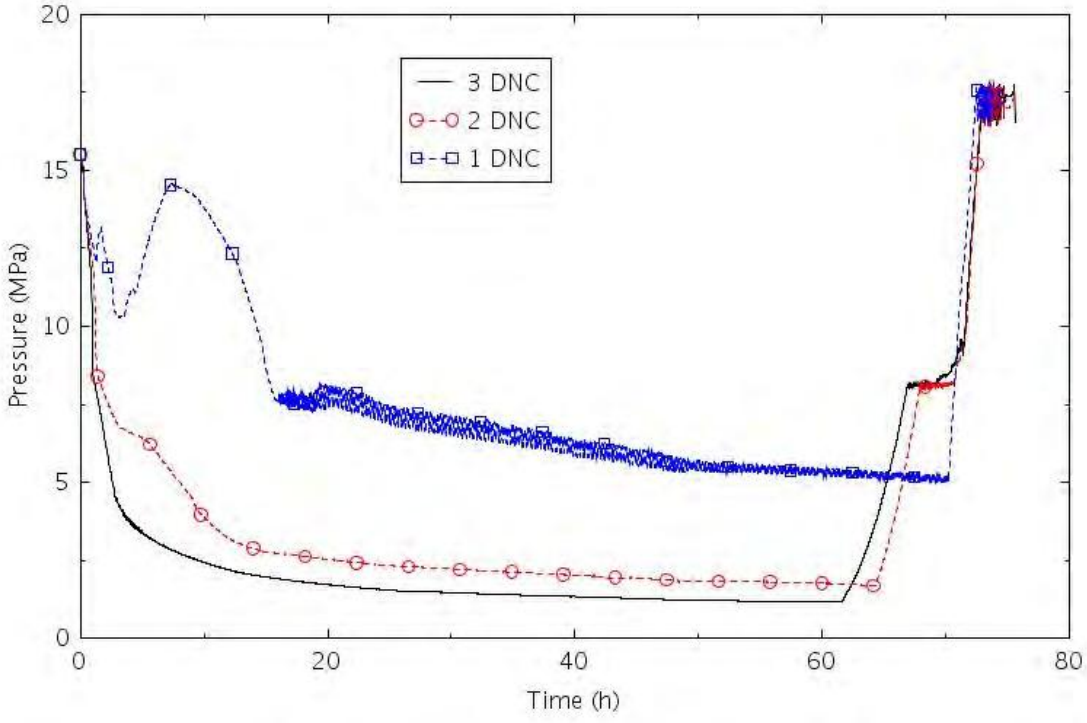

Figure 4-12. The Effects of the Number of DNC Systems Available on Pressurizer Pressure (SBO-1.0).

Table 4-2. Sequence of Events for Scenario SBO-1.0 with Different Number of DNC Systems Available.

Event	Time (hr:min)		
	3 DNC	2 DNC	1 DNC
SBO occurs	0:00	0:00	0:00
RCP leakage begins	0:13	0:13	0:13
SIAS	0:38	0:46	0:56
Accumulator flow initiated	3:16	9:23	NA
Batteries depleted	4:00	4:00	4:00
Accumulator flow terminated	56:25	63:38	NA
DNC feedwater flow terminated	61:36	64:18	70:13
SG SRVs begin to cycle	66:56	67:56	NA
All SGs empty	71:30	71:41	70:17
Pressurizer SRVs begin to cycle	73:02	72:57	72:30
PRT rupture disk opens	73:03	72:58	72:31
Core begins to uncover	73:38	73:36	72:49
0.5 kg H_2 generation	74:32	74:25	73:46
First cladding rupture	75:32	75:27	74:53
Core damage	75:36	75:31	74:55

4.2.2 SBO-4.0

This scenario was identical to Scenario SBO-1.0 except that the nominal pump leakage was assumed to be 480 gpm per pump. As with Scenario SBO-1.0, the MFW, AFW, and HPSI systems were not available during the SBO. All three DNC systems were assumed to be available. The only cooling mechanisms present were due to the inventory of water stored in the DNC pool, SGs, and RCS. The calculated sequences of events are shown in Table 4-3. The reactor scram, RCP pump trip, termination of MFW, and the closure of the turbine stop valves all occurred within the first second of the event. The DNC systems began to operate at 15 s. RCP seal leakage began at 13 minutes. The nominal leakage was 480 gpm per pump. The cooling due to the DNC and the depressurization due to the seal leakage resulted in the SIAS at 14 minutes, but the HPSI pumps were assumed to fail. Accumulator injection began at about 1 hour and 40 minutes. The station batteries were assumed to be depleted at 4 hours, but their failure had no impact on the passive DNC systems. There was considerable variation in the time that the accumulators emptied. The accumulators emptied at about 11 hours with FeCrAl cladding, but were not quite empty when the calculation was terminated with Zircaloy cladding. The core began to uncover near 13 hours. The calculations were terminated when the hottest cladding reached its maximum temperature. The amount of hydrogen produced was 0.5 kg for FeCrAl, 11.1 kg for Chromite, and 11.5 kg for Zircaloy.

Table 4-3. Sequence of Events for Scenario SBO-4.0.

Event	Time (hr:min)		
	Zircaloy	FeCrAl	Chromite
SBO occurs	0:00	0:00	0:00
RCP leakage begins	0:13	0:13	0:13
SIAS	0:14	0:14	0:14
Accumulator flow initiated	1:38	1:39	1:38
Batteries depleted	4:00	4:00	4:00
Accumulators empty	NA	11:17	15:11
Core begins to uncover	12:51	13:49	12:39
First cladding rupture	13:44	14:58	13:31
0.5 kg H_2 generation	13:48	15:31	13:45
Core damage	14:10	15:31	15:30

The following figures illustrate the effects of the cladding on various parameters. Results are presented for SG B, which are representative of the other steam generators in this scenario. The steam flow into the DNC system in SG B is shown in Figure 4-13. The liquid flow delivered to the SG from the DNC system was approximately the same as the steam flow, so the liquid level was maintained at a high value. The calculated pressure in SG B is illustrated in Figure 4-14. The pressure increased initially in response to the closure of the turbine stop valves and then decreased due to the opening of the DNC steam valves. The DNC automatically depressurized and cooled the SG. The maximum cooldown rate was about 30 K/h based on the change in the pressure.

The temperature of the feedwater delivered to SG B by the DNC system is shown in Figure 4-15. The subcooling was greater than 25 K during the transient.

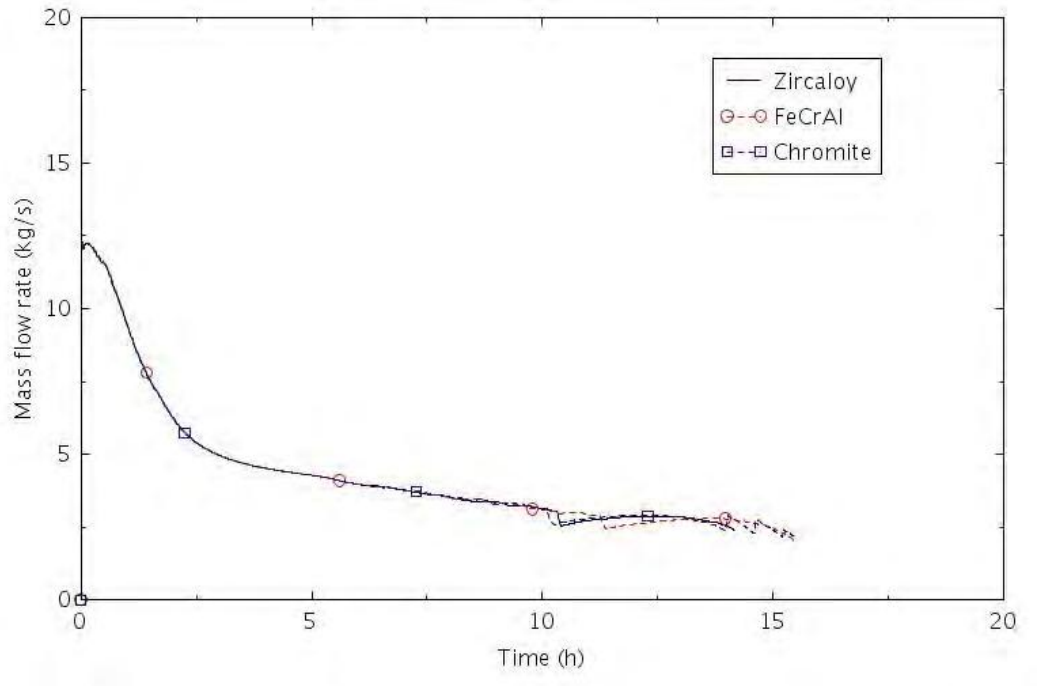

Figure 4-13. Steam Flow to the DNC System in SG-B (SBO-4.0).

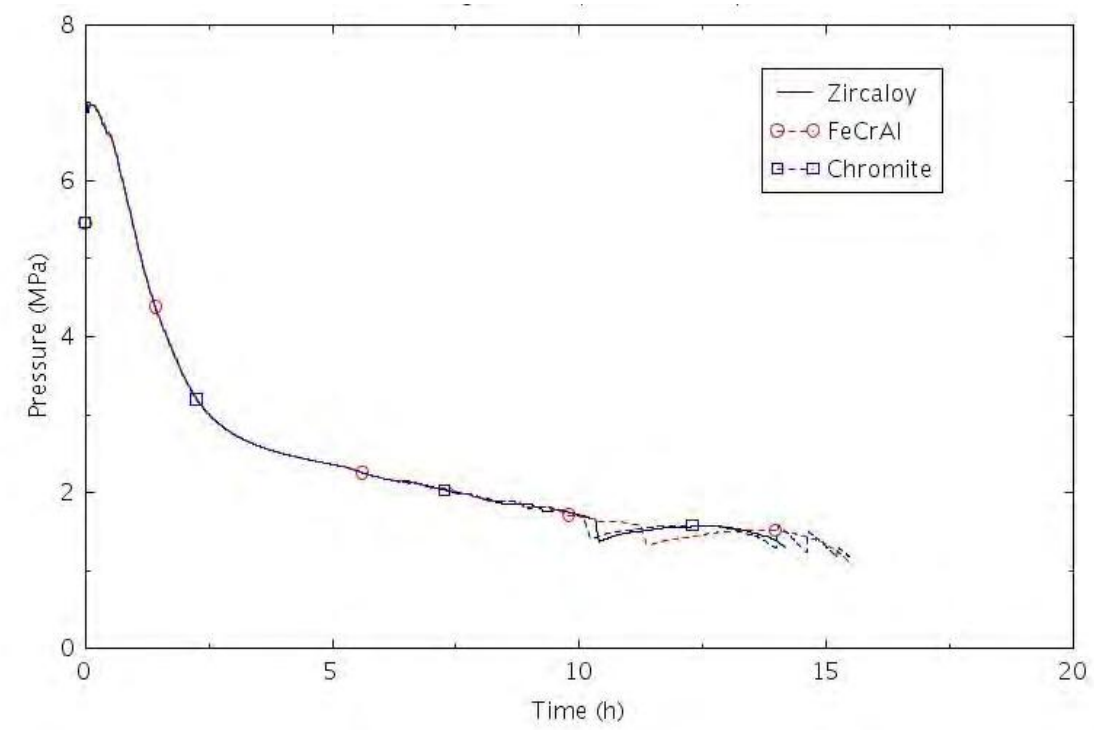

Figure 4-14. Pressure in SG-B (SBO-4.0).

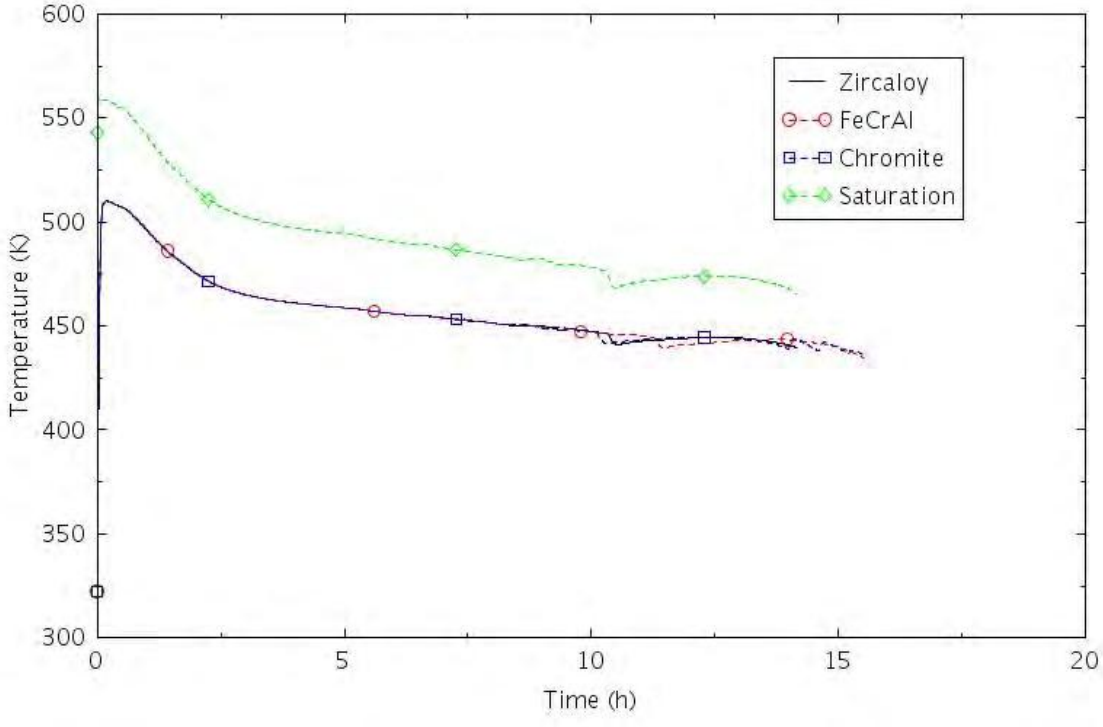

Figure 4-15. Feedwater Temperature Supplied to SG-B (SBO-4.0).

The mass flow through the seals in RCP B is illustrated in Figure 4-16. The flow area of the leakage path provides a flow rate of 480 gpm per pump at normal operating conditions. The combined leakage area for all three pumps corresponds to a 2.8 cm (1.1 inch) break. Mostly liquid passed through the seals until about 1 hour. Thereafter, a significant amount of steam passed through the seals.

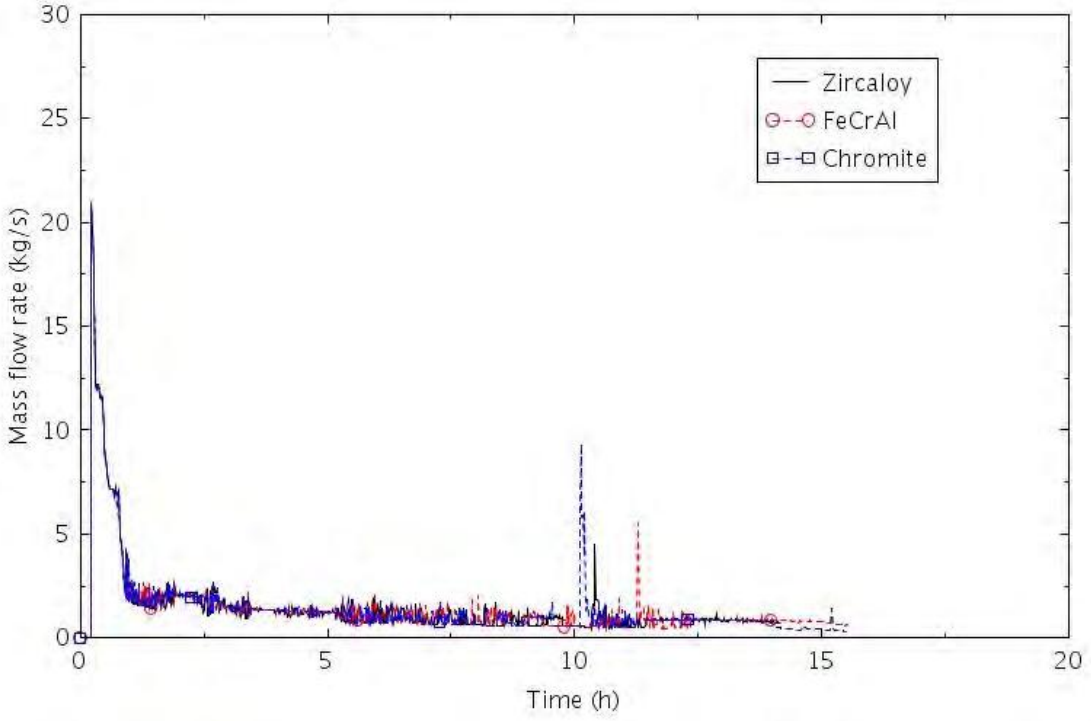

Figure 4-16. Mass Flow Rate through the Seals of RCP B (SBO-4.0).

The calculated pressurizer pressure is shown in Figure 4-17. The combination of the cooling provided by the DNC systems and the LOCA created by leakage of the pump seals caused the RCS to depressurize enough to initiate accumulator injection near 1 hour and 40 minutes as shown in Figure 4-18. The accumulator injection was initially continuous, but became intermittent after about 6 hours. A rapid decrease in level occurred near 10 hours in each case, which caused the accumulators to completely empty in the calculation with FeCrAl and nearly empty in the calculations with Zircaloy and Chromite. The accumulators eventually emptied near 15 hours in the calculation with Chromite, but did not empty in the calculation with Zircaloy. The calculation with Zircaloy would have emptied if the calculation had been run longer. The variability in the emptying of the accumulators is more likely due to numerical causes than to the differences between the claddings.

The combination of the cooling by the DNC systems and the leakage of the pump seals caused the pressurizer to empty early in the transient as shown in Figure 4-19.

The collapsed liquid level in the core and the maximum cladding temperature are shown in Figure 4-20 and Figure 4-21, respectively. The collapsed liquid level in the core began to decrease at about 0.5 hour due to boiling in the core, but the core was adequately cooled until about 13 hours when the collapsed level began to decrease rapidly, and the maximum cladding temperature began sustained increases. The variation in the cladding temperatures during the heatups was caused by the variation in the accumulator behavior discussed previously. The brief accumulator injections near 14 hours in the calculation with Chromite caused increases in core level and decreases in cladding temperature.

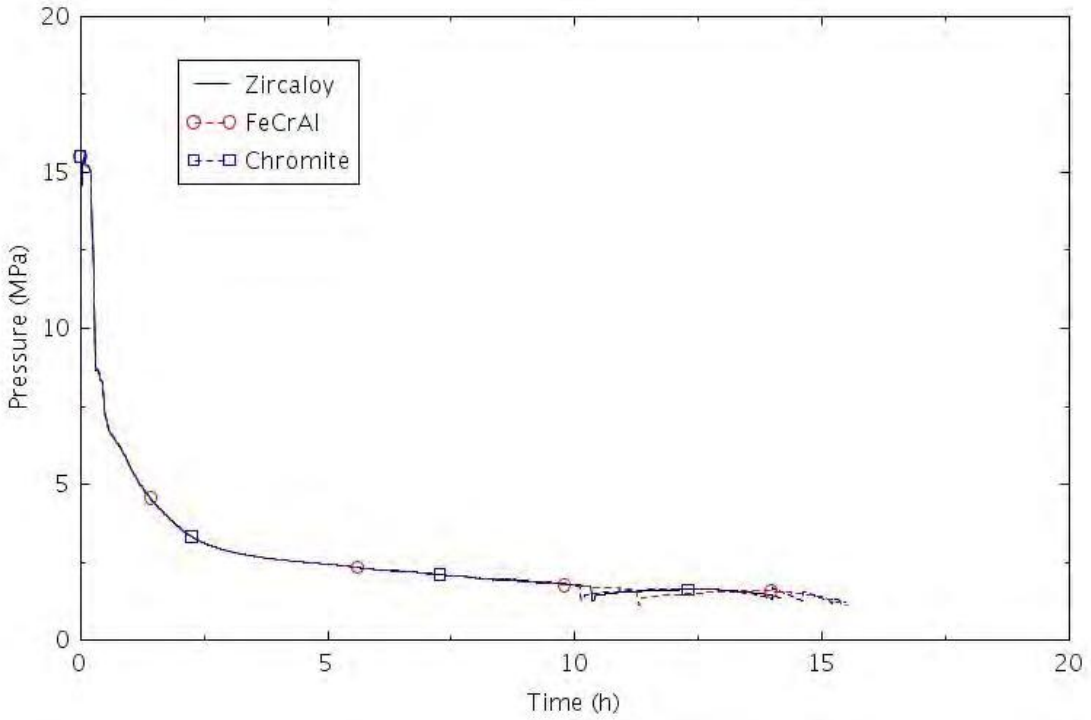

Figure 4-17. Pressure in the Pressurizer (SBO-4.0).

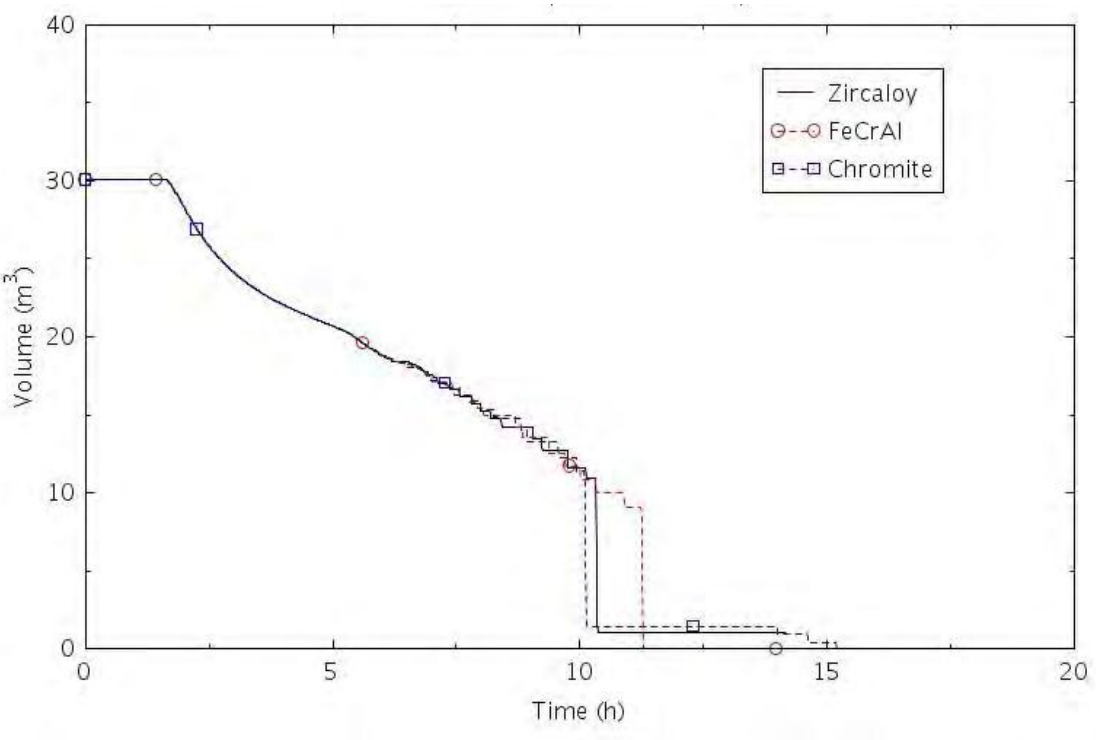

Figure 4-18. Liquid Volume in the Accumulator in Loop B (SBO-4.0).

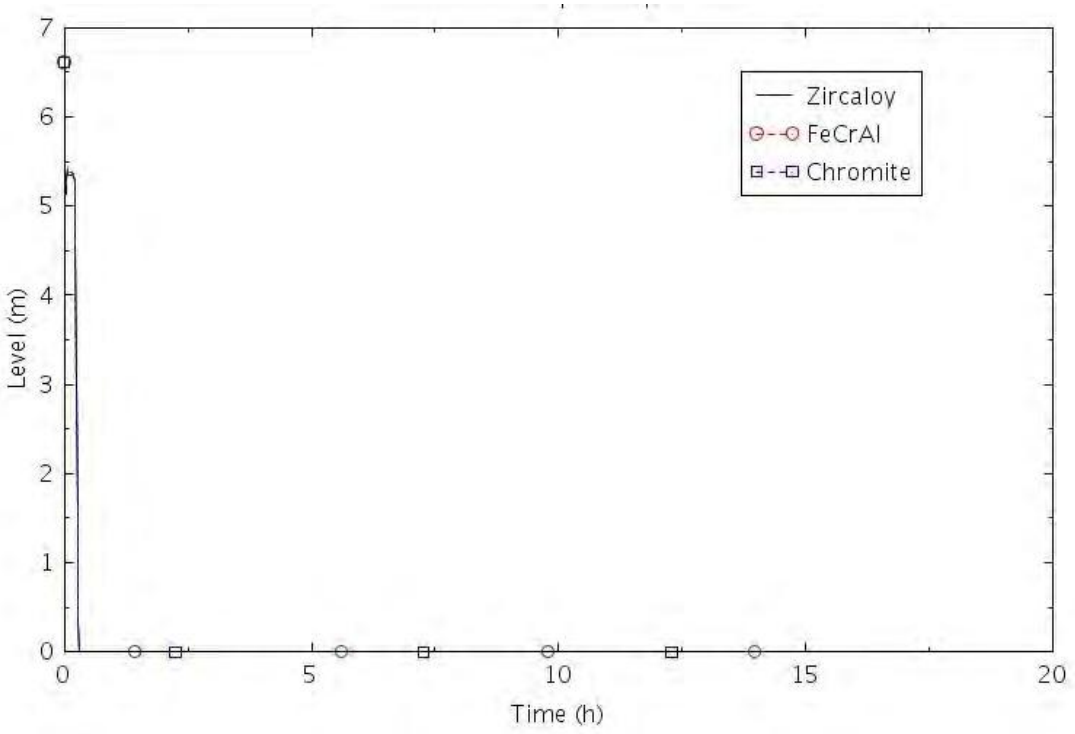

Figure 4-19. Collapsed Liquid Level in the Pressurizer (SBO-4.0).

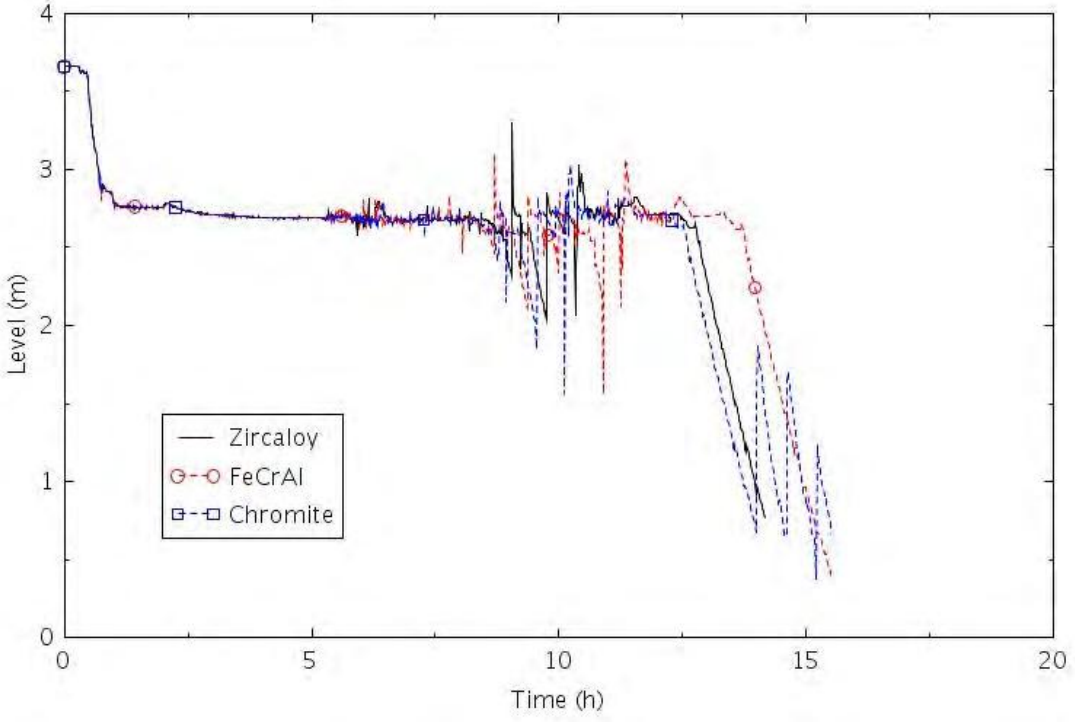

Figure 4-20. Collapsed Liquid Level in the Central Core Channel (SBO-4.0).

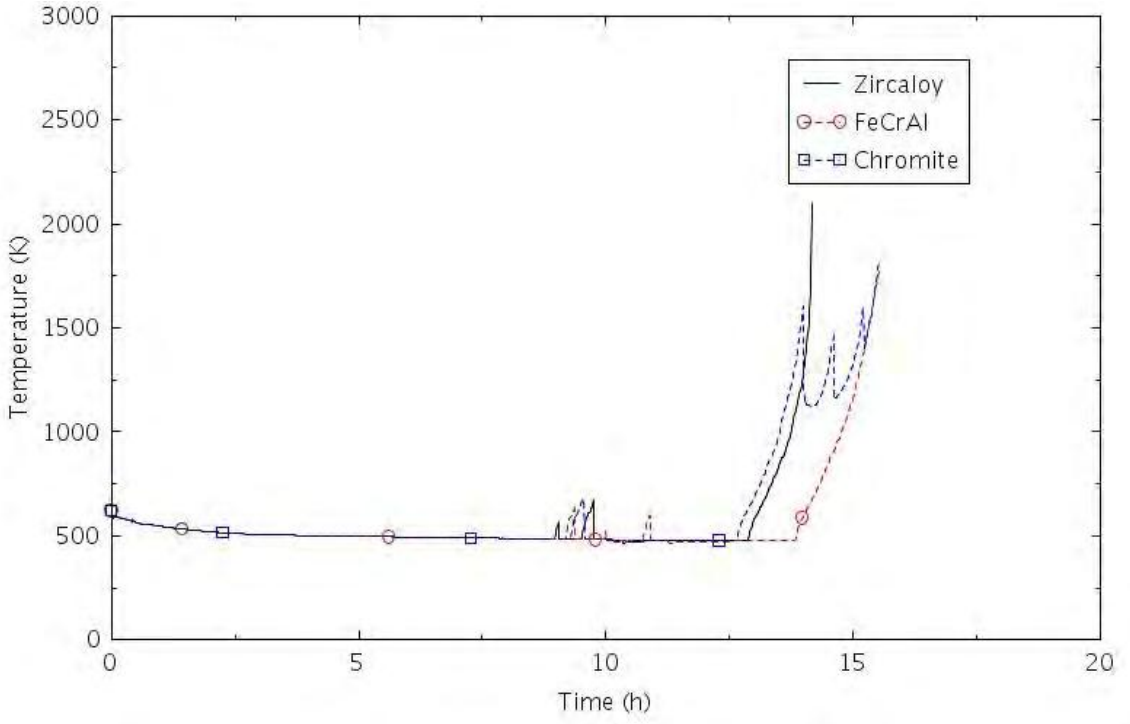

Figure 4-21. Maximum Cladding Temperature (SBO-4.0).

The calculations for Scenario SBO-4 showed that core damage occurred at about 14 hours. In contrast, the calculations of Scenario SBO-1.0 showed core damage did not occur until about 72 hours. The difference between the two scenarios was due to the increased leakage through the RCP seals in Scenario SBO-4. Even though the DNC systems are efficient in removing core decay heat via the steam generators, they do not inject liquid into the RCS and therefore cannot make up for inventory lost during an LOCA. These results indicate that the DNC becomes less effective in delaying the time of core damage as the size of the break increases.

The large decay heat removal capacity of the DNC pool does provide some benefit compared to traditional AFW systems even for transients involving LOCAs. For example, Table 4-9 of (Ma & al., 2018) showed that core damage occurred at 10 hours and 32 minutes for a nominal leakage of 21 gpm per pump and 5 hours and 25 minutes for a nominal leakage of 480 gpm per pump when the turbine-driven AFW system was assumed to operate for 4 hours. The results with three DNC systems available showed that the core damage was delayed until 75 hours and 36 minutes for a nominal leakage of 21 gpm per pump and 14 hours and 10 minutes for a nominal leakage of 480 gpm per pump. The gain in coping time due to the DNC systems is about 65 hours for a nominal leakage of 21 gpm per pump and about 5 hours for a nominal leakage of 480 gpm per pump. The gain in coping time is expected to decrease further as the break size increases.

The SBO-4.0 calculation described previously assumed that all three DNC systems were available. Sensitivity calculations were performed with two DNC systems available and with one system available. These sensitivity calculations were performed with Zircaloy cladding.

The effects of the number of DNC systems available on the sequence of events are shown in Table 4-4. The loss of one or two DNC systems resulted in less depressurization of the RCS as shown in Figure 4-22. The accumulator injection was significantly delayed with two DNC systems available and did not occur at all when only one system was available as shown in Figure 4-23. Figure 4-24 shows that the time that core damage occurred was reduced by almost 8 hours with only two operating DNC systems and by about 11 hours with only one operating system. The rate of temperature rise in the cladding was significantly slower when two DNC systems

were operating because the accumulators were injecting as the core was heating up. Even though the accumulators were not empty in the case with 3 operating DNC systems, they were not injecting as the core was heating.

Table 4-4. Sequence of Events for Scenario SBO-4.0 with Different Number of DNC Systems Available.

Event	Time (hr:min)		
	3 DNC	2 DNC	1 DNC
SBO occurs	0:00	0:00	0:00
RCP leakage begins	0:13	0:13	0:13
SIAS	0:14	0:14	0:14
Accumulator flow initiated	1:38	3:07	NA
Batteries depleted	4:00	4:00	4:00
Accumulators empty	NA	NA	NA
Core begins to uncover	12:51	3:14	2:17
First cladding rupture	13:44	4:28	2:49
0.5 kg H_2 generation	13:48	4:17	2:46
Core damage	14:10	6:29	2:59

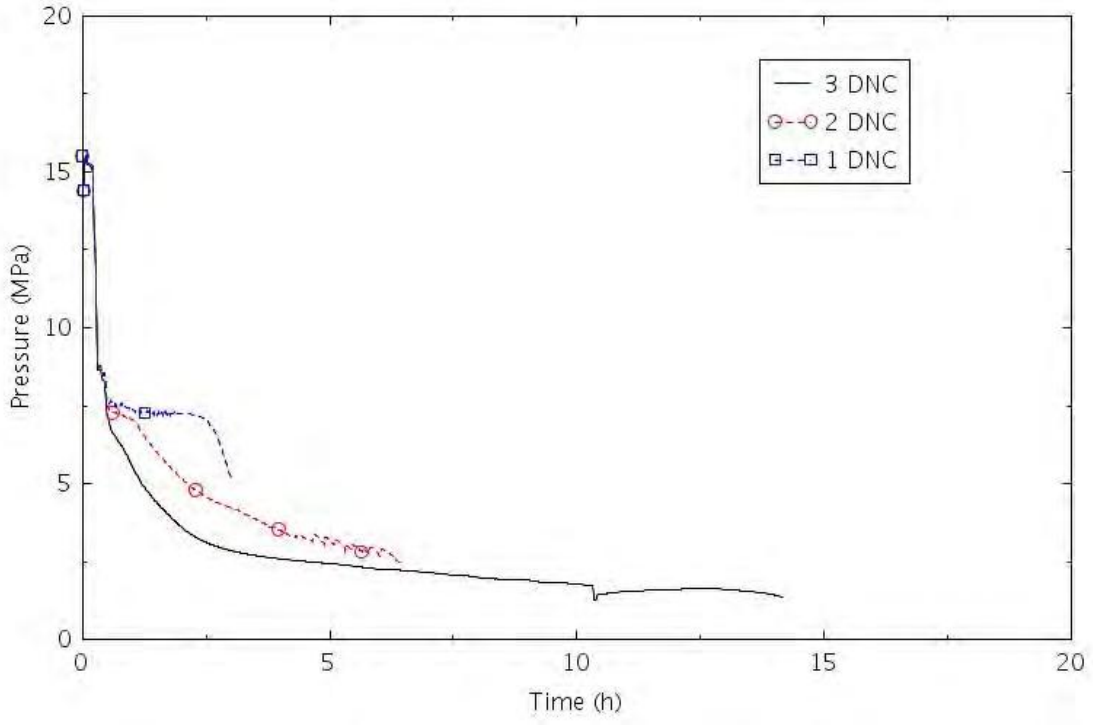

Figure 4-22. The Effects of the Number of DNC Systems Available on Pressurizer Pressure (SBO-4.0).

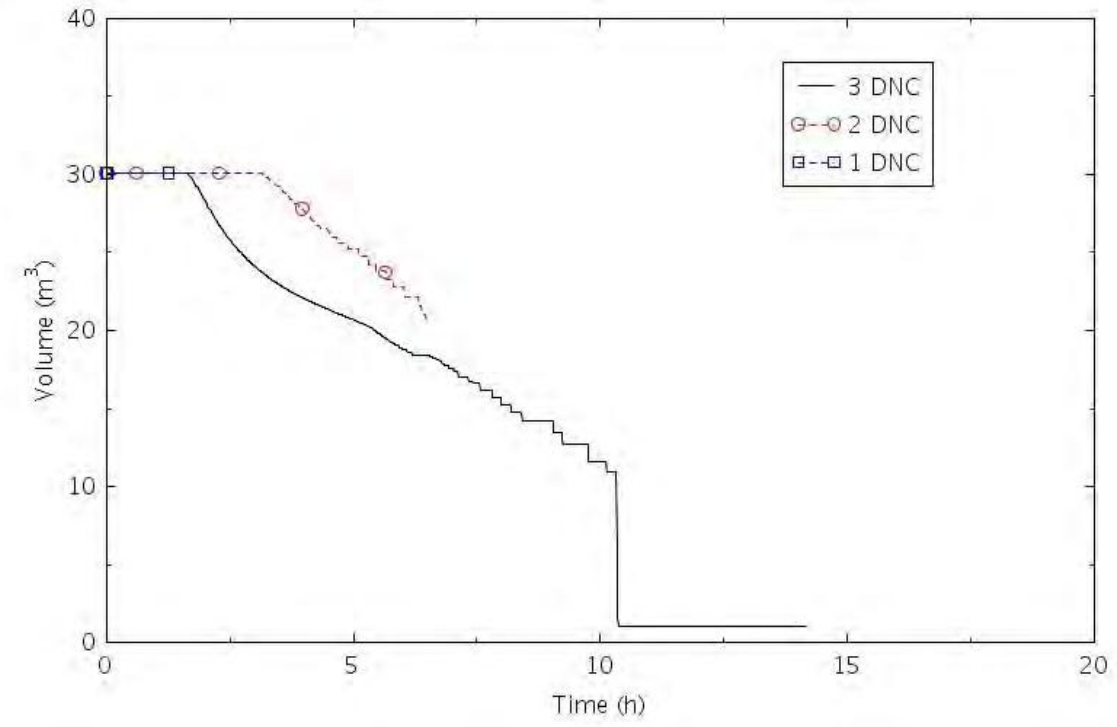

Figure 4-23. The Effects of the Number of DNC Systems Available on Liquid Volume in the Accumulator in Loop B (SBO-4.0).

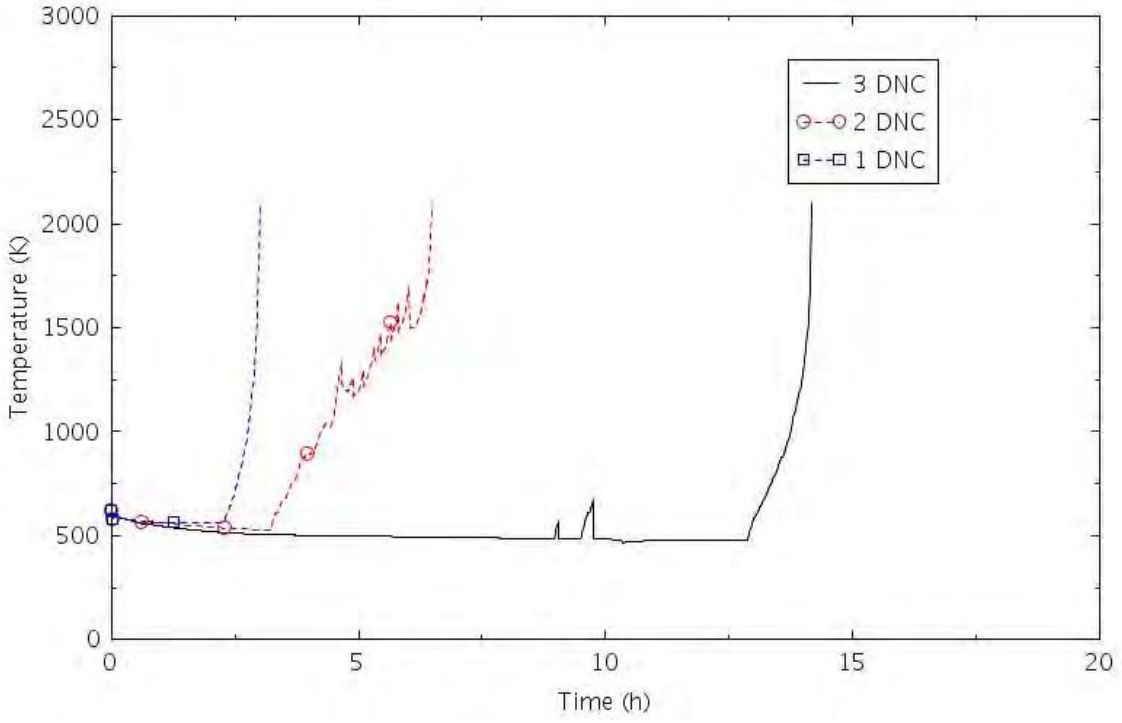

Figure 4-24. The Effects of the Number of DNC Systems Available on Maximum Cladding Temperature (SBO-4.0).

4.2.3 SBO-6.0

This scenario is identical to SBO-1.0 except that the pressurizer PORV was assumed to stick open after its first lift. In Scenario SBO-1, the pressurizer pressure did not reach the open setpoint of the PORV until about 73 hours. In that scenario, the PORV was assumed to be unavailable and the pressurizer SRVs opened as necessary to relieve the pressure. The RELAP5-3D model represents the three SRVs on the pressurizer as a single valve. Since all three SRVs would not be expected to stick open, the PORV was assumed to be available for this scenario. The capacity of a single SRV is greater than that of a single PORV. Therefore, core damage would have occurred a little earlier than reported here if the stuck open valve had been assumed to be an SRV rather than a PORV.

The calculated sequences of events are shown in Table 4-5. The results are identical to those reported previously in Table 4-1 until the pressurizer PORV stuck open on its first lift near 73 hours. Core damage occurred about 1 hour earlier than was calculated for Scenario SB0-1. The sticking open of the valve did not affect the core damage time very much because the first lift of the pressurizer PORV occurred so late in the transient. The amount of hydrogen produced was 1.2 kg for FeCrAl, 8.0 kg for Chromite, and 25.8 kg for Zircaloy.

Table 4-5. Sequence of Events for Scenario SBO-6.0.

Event	Time (hr:min)		
	Zircaloy	FeCrAl	Chromite
SBO occurs	0:00	0:00	0:00
RCP leakage begins	0:13	0:13	0:13
SIAS	0:38	0:38	0:38
Accumulator flow initiated	3:16	3:16	3:16
Batteries depleted	4:00	4:00	4:00
Accumulator flow terminated	56:25	56:24	56:26
DNC feedwater flow terminated	61:36	61:35	61:36
SG SRVs begin to cycle	66:56	66:56	66:56
All SGs empty	71:30	71:31	71:30
Pressurizer PORV sticks open	72:45	72:45	72:43
PRT rupture disk opens	72:47	72:47	72:46
Core begins to uncover	73:26	73:24	73:26
0.5 kg H_2 generation	73:58	74:54	74:14
First cladding rupture	74:09	74:03	74:09
Core damage	74:28	74:54	74:37

The calculated mass flow rate through the PORV is shown in Figure 4-25. The pressurizer PORV was assumed to stick open after its first lift, which occurred near 73 hours. The flow through the PORV caused a rapid depressurization of the RCS as shown in Figure 4-26.

The maximum cladding temperature is shown in Figure 4-27. The time between when the core began to uncover and the onset of core damage was 62 minutes with Zircaloy, 90 minutes with FeCrAl, and 71 minutes with Chromite. The loss of mass through the stuck-open PORV resulted in about one hour less between the time the core began to uncover and onset of core damage than in Scenario 1.0.

The other calculated parameters were similar to those shown previously for Scenario SBO-1.0.

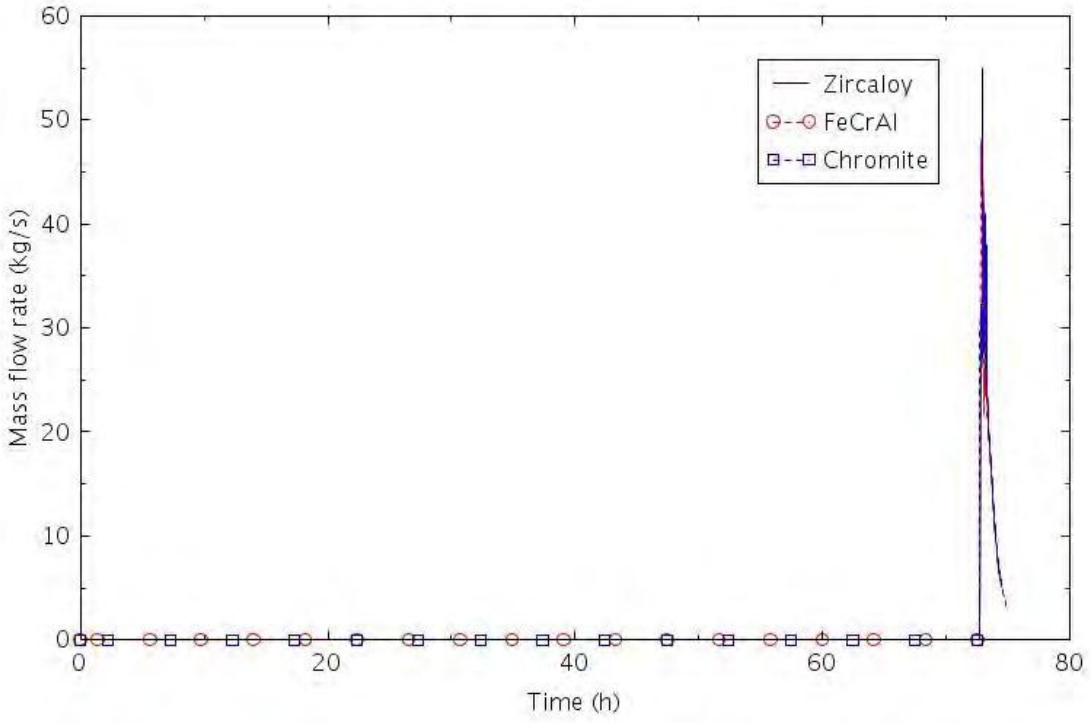

Figure 4-25. Mass Flow Rate through the Pressurizer PORV (SBO-6.0).

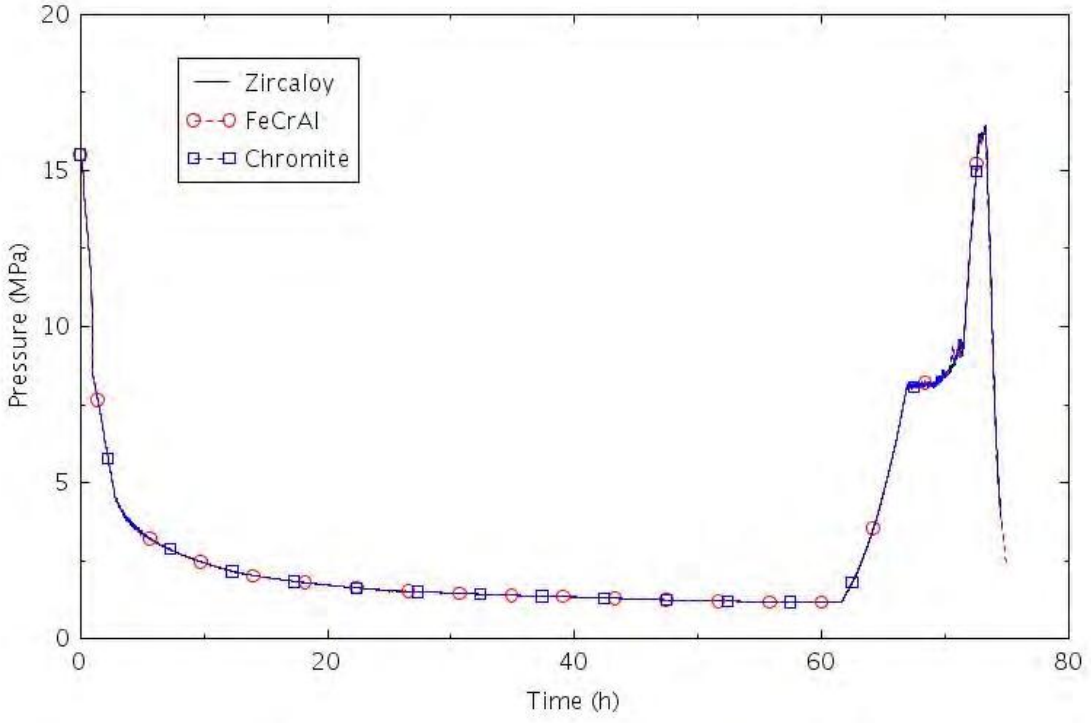

Figure 4-26. Pressure in the Pressurizer (SBO-6.0).

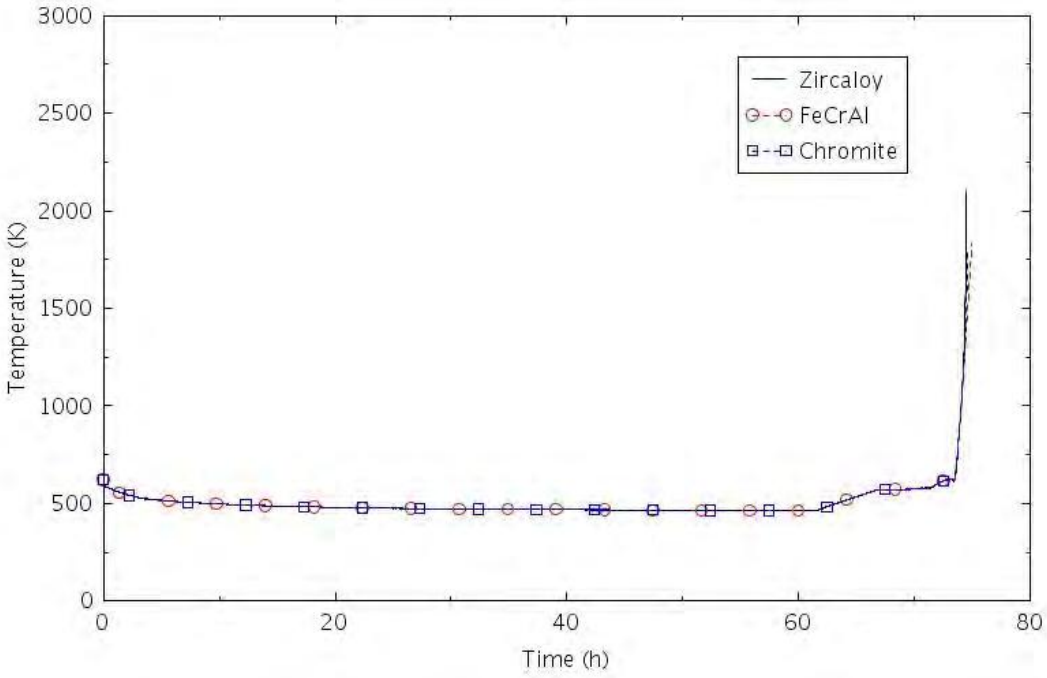

Figure 4-27. Maximum Cladding Temperature (SBO-6.0).

4.2.4 DNC ATF SBO Analysis Summary

Table 4-6 presents a summary of the RELAP5-3D simulation results for time to core uncovery, time to 0.5 kg hydrogen production, and time to core damage for DNC SBO scenarios and for Zircaloy and ATF clads (FeCrAl and Chromite). Table 4-7 compares the times to core damage for ATF designs (FeCrAl and Chromite) with those for existing Zircaloy clad design in different SBO scenarios. The table shows that the gain of coping time, or the delay of time to core damage, can be from about 10 minutes to as much as one and a half hours for SBO-4.0 scenario. Table 4-8 compares the hydrogen production for ATF designs (FeCrAl and Chromite) with those for existing Zircaloy clad design in different LOFW scenarios. The table shows the hydrogen production for FeCrAl is less than 5% of those for Zircaloy. For Chromite, the hydrogen production results vary significantly depending on the scenarios, from no hydrogen production at all in SBO-1.0, to about 30% and 96% of those from the Zircaloy clad in SBO-6.0 and SBO-4.0, respectively. For Chromite, hydrogen production does not occur until after the cladding ruptures. No rupture was calculated in SBO-1.0, but rupture and hydrogen production would have occurred had the calculation been continued for 4 more minutes. The calculated accumulator injection during the core heatup in SBO-4 with Chromite resulted in a relatively long heatup time, which caused an increase in coping time, but also resulted in a relatively large amount of hydrogen production. The variability in accumulator injection in SBO-4 is more likely due to numerical causes than to the differences between the claddings.

Table 4-6. Summary of RELAP5-3D Time Results for DNC SBO Scenarios – Zircaloy and ATF

Scenario	Time to Core Uncovery (hr:min)			Time to 0.5 kg H_2 (hr:min)			Time to Core Damage (hr:min)		
	Zircaloy	FeCrAl	Chromite	Zircaloy	FeCrAl	Chromite	Zircaloy	FeCrAl	Chromite
SBO-1.0	73:38	73:43	73:46	74:32	75:52	NA	75:36	76:10	76:10
SBO-4.0	12:51	13:49	12:39	13:48	15:31	13:45	14:10	15:31	15:30
SBO-6.0	73:26	73:24	73:26	73:58	74:54	74:14	74:28	74:54	74:37

Table 4-7. Time to Core Damage Comparison for DNC SBO Scenarios with ATF Designs

Section	Scenario	Description	Time to Core Damage (hr:min)				
			Zircaloy	FeCrAl	Δt (FeCrAl)	Chromite	Δt (Chromite)
4.2.1	SBO-1.0	DNC with 21 gpm	75:36	76:10	00:34	76:10	00:34
4.2.2	SBO-4.0	DNC with 480 gpm	14:10	15:31	1:21	15:30	1:20
4.2.3	SBO-6.0	DNC with Late PORV LOCA	74:28	74:54	00:26	74:37	00:09

Table 4-8. Comparing H_2 Productions for DNC SBO Scenarios with ATF Designs

Section	Scenario	Description	Total H_2 (kg)				
			Zircaloy	FeCrAl	H_2% (FeCrAl)	Chromite	H_2% (Chromite)
4.2.1	SBO-1.0	DNC with 21 gpm	134.1	2.0	1.5%	0.0	0.0%
4.2.2	SBO-4.0	DNC with 480 gpm	11.5	0.5	4.3%	11.1	96.5%
4.2.3	SBO-6.0	DNC with Late PORV LOCA	25.8	1.2	4.7%	8.0	31.0%

4.3 DNC System Risk Analysis

This section presents the risk impact analysis for the DNC system. The DNC system was modeled and incorporated into the generic PRA model. In this analysis, the DNC system is assumed to be able to replace AFW to provide secondary cooling safety function after an IE is occurred. The original AFW fault tree was revised to add the DNC system model, with a house event, DNC-HE, as the switch to turn on or off the DNC system in the PRA model with the benefit that event trees are not needed to change in order to incorporate the DNC. Figure 4-28 shows the revised AFW fault tree with the DNC system added to the logic. As a passive system, the DNC system has fewer failure modes with fewer components to be modeled. The following basic events were included in the revised AFW fault tree with DNC:

- DNC starting steam valve (V001/002/003) fails to open; the type of the DNC starting valve has not yet been determined; after discussions with the system designer, solenoid operated valve was used in the analysis
- Common cause failure (CCF) to open of the steam valves V001, V002, and V003
- DNC heat exchanger (HTX001/002/003) fails
- CCF of HTX 001, 002, and 003
- DNC jet ejector (ORF001/002/003) fails to operate; the failure data of orifice is used in the model for the jet ejector
- DNC condensate tank fails
- DNC heat exchanger is not available due to test or maintenance, which is used to represent the unavailability of DNC system due to test or maintenance.

The results of the latest nuclear industry average parameter estimates (NRC, 2017) were used in the model. Table 4-9 shows the DNC system basic event data in the PRA model.

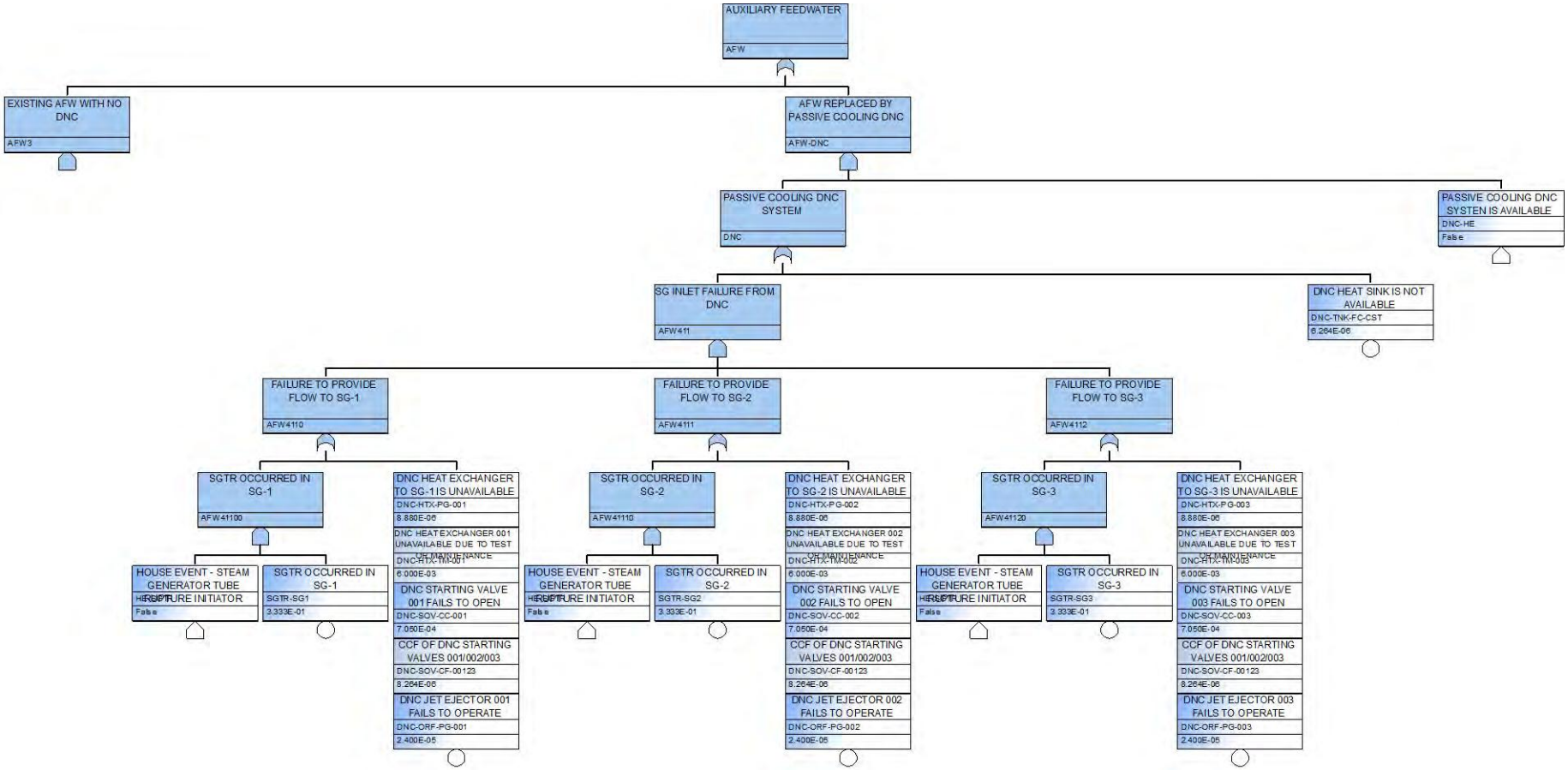

Figure 4-28. Revised AFW Fault Tree with DNC System Added.

Table 4-9. DNC System Basic Event Data.

Name	Description	Failure Probability	Failure Rate (/hour)	Mission Time (hour)
DNC-HTX-PG-001	DNC HEAT EXCHANGER TO SG-1 IS UNAVAILABLE	8.88E-06	3.70E-07	24
DNC-HTX-PG-002	DNC HEAT EXCHANGER TO SG-2 IS UNAVAILABLE	8.88E-06	3.70E-07	24
DNC-HTX-PG-003	DNC HEAT EXCHANGER TO SG-3 IS UNAVAILABLE	8.88E-06	3.70E-07	24
DNC-HTX-TM-001	DNC HEAT EXCHANGER 001 UNAVAILABLE DUE TO TEST OR MAINTENANCE	6.00E-03		
DNC-HTX-TM-002	DNC HEAT EXCHANGER 002 UNAVAILABLE DUE TO TEST OR MAINTENANCE	6.00E-03		
DNC-HTX-TM-003	DNC HEAT EXCHANGER 003 UNAVAILABLE DUE TO TEST OR MAINTENANCE	6.00E-03		
DNC-ORF-PG-001	DNC JET EJECTOR 001 FAILS TO OPERATE	2.40E-05	1.00E-06	24
DNC-ORF-PG-002	DNC JET EJECTOR 002 FAILS TO OPERATE	2.40E-05	1.00E-06	24
DNC-ORF-PG-003	DNC JET EJECTOR 003 FAILS TO OPERATE	2.40E-05	1.00E-06	24
DNC-SOV-CC-001	DNC STARTING VALVE 001 FAILS TO OPEN	7.05E-04		
DNC-SOV-CC-002	DNC STARTING VALVE 002 FAILS TO OPEN	7.05E-04		
DNC-SOV-CC-003	DNC STARTING VALVE 003 FAILS TO OPEN	7.05E-04		
DNC-SOV-CF-00123	CCF OF DNC STARTING VALVES 001/002/003	8.26E-06		
DNC-TNK-FC-CST	DNC CONDENSATE TANK IS NOT AVAILABLE	6.26E-06	2.61E-07	24

The PRA model was quantified with the DNC system to replace AFW. Comparing to the baseline PRA model with the AFW system, the SBO core damage frequency (CDF) is reduced from 2.28E-6 to 9.79E-7 per year, which represents a significant 57% reduction (Table 4-10).

After applying the DNC system to other event trees, the plant total CDF is reduced from 3.17E-5 to 2.34E-5 per year, with about 25% reduction (Table 4-11). From Table 4-11, the DNC system may have no to little impact to initiators such as loss-of-coolant accidents (LOCAs), loss of component cooling water (LOCCW), and general transients (TRANS), or have much more significant impact to other initiators such as LOOP and loss of one ac bus, due to the importance of the AFW system in different initiators.

It should be noted while the DNC system has significant impact on behalf of the plant risk metric in CDF, it could also have significant contributions to other risk-informed applications and the economic benefits to plant operations. For example, replace AFW system with the passive DNC system would mean a big relief on the maintenance of AFW including the turbine-driven AFW pump (TDAFP), motor-driven AFW pump (MDAFP), and the valves. The DNC system could also bring immediate benefits to a plant that has troubles in TDAFP or MDAFP MSPI index. A detailed analysis on such impact could be conducted in the future.

It should also be noted that the above DNC system analysis is based on a generic RELAP5-3D model and generic PRA model with early system design concepts. Detailed plant-specific analysis with more matured DNC system design could provide a better and more realistic assessment on the risk impact from the DNC system.

Table 4-10. DNC Risk Impact on SBO CDF.

ET	CDF with AFW (/year)	CDF with DNC (/year)	ΔCDF (/year)	ΔCDF%
LOOPGR	1.07E-06	4.61E-07	-6.06E-07	-56.8%
LOOPPC	6.21E-08	2.20E-08	-4.01E-08	-64.6%
LOOPSC	4.57E-07	1.84E-07	-2.72E-07	-59.7%
LOOPWR	6.89E-07	3.11E-07	-3.78E-07	-54.8%
Total	2.28E-06	9.79E-07	-1.30E-06	-57.0%

Table 4-11. DNC Risk Impact on Plant Total CDF.

Event Tree	CDF with AFW (/year)	CDF with DNC (/year)	ΔCDF (/year)	ΔCDF%
ISL-HPI	3.85E-09	3.85E-09	0.00E+00	0.0%
ISL-LPI	3.84E-08	3.84E-08	0.00E+00	0.0%
ISL-RHR	6.65E-07	6.65E-07	0.00E+00	0.0%
LLOCA	2.01E-08	2.01E-08	0.00E+00	0.0%
LOACA	1.14E-05	4.60E-06	-6.81E-06	-59.7%
LOCCW	1.35E-09	1.33E-09	-1.30E-11	-1.0%
LOCHS	1.46E-07	1.35E-07	-1.13E-08	-7.8%
LODCA	3.71E-07	3.05E-07	-6.57E-08	-17.7%
LODCB	3.72E-07	3.05E-07	-6.71E-08	-18.0%
LOMFW	1.08E-07	9.98E-08	-8.29E-09	-7.7%
LONSW	1.43E-05	1.43E-05	0.00E+00	0.0%
LOOPGR	1.07E-06	4.61E-07	-6.06E-07	-56.8%
LOOPPC	6.21E-08	2.20E-08	-4.01E-08	-64.6%
LOOPSC	4.57E-07	1.84E-07	-2.72E-07	-59.7%
LOOPWR	6.89E-07	3.11E-07	-3.78E-07	-54.8%
MLOCA	6.28E-07	6.28E-07	0.00E+00	0.0%
SGTR	1.07E-07	1.12E-07	4.80E-09	4.5%
SLOCA	7.78E-08	7.78E-08	-5.00E-11	-0.1%
TRANS	1.07E-06	1.05E-06	-2.30E-08	-2.1%
XLOCA	1.00E-07	1.00E-07	0.00E+00	0.0%
Total	3.17E-05	2.34E-05	-8.28E-06	-26.1%

5. CONCLUSIONS AND FUTURE WORK

This report documents the FY 2019 activities on enhanced resilient plant (ERP) research and development (R&D). These activities continued the investigation of integrated evaluation approaches that combine the plant probabilistic risk assessment (PRA) models with multi-physics best estimate analyses and perform detailed risk and benefit assessments of accident-tolerant fuel (ATF) designs, diverse and flexible coping strategy (FLEX), and passive cooling system designs for current nuclear power plants. These studies will help achieve both safety and operational performance enhancements.

Risk analysis was conducted for the FeCrAl and Cr-coated cladding design impact on a generic Westinghouse 3-loop PWR for postulated loss of feedwater (LOFW) and steam generator tube rupture (SGTR) accident scenarios using the generic SAPHIRE and RELAP5-3D models. The FLEX analysis was presented as an overview of FLEX equipment and strategies implemented in the nuclear industry after the Fukushima accident. A FLEX model was developed and incorporated into the generic SAPHIRE model to assess the risk impact. A FLEX human reliability analysis (HRA) was performed which suggested an approach to HRA with FLEX strategies. Passive cooling system analysis includes an overview of the DNC system, the RELAP5-3D simulations of the DNC system in selected SBO scenarios, and the evaluation of the DNC system risk impact using the generic PRA model.

In the ATF LOFW analysis, the RELAP5-3D simulation results show that the gain of coping time, or the delay of time to core damage due to the ATF designs is less than 20 minutes for most LOFW scenarios. For FeCrAl, four of the seven analyzed LOFW scenarios have a gain of coping time from 6 to 14 minutes. The other three scenarios have a gain of coping time from 18 to 49 minutes, which are relatively small when comparing the time to core damage with Zircaloy in the associated scenarios (about 13 hours). For Chromite, four of the seven analyzed LOFW scenarios have a gain of coping time from 4 to 9 minutes. The other three scenarios have a gain of coping time from 16 to 22 minutes. With these relatively small increases of the time to core damage, the risk-benefit on behalf of the core damage frequency (CDF) brought by the ATF designs would be very small and they are not conducted in this analysis. However, the RELAP5-3D simulation results show a clear benefit in adopting ATFs with much less hydrogen produced at the time of core damage, which can be one or two orders of magnitude lower than the Zircaloy-clad cases.

In the ATF SGTR analysis, the SGTR accident sequences based on the PRA model do not reach core damage conditions within 48 hours. The reasons they were defined in the PRA model with the end state of core damage are probably from the conservative and qualitative assessment when developing the PRA model. With the slow progressing nature in an SGTR event, the time to core damage for most SGTR accident sequences could be much longer than the 24 hours one would see in other initiating events.

Additional SGTR accident scenarios were developed based on the U.S. NRC SOARCA report, which assumes no operator actions for an extended time interval. The RELAP5-3D analysis results show similar ATF impacts to those in the LOFW analysis. Similarly, the risk impact on behalf of the CDF brought by the ATF designs was not conducted for SGTR. However, the benefit of much less hydrogen produced at the time of core damage is obvious. The calculated amount of hydrogen produced during the transients for Zircaloy is 72.5 kg, but only 1.1 kg for FeCrAl (1.5% of the hydrogen production for Zircaloy), and 18.5 kg for Chromite (25% of the hydrogen production for Zircaloy).

The FLEX analysis presents an overview of FLEX, including FLEX characterizations and the crediting of FLEX in PRA, an effort to develop and incorporate FLEX to the generic LOOP/SBO SAPHIRE model, and a case study of how to perform HRA for FLEX applications. The total loss of offsite power (LOOP) CDF with FLEX from the generic model is 1.68E-6 per year, which is a 26% reduction when compared with the total LOOP CDF with no FLEX (2.28E-6 per year). These results represent the risk impact on a generic pressurized-water reactor (PWR) plant. Plant-specific FLEX analyses should be conducted to evaluate plant-specific risk impacts from the planned or implemented FLEX equipment and strategies, which might be different from the results due to specific structure, system, and component (SSC) configurations, their risk contributions and significance, and plant-specific risk profiles.

The FLEX HRA in this report provides a case study on how to perform HRA for FLEX applications. It utilizes South Korean operating experience and tries to use existing HRA methods for FLEX. The South Korean examples are particularly relevant to multi-unit sites but can be generalized to single-unit plants. The analyses characterize different types of accident scenarios that would require FLEX. To date, most U.S. PRAs have on FLEX has taken minimal HRA credit for FLEX deployment. The examples provided in this report demonstrate ways to account for FLEX and to use existing HRA methods without the need necessarily to adopt newer HRA techniques specifically to account for FLEX.

In the passive cooling system analysis, the dynamic natural convection (DNC) system designed by DYNAC Systems was reviewed and simulated with RELAP5-3D in selected station blackout (SBO) scenarios. The DNC system was modeled and incorporated into the generic PRA model by assuming that the DNC system is able to replace auxiliary feedwater (AFW) to provide secondary cooling safety function after an initiating event (IE) occurs. The quantification results show that the SBO CDF with DNC system is reduced from 2.28E-6 to 9.79E-7 per year, which represents a significant 57% reduction. After applying the DNC system to other event trees, the plant total CDF is reduced from 3.17E-5 to 2.34E-5 per year, with about a 25% reduction. The smaller risk reduction on the total plant CDF is attributed to the possibility that the DNC system may have little or no impact to initiators such as loss-of-coolant accidents (LOCAs), loss of component cooling water (LOCCW), and general transients.

Part of the FY 2019 ERP activities will be documented in the other project report. These activities include the ATF analysis for other accident scenarios such as anticipated transient without scram (ATWS), as well as general transients with turbine trip and PWR locked rotor. A more in-depth risk analysis on FLEX and passive cooling system will also be documented in that report.

For future work, we recommend the following activities for the ERP research:

- Develop generic BWR SAPHIRE Level 1 model and perform ERP risk analyses for selected boiling water reactor (BWR) accident scenarios
- Continue to investigate approaches that could maximize the benefits from the industry investment of FLEX and collaborate with industry to conduct plant-specific FLEX analysis
- Collaborate with the industry to work on the FLEX HRA
- Collaborate with the industry to conduct plant-specific dynamic natural convection system analysis
- Investigate other passive cooling system designs including Terry turbine and their impact on enhancing plant resilience.

6. REFERENCES

Ainsworth, L. K., & Kirwan, B. (1992). *A guide to task analysis.* Taylor & Francis.

Aldemir, T. (2013). A Survey of Dynamic Methodologies for Progabilistic Safety Assessment of Nuclear Power Plants. *Annals of Nuclear Energy, 52*, 113-124.

Aldemir, T., & et al. (2010). Probabilistic Risk Assessment Modeling of Digital Instrumentation and Control Systems using Two Dynamic Methodologies. *Reliability Engineering and System Safety, 95*, 1011–1039.

Alfonsi, A., Rabiti, C., Mandelli, D., Cogliati, J., Wang, C., Talbot, P. W., . . . Smith, C. L. (2017). *RAVEN Theory Manual and User Guide.* Idaho National Laboratory. Idaho Falls: Idaho National Laboratory.

Altman, N. S. (1992). An Introduction to Kernel and Nearest-Neighbor Nonparametric Regression. *The American Statistician, 46:3*, 175-185.

Arigi, A. M., Kim, G. P., & Kim, J. (2019). Human and organizational factors for multi-unit probabilistic safety assessment: Identification and characterization for the Korean case. *Nuclear Engineering and Technology*(51), 104-115.

ASME and ANS. (2013). *Addenda to ASME/ANS RA-S-2008 Standard for Level 1/Large Early Release Frequency Probabilistic Risk Assessment for Nuclear Power Plant Applications.* ASME and ANS.

Baumont, G., Menage, F., Schneiter, J., Spurgin, A., & Vogel, A. (2000). Quantifying human and organizational factors in accident management using decision trees: the HORAAM method. *Reliability Engineering & System Safety*(70), 113-124.

Bayless, P. D. (1987). *Natural Circulation during a Severe Accident: Surry Station Blackout.* EG&G. Idaho Falls: EG&G.

Boring, R., Germain, S. S., Banaseanu, G., Chatri, H., & Akl, Y. (2015). Applicability of simplified human reliability analysis methods for severe accidents. *7th International Conference on Modelling ans Simulation in Nuclear Science and Engineering.*

Bragg-Sitton, S. (2014). Development of Advanced Accident Tolerant Fuels for Commercial LWRs. *Nuclear News*(83).

Carlo Parisi, e. a. (2016). *Demonstration of External Hazards Analysis.* Idaho Falls: Idaho National Laboratory.

Cathcart, J. V., & et al. (1977). *Reaction Rate Studies, IV, Zirconium Metal-Water Oxidation Kinetics.*

CNSC. (2014). *Summary report of the international workshop on multi-unit probabilistic safety assessment.* Ottawa, Ontario, Canada: Canadian Nuclear Safety Commission.

Davis, C. B. (2017). *Evaluation of the DNC System Using RELAP5-3D.* Idaho Falls: INL.

Dominion. (2007). *Surry Power Station Units 1 and 2. Updated Final Safety Analysis Report. Rev. 39.* Virginia Electric and Power Company (Dominion). Washington, DC: US NRC.

Eide, S., & al., e. (2007). *Industry-Average Performance for Components and Initiating Events at U.S. Commercial Nuclear Power Plants.* Washington, DC: Nuclear Regulatory Commission.

Eide, S., Gentillon, C., Wierman, T., & Rasmuson, D. (2005). *Reevaluation of Station Blackout Risk at Nuclear Power Plants - Analysis of Loss of Offsite Power Events: 1986-2004.* Nuclear Regulatory Commission.

EPRI. (2012, April 16). *Modular Accident Analysis Program: A Software Toll for Analyzing Nuclear Plant Accident Scenarios.* Electric Power Research Institute. Retrieved April 16, 2018, from https://www.epri.com/#/pages/product/000000000001025795

EPRI. (2014). *Incorporating Flexible Mitigation Strategies into PRA Models: Phase 1: Gap Analysis and Early Lessons Learned.* Electric Power Research Institute.

EPRI. (2016). *An Approach to Human Reliability Analysis for External Events with a Focus on Seismic.* Electric Power Research Institute.

EPRI. (2018). *Accident Tolerant Fuel Technical Update.* Electric Power Research Institute.

Federal Register. (1995). *Use of Probabilistic Risk Assessment Methods in Nuclear Activities: Final Policy Statement.* Washington, DC: Federal Register.

Field, K. G., Snead, M. A., Yamamoto, Y., & Terrani, K. A. (2017). *Handbook on the Material Properties of FeCrAl Alloys for Nuclear Power Production Applications.* Oak Ridge National Laboratory, Nuclear Technology R&D.

Gamble, K. A., & et al. (2017). An investigation of FeCrAl cladding behavior under normal operating and loss of coolant conditions. *Journal of Nuclear Materials, 491*, 55-66.

Gaston, D., Hansen, G., & Newman, C. (2009). MOOSE: A Parallel Computational Framework for Coupled Systems for Nonlinear Equations. *International Conference on Mathematics, Computational Methods, and Reactor Physics.* Saratoga Springs, NY: American Nuclear Society.

Gauntt, R. O., Cash, J., Cole, R. K., Erickson, C. M., Humphries, L., Rodriguez, S. B., & Young, M. F. (2005). *MELCOR Computer Code Manuals.* Nuclear Regulatory Commission.

George, N. M., Terrani, K., Powers, J., Worrall, A., & Maldonado, I. (2015). Neutronic analysis of candidate accident-tolerant cladding concepts in pressurized water reactors. *Annals of Nuclear Energy, 75*, 703-712.

Gertman, D. I., & et al. (1992). INTENT: a method for estimating human error probabilities for decision-based errors. *Reliability Engineering & System Safety*(35), 127-136.

Gertman, D., & et al. (2005). *The SPAR-H human reliability analysis method.* Washington, DC: Nuclear Regulatory Commission.

Groth, K., & Swiler, L. P. (2012). Use of a SPAR-H Bayesian Network for predicting Human Error Probabilities with missing observations. *11th International Probabilistic Safety Assessment and Management Conference.*

Hales, J. D., & al., e. (2015). *BISON Theory Manual, The Equations behind Nuclear Fuel Analysis.* Idaho National Laboratory.

Han, S. H., Oh, K., Lim, H., & Yang, J. (2018). AIMS-MUPRA software package for multi-unit PRA. *Nuclear Engineering and Technology*.

Hollnagel, E. (1998). *Cognitive reliability and error analysis method (CREAM).* Elsevier.

Holzwarth, U., & Stamm, H. (2002). Mechanical and thermomechanical properties of commercially pure chromium and chromium alloys. *Journal of Nuclear Materials, 300*, 161-177.

IAEA. (1966). *Thermal Conductivity of Uranium Dioxide.* International Atomic Energy Agency.

INL. (2018). *Light Water Reactor Sustainability Program Integrated Program Plan.* Idaho National Laboratory.

Jung, W. (2005). *A standard HRA method for PRA in nuclear power plant: K-HRA method.* KAERI.

Kim, J. J., Wondea, & Park, J. (2018a). *A Case Study on Human Reliability Analysis for Mitigation Strategies using Portable Equipment in an Extended Loss of AC Power (ELAP) Event of Nuclear Power Plants.* KAERI.

Kim, J. J., Wondea, & Park, J. (2018b). Human Reliability Analysis of the FLEX/MACST Actions deploying Portable Equipment. *Transactions of the Korean Nuclear Society Autumn Meeting.* Yeosu, Korea.

Kim, Y., Park, J., & Jung, W. (2017). A classification scheme of erroneous behaviors for human error probability estimations based on simulator data. *Reliability Engineering & System Safety*(163), 1-13.

Larson, F. R., & Miller, J. (1952). A Time-Temperature Relationship for Rupture and Creep Stress. *Transactions of the ASME*, (pp. 765-775).

Lee, S. M., Ha, J. S., & Seong, P. H. (2011). CREAM-based communication error analysis method (CEAM) for nuclear power plant operators' communication. *Journal of Loss Prevention in the Process Industries*(24), 90-97.

Linthicum, R., & Powell, M. (2019). FLEX Equipment Reliability Data. *PRA 2019* (pp. 458-461). Charleston: American Nuclear Society.

Ma, Z., & al., e. (2018). *Plant-Level Scenario-Based Risk Analysis for Enhanced Resilient PWR – SBO and LBLOCA.* Idaho National Laboratory.

Ma, Z., & et al. (2017). A Simulation-based Dynamic Approach for External Flooding Analysis in Nuclear Power Plants. *Proceedings of the 20th Pacific Basin Nuclear Conference.* Springer.

Matev, A. (2006). Analysis of Operator Response to Station Blackout. *International RELAP5-3D User Group Meeting* . West Yellowstone: Idaho National Laboratory.

Matos, J. E., & Snelgrove, J. L. (1992). *Research Reactor Core Conversion Guidebook.* International Atomic Energy Agency.

Modarres, M. (2015). Multi-unit nuclear plant risks and implications of the quantitative health objectives. *Proceedings of the International Topical Meeting on Probabilistic Safety Assessment and Analysis.* Sun Valley, Idaho: American Nuclear Society.

Murabayashi, M., Tanaka, S., & Takahashi, Y. (1975). Thermal Conductivity and Heat Capacity of Zircaloy-2,− 4 and Unalloyed Zirconium. *Journal of Nuclear Science and Technology, 12*(10), 661-2.

NEI. (2012). *Diverse and Flexible Coping Strategies (FLEX) Implementation Guide.* Nuclear Energy Institute.

NEI. (2016). *Crediting Mitigating Strategies in Risk-Informed Decision Making.* Nuclear Energy Institute.

Nelson, A., White, J., Byler, D., Dunwoody, J., Valdez, J., & McClellan, K. (2014). Overview of properties and performance of uranium-silicide compounds for light water reactor applications. *Transactions of the American Nuclear Society. 110*, pp. 987-9. American Nuclear Society.

Nilsson, O., Mehling, H., Horn, R., Fricke, J., Hofmann, R., Müller, S. G., & al., e. (1997). Determination of the thermal diffusivity and conductivity of monocrystalline silicon carbide (300-2300 K). *High Temperatures High Pressures, 29*(1), 73-9.

NRC. (2008). *NRC Staff Position on Crediting Mitigating Strategies Implemented in Response to Security Orders in Risk-Informed Licensing Actions and in the Significance Determination Process.* Washington, D.C.: Nuclear Regulatory Commission.

NRC. (2010). *Confirmatory Thermal-hydraulic Analysis to Support Specific Success Criteria in the Standardized Plant Analysis Risk Models – Surry and Peach Bottom.*

NRC. (2012). *State-of-the-Art Reactor Consequence Analyses Project / Volume 2: Surry Integrated Analysis.* Nuclear Regulatory Commission.

NRC. (2012). *TRACE V5.0 Theory Manual: Field Equations, Solution Methods, and Physical Models*. (N. R. Commission, Producer) Retrieved April 16, 2018, from https://www.nrc.gov/docs/ML0710/ML071000097.pdf

NRC. (2017). *Industry Average Parameter Estimates 2015 Update.* Nuclear Regulatory Commission. Retrieved from Reactor Operational Experience Results and Databases: https://nrcoe.inl.gov/resultsdb/AvgPerf/

NRC. (2017). *Loss of Offsite Power.* Retrieved 07 28, 2017, from US NRC: http://nrcoe.inel.gov/resultsdb/publicdocs/LOSP/loop-glossary.pdf

NRC. (n.d.). *NRC Industry Average Parameter Estimates*. (N. R. Commission, Producer) Retrieved from NRC Reactor Operational Experience Results and Database: https://nrcoe.inl.gov/resultsdb/AvgPerf/

Parisi, C., Prescott, S. R., Szilard, R. H., Coleman, J. L., Spears, R. E., & Gupta, A. (2016). *Demonstration of External Hazards Analysis.* Idaho National Laboratory. Idaho Falls: Idaho National Laboratory.

Park, J. K., & et al. (2018). Analysis of Mobile Diesel Generator Operation to cope with Extended Loss of all AC Power in Nuclear Power Plant. *53rd International Universities Power Engineering Conference* (pp. 1-4). IEEE.

Park, J., Arigi, A. M., & Kim, J. (2019). Treatment of human and organizational factors for multi-unit HRA: Application of SPAR-H method. *Annals of Nuclear Energy*(132), 656-678.

Parry, G., & et al. (1992). *An approach to the analysis of operator actions in probabilistic risk assessment.* Electric Power Research Institute.

Pastore, G., & et al. (2017). *LOCA Demonstration with Experimental Assessment (IFA-650.10).*

Petruni, A., Giagloglou, E., Douglas, E., Geng, J., Leva, M. C., & Demichela, M. (2017). Applying Analytic Hierarchy Process (AHP) to choose a human factors technique: Choosing the suitable Human Reliability Analysis technique for the automotive industry. *Safety Science*.

Popov, S., Carbajo, J., Ivanov, V., & Yoder, G. (2000). *Thermophysical properties of MOX and UO2 fuels including the effects of irradiation.* ORNL,Fissile Materials Disposition Program.

Prosek, A., & Cizelj, L. (2013, April). Long-Term Station Blackout Accident Analyses of a PWR with RELAP5/MOD3.3. *Science and Technology of Nuclear Installations, 2013*.

Pyy, P. (2000). *Human reliability analysis methods for probabilistic safety assessment.* VTT Publications.

Rasmussen, M., Standal, M. I., & Laumann, K. (2015). Task complexity as a performance shaping factor: a review and recommendations in standardized plant analysis risk-human reliability analysis (SPAR-H) adaption. *Safety Science*(76), 228-238.

RELAP5-3D Code Development Team. (2003). *SCDAP/RELAP5-3D Code Manual. Volume 2: Modeling of Reactor Core and Vessel Behavior During Severe Accidents.* Idaho Falls: INEEL.

RELAP5-3D Code Development Team. (2018). *RELAP5-3D Code Manual Volume I.* Idaho National Laboratory. Idaho Falls: Idaho National Laboratory.

Richner, M. (2006). Modeling of SAMG Operator Actions in Level 2 PRA. *Proceedings of the 8th International Conference on Probabilistic Safety Assessment & Management (PRAM).* ASME.

Robb, K. R., Howell, M., & Ott, L. J. (2017). *Parametric and Experimentally Informed BWR Severe Accident Analysis Using FeCrAl.* Oak Ridge National Laboratory, Nuclear Technology R & D.

Schroer, S., & Modarres, M. (2013). An event classification schema for evaluating site risk in a multi-unit nuclear power plant probabilistic risk assessment. *Reliability Engineering & System Safety*(117), 40-51.

Schultz, R. R. (2015). *RELAP5-3D(c) Code Manual Volume V: User`s Guidelines.* Idaho National Laboratory. Idaho Falls: Idaho National Laboratory.

Scikit-Learn. (2017). Retrieved 07 28, 2017, from Scikit-Learn: http://scikit-learn.org/stable/

Siu, N. (1994). Risk Assessment for Dynamic Systems: an Overview. *Reliability Engineering and System Safety, 41*, 43–73.

Smith, C. L., & Wood, S. T. (2011). *Systems Analysis Programs for Hands-on Integrated Reliability Evaluations (SAPHIRE).* Idaho National Laboratory. Idaho Falls: US NRC.

St Germain, S., & et al. (2017). *Multi-Unit Considerations for Human Reliability Analysis.* Idaho Falls, Idaho: Idaho National Laboratory.

Swain, A. D. (1987). *Accident sequence evaluation program: Human reliability analysis procedure.* Albuquerque, NM: Sandia National Laboratory.

Swain, A. D. (1990). Human reliability analysis: Need, status, trends and limitations. *Reliability Engineering & System Safety*(29), 301-313.

Swain, A. D., & Guttmann, H. E. (1983). *Handbook of human-reliability analysis with emphasis on nuclear power plant applications.* Albuquerque, NM: Sandia National laboratory.

Szilard, R. H., Coleman, J. L., Prescott, S. R., Parisi, C., & Smith, C. L. (2016). *RISMC Toolkit and Methodology Research and Development Plan for External Hazards Analysis.* Idaho National Laboratory. Idaho Falls: Idaho National Laboratory.

Takahashi, Y., Yamamoto, K., Ohsato, T., Shimada, H., Terai, T., & Yamawaki, M. (1989). Heat capacities of uranium-zirconium alloys from 300 to 1100 K. *Journal of Nuclear Materials, 167*, 147-51.

Takahashi, Y., Yamawaki, M., & Yamamoto, K. (1988). Thermophysical properties of uranium-zirconium alloys. *Journal of Nuclear Materials, 154(1)*, 141-4.

Virginia Electric and Power Company. (2010). *Measurement Uncertainty Recapture Power Uprate.* Richmond.

Williamson, R. L., & et al. (2012). Multidimensional multiphysics simulation of nuclear fuel behavior. *Journal of Nuclear Materials, 423(1)*, 149-163.

Yalaoui, S. X., & Yolande, A. (2018). *WGRISK Task (2) Phase 1: Summary Results of the "Multi-Source Interactions and Dependencies" Focus Area, International workshop on Site Level PRA Developments.* Munich, Germany: OECD/NEA.

Zhang, H., Szilard, R., & Hess, S. (2018). *R&D Roadmap for Enhanced Resilient Plant Systems, Metrics, Scenarios, Risk Analysis, and Modeling and Simulation.*